An experimental study of the flow around and the forces developed by, hypersonic lifting vehicles.

Theodor Pinkus Selig Opatowski.

D.C.Ae.; C.Eng.; A.F.R.Ae.S.

September 1967.

A thesis submitted for the Degree of Doctor of Philosophy in the Faculty of Engineering of the University of London.

An experimental study of the flow around and the forces developed by, hypersonic lifting vehicles.

Abstract

The forces developed by sharp delta wings with vee roofs at hypersonic speeds have been experimentally investigated and theoretical consideration given to the relationship of these results to full scale conditions.

The theoretical development considered the case of streamwise upper surfaces and the maximum lift/drag ratio and optimum thickness (θ') which result from applying this restraint. Simple expressions for both these quantities and their variation with Mach No., Reynolds No. and surface heat transfer have been obtained using a new formula for pressure versus flow deflection at hypersonic speeds developed for this purpose. When related to practical cruise vehicles operating in the atmosphere, these optimum configurations proved to be unrealistic as they corresponded to vehicles that were only 1° to 2° thick or had very low wing loadings.

Numerical estimates for vehicles having practical wing loadings and thicknesses showed that reasonable lift/drag ratios could only be obtained at the lower altitudes, i.e. up to about 150,000 ft. and at these altitudes base drag had a significant effect. It was also shown that for these conditions the maximum lift/drag ratio occurred when the upper surfaces were streamwise for a thickness of about 5°.

For a wing operating at optimum condition θ', the viscous drag is significant, being about half the total drag. Conversely, the viscous drag is only a minor part of the total drag of wings that are much thicker than θ'. While the latter condition is that relevant to practical cruise vehicles in the atmosphere, this is not the case in many tunnel tests where optimum thicknesses, appropriate to Reynolds numbers between 1×10^6 and 4×10^6 are in the range 5^o to 8^o. This means that tunnel tests in these conditions will be Reynolds number sensitive and many of the results which arise from viscous effects will be markedly different at higher Reynolds numbers. Extreme caution is indicated in translating test results to full scale. Tests of such thin wings at low Reynolds numbers, if intended for high Reynolds numbers, are useful mostly for substantiating theoretical methods of estimation.

The experimental programme was carried out in the Imperial College gun tunnel at a Mach No. of 8·3 and two strain gauge balances were developed for this purpose. The models were sharp deltas with vee roofs and included two thicknesses, two aspect ratios, flat bottomed, caret and twisted shapes which were tested at Reynolds numbers of $0{\cdot}9 \times 10^6$ to $3{\cdot}5 \times 10^6$.

The results agreed with theoretical estimates to within the estimated experimental accuracy. The lift of the flat wings was seen to be closely predicted by the two-dimensional oblique shock equations assuming each surface to be part of an infinite unswept plane, the difference being the order of 3-5% as predicted by

Babaev for almost similar conditions. The loss of lift with leading edge shock detachment was seen to be small.

Within the margin of unknowns, the skin friction was adequately predicted by strip theory and the intermediate enthalpy method. There was some evidence of transition on a flat bottomed wing which was not so evident on a similar wing of lower aspect ratio, an apparent increase of transition Reynolds number with increasing sweep. There was also evidence of viscous effects on the caret wings and on the twisted wing.

At the Reynolds numbers of the tests there was little to choose between the three different cross-sectional shapes in terms of maximum lift/drag ratio. The caret and twisted wings developed their maximum lift/drag ratio at a higher value of lift coefficient which is advantageous for cruise vehicles in the atmosphere, and this benefit would be expected to remain at the appropriate full scale Reynolds numbers, at least in the case of the caret wing. The twisted wing had its centre of pressure 2% further forward - also advantageous - and a more useful cross-sectional area distribution.

The experimental results also substantiated the theoretical estimates of optimum thickness with streamwise upper surfaces (θ') for the conditions of the tests.

Acknowledgements

In any endeavour such as that involved in the work described herein, one is inevitably helped in many ways by numerous people, some of whom I may unwittingly have forgotten about. Let me first, therefore, thank all who have helped, if only with their good wishes and encouragement.

The work was carried out under a Ministry of Technology contract and monitored by the National Physical Laboratory, represented by Dr. L. Pennelegion whose interest and advice throughout was much appreciated. Much useful advice was also obtained from several members of the R.A.E. (Farnborough) High Speed section and from my colleagues at Imperial College.

My special thanks go to my supervisor, Mr. J.L. Stollery, without whom none of this would have been possible. He has that uncommon knack of being able to provide the right word at the right time, allowing one to proceed more or less as one wishes without allowing any disasterous mistakes, being encouraging in black moments while not allowing one to be carried away by small successes. Thanks are also due to Dr. J. Harvey who "stood-in" for Mr. Stollery while he was in the U.S.A. and who suggested the pressure recovery cone for flow inclination measurement.

A large part of the work was concerned with the design and construction of the balances. The design of the MKIII balance benefited greatly from the experience of Mr. G. Smith of the

N.P.L. who gave freely of his knowledge and was very helpful in all ways. The college workshop under Mr. W. Davies was extremely helpful and my special thanks go to Mr. J. Cunningham who was ever capable, helpful and concerned and to Mr. F. Fone who carried out the difficult machining on the MKIII balance; a good job of which they can all be justifiably proud. I would also like to thank Mr. O'Leary, the college photographer for his help including the manufacture of the printed circuits for the balance.

My gratitude and thanks go also to Mrs. L. Fancett who so ably and cheerfully typed this thesis through many long evenings and weekends.

One way or another, over the last four years my wife and children have made considerable sacrifices in order that this work could proceed. I hope they know how much I appreciate it but they might like to see it in print; thanks-a-million, family.

Contents

Page

List of figures

The first digit of each figure number indicates the paragraph in which the figure is discussed.

Figure		Page

Notation

a   speed of sound

b   base pressure ratio, see eqn. 2.8.

C   constant in Sutherland viscosity law

$\bar{C}$ constant in simplified viscosity law

see equations B.9. and B.10.

C_D drag coefficient, $\dfrac{D}{0.5\,\gamma M_\infty^2\, p_\infty\, S}$

C_p pressure coefficient, $\dfrac{p - p_\infty}{0.5\gamma M_\infty^2\, p_\infty}$

C_L lift coefficient, $\dfrac{L}{0.5\,\gamma M_\infty^2\, p_\infty\, S}$

D   drag

E_U E_L ratio of surface areas, see eqn. B.13.

H   constant related to surface cooling

see equations B.15. and B.17.

$\bar{H}$ $\left[\dfrac{H(\gamma - 1)}{2}\right]^{\frac{1-n}{2}}$, see eqn. B.21.

K   skin friction parameter, see eqn. B.31.

L   lift

l   overall length of vehicle

M   Mach number

n   power in viscosity law, see eqn. B.9.

p   pressure

$Q_{1,2..}$ ratio of dynamic pressures $\dfrac{\rho_{1,2...}U^2_{1,2...}}{\rho_\infty\ U^2_\infty}$

R_e	Reynolds number
R_{e_1}	Reynolds number based on unit length
S	wing plan area
s	semi-span
T	temperature
U	velocity
V	volume
$\bar{V}$	volume parameter $\frac{V}{S^{3/2}}$ (sometimes $\frac{V^{2/3}}{S}$)
x	distance aft of leading edge
α_o	incidence of wing centre line, see Appendix A and fig. 4.1
β	wing semi-thickness angle, see Appendix A.
γ	ratio of specific heats, taken as 1·4
δ	flow deflection angle
θ	wing thickness angle
θ'	wing thickness angle for maximum lift/drag ratio with upper surfaces streamwise.
μ	viscosity
ρ	density
σ	relative density
τ_o	surface skin friction
$\varkappa$	leading edge interaction parameter, see eqn. 2.1
ω	wing loading, $\frac{W}{S} = \frac{L}{S}$

Suffixes

B	base
D	drag
F	total skin friction
f	local skin friction
L	lower surface
l	based on vehicle length
S	standard
U	upper surface
W	at wall
W_o	adiabatic recovery at wall
x	distance from leading edge
∞	free stream
1	lower surface with upper surface streamwise
3	at deflection equal to half thickness angle
*	based on intermediate temperature defined by equation B.15.
'	optimum values
max	maximum obtainable at any incidence
θ'	maximum with upper surface streamwise.

Section 1. Introduction and review of information on wings and lifting bodies.

1.1. Introduction.

As the title implies, the original aims of this investigation were extremely broad and capable of applying to a large variety of configurations. In order to achieve a useful result with the available effort it was necessary to select and define a smaller area for detailed study. For the last few years, two related topics have aroused considerable interest and effort in this country, namely hypersonic cruise vehicles (refs. 1 to 4) and waverider designs (refs. 5 to 15). It was therefore thought most suitable to concentrate efforts in these general areas, thus enabling comparisons to be drawn with various estimates (refs. 16 to 22) and in the hope that the results would be useful to others.

Hypersonic lifting vehicles can be roughly divided into those in which lift is used only transiently as a control, as in lifting re-entry vehicles (eg.ref. 23), and those in which a proportion of the weight is borne by aerodynamic means in an equilibrium condition, such as cruise vehicles. The former are distinguished by very high Mach numbers, high incidence and high heating rates, low Reynolds numbers and low lift/drag ratios, large amounts of blunting and the possibility of significant variations arising from non-equilibrium, dissociation and possibly ionization effects. The provision of volume is not usually a problem.

Among cruise vehicles there is a division between the lower speeds where the majority of the weight is borne by aerodynamic means and air breathing engines are possible and higher, near orbital speeds where only a fraction of the lift is aerodynamic. The test Mach No. of 8·3 implies the former of the two above alternatives and the latter has not been explicitly examined, though it is not difficult to read from one to the other in some cases. These lower speed vehicles operate at comparatively high Reynolds numbers, high lift/drag ratios and low incidences and can have effectively sharp leading edges (Ref. 29.). The main aerodynamic problems are those of providing adequate lift and volume at reasonable lift/drag ratios.

Cruise vehicles can be further sub-divided into interference and non-interference designs, a typical example of the former being the flat delta wing with underslung half-cone (eg.ref.34.). These shapes compare favourably with the merged configurations such as wave riders at Mach numbers below about 8 but begin to lose this advantage as Mach number is increased and require increasingly complicated shapes in order to derive the full benefits available (refs. 24 to 27.). These shapes have not been investigated.

The particular object of the present work therefore, was to experimentally study the factors affecting the performance of hypersonic lifting cruise vehicles of the merged wing-body type. *

(See footnote on next page.)

In order to adequately assess the experimental results, a theoretical study was carried out and this forms an important part of the results.

An ancilliary problem, which required a considerable amount of effort, was that of providing a satisfactory balance for use in the gun tunnel. Two such balances were built. The first was an extensive modification of one left by a previous investigator, Mr. P. Church, while the second was entirely new. The two balances are described in detail in section 3 and ref.70, as a considerable amount of information was obtained from their development which, it is considered, could be of use to others in this field.

1.2. Experimental results in the literature.

1.2.1. Force measurements.

There exists a moderate amount of experimental data on the forces developed by bodies in hypersonic flow. Because the range of bodies and conditions is large, the coverage tends to be thin. Those discovered by the author are tabulated below.

---

* These bodies are included in the designation 'wave-riders' which can be applied to any bodies with attached leading edge shocks including interference designs.

Ref.	Configurations.	Test conditions and measurements.	Remarks.
(a) Plain wings.			
Penland (30)	Triangular and rectangular planform. 'Vee' roofs 5°&10° thick.	$R_e = 0{\cdot}6 \times 10^6$ to $4{\cdot}2 \times 10^6$ $M = 6{\cdot}9$ C_L. C_D. C_M.	Directly comparable to results of present investigation. Compares the performance of the tested configurations.
Blackstock & Ladson (31)	Triangular and rectangular planform. 'Vee' roofs 11° thick.	C_L. C_D. C_M. $M = 6{\cdot}8, 9{\cdot}6, 10{\cdot}8, \& 18{\cdot}0$ $R_e = 0{\cdot}33 \times 10^6$ to $2{\cdot}42 \times 10^6$	Includes effect of blunting. High M and R_e in helium.
Fetterman et al. (27)	Many, including rectangular, sharp deltas, bodies and interference.	$M = 6{\cdot}8$ and 20 $(L/D)_{max}$. only. $R_e = 1{\cdot}5 \times 10^6$ and $3{\cdot}5 \times 10^6$	Compares performance of wide range of wings, bodies and wing/body combinations. High M and R_e in helium.

Ref.	Configurations.	Test conditions and measurements.	Remarks.
Becker (32)	Many. Includes most of above results plus others on interference etc.	$(L/D)_{max}$. only. Conditions as above.	Review paper covering comparative performance in addition to other hyp. vehicle problems.
McLellan and Ladson (25).	Vehicle shapes. Includes one plain delta with Vee roof.	$(L/D)_{max}$. only. $M = 0$ to 20 $R_e = 0{\cdot}7 \times 10^6$.	Compares performance of wide range of wings, bodies and wing/body combinations including results from other sources.
Weinstein & Neal, (88).	Flat delta and diamond cross-section.	C_L. C_D. C_M. $M = 6{\cdot}8$ & $9{\cdot}7$ $R_e = 3 \times 10^6$	Investigates effect of geometric modifications. Includes 6^o flat delta.

Ref.	Configurations.	Test conditions and measurements.	Remarks.
(b) interference and inverted wings			
Fetterman (26)	Interference delta/half cone with dimensional variations.	$M = 6{\cdot}8$ $Re = 1{\cdot}5 \times 10^6$ C_L, C_D, L/D.	Compares performance resulting from various geometric modifications.
Geiger (33)	Interference delta. Blunt half cone.	$M = 12, 17$ $Re = 5 \times 10^4$ to 5×10^5 $\alpha = \pm 12^\circ$ for wings C_L, C_D, L/D.	Force measured by free flight technique.
Small & Bertram (35)	Arbitary wing-body combinations	$M = 6{\cdot}8$ & $9{\cdot}6$ $Re = 1{\cdot}5 \times 10^6$ C_L, C_D, L/D.	Compares performance resulting from various geometric modifications.

Ref.	Configurations.	Test conditions and measurements.	Remarks.
Mead et al (36)	Wing body combinations. Slab wings with champhered leading edges/half cones. Geometric variations.	$M = 8$ $Re = 2{\cdot}5 \times 10^6$ C_L, C_D, C_M, L/D.	Wide variety of configurations.
(c)	lifting bodies.		
Trimpi et al (23)	Lifting bodies.	-	Review paper. Problems of re-entry. Extensive bibliography.
Penland (37)	Cones, cone cylinders $5^\circ, 10^\circ, 15^\circ, 20^\circ, 30^\circ, 45^\circ$, half angle.	$M = 8{\cdot}6$ $Re = 0{\cdot}2 \times 10^6$ to 1×10^6 $\alpha = 0$ to 130° C_L, C_D, L/D.	Compares L/D_{max}. of the various shapes.

Ref.	Configurations.	Test conditions and measurements.	Remarks.
Penland (38)	Cones. $5^{\circ}, 10^{\circ}, 20^{\circ}, 30^{\circ}, 40^{\circ}, 50^{\circ}$, half angle.	$M = 6 \cdot 8$ $Re. = 0 \cdot 2 \times 10^{6}$ $\alpha = 0 - 180^{\circ}$ C_M, C_L, C_D.	Accurate centre of pressure data. Stability considered.
Ladson and Blackstock (39)	Cones. $5^{\circ}, 10^{\circ}, 15^{\circ}, 20^{\circ}$ half angle.	$M = 6 \cdot 8$ & $9 \cdot 6$ & $10 \cdot 9$ & 18. $Re = 5 \times 10^{5}$ to $1 \cdot 2 \times 10^{6}$. $\alpha = 0$ to 90° C_L, C_D, L/D.	High two M's in helium.
Spencer & Fox. (40)	Elliptic power law bodies. Also min drag bodies.	$M = 10 \cdot 8$ C_L, C_D, C_M, & L/D.	Includes right circular and elliptic cones and explores optimum longitudinal profiles.

Ref.	Configurations.	Test conditions and measurements.	Remarks.
Wells and Armstrong (41)	Bodies, cones and half cones.	$M = 9{\cdot}6$ C_L, C_D, C_M, $(L/D)_{max}$.	Also gives tabulated theoretical forces for various conic and hemispherical shapes using Newtonion theory.
Betram et al (48)	Wings and bodies including deltas.	$M = 6 - 10$. Includes heat transfer and surface flow on flat delta.	Review paper, considers many problems including streamwise corners. Comprehensive bibliography.

1.2.2. Pressure distributions

Pressure distributions have been measured by several investigators ; details are given in the table below.

(a) Wings of shape directly comparable to those of the present tests.

Ref.	Configuration.	Conditions.	Remarks.
Squire (20)	Deltas, plain and caret. Top and bottom surfaces.	$M = 4$ & 5, $\alpha = 0$ to 25°	Affected by shock detachment. Includes surface streamlines. Caret on and off design.
Peckham (42)	Deltas with various upper surfaces. Also caret and other waveriders. Top and bottom surfaces.	$M = 6{\cdot}85$ & $8{\cdot}6$. $\alpha = 0 - 25^{\circ}$	Affected by shock detachment.
Peckham (16)	Caret, lower surface.	$M = 4{\cdot}3$	One pressure point.
Pennelegion and Cash. (21)	Caret, lower surface.	$M = 8{\cdot}8$, $\alpha = -5^{\circ}$ to $+20^{\circ}$	One pressure point.
Mead & Koch (36)b	Deltas, rectangular, interference and merged shapes. $\Lambda \leqslant 65^{\circ}$.	$M = 5$ & 8	Extensive range of models. Flow visualization by vapour screen.

Ref.	Configuration.	Conditions.	Remarks.
Dunavant (47)	Caret and flat deltas $\Lambda = 75^\circ$.	$M = 6\cdot8$ & $9\cdot6$ $0 \leq \alpha < 90^\circ$.	Also includes heat transfer measurements and surface streamlines. Summary of these results in ref.48 &49.
Crabtree and Treadgold. (83)	Caret and flat deltas.	$M = 4$, 5 & $8\cdot6$ on and off design.	Review paper. Contains results from other R.A.E. reports.
Crane (87)	Caret and flat deltas. 'Vee' roofs. Both surfaces.	$M = 8\cdot6$ $-15^\circ \leq \alpha \leq 15^\circ$.	Some of these results are contained in ref.(83).
Polak. (50)	Flat delta.	$\alpha >$ shock detachment.	Shock detached at high incidence. Surface streamlines. Very low Re. Viscous interaction region.

(b) Other wings and lifting bodies.

These fall roughly into three groups :- slab wings, interference designs and lifting bodies. While not directly comparable with the wings of the present tests, these results can give useful indications of the effect of various geometric variations, such as blunting. The table below is not intended to be exhaustive.

Ref.	Configuration.	Conditions.	Remarks.
Nagel et al (43)	Slab deltas. Round leading edge.	Pressure and heat transfer. $M = 2{\cdot}2, 6, 7, 8, \& \ 15$. $\alpha = 0$ to 45°.	Comprehensive bibliography.
Hopkins et al. (52)	Rect. and delta slab wings with camber and twist.	$M = 12 \ \& \ 19$. $\alpha = 0$ to 15°.	Includes a twisted rectangular wing.
32,36,42 & 44.	Interference designs.	Various.	Ref. 44 includes surface streamlines and heat transfer.
45 & 46.	Cones. Sharp and blunt. 5° up to 45°.	$M = 3{\cdot}8, 6{\cdot}8 \ \& \ 8{\cdot}6$. $\alpha = 0\text{-}100^{\circ}$.	-
Peckham (42)	Lifting bodies, various, including caret under surfaces.	$M = 6{\cdot}8 \ \& \ 8{\cdot}6$ $\alpha = 0\text{-}29^{\circ}$.	Detached shock, wing-like bodies.

1.3. Theoretical estimates in the literature.

1.3.1. Estimates of pressure forces.

There exist a few exact results and many approximations to the inviscid pressure on bodies in hypersonic flow, covering the range from the simple pressure versus flow deflection on a plane surface to the integrated force developed on an arbitary body at an arbitary incidence. Some pertinent references are reviewed in the table below.

Ref.	Theory.	Applicable to.	Remarks.
Ames Research Staff. (53)	Exact. Oblique shock equations. Conical flow results.	Plane 2-D and Conical flows.	Also gives Busemann's expansion for pressure versus flow deflection for small deflections.
Taylor & Macoll. (54)	Exact conical flow.	Cones at zero incidence.	
Kopal et al (55)&(56)	Conical flow.	Cones at incidence.	Tabulated results. Other authors have presented methods of easing the use of these tables.

Ref.	Theory.	Applicable to.	Remarks.
Fowel. (62)	Conical flow.	Flat deltas with attached L.E. shocks.	-
Babaev. (63)	Exact numerical calculation.	Flat deltas with attached L.E. shocks. Results for, $M = 4, 6$. $\Lambda = 50^{\circ}, 60^{\circ}$. $\alpha = 5^{\circ}, 9^{\circ}, 10^{\circ}, 15^{\circ}$.	Exact result for the cases considered.
Trimpi & Jones. (61)	Exact oblique shock equations.	Plane 2-D flow with sweep and various values of γ.	Extensive tabulated results.
Opatowski (74)	Approximation to oblique shock for small deflections.	Plane 2-D flow for low $M\delta$ at hyp. speeds.	Also briefly reviews similar approximations in refs. 22, 57, 58, 59, and 60.

Ref.	Theory.	Applicable to.	Remarks.
Crabtree (64)	Small perturbation. Tangent wedge. Tangent cone. Shock expansion and Newtonion.	Arbitary bodies.	Survey paper.
Love & Henderson. (65)	Newtonion and other approximations. Effect of varying γ.	2-D plane flows.	Comprehensive survey of accuracy of various approximations and effect of various assumptions.
Scheuing et al. (66)	Shock expansion. Shock layer and others.	Deltas and arbitary bodies.	Attempt to improve applicability of theories with only moderate success.
Gentry. (67)	Tangent wedge/cone combination.	Arbitary bodies.	Computor programme to integrate forces on a numerically defined arbitary body.

1.3.2. Overall forces and aerodynamic performance.

Several authors have made estimates of the overall forces and aerodynamic performance of thin wings, suitable for hypersonic cruise vehicles. Some characteristics of the plain two-dimensional wedge in inviscid flow are tabulated and plotted by Edwards in ref. 68 while the same flow but translated to the single or multiple shock, caret type wing is dealt with by Peckam in ref. 16. The characteristics of caret wings with boundary layer effects included are estimated by Catherall for laminar flow in ref. 17 and for turbulent flow in ref. 19.*

An extensive variational study of caret wings with various assumptions about the skin friction is presented by Collingbourn and Peckham in ref. 22. This report, which attempts a similar analysis to that of section 2 of this thesis is discussed in detail in section 7.

All the above work on the estimated aerodynamic performance of wings suitable for hypersonic cruise vehicles is of British origin. The U.S.A. does not seem to have been interested in this type of vehicle until quite recently and much of their work on this subject, has been classified. Another reason may have been that they have not taken advantage of the caret wing concept, (Nonweiler ref. 5) which enables simple but exact estimates to be made for a large

---

* Upper surface skin friction was neglected in these reports.

variety of conditions.

One report which, although not directly applicable is however worth mentioning is that of Dewey (ref. 69). This report is concerned with slender wings and the effects of blunting and viscous interaction and presents estimates of lift/drag ratio with increasing Mach number and altitude. The altitudes considered are above those relevant to the present investigation but show that for a considerable altitude range, equivalent to $2 < \chi_{\infty_L} < 25$, the effect of viscous interaction is to reduce the lift/drag ratio by about 5%. At lower altitudes (and values of χ_{∞_L}) the difference in lift/drag ratio due to viscous interaction would be less than 5% while for values of $\chi_{\infty_L} > 25$, ref.69 shows that viscous interaction can result in a value of L/D greater than that which would be obtained if viscous interaction were ignored.

Section 2. General theory of delta wing cruise vehicles.

2.1. General considerations.

Studies of the aerodynamic efficiency of lifting shapes at hypersonic speeds have often been presented in terms of a volume parameter $\overline{V}$, e.g. refs. 25, 26, 27, 30, 32, 48, 88. This parameter contains many shape variables and its use makes the separation of the effects of these variables difficult. It was felt that a greater insight into the factors affecting the performance of hypersonic cruise vehicles could be obtained by looking more closely at a single configuration.

To this end an analysis has been carried out on sharp, flat bottomed or caret delta wings with vee roofs and attached leading edge shocks. The object has been to find the conditions giving the highest value of lift/drag ratio with reasonable volume and wing loading, to investigate the characteristics of these wings in the atmosphere and to obtain an indication of the relevance of tunnel tests to free flight conditions.

2.2. Analysis

2.2.1. Assumptions

Wing shape

The basic shape considered in this section is a flat bottomed delta with a vee roof. A delta was chosen as being representative of the sort of shape that would be practical as a cruise vehicle since low speed handling and transonic stability are as essential as good hypersonic performance. Since the theory used herein assumes an average pressure over each surface equal to the two-dimensional oblique shock pressure applied to a streamwise section, the basic equations are equally applicable to caret wings and, with an appropriate change of numerical constant, to waverider wings of any planform, provided leading edge shock attachment is maintained.

The assumption of sharp leading edges should not be a severe limitation. Some calculations presented in ref. 28 show typical leading edge radii of one or two inches in the range of speeds and heights of interest to cruise vehicle design and Capey (ref. 29) shows that if provision is made for heat conduction, the leading edge can be made arbitraraly sharp. Additionally, ref. 31 shows that for highly swept edges, even quite large amounts of blunting have only a small effect on the lift/drag ratio.

Flow conditions

Air is assumed to behave as a perfect gas and the entire boundary layer flow is assumed laminar. For the 200 ft. vehicle in the atmosphere for which numerical calculations have been made, the average Reynolds number is of the order of 40×10^6 and the assumption of completely laminar flow is probably optimistic. Information on transition at hypersonic speeds is sparse and there are known variations between different tunnels and between tunnel and free flight. From some recent free flight measurements on a caret wing, Picken and Greenwood (ref. 75) obtained a maximum transition Reynolds number of 8×10^6 at a Mach number of 3.

With the known tendency of transition Reynolds number to increase with Mach number, the above assumption may not be impossible but the position of transition must remain one of the largest unknowns especially when the possible effects of blunting and sweep are included.

Leading edge interaction has been assumed negligible. Cooke in ref. 18 gives the following criterion for interaction to affect less than 5% of a delta surface

$$\chi_1 = \frac{M^3}{\sqrt{R_{e1}}} < 0.22$$

where M = Mach number

R_{e1} = Reynolds number based on overall length.

For a 200 ft. vehicle at Mach 10 and 100,000 ft. χ_1 = 0·07, and hence the above assumption is likely to be adequate.

Theoretical methods used

The average pressure on each plane surface has been assumed to be given by the two-dimensional oblique shock equations, assuming the surface to be part of an infinite unswept plane. Babaev, ref. 63, has solved the problem of flow over such surfaces numerically, and has demonstrated that for the sweep angles considered (0 - 50^{o}), the loss of average pressure from the 2 - D value is only 2 - 4% up to an incidence of 21^{o} on the pressure surface, and less than 2.5% up to -7^{o} incidence on the suction surfaces at a Mach number of 4 to 5.

The present experimental results tend to confirm that the appropriate figure for the higher Mach numbers and sweep angles of these tests, is also less than 5%. The lift/drag ratio is rather insensitive to small variations in the assumed pressure.

Strip theory has been used in calculating the laminar skin friction, assuming that each streamwise strip behaved as a sharp flat plate at zero incidence and with free stream conditions equal to those after the oblique shock. No allowance has been made for boundary layer displacement in the approximate development of this section. (Boundary layer displacement is included in the comparative theoretical results of section 4.)

Other assumptions

Since maximum lift/drag ratio is achieved with a wing of zero thickness, another form of optimum must be sought if one wants a practical vehicle. A maximum in lift/drag ratio verus thickness other than zero thickness, can be obtained by fixing the incidence of the upper surface at some appropriate value. A convenient value is zero, i.e. the upper surfaces are held streamwise and the resulting relationship between the $^L/D$ for this condition and the $^L/D$ for any thickness and incidence is shown schematically in figures 2.1 and 2.2 and the appropriate equations being given in Appendix A. If a negative upper surface incidence (i.e. suction) has been chosen, the curve would have started at some positive value of $^L/D$ and touched the full curve at a lower thickness with an opposite trend for fixed positive upper surface incidences. Anticipating the results, the upper surface streamwise condition coincides with the maximum lift/drag ratio condition for thicknesses around 5^{o}. A large proportion of the analysis and results presented here is related to the condition of upper surface streamwise. (See also paragraph 4.)

Another important unknown is the base drag. It was felt that no realistic estimates could be made and so the numerical results have been presented for no base drag and for a base drag corresponding to a base pressure equal to half the free stream static pressure.

2.2.2 Theory

A full derivation of the theory is given in Appendix B, it being given only in outline here. Pressure versus flow deflection was obtained, as shown in ref. 74 from the expression

$$\left(\frac{p}{p_{\infty}} - 1\right) = \gamma M\delta \pm 1{\cdot}1\ (M\delta)^{2{\cdot}15} \qquad \ldots\ldots\ldots(2.1.)$$

For the case of upper surface streamwise, all pressure forces are generated on the lower surface whose incidence is equal to the thickness angle θ. For slender wings the normal force is nearly equal to the lift force and hence with equation (2.1.) above,

$$C_L \simeq \frac{2\theta}{M} + 1{\cdot}5M^{0{\cdot}15}\ \theta^{2{\cdot}15} \qquad \ldots\ldots\ldots(2.2.)$$

$$\text{for } \gamma = 1{\cdot}4$$

It is shown in Appendix B (equation B26a and equation 3.6 below) that the skin friction on any surface, can be expressed by

$$C_{D_F} \sim \left(\frac{p}{p_\infty}\right)^{\frac{1}{2}} \qquad \ldots\ldots\ldots(3.3.)$$

For slender wings the rates of change of pressure with incidence of upper and lower surfaces are nearly equal in magnitude and opposite in sign and therefore so also is the rate of change of skin friction. Hence total skin friction is approximately invariant with wing incidence at fixed thickness.

Using the Blasius solution of the laminar boundary layer on a flat plate with zero pressure gradient, the reference temperature method of reference 71 and performing the necessary integration for the triangular planform (ref. 19) the total skin friction drag becomes,

$$C_{D_F} = 1{\cdot}77 Q_3 \,(E_L + E_U)\sqrt{\frac{\bar{C}_3}{Re_{3L}}} \qquad \ldots\ldots\ldots(3.4.)$$

where upper and lower surfaces are taken at $\theta/2$ incidence, and Q_3 is $\frac{\rho_3 U_3^2}{\rho_\infty U_\infty^2}$; E_U and E_L , upper and lower surface area$/S$ respectively, and $\bar{C}_3 = \left(\frac{T^*}{T_3}\right)^{1-n}$ $\qquad \ldots\ldots\ldots(2.5.)$

where n is the exponent in the assumed power relationship between temperature and viscosity and can be found for any temperature range, by using Sutherlands law. T^*, the intermediate temperature can be incorporated in a parameter $\bar{H}$ which only varies over narrow limits (0·7 to 0·8) as the wall temperature varies from static to adiabatic wall temperature, i.e. as the cooling varies from 100% to zero.

After some manipulation, given in Appendix B, the total skin friction drag is,

$$C_{D_F} = \frac{1{\cdot}77\,(E_L + E_U)}{\bar{H}\;M_\infty^{1-n}\sqrt{R_{e_L}}} \cdot \left(\frac{p_3}{p_\infty}\right)^{1/2} \qquad \ldots\ldots\ldots\ldots\ldots(2.6)$$

and from a graphical solution using the exact relation for the pressure rise through an oblique shock

$$\left(\frac{p_3}{p_\infty}\right)^{1/2} = 1 + \tfrac{1}{4}\,\gamma M\theta + 0{\cdot}0485\,(M\theta)^{1{\cdot}77} \qquad \ldots\ldots\ldots\ldots\ldots(2.7)$$

where, for the condition given by the suffix 3 the flow deflection angle δ is half the thickness angle θ.

In considering the lift/drag ratio, it is easier to treat the reciprocal, i.e. draf/lift ratio. From Appendix B.

$$\frac{C_D}{C_L} = \theta + \frac{1{\cdot}77(E_L + E_U)M^{(1+n)}\left[1 + 0{\cdot}35(M\theta) + 0{\cdot}048(M\theta)^{1{\cdot}77}\right]}{\bar{H}\sqrt{R_{e_{\infty L}}}\;\left[2\theta M + 1{\cdot}5\,(M\theta)^{2{\cdot}15}\right]}$$

$$+ \frac{b\,\theta}{1{\cdot}4M\theta + 1{\cdot}05(M\theta)^{2{\cdot}15}}$$

$$\text{where } b = \frac{p_\infty - p_b}{p_\infty} \qquad \ldots\ldots\ldots\ldots\ldots(2.8.)$$

This expression has a minimum with respect to thickness θ which is the optimum thickness θ' as defined in paragraph 2.1.4. and figure 2.2. Putting b = 0, i.e. assuming that base drag has only a small effect on the thickness angle for maximum lift/drag ratio (see paragraph 3) a relationship is obtained,

$$f(M\theta') = K(M\theta') \qquad \ldots\ldots(2.9.)$$

where

$$K = \frac{1{\cdot}77(E_L+E_U)\ M^{(2+n)}}{\bar{H} \cdot \sqrt{Re_{\omega l}}} \qquad \ldots\ldots(2.10.)$$

The solution to equation (2.9.) is,

$$M\theta' = 0{\cdot}688K^{0{\cdot}477} \qquad \ldots\ldots(2.11.)$$

which enables θ' to be found, given the vehicle geometry and the flight or test conditions. Substituting equation (2.11.) into equation (2.8.) and solving (graphically) gives

$$M\left(\frac{D}{L}\right)_{\theta'} = 1{\cdot}28K^{0{\cdot}466} + \frac{b}{1{\cdot}38 + 0{\cdot}68K^{0{\cdot}553}} \qquad \ldots\ldots(2.12.)$$

which is the maximum lift/drag ratio with upper surfaces streamwise.

Combining the Mach number terms to obtain the variation with M gives

$$\theta' \sim \left[M^{n-0{\cdot}6}\right]^{0{\cdot}477}$$

$$\theta' \sim M^{0{\cdot}076} \qquad \text{for } n = 0{\cdot}76 \qquad \ldots\ldots(2.13.)$$

and

$$\left(\frac{D}{L}\right)_{\theta'} \sim \left[M^{n-0{\cdot}66}\right]^{0{\cdot}466}$$

$$\left(\frac{L}{D}\right)_{\theta'} \sim M^{-0{\cdot}047} \qquad \text{for } n = 0{\cdot}76 \qquad \ldots\ldots(2.14.)$$

2.3. Numerical illustration

The theory of paragraph 2.2.2 has been illustrated by applying it to a delta wing in the atmosphere. Values have been obtained for the optimum thickness, θ' together with the corresponding lift/drag ratios and wing loadings.

The results cover heights from 75,000 to 200,000 ft. and Mach numbers from 5 to 20. A 200 ft. long vehicle has been used as was done in reference 19. The heat transfer parameter, $\bar{H}$, was taken as 0·75, a value representative of the condition half way between the adiabatic wall condition and 100% cooling ($T_W = T_\infty$). Atmospheric data were obtained from reference 73.

Figure 2.3. gives the results for the optimum thickness angle θ', versus Mach number and altitude and figure 2.4. gives the corresponding lift/drag ratios and wing loadings.

Some interesting points emerge. The optimum thickness angles are extremely small, except at very high altitudes. The wing loadings corresponding to θ' are impossibly small except at low altitudes and high Mach numbers. It is evident that the optimum (θ') vehicle is not a practical design and that wing loading is a major factor.

This being so, some calculations were performed to illustrate the performance of non-optimum vehicles (but still with upper surfaces streamwise), having practical wing loadings. Lift/drag ratios corresponding to the range of wing loadings from 20 to 90 lb/sq ft are given versus height for Mach number of 5, 10 and 15 in figures 2.5 (a)(b)&(c) respectively. The corresponding thickness angles are plotted in figures 2.6 (a)(b)& (c). The lift/drag ratios are given both for the case of zero base drag and for a base drag corresponding to a base pressure equal to half the free stream static pressure.

If a lift/drag ratio of 5 is arbitrarily taken as a minimum, then the usable area of the flight spectrum is reduced to the lower altitudes. The following table shows the position with base drag included.

Wing loading	Maximum altitude for $^{L}/D \nless 5$		
	M = 5	M = 10	M = 15
20lb/sq. ft	110,000ft	150,000ft	170,000ft
90lb/sq. ft	80,000ft	112,000ft	125,000ft

Figures 2.5 clearly show the considerable effect of base drag, especially in the area of interest, i.e. low altitudes, moderate Mach numbers and high lift/drag ratios. Base drag must rank as one of the major uncertainties in estimating lift/drag ratio.

The results also show that the inclusion of base drag produces little change in the thickness angle for maximum lift/

drag ratio, thus substantiating an assumption made in paragraph 2.2 and Appendix B.

Results for constant thickness angles of 6^o and 10^o have been extracted from the figures and are given in figure 2.7. The lift/drag ratios achieved depend mainly on the thickness and secondly on the Mach number. Altitude, and hence Reynolds number, has little effect except on wing loading. This is because the thickness angles are well away from the optimum and hence the skin friction drag is small in comparison with the pressure drag.

2.4. Discussion

Summarizing the development so far, a detailed study of a specific hypersonic cruise vehicle configuration has been carried out. Delta wings were chosen because they represent a credible cruise vehicle shape and because there exists a reasonable amount of experimental data with which the theory can be checked, in addition to the results of the present investigation.

Since, in obtaining the forces on the wing, the assumption has been made that the average pressure over a surface is equal to that obtained if the surface were part of an infinite unswept plane, the results must apply to any wing for which this is a good approximation; except that different planforms will require different constants in the skin friction term. This will include all single shock waveriders such as

Nonweiler wings and the infinite unswept wedge. Excluding interference designs, the infinite wedge would be expected to give an upper bound to the efficiencies obtainable and delta wings should be close to this, the main loss being viscous due to the average Reynolds number being less than the overall Reynolds number, and this loss being small in the region of interest for practical cruise vehicles.

The maximum lift/drag ratio is evidently achieved with a wedge of zero thickness at an incidence determined by the skin friction, (see Appendix A and figures 2.1 and 2.2). The upper surface is at a negative angle equal to the lower surface flow deflection angle which is usually small (say 1° to 2°) for practical Reynolds numbers. As thickness, and hence volume, is introduced, the maximum $^{L}/D$ is reduced continuously while the lower surface incidence is increased, and that of the upper surface becomes less negative until, again for practical Reynolds numbers, it becomes streamwise as the lower surface reaches about 5°. For greater thickness angles, the optimum condition corresponds to slightly positive values of the upper surface incidence. Taking the upper surface streamwise condition as constant in this report has introduced an optimum thickness θ' and corresponding maximum lift/drag ratio, with the $^{L}/D$ falling to zero as the thickness and incidence fall to zero. For thicknesses greater than θ', the absolute $^{L}/D_{max}$ has been slightly underestimated with the optimum incidence being slightly greater below about 5° and slightly lower above it.

From the Newtonian standpoint, negative upper surface incidence would have no effect on the lift/drag ratio, thus reducing the volume for no gain. In practice, the upper surface is capable of, but less efficient at, producing lift than the lower surface and thus the optimum thickness θ' may be regarded as a point of diminishing returns below which the gain in $^{L}/D$ is not worth the loss of volume. At θ', numerical results show, that the viscous drag is approximately equal to the pressure drag.

Simple expressions have been obtained for θ' and the corresponding $^{L}/D_{max}$, enabling their value to be obtained quickly for any particular conditions. While practical cruise vehicles would be mainly well away from these optimum conditions, this does not apply to tunnel tests or to tests of small models in the atmosphere. The relative importance and effect of several of the variables is different, depending on whether the case being considered is near or far from θ', and a knowledge of θ' is helpful in making any comparisons or extrapolations.

The curves of figures 2.3 and 2.4 show the position for a typical vehicle of 200 ft length in the atmosphere. Optimum thicknesses are entirely ruled out in this case, mainly due to insufficient wing loading and in the small area of very high Mach number and low altitude where the wing loading is adequate,

θ' is ruled out due to insufficient volume, (thicknesses of 1° to 2°).

The provision of adequate wing loadings has the effect of moving the point of operation well away from θ'. Viscous effects become considerably less important while thickness angles, which are now reasonable, become of primary importance. Thus, comparisons made at or near θ' become entirely different when transposed to the region of practical operation. This change is particularly important since many tunnel tests are performed near θ', (e.g. a 6° thick vehicle in a wind tunnel would be operating at its optimum, θ' condition at a Reynolds number of $2 \cdot 5 \times 10^{6}$ while in the atmosphere the relevant value of θ' would be $< 2^{\circ}$.)

The spectrum of practical operation is covered by figures 2.5 and 2.6. Increasing Mach number at constant wing loading and altitude reduces the thickness and hence increases $^{L}/D$. Alternatively, the effect of keeping the thickness constant is shown in figure 2.7. Increasing the Mach number still tends to increase the lift/drag ratio though not so markedly. Thus it is advantageous to have the highest Mach number possible.

The lift/drag ratio varies little with wing loading. This is due partly to the smallness of the viscous drag compared to the pressure drag and partly to the fact that the change of base drag with altitude tends to cancel the change of viscous drag. Thus the lift/drag ratio is firstly a function of wing thickness, secondly of Mach number and is almost independent of the wing loading which only determines the required altitude.

In practice, the design Mach number could well be limited by heating and the minimum thickness limited by the need for volume. Typical figures could be Mach number of 10, 5^{o} thickness and 50lb/sq. ft. wing loading giving an altitude of about 100,000 ft. and $^{L}/D$ of about 8·5 for the case of base pressure equal to half static pressure. If 10^{o} thickness were required, the figures would be 112,000 ft. and $^{L}/D$ of 5.

It is evident that altitudes greater than about 150,000 ft. are unlikely to be useable (for cruise) and even this height will require very high Mach numbers with very high heating rates. One result of this is that base drag has a comparatively large effect, being largest at the lower altitudes and Mach numbers. At present, base drag seems to be a major uncertainty.

In looking for experimental confirmation of the theoretical estimates from tests performed in low Reynolds numbers facilities, the best quantity to compare is the thickness for maximum lift/drag ratio with upper surfaces streamwise (θ'). This is because, as has been shown, θ' is relatively insensitive to the value of base drag while the actual value of $^{L}/D_{max}$ is very sensitive to it. Such a comparison is made in section 4 where the values of θ' and $(^{L}/D)_{\theta'}$ appropriate to the tunnel conditions of the present tests are also given.

Section 3. Development of the force balances and calibration of the tunnel.

3.1. Introduction

The present investigation was started using a strain gauge balance inherited from Mr. P. Church, and termed MK.1. in this thesis. This balance had certain drawbacks and was extensively modified in an attempt to improve its performance. The modified balance is termed MKII. The main problems were those of model mounting and incidence adjustment, poor accuracy of pitching moment measurement and comparatively low natural frequency.

The modifications introduced to overcome the first three problems resulted in an increase in bulk and a decrease in the natural frequency which was so low as to make electronic filtering impossible. In this situation viscous damping proved very successful in that it not only damped the vibratory signal sufficiently to obtain a reading in the running time but also absorbed a substantial proportion of the starting load.

The development of the MKII balance was largely dictated by what was possible rather than by what was desirable. Nevertheless, certain of the features used in the MKIII balance were pioneered on this one, these being the use of silicon gauges and associated method of temperature compensation and the layout of the sensing elements. The MKII balance and results obtained on it are fully described in ref. 70.

At the beginning of the present work, the Imperial College gun tunnel was fitted with a conical nozzle. While force data had been reported from tests in conical nozzles and various attempts had been made to apply corrections to the results, it was clear that the answers so obtained were far from satisfactory.

We were fortunate - the present writer particularly so - in having for trial a Mach 8 contoured nozzle designed and largely manufactured by Bristol Siddely Engines Ltd. The flow achieved, while not perfect, was good especially with respect to Mach number gradient which was virtually zero. Details of the calibration of the test flow are included in this section.

Following the tests on the first (MKII) balance it was decided to use the experience gained from its development to design a new (MKIII) balance in order to measure higher lift/drag ratios. The prime design requirement therefore was to be able to mount thinner wings. At the same time it was desirable to increase the accuracy of measurement, especially of pitching moment and to widen the range of tunnel conditions in which the balance could be used so that the Reynolds number effect on force coefficients could be determined. Ancillary design aims were greater sensitivity, higher natural frequency and lower interactions.

Since the balance was to be entirely new, the opportunity was taken to design a complete balance system incorporating means for setting incidence and roll and for calibrating the balance both in and out of the tunnel.

In the event, nearly all the design aims were achieved but some unexpected difficulties were encountered, requiring solutions that were not entirely satisfactory.

The manufacture of the balance was a very difficult task, made more difficult by being machined from EN24 steel in the hardened condition. The fact that it was successfully made, at the first attempt, does credit to the skill and enthusiasm of the workshop staff.

3.2. Tunnel calibration

3.2.1. Nozzle details

The contoured nozzle was made of resin bounded fibreglass except for a section near the throat which was made of light alloy and into which a stainless steel throat insert was screwed. The following details of its design were obtained from Bristol Siddely Engines Ltd. The method of I.M. Hall (ref. 89) was used to determine the transonic flow characteristics of the constant radius throat to a Mach number of 1·05 to 1·1, thus giving a starting line for the characteristics solution. For this, the Mach number distribution down the centre line was specified in the form of a conic fitted to the Mach number and first and second derivatives at the starting line and Mach number and zero gradient at the exit. The maximum divergence half-angle was 21.7^{o}, close to the maximum possible of 24^{o}, in order to keep the nozzle as short as possible. The resulting contour was corrected for boundary layer growth, the correction being based on Stratford and Beavers (ref. 90) assuming zero thickness at the throat with turbulent flow everywhere downstream and zero heat transfer.

3.2.2. Pitot pressure survey

A full description of the tunnel and calibration of the driver section is given by Needham in ref. 76. A special pitot rake capable of being traversed along and across the working section was built for the calibration of the flow from the contoured nozzle.

The pitot tubes were arranged 1" apart except that the upper set were displaced an extra half inch relative to the lower set. Thus, by inverting the whole rake, a vertical coverage of every half inch could be obtained. Lateral location was also at every half inch and the longitudinal fixing was infinitely variable within the area of interest.

The measured pitot pressures have been converted to values of Mach number using the Rayleigh pitot formula, assuming isentropic expansion from the stagnation conditions of ref. 76.

Readings were taken with the rake on the centre line at every inch from the exit plane to 8" aft and at every inch across the jet at a station 3" aft of the exit plane for the normal running condition of 2,000 p.s.i. driver pressure and atmospheric pressure in the barrel. With the barrel pressurized to 100 p.s.i.a., readings were obtained on the centre line, at the exit plane and at 3" and 6" aft.

3.2.3. Mach number distribution results.

The results of the longitudinal survey at normal barrel pressure are plotted in terms of Mach number in fig. 3.1.(a) and a lateral cross section at 3" aft of the exit plane in fig. 3.1.(b).

The results with the barrel pressurized are tabulated below. In this condition the pressure trace was not constant in the first wave and gave a slightly different answer in the second and subsequent waves. Typical traces are shown in figs. 3.2.

	MACH No.		
DISTANCE FROM CENTRE LINE	EXIT PLANE	3" AFT	6" AFT
0.5" UP	8.18	8.26	8.22
	8.32	8.35	8.35
1.5" UP	8.12	8.16	8.14
	8.21	8.23	8.28
2.5" UP	8.12	8.19	8.19
	8.21	8.25	8.28

DISTANCE FROM CENTRE LINE	EXIT PLANE	3" AFT	6" AFT
CENTRE LINE	7·965 8·21	8·13 8·18	8·025 8·14
1" DOWN	8·11 8·22	8·11 8·15	8·19 8·25
2" DOWN	8·17 8·3	8·25 8·28	8·17 8·26
3" DOWN	8·09 8·17	8·12 8·17	

Upper value is 1st wave and lower, second and subsequent waves.

The accuracy of the results is estimated to be about equivalent to $\pm 0{\cdot}1 M_N$. though the lines in fig. 3.1. have been drawn through the measured points (or means positions where more than one reading was taken).

Measurements were taken on the centre line and 0·5" above it and this latter point has been reflected about the centre line in order to facilitate the drawing of the curve in this region of large variations. Fig. 3.1. shows clearly the focusing effect of the axially symetric nozzle, and it is probable that the fluctuations are even more localised to the centre than drawn.

Other than on the centre, within the accuracy of the tests, the flow is sensibly steady at a Mach no. of about 8·25. This is born out by the lateral distribution shown in fig. 3.1.(b).

The results with the barrel pressurized were very similar to those for normal pressure. The shape of the pressure trace suggests that consistent results would be more difficult to obtain but the values of Mach no. were much the same and the difference between the first and subsequent waves was small (of the order of the accuracy of the results). Hemisphere drag measurements showed that the Mach no. when running pressurized was nearer 8·3 and this value has been used where appropriate.

Schlieren photographs taken of the flow in both conditions were entireley normal and showed no obvious discontinuities.

The running time in normal operation ($\frac{\text{driver pressure}}{\text{barrel pressure}}$ = 136) as taken from the traces was about 28 milliseconds.

3.2.4. Flow inclination

An incidence probe was built in order to check the inclination of the flow relative to the floor of the tunnel working section. This was of the blunted cone "pressure recovery" type (e.g. Album ref. 84) in which the differential pressure from two pitot tubes embedded in the entropy layer of a blunted cone is used as an indication of flow incidence. The probe is shown in fig. 3.3.(a) and a schlieren photograph of the flow about it in fig. 3.3.(b) The cone diameter was 0·5" , tip diameter 0·08" and included angle 30°.

The probe was experimentally developed and calibrated. To obtain satisfactory characteristics the cone had its blunting successively increased and was found to be satisfactory after the first adjustment. It was calibrated by rotating the sensing head through 180° to determine the zero error and by varying the incidence at one location (measured by 'clocking' the height from the working section floor to datum surfaces at front and rear of the probe) to determine the sensitivity to flow inclination.

Results obtained at a position 1" below the centre line and 3" from the exit plane are presented in fig. 3.4. The sensitivity near zero inclination was 14 p.s.i./degree inclination or in terms of pressure coefficient, $2\cdot3/^{\circ}$. The flow was parallel to the working section floor to within $0\cdot1^{\circ}$.

3.2.5. Repeatability

As an indication of the repeatability of the tunnel, one measurement was repeated several times during the calibration of the nozzle. A repeatability of 97% over 6 runs was achieved. Since these runs included instrumentation errors, the variation due to changes in tunnel running conditions would be expected to be less than $\pm 3\%$.

3.3. Balance design considerations

3.3.1. General

There are many factors to be considered in the design of a balance, some are applicable to all wind tunnel balances and others are unique to gun tunnel (or even more critically to shock tunnel) applications. For convenience and also in order to demonstrate the scope of the problem, they are listed below:

high natural frequency

sensitivity

small size and frontal area

accuracy

ease of calibration

low interactions

strength

incidence accuracy and range

compatibility with tunnel and models

ability to be produced in time and cost

reliability.

In general, the forces applied by the airstream to the model are reacted by a combination of inertia and support forces. Inertial forces arise both from the model and from parts of the balance (and supporting structure) while the remaining forces are reacted by the balance and constitute its output. Thus the error that the inertia forces represent must either be measured and added to the result or allowed for in some other way. The various system stiffnesses can be such that the proportion of inertia force to support force varies from all inertia, through various proportions to virtually all support. At the one extreme, forces are derived from measurement (usually but not necessarily photographic) of acceleration on free flying or very lightly supported models (ref 92)

In the central range are inertia compensated balances while at the latter end of the range are the more usual, uncompensated balances with various ways of dealing with the residual oscillations.

Only balances incorporating accelerometers are capable of giving a true instantaneous measurement of the force on a model. All the others give an average over some period of time and the problem is to make this period short enough in relation to the characteristics of the tunnel for which the balance is intended.

Each type of balance has its problems. It is very difficult to control or measure the incidence of models when they are only lightly supportd and the measurement of acceleration is also not very accurate in these circumstances. One major advantage of this type of measurement is that sting interference effects are entirely absent, though this makes the measurement of base pressure for correction purposes very much more difficult. The inertia compensated balance on the other hand, while inherently the most versatile and accurate, is complicated, expensive and difficult to calibrate. While good results have been obtained with both the above types of measurement, it was though preferable to continue development of the existing type of balance rather than change to a new type.

The main problem therefore was that of obtaining a true average reading in the available time. A recent development that promises a considerable improvement in this type of measurement is the use of field effect transistors (F.E.T.) with piezo-electric transducers, (ref. 93). The F.E.T.'s appear to eliminate many of the problems associated with the use of these highly stiff transducers as well as giving a useful amplification of the signal.

3.3.2. Design principles of the MKIII balance

Most of the requirements are conflicting and any improvement in one attribute is usually obtained only at the expense of another. In the present (MKIII) balance, four important design features gave improvements which would be shared between the conflicting requirement. These were; use of high strength steel, tension link sensing elements, silicon gauges and the layout of the sensing elements.

The high strength steel, (details of which are given in paragraph 3) enabled the sting size to be brought down to 0·25" diameter making 6^{o} thick models possible.

The use of tension links in place of the more usual cantilevers for sensing elements, can give more than five times the stiffness for the same sensitivity, even when compared to the shortest practical cantilever. This is a direct gain to the performance of a balance. The only problem, for the order of loads available, was that the links were so thin that their strength in buckling was critical. This required the use of miniature gauges (with some associated un-reliability) in order to keep the link lengths short.

The considerable increase in sensitivity available from silicon gauges (and their associated problems) have already been discussed in ref. 70. These problems are less with the normal foil and wire gauges and, though expensive, good d.c. amplification is available. However, one important consideration is the signal to noise ratio, as any noise originating before the amplifier will also be amplified. With the existing electrical environment it was felt safer (and cheaper) to rely on a high gauge output than on subsequent amplification.

In appendix B of ref. 70. it is shown that the accuracy of measurement of pitching moment is highly dependent on the distance between the point of measurement and the centre of pressure. An accurate knowledge of the position of the centre of pressure is also needed in deriving the value of the lift force. Thus it is of paramount importance that the moment sensor should be buried in the model, close to the C.P. and if this is so, the lift and drag can be measured behind the model with little loss of accuracy. (It is possible to reduce the sensitivity to C.P. position by a parallelogram linkage but at the expense of an increase in the bulk and in the difficulty of manufacture e.g. see ref. 79.)

The above comments have indicated the philosophy behind the design; paragraph 3.4. below describes the balance in detail.

3.4. Description of balance and associated equipment.

3.4.1. The balance 'plug-in' unit.

The main part of the balance containing all the active elements is shown with covers off in fig. 3.6.

The models were screwed onto thread A and located by the spigot B and taper C. Two gauges, measuring pitching moment, were cemented onto the flats D and the leads from them ran back in channels E (one each side). The gauges and wires were cemented over to give a smooth 0.25" diameter cylindrical sting.

Lift was measured by four gauges stuck, one on each surface of the two tension links F, each of which was 0·010" thick. Drag was measured by a similar arrangement on the links G.

The wiring between upper and lower lift gauges and between the gauges and the 15 way miniature McMurdo plug J, was by means of two printed circuits * H, one each side of the balance.

The whole balance unit was bolted to the incidence gear by a bolt K and locating pin L. The shield M had a replaceable portion N screwed into it, to cater for different length models.

In its original form the balance had light covers screwed onto each side but these were changed to 0·125" gauge plate and attached by taper pins in order to reduce the lift interaction on drag. Finally, since the balance proved sensitive to loads on its external structure, a separate wind shield was added.

---

* These circuit boards were made at Imperial College by the departmental photographer, Mr. O'Leary.

The main part of the balance, (parts A to L inclusive) was machined out of a single piece of EN 24W steel, heat treated to a Brinell hardness no. of 320 and giving an ultimate strength of 70 tons/sq. in.

3.4.2. Incidence adjustment.

For incidence adjustment the balance unit was bolted onto the linkage shown in fig. 3.7.(a). By sliding the top and bottom plates horizontally in the exisiting channels of the gun tunnel the unit was made to rotate about the upper pivot point which was so placed as to give the least vertical movement of the model centre of pressure. The vertical movement was about 0.25" through the incidence range of 0 to $+30^{o}$ (available range $\pm 30^{o}$).

The attachment shown dotted on fig. 3.7. which was held by two pins registering in accurately located holes, enabled the incidence to be set by means of an inclinometer to within 2'. The attachment could also be located with the horizontal bar across the tunnel in order to set the position of the model in roll. The final position of a model in roll was determined by the position of the taper on the sting. If the model position was not correct it could be adjusted by relieving the taper in the model with a special tool, or by inserting thin paper washers. The edge of the incidence attachment also served as a datum from which horizontal distances were measured.

The balance was so stiff that there was negligible change of incidence with the loads of the present tests.

3.4.3. Circuit arrangement.

A complete circuit diagram is given in figure 3.8. The gauges were miniature silicon gauges, type 2A-3A-120P supplied by Ether Ltd. These were chosen in preference to more sophisticated gauges, (smaller size, better temperature characteristics) which are obtainable from the U.S.A., because they were more readily available. Several had to be replaced.

The gauges were arranged in conventional Wheatstone bridges; full bridges for lift and drag and, because of limited space, a single active leg with dummy second leg for the pitching moment as shown in fig. 4.5. They were supplied from a common 3v stabalized voltage source (Farnell Instruments Ltd.) but with individual return leads. By keeping the supply voltage down to 3v the self heating was reduced to negligable proportions. Inserted in each return lead was a small calibration resistor the voltage across which was a measure of the current through the corresponding bridge and hence of the bridge total resistance. To avoid errors, the balancing circuits were disconnected from the bridges before the voltages across these resistors were measured.

All setting up and calibration measurements were made using a Solartron 1420 digital voltmeter. This was used for balancing the circuits, taking readings on calibration, measuring the value of the stabilized voltage, and the voltages across the calibration resistors. These latter resistors were used to compensate for the effect of temperature on the silicon gauges in the same nammer as described in ref. 70, except that all the gauges of a bridge were taken together and assumed to be at equal temperature.

Balance outputs during tunnel runs were displayed on a Tektronix 502 oscilloscope and recorded with a Land Polaroid camera.

3.4.4. Filter units.

In its original form, the balance was fitted with convential low-pass filters on each channel. These eliminated much of the noise and gave some 30% attenuation to natural frequencies of around 200 cycles/sec. When this type of filtering was increased to the point where the maximum permitted rise time was obtained - about 15 - 20 m.sec. - about 70% of the oscillating component could be removed. As a result of a suggestion by Dr. Pennelegion of the N.P.L. some parallel T or 'notch' filters were added and the low pass filters time constants reduced to keep the rise time below the permitted limit.

The parallel T filter (shown in fig. 3.9.(a) in its most usual form) is capable of being tuned to give an infinite impedance to a particular frequency given by :-

$$f = \frac{1}{2\pi R_1 C_1} \qquad \text{........3.1.}$$

for zero load.

The actual achieved performance depends on the quality and matching of the componants and on the loading conditions.

These filters work from a low impedance into a high one.

Commercial notch filters all seemed to have one side earthed and this proved to be incompatible with the balance and with the rest of the electronics. Some special filters were therefore constructed (fig. 3.9.(b)), being tuned to the known frequency of the balance. These were originally adjustable to several frequencies but this feature was dropped as it caused considerable noise pick-up.

Despite the lack of component matching, between 95% and 98% of the oscillatory component could be removed at the tunnel frequency, with a fairly rapid drop-off of performance with frequency away from the optimum.

3.4.5. Calibration equipment.

The calibration set-up for static calibration and for dynamic interaction are shown in fig. 3.7.(b). The equipment could be used in-situ in the tunnel in both cases.

Lift and moment were calibrated by direct application of weights, hung from the grooves of the calibration bar shown. For drag, the special bracket was pinned onto the incidence gear and the drag load applied via a 2:1 bell crank, supported on knife edges. This mechanical advantage enabled high loads to be achieved in the restricted space of the tunnel. The drag linkage was levelled by the pointed screw at the front. Because of the high rigidity of the balance, it was not necessary to compensate or allow for the deflection under load on calibration.

(The deflection under lift load was 5×10^{-4} ins/lb. at the tip of the balance and about 4×10^{-6} ins/lb for drag.)

Fig. 3.7.(b) shows the arrangement for calibrating the interaction of lift on drag under dynamic loading. For this, the lift and drag outputs were fed to the x and y plates of an oscilliscope with appropriate amplifications and produced a line whose slope was proportional to the interaction. With this system the interaction could be determined to 0·2%. To ensure that no interaction was being fed in by the calibration mechanism, the loading bar A was raised until the drop arm B had found its own vertical. The loading bar was then lowered onto the spherical nut at the bottom of the drop arm which had been previously set to make the loading bar horizontal. Weights were dropped by hand onto the loading platform at the front of the loading bar.

3.5. Development and calibration.

3.5.1. Initial results and modifications.

Some of the problems encountered are described below as it is felt that the information could be useful to others in assessing the possibilities and usefulness of this type of design.

The first problem encountered was one of inconsistency in the bridge balance points and the lift interaction on drag which was non-linear and varied from time to time from near zero to 14%. This was coupled to an extreme sensitivity to loads on the external structure. The trouble was traced to variations in the strength of attachment (screw tightening) of the side covers, without which the interaction was consistently -14%. It would seem that the tension links were so stiff and sensitive that the supporting structure was not sufficiently rigid in comparison and fed loads back into the drag channel. The only solution available was to replace the side covers by load carrying side plates which were held by taper pins to minimize any lost movement. These reduced the static interactions to less than 1% and consistent results were obtained. The sensitivity to external loads was also reduced, though not eliminated.

Apart from the difficulty of access to the internals of the balance, the taper pinned side covers were not entirely satisfactory as they introduced a possible source of non-linearity, hysteresis and temperature sensitivity. The latter effect could be dealt with by the existing temperature calibration procedure but the first two effects made a dynamic calibration to measure interactions a necessity.

Since the tension links also acted as flextures, a certain amount of interaction on individual gauges was expected. This was expected to be small because of the high stiffness of the balance and any remaining interaction was to be balanced out by the bridge arrangement of the gauges. Because of the fixed ends, the links deflected in an 'S' shape and hence it was possible to obtain variations of interaction on any particular gauge depending on precisely where it was positioned along the length of the link. This arrangement produced unexpected interactions but also provided a mechanism by which any desired variation of interaction could be achieved. To take advantage of this, a rig was constructed by which the output of any individual gauge could be measured. This was merely inserted in series with the output of the balance and proved useful in tracing faulty gauges and indicating which gauges to move in reducing interaction.

The principle of operation of the apparatus was simply that in any leg of a bridge the companion gauge to the one being examined was shorted out by a small resistor and the voltage charge across this resistor was then a direct indication of the resistance change of the subject gauge. The supply voltage was adjusted to give the correct current through the subject gauge.

An additional problem was that calibrations performed outside the tunnel differed from those obtained in-situ and there were some inconsistencies in the calibrations obtained in the tunnel. These variations were traced to variations in resistance of connecting cables and connectors. Consistency for in-situ calibrations was obtained by putting the temperature calibration resistors in a box in the tunnel and taking all voltage measurements from this point. Thermo-electric effects were also reduced by increasing the size of these resistors. However, external calibrations could not be directly related to in-situ calibrations and only the latter could be used for test results. The relationship between sensitivity and reading of the temperature calibration resistor was still not entirely consistent but the temperature varied little and the problem was overcome by frequent calibration.

3.5.2. Static calibration, direct.

The more comprehensive calibrations for linearity and the effect of temperature were carried out on the calibration rig with rather briefer checks in the tunnel. Figures 3.10. show results obtained on the rig, for lift, drag, and pitching moment. The calibration was linear on all channels.

Also shown on the figures in the variation of sensitivity with temperature. This variation was used with the in-situ calibrations for reducing the results. The fact that the temperature sensitivity of the drag channel was of opposite sign to that of the other two channels suggest a variation in the gauge characteristics, probably in those used for the drag measurement. During the period of the tests the lift and moment channels were consistent throughout and corrections due to temperature on the drag channel were less than 1%.

The sensitivities obtained from the in-situ calibrations and the temperature corrections used are summarized below.

CHANNEL	DATUM RESISTANCE READING	SENSITIVITY AT V=2·91	%CHANGE IN SENSITIVITY PER 1% CHANGE OF RESISTANCE
Moment	1696	0·195lb/mv	-0·6

CHANNEL	DATUM RESISTANCE READING	SENSITIVITY AT V=2·91	%CHANGE IN SENSITIVITY PER 1% CHANGE OF RESISTANCE
Lift$(L+\frac{M}{4\cdot 5})$	1725	0·274lb/mv	-2·5
Drag	1755	0·548 0·575 lb/mv	+0·8

where V is the applied voltage as measured at the balance, having dropped from 3·02 at the voltage source in passing through the cables and connectors.

Two figures are given for the drag as there was a single change of calibration about a third of the way through the tests. In the interval between the two calibrations in question, there was also an overnight change in bridge balance position and it was therefore assumed that the two changes occurred together. The total change in calibration was 5%. There were no further changes.

The method of obtaining the lift from the readings was the same as that used with the first (MKII) balance and given in appendix B of ref. 70.

3.5.3. Interaction.

Measurements of interaction under static loading were made between all channels and both in the loaded and unloaded conditions. These calibrations were carried out on the calibration stand. The interactions, which are tabulated below, were so small that it was not possible to determine linearity. There was no change as between loaded and unloaded conditions.

Effect of	on	Interaction
Lift	Drag	-0·8% at zero moment
Drag	Lift	-0·9%
Lift	Moment	Included in normal calibration curves.
Moment	Lift	Included in normal calibration curves.
Drag	Moment	zero
Moment	Drag	Included in normal calibration.

The lift interaction on drag varied with the position of application of the lift load but as the C.P. for the tests was known to be very close to the zero moment position, only this condition was taken.

As the proportion of vibration being fed through from the lift to the drag channel seemed higher than could be accounted for from the above figures, it was decided to carry out a dynamic interaction calibration. This was accomplished by the method described in paragraph 3.4.5. with the following results.

Lift on drag	-2 to 2·5%
Drag on lift	-0·9%

The dynamic interaction of the lift on drag appeared to reduce slightly through the period of the tests as indicated by the range quoted.

Typical dynamic interaction traces are shown in fig. 3.11. The vibrations evident on the drag interaction on lift trace, were due to the various components of the drag linkage.

3.5.4. Natural frequencies.

The natural frequencies of the balance plus various weights of models were obtained on the calibration stand by using an audio-frequency oscillator driving a permanent magnet loud-speaker which was placed on the top support plate. The outputs of the balance were displayed on an oscilliscope with the following results.

MODEL	WEIGHT gms.	LIFT	MOMENT	DRAG
No model	zero	350c/s	3,500c/s	2,600c/s
10° plain delta AR = 1	73·3	230c/s	345c/s	> 2,000c/s
10° caret delta "	66·6	220c/s	230c/s	"
6° plain delta "	43·8	270c/s	360c/s	"

The proximity of the moment natural frequency to that of lift for the 10° caret delta indicated a possible difficulty which the tests confirmed. There was considerable mechanical coupling resulting in extremely high oscillatory moment loads. The two frequencies were just sufficiently de-coupled by reducing the model inertia in pitch. A similar coupling occurred with the 20° cone which had been tested on the MKII balance (ref. 70.) and as it was not possible to separate the frequencies in this case it could not be tested on the MKIII balance.

3.5.5. Filter attenuation and response.

3.5.5. (Cont.)

The characteristics of the low-pass filters were checked by recording their response to a step input. Since the minimum running time available was 28msec (36msec and 44msec for the 2 test conditions) the filters were adjusted to record within 1% of the true value in less than 18msec in order to give a minimum of 10msec steady trace. The attenuation of these filters was negligible.

The addition of the notch filters (paragraph 3.4.) reduced the response and so the low-pass filters were changed in order to keep the overall response about the same. These adjustments were made between test runs and judged on the results so that the exact response time was not known but as the test conditions gave greater than minimum running times, it was felt that there was a sufficient margin. The attenuation of the notch filters was 0·2%.

3.5.6. Tare calibrations.

Recordings were taken both with wind-off and with no model on the balance. In the former case the nozzle throat was replaced by a plug while in the latter case a slender cone and wedge were separately supported in front of the balance sting. Fig. 3.12. shows the resulting traces for the test conditions.

This calibration was incorporated in the reduction of the test results by drawing a mean line through the record and measuring the correction at a given time from the start of the run. Readings were then taken at this standard point for all test runs.

The oscillation visible on the trace of fig. 3.12.

was caused by movement of the complete working section, probably relative to the dump tank. Its amplitude was reduced by a modification which eliminated the friction between the nozzle and working section but the residual oscillation still made accurate reading of the drag trace difficult.

The balance centre of rotation was virtually on the tunnel centreline where disturbances were at a maximum (see para. 3.2.2.) This arrangement was prefered as variations could arise from parts of models moving into the central region with incidence. To check whether the disturbances averaged themselves out over the models, several readings were repeated at different positions from the nozzle exit. There were no variations that could be seen above the general experimental scatter.

3.5.7. Hemisphere check.

An additional check on the drag channel under dynamic conditions was carried out by measuring the drag of the hemisphere which was used on the MKII balance, (see ref. 70.) under the same tunnel conditions. The resulting value of drag coefficient was within 2% of that previously obtained and within 2% of the theoretical value of 0·92.

3.6. Performance and accuracy.

3.6.1. Performance.

The performance of the balance is summarized below.

OVER.

Characteristic	Lift	Drag	Pitching Moment
Design Max Load	50lb	50lb	50lb ins
Reserve factor (proof)	3·5	$>$5	2
Limiting quantity	Sting yield	gauge extension	gauge extension
Calibrated range	15lb	12lb	20lb ins
Sensitivity at 3V excitation (approx. see para. 3.5.2.)	3·6mv/lb	1·8mv/lb	5mv/lb ins
Interaction - static	-0·8% drag	-0·9% lift	0
" dynamic	-0·9%drag	-2 to -2·5% lift	0
Natural frequency - no models	350 c/s	3,500 c/s	2,600 c/s
Natural frequency - design models	220 - 270 c/s	$>$2,000 c/s	230 - 360c/s
*Accuracy (see below)	$\pm$7·5%	$\pm$10·5%	$\pm$4%
Incidence range	$\pm 30^{\circ}$		
Model base	0·3"dia.min.		

3.6.2. Accuracy

Errors could arise from the various sources tabulated below. They fall into several categories, i.e. random errors, consistent errors, those that vary with the applied loads and those that do not.

---

* for max design loads. Total of maximum possible random and consistent errors.

Source of Error	Normal Force		Axial Force		Moment	
	Random	Consis-tent	Random	Consis-tent	Random	Consis-tent
Static Calibration	--	$\pm 1\%$	--	$\pm 2{\cdot}5\%$	--	$\pm 1\%$
Temperature Correction	$\pm 0{\cdot}5\%$	--	$\pm 1\%$	--	$\pm 0{\cdot}5\%$	--
Trace reading	$\pm 3\%$	--	$\pm 3\%$	--	$\pm 3\%$	--
Lag effect	--	$\pm 2\%$	--	$\pm 2\%$	--	$\pm 2\%$
Oscilloscopes	$\pm 1\%$	--	$\pm 1\%$	--	$\pm 1\%$	--
Interaction	--	--	--	$\pm 0{\cdot}2\%$ Lift	--	--
Tare loads	--	--	--	$\pm{\cdot}005$ qlb	--	--
TOTAL	$\pm 4{\cdot}5\%$	$\pm 3\%$	$\pm 5\%$	$\pm 4{\cdot}5\%$ $\pm 0{\cdot}2\%$Lift $\pm{\cdot}005$qlb	$\pm 4{\cdot}5\%$	$\pm 3\%$

The large consistent error on the axial force (drag) calibration came from the shift of calibration discussed in paragraph 3.5.2.

The maximum errors for any test condition will evidently depend on the test conditions, model and incidence and can be obtained by using the errors tabulated above. These errors have been calculated for five typical cases and are given below.

Case 1. 6^{o} plain delta AR=1 $R_e=3{\cdot}5\times10^{6}$ at $(\frac{L}{D})$ max

2. 6^{o} " " AR=1 $R_e=3{\cdot}5\times10^{6}$ at 12^{o} incidence

3. 10^{o} plain delta AR=1 $R_e = 0{\cdot}9 \times 10^6$ at $(\frac{L}{D})$ max

4. Hemisphere at $R_e = 3{\cdot}5 \times 10^6$

5. At balance max, design loads.

Max. possible errors for	Case 1	Case 2	Case 3	Case 4	Case 5
Lift, random	±4·5%	±4·5%	±4·5%	--	±4·5%
" consistent	±3%	±3%	±3%	--	±3%
Drag, random	±5%	±4·5%	±5%	±5%	±5%
" consistent	±17%	±10%	±14%	±4·5%	±5·5%
C.P. Position, random	±0·4%	±0·4%	±0·4%	--	±2·5%
" " " consistent	±0·3%	±0·3%	±0·3%	--	±1·5%
Lift/drag ratio, random	±9·5%	±9%	±9·5%	--	±9·5%
" " " consistent	±20%	±13%	±17%	--	±8·5%

The probable error of results, arising from random errors depends on the number of data points from which an average is taken. The above figures represent maximum errors and are not too likely even for a single point.

3.7. Discussion.

In general, the design concepts outlined in the introduction were vindicated by the results. The balance gave good repeatability and hence would also have given good accuracy if the difficulties of calibration had not arisen.

The uncertainties of calibration arose from the need to have taper pinned, load carrying members, which in turn were made necessary by high interactions and high sensitivity of the supporting structure to aerodynamic loading. The root of the trouble was that the supporting structure had insufficient margin of stiffness over the sensing elements and indeed it would be difficult to achieve the required stiffness because of the high stiffness of the tension links. Some improvement could be affected by redesign of the supporting structure e.g. by making the balance fill the space up to the incidence gear arms and by reducing the overall length of the sting beam in the balance.

However, the drag sensor was both unnecessarily stiff and unnecessarily strong, due to the impracticability of producing thinner tension links, and hence in this application a considerable improvement could probably be achieved by reverting to a cantilever for this channel.

With the exception of the above problem, the balance functioned satisfactorily. In assessing the possible errors of paragraph 3.6.2. it should be noted that in the worst case, the measured drag was 0·25% of the design maximum load. Thin, high lift/drag ratio wings, considerably increase the problems of gun tunnel balances. The high design strength was necessary because of starting and vibrating loads, the wide range of possible conditions and models and handling considerations.

Section 4. Experimental results and analysis.

4.1. Model and test conditions.

4.1.1. Model design.

The six delta wing models tested are listed below and shown in figs. 4.1.(a)(b) and (c) together with their leading particulars. All models had vee roofs and the thickness angles quoted refer to angles in the vertical plane parallel to the centre-line chord. All were 5" long with sharp leading edges of 0·003" to 0·007" diameter.

Model	Cross sectional shape	Thickness angle	AR	Sweep
1	Flat bottom	10°	1	76°
2	Caret	10°	1	76°
3	Flat bottom	6°	1	76°
4	Flat bottom	6°	$^3/_2$	$69{\cdot}5^\circ$
5	Caret	6°	$^3/_2$	$69{\cdot}5^\circ$
6	Twisted	6° Nominal	$^3/_2$	$69{\cdot}5^\circ$

The angle between the plane of the leading edge and the lower ridge line of both caret wings was 6°. For inviscid flow at the test Mach number of 8·3, the shock would lie in the leading edge plane at lower ridge line incidences of 4° and 16° and be within $0{\cdot}7^\circ$ of this plane between the above angles (e.g. ref. 53.) Thus essentially two-dimensional flow would be expected at close to these incidences, with probably only small departures in the intervening range. Large departures from this state would probably indicate significant viscous effects.

The twisted wing was designed to have the same volume as the 6^{o} wings of equal aspect ratio and to have a linear reduction of lower surface incidence from centre-line to tip such that the centre-line incidence was twice that at the tip. The object of the design, apart from merely testing the effect of twist, was to try to obtain some of the benefits of interference designs by utilizing the effect of the boundary layer in spreading pressures laterally, as has been noted in the case of delta wings with underslung half cones where the leading edges were outside the conical shock from the half cone e.g. ref. 32. In these cases, pressures at the leading edges were obtained that were much higher than those to be expected in inviscid flow and this difference was attributed to the presence of the boundary layer and a resulting spreading of the shock induced pressures, outwards to the tips. A similar phenomenon occurring on the twisted wing would produce a high pressure towards the tips than that appropriate to the local incidence and hence a higher lift for a given lift/drag ratio. Appendix C gives the derivation of the expressions by which the ordinates of the twisted wing were obtained.

The MKIII balance and associated models were designed to achieve the thinnest wings possible in order to provide a direct comparison with the theory of section 2. For this purpose the thickness had to be that for maximum lift/drag ratio with upper surfaces streamwise for a Reynolds number within the available range, i.e. a thickness of between $5{\cdot}5^{o}$ and $7{\cdot}5^{o}$.

4.1.2. Tunnel conditions.

The calibration of the tunnel is fully described in paragraph 3.2. Fig. 4.2. shows the available tunnel unit Reynolds numbers against driver conditions extracted from ref. 76 with Mach 8·3 nozzle conditions added and the conditions of the present tests marked. The following conditions were obtained for the 5" chord models used.

Driver pressure	Barrel pressure	Mach No.	Reynolds No.	q p.s.i.	T_T ^{o}K	T_O ^{o}K	Balance
1,000 p.s.i.	14·7 p.s.i.a.	8·3	$0{\cdot}9\times10^{6}$	3·05	1030	70	MKIII
1,000 p.s.i.	40 p.s.i.a.	8·3	$1{\cdot}5\times10^{6}$	3·05	740	50	MKII
2,000 p.s.i.	95 p.s.i.a.	8·3	$3{\cdot}5\times10^{6}$	6·1	700	47	MKIII

4.1.3. Tests made.

Model and test conditions were as follows.

Model	Incidence	M_N	R_e	Balance
Wings 1-6	$0\text{-}12^{0}$	8·3	$0{\cdot}9\times10^{6}$ $3{\cdot}5\times10^{6}$	MKIII
Wings 1 & 2	$0\text{-}11^{o}$	8·3 ,	$1{\cdot}48\times10^{6}$	MKII
20^{o}half angle cone	$0\text{-}30^{0}$	8·3	$1{\cdot}48\times10^{6}$	MKII
Hemisphere	0^{o}	8·3	$0{\cdot}9\times10^{6}$ $1{\cdot}48\times10^{6}$ $3{\cdot}5\times10^{6}$	MKII and MKIII

(For wing details refer to table of model geometry Page 81 and Fig. 4.1.)

In each case the quoted incidence is that of the line joining the tip to the mid-point of the trailing edge in the plane of the centre-line chord except for the twisted wing where a line 3^{o} from the upper ridge line was used as datum.⊛

Measurements were made of lift, drag, and pitching moment (axial force, normal force and pitching moment in the case of the MKIII balance). In addition Schlieren photographs of the flow in side and plan views were obtained for the two 10^{o} models and some 6^{o} models.

4.2. Comparative theory.

Details of the theoretical estimates used for comparison with the results obtained on the MKII balance are contained together with the results in ref. 70. For the results obtained on the MKIII balance, the theoretical estimates shown on figures 4.3. to 4.10 were obtained using the methods outlined in section 2 but applied individually to each plane surface and including a boundary layer displacement correction obtained by the methods of ref. 72. The correction was applied by calculating the displacement thickness δ_1^* at the trailing edge of the root chord and assuming a uniform angular displacement over the surface of $\frac{\delta^*}{l}$. The value of n in the expression $\frac{\mu}{\mu^*} \sim \left(\frac{T}{T^*}\right)^n$ taken as appropriate to the tunnel conditions was n = 0·84.

Newtonian theory was shown to be very inaccurate under the conditions of the present tests (ref. 70.) and has therefore

---

⊛ This datum was chosen so that upper surface conditions would be identical between models at the same incidence. Thus differences would be due to the lower surfaces alone.

not been considered again.

Convenient and significant parameters for comparing the theory of section 2 with the experimental results are the thickness angle required for maximum lift/drag ratio to occur with upper surfaces streamwise and the associated maximum lift/drag ratio. Applying the tunnel conditions to the appropriate equations, i.e.

$$M\theta' = 0{\cdot}688K^{0{\cdot}477} \qquad \ldots\ldots\ldots(4.1.)$$

and $$M\left(\frac{D}{L}\right)_{\theta'} = 1{\cdot}28K^{0{\cdot}466} \text{ for zero base drag} \qquad \ldots\ldots\ldots(4.2.)$$

where $$K = \frac{1{\cdot}77(E_1+E_u)M^{(2+n)}}{\bar{H}\ R_{e_{c_L}}^{0{\cdot}5}} \qquad \ldots\ldots\ldots(4.3.)$$

gives,

Reynolds No.	θ'	$\left(\frac{L}{D}\right)_{\theta'}$
$0{\cdot}9 \times 10^6$	$7{\cdot}45^\circ$ $(6{\cdot}4^\circ)$	$4{\cdot}16$ $(4{\cdot}85)$
$1{\cdot}50 \times 10^6$	$6{\cdot}6^\circ$ $(5{\cdot}7^\circ)$	$4{\cdot}66$ $(5{\cdot}42)$
$2{\cdot}65 \times 10^6$	$6{\cdot}0^\circ$ $(5{\cdot}1^\circ)$	$5{\cdot}1$ $(5{\cdot}95)$
$3{\cdot}5 \times 10^6$	$5{\cdot}4^\circ$ $(4{\cdot}7^\circ)$	$5{\cdot}71$ $(6{\cdot}65)$

where $n = 0{\cdot}84$ for the tunnel conditions and the figures in brackets give the corresponding values if n were taken as 0.76, the usual value in the atmosphere.

It can be seen that for the 6° wings a maximum $^L/D$ of $5{\cdot}1$ should be achieved when the upper surfaces are streamwise at a Reynolds number of $2{\cdot}65 \times 10^6$. Keeping the upper surfaces streamwise and increasing the Reynolds number will raise the lift/drag ratio. The condition for (^{L}/D)max however will no longer be with upper surfaces streamwise.

4.3. Results obtained with the MKIII balance.

(Those from the MKII balance are contained in ref. 70 a copy of which is included with the thesis.)

4.3.1. Magnitude of significant variations.

For differences in the results to be significant, it is necessary for them to be greater than the differences to be expected from experimental sources and other unknowns. The magnitude of the unknown errors vary according to the particular quantities being compared. Thus, for example, in comparing the experimental results of different models with each other, only the random part of the balance error is important while in a comparison between the experimental results and the theoretical predictions consistent errors are involved.

It is possible to divide the incidence range into three parts in each of which the relationship of pressure to viscous forces is different and from which, in consequence, different deductions can be made. These are; near zero incidence, at maximum lift/drag ratio and at the highest incidences tested. The minimum significant variation for each type of comparison and each incidence range is:-

OVER

Parameter	Comparisons between models and incidences			Absolute comparison with theory and data from other balances.		
	$\alpha_o=0^o$	$(^L/D)max$	$\alpha_o=12^o$	$\alpha_o=0^o$	$(^L/D)max$	$\alpha_o=12^o$
Axial force	16%	15%	9%	29%	27%	25%
C_{D_F} + base drag	24%	24%	22%	44%	40%	30%
C_D	16%	12%	8%	29%	21%	10%
C_L	9%	9%	9%	3%	3%	9%
$^L/D$	25%	21%	17%	32%	24%	19%

In the above table the consistent errors includes a contribution for base drag equal to half the free stream static pressure (14% of zero lift/drag) and a further contribution for balance induced surface separation which occurred at high incidence (6% Lift at $\alpha_o=12^o$) but no contribution from random errors since the figures refer to the mean line in every case. The figures for random error include twice the balance error and an allowance for possible variations of base drag up to a quarter of the free stream static pressure.

In the absence of sting effects, the expected variation of base pressure with Reynolds number is given, for example, by Hana, Ref. 85. Base pressure reduces with increasing Reynolds number as transition moves upstream from the far wake to the body. The evidence of Hana (ref. 85.), King (ref. 78.) and McLellen et al. (ref. 80.) would suggest a value of $\frac{p_b}{p_\infty}$ of 0.5 to 0.8 for fully laminar flow reducing to 0.2 to 0.3 for the fully turbulent case.

The schlieren photographs presented as figures 4.5. however, clearly show that the presence of the sting and balance has severely modified the base flow and caused upper surface separation which is just visible at $\alpha_o = 5^o$ for the 6^o wings, and becomes progressively more extensive with increasing incidence. In these circumstances the base pressure would be expected to be higher than that for a free wake and probably close to the free stream static. Thus the allowance for variations of base pressure incorporated in the table of significant magnitudes should be entirely adequate.

The effect of the observed upper surface separation has been estimated on two assumptions; that the separated area lay parallel to the leading edges and that the leading edge of the separated area was at right angles to the centreline. Both lift and drag were considered and the worst result incorporated in the table. Only the high incidence case was affected as the separation occurred only at incidences higher than those for maximum lift/drag ratio.

4.3.2. Axial force, figs. 4.3. and 4.4.

Referring to the figures, the difference in theoretical axial force as between plain wings and caret wings is due to a combination of higher pressure drag from the greater pressure recovery of the caret wing and its greater skin friction drag resulting from greater wetted area. There is also a compensating contribution due to a smaller pressure difference $p-p_{\infty}$ on the roof surfaces resulting from their greater angling relative to the flow.

The experimental results show a pattern of variation as between different models which is significantly different to the theoretical pattern. The differences are more noticeable at the lower Reynolds number of $0{\cdot}9 \times 10^6$ but many of the differences are also present at $R_e = 3{\cdot}5 \times 10^6$. Near zero incidence, at $R_e = 0{\cdot}9 \times 10^6$ the twisted wing has a higher drag than the plain wings and so, to some extent has the caret wing, but these variations are no longer significant at the incidence for maximum lift/drag ratio. The fact that the discrepancy occurs at low Reynolds numbers and incidence suggests a boundary layer effect, on the concave lower surfaces.

At both Reynolds numbers there is a significant difference of axial force between the results for the two 6° plain wings of different aspect ratio at intermediate and high incidences. At the higher incidences, the axial force contains a substantial contribution from the lower surface pressure and a smaller contribution from the upper surface suction. In order to trace the source of the observed differences in axial force, these contributions have been subtracted from the observed values of axial force, using the measured values of normal force together with a theoretical estimate of the relative contributions from upper and lower surfaces to deduce the average pressures. The resulting values of $C_{D_F}^{*}$ + base drag are shown in figs 4.4.

Comparing the results for the two 6^{o} plain wings and recalling that differences greater than 24% are significant, it can be seen that the higher aspect ratio wing has the higher drag in all conditions except at low incidence and high Reynolds number. Low aspect ratio appears to be beneficial, especially at low Reynolds numbers. The amount by which the experimental value of C_{D_F} + base drag exceeds the theoretical for the AR=$^3/2$ wing at R_e=3.5 x 10^6 and α_o=12^o is also significant (> 100%) and this could be due to the onset of transition. If this is the case, the figures suggest that transtition is delayed by increased sweep, at least under the test conditions.

Comparing plain and caret wings (figs. 4.4.(d) and (e)) there is little to choose between the two for the higher aspect ratio, 6^o thick wings except for the near zero incidence effect previously noted. In the case of the lower aspect ratio, 10^o thick wings figs.4.4.(a) and (b), the caret wings show a marked increase in C_{D_F} plus base drag over both the plain wing results and the theoretical estimates at the highest incidences, most probably due to viscous effects in the streamwise corner of the under surface (ref. 48.) which was. of course, more accute

---

* These values are strictly the axial components of skin friction and base drag but $\Delta C_D = \Delta C_A \cos\alpha$ and $\cos\alpha \simeq 1$ for the range of α of these tests.

on the AR = 1 wing than on the AR=$^3/2$ wing.

4.3.3. Lift. Figs 4.6. and 4.7.

Referring to the figures, the theoretical differences in C_L between caret and plain wings are very small as they arise only from differences in upper surface geometry. At low incidences, in all cases, the experimental lift coefficients for the plain wings lie close to the 2-D values while, in contrast, the caret wing results are above. This is another indication of the viscous effects on the caret wings at low incidence noted in the axial force results and this is further substantiated by the fact that the effect in question is greater at the lower Reynolds number.

With increasing incidence the caret wing results become equal to the 2-D values while the plain wings fall away, partly as would be expected from the numerical calculations of Babaev already discussed (section 2), partly due to the upper surface separation mentioned in paragraph 4.3.1., and partly due to leading edge shock detachment which would occur at about 6·8^o pressure surface incidence for wings of AR=1 and at about 14·7^o for wings of AR=$^3/2$.

The values of lift coefficient obtained at zero incidence reflect the different geometries of the models with caret wings giving more lift than plain wings due both to the lower losses on the lower surfaces as a result of more 2-D flow (and viscous effects previously mentioned) and to lower losses from the upper surfaces as a result of the greater angling of these surfaces. The above effects are accentuated on thicker wings, resulting in greater zero incidence lift on 10^{o} wings than on 6^{o} wings.

4.3.4. Drag

The drag coefficients are geometric resolutions of the axial and normal forces and are presented in figures 4.8.

4.3.5. Centre of pressure position fig. 4.9.

The MKIII balance was extremely sensitive to pitching moment (paragraph 3.6.1.) and much of the scatter on fig. 4.9. may be due to small variations in tunnel conditions. In a number of cases the pitching moment (and, by comparison with the lift trace, therefore the centre of pressure also) could be seen to vary gradually through a run. The C.P. positions at zero incidence were nearly indeterminate and these points have been disregarded.

There appears to be a tendency for the C.P. to move initially forward with increasing incidence and then to move slightly aft with a total movement of about 1% root chord. This pattern is followed to some extent by all the models.

The moment about the model moment datum is made up of a contribution from the normal force and a contribution from the axial force, for all the models except the caret wings, the axial force moment would be negligible, but the anhedral of the caret wings would have produced a nose down drag moment and hence these wings have a C.P. position slightly aft of that which can be attributed to the normal force alone. The 6° wings have C.P. positions forward of those for the 10° wings due, at least in part, to the trailing edge planes being perpendicular to the centre line for the 6° wings and perpendicular to the upper surfaces for the 10° wings.

As would be expected, the twisted wing gave C.P. positions further forward (2%) than any other wings as a result of having a larger proportion of its lift in the central area of the wing.

4.3.6. Lift/drag ratio Figs. 4.10.

The figures for minimum significant differences in results for the different models, given in paragraph 4.3.1., for $^{L}/D$ include twice the random errors for both lift and drag. Within the quoted margins, only the differences at zero incidence are significant and these reflect the differences in the lift results. However, the likelihood that all the worst errors will combine is small and this is substantiated by the general consistency of the experimental points.

At maximum lift/drag ratio, the differences primarily reflect the significant variations in 'C_{D_F} plus base drag' discussed in paragraph 4.3.2. This is also true of the results at high incidence, largely because in terms of pressure forces, the lift/drag ratio is almost entirely a function of the incidence alone for the models under consideration and hence at a given incidence only viscous forces and possibly base drag differ significantly.

The difference between the experimental points and the theoretical estimates is less than that which can be expected from the various sources of possible error. This also applies to the difference between the results obtained on the two balances where the errors appear to have been of opposite sign.

A good curve of $^L/D$ versus incidence can be obtained by using smoothed curves of lift and drag, both of which have only gentle variations with incidence. Such curves are shown in figures 4.1.(a) and (b). Being derived from smoothed curves, their random error would be expected to be better than the figures given in paragraph 4.3.1. and this should be especially so for the angle for maximum lift/drag ratio since this quantity would, in addition, be largely unaffected by consistent errors. Thus the angle for maximum lift/drag ratio so obtained is a good parameter with which to compare the theory of section 2.

The relevant estimates, given in paragraph 4.2. show that for a thickness of 6^o, the maximum lift/drag ratio should occur with the upper surfaces streamwise for a Reynolds number of $2{\cdot}65 \times 10^6$. It follows from the arguements of section 2 that at lower Reynolds numbers the $(^L/D)_{max}$ will occur at higher incidences i.e. with the upper surfaces developing suction. Higher Reynolds numbers will result in $(^L/D)_{max}$ occurring with the upper surfaces developing pressure.

This pattern is closely followed by the experimental results of figures 4.11 which have been plotted against top surface ridge line incidence to facilitate the comparison. At the test Reynold number of $3 \cdot 5 \times 10^6$ which is close to the required value of $2 \cdot 65 \times 10^6$, $(^L/D)_{max}$ occurred on the plain wings with the upper surfaces developing a slight amount of pressure while for $R_e = 0 \cdot 9 \times 10^6$ $(^L/D)_{max}$ occurred with suction on the upper surfaces. These characteristics are in good agreement with the estimates presented above.

Section 5. Discussion and conclusions.

5.1. The experimental results.

5.1.1. Force data

The measured drags include two important unknown factors; the position of transition and the value of the base drag. Base pressures were not measured, largely because of the experimental difficulties involved in measuring very low pressures in very short times in very small spaces. For the size of models involved, determining the position of transition, if it occurred, would also have been difficult. There was no sign of transition on the schlieren photographs (e.g. see fig. 4.5.(a) and ref. 70).

Base pressures were evidently affected by the presence of the balance and estimates of pressures to be expected in isolation will have little relevance. The allowance of $\pm 0{\cdot}5p_{\infty}$ for absolute comparisons and $\pm 0{\cdot}25p_{\infty}$ for relative comparisons incorporated in the table of minimum significant quantities given in paragraph 4.3.1. should be entirely adequate and the base pressure would be expected to be close to free stream static in the separated condition, especially since separation did not occur until the upper surfaces were developing suction.

That being so, there is evidence of a rise of skin friction drag with incidence in the case of the 6^{o} high aspect ratio plain wing, almost certainly due to the onset of transition, and evidence that this rise was absent or delayed for the lower aspect ratio wing. It would appear that increased sweep delayed the onset of transition.

This apparently beneficial effect of sweep on transition is in the opposite sense to the normally accepted effect of sweep as given for example by Deem and Murphy (ref. 91.). Examination of their results shows that transition started slightly earlier with increasing sweep but also that the rate of development of transition was no quicker and sometimes slower than the corresponding result for an unswept plate. Thus earlier transition need not necessarily result in higher total skin friction and the present results do not necessarily contradict the existing experimental evidence.*

Some recent results presented by Weinstein and Neal (ref. 88.) tend to confirm the results of the present tests. They compare the measured skin friction drags on three diamond-cross-section wings at zero incidence with the estimated laminar values and show the onset of transition with increasing Reynolds number. Their results show the wings of higher aspect ratio also to have higher transition Reynolds numbers.

Using the assumptions of section 2, the local Reynolds number on a slender wing is given by:-

$$\frac{R_e}{R_{e\infty}} = \left(\frac{p_\infty}{p}\right)^n \left(\frac{\frac{p_\infty}{p} + 6}{6\frac{p_\infty}{p} + 1}\right)^{1+n} \qquad \ldots\ldots.5.1.$$

---

* An additional difference is that the result of ref. 91. were obtained on a yawed flat plate and the effect of sweep on this configuration is not necessarily the same as on 3 dimensional bodies.

giving, for the conditions of the present tests,

δ	=	0	10°	20°
$\frac{R_e}{R_{e_\infty}}$	=	1·0	1·7	1·5
M	=	8·3	5·8	3·9

Increases of skin friction with incidence would be expected partly due to earlier transition with increasing local Reynolds number and decreasing local Mach number and partly due to the decreasing length of the transition region with decreasing Mach number.

If the local Reynolds number at which a significant rise in skin friction drag occurred is taken as an indication of transition then an estimate of transition Reynolds number (R_{e_t}) can be obtained from the results for the two plain 6° wings to give $R_{e_t} \simeq 1{\cdot}5 \times 10^6$ for the AR = $^3/2$ wing and $R_{e_t} \simeq 3{\cdot}5 \times 10^6$ for the AR = 1 wing. These values compare with a value of about 2×10^6 for the start of transition to about 6×10^6 for M = 8·3 reducing to 4×10^6 for M = 6·5 for the end of transition, obtained by Richards (ref. 86.) on an unswept flat plate in the same tunnel

The lift coefficient results for the AR = $^3/2$ plain wing clearly demonstrate the very small loss of lift compared to the 2-Dvalue, predicted by Babaev (ref. 63.). With allowance for the loss of lift from upper surface separation, the difference between the theoretical estimates and experimental results is less than the possible consistant experimental error of 3%.

The AR = 1, 6^{o} plain wing at 12^{o} incidence shows a lift coefficient which has only 7% less lift relative to the 2-D value than the AR = $^{3}/2$ wing despite leading edge shock detachment which would start at an incidence of about 4^{o} for the AR = 1 wing. This shows the relatively small loss of lift due to shock detachment also found in pressure surveys such as those by Squire (ref. 20.) and Peckham (ref. 42.).

The agreement with theory in general has been good and within the expected order of accuracy of the experimental results. The departures from theory can all be explained in terms of known phenomena, i.e. boundary layer transition and viscous effects in the streamwise corner on the lower surface of the caret wings, (ref .48.)

The comparison with other experimental data in the literature is reasonable. The only direct comparison is with the results of Penland (ref. 30.) for the case of the 10^{o} plain wing of AR = 1. The comparable figures for maximum lift/drag ratio are - Penland's results first - 3·6 and 4·1 for $R_e = 0{\cdot}9 \times 10^{6}$ and 4·3 and 4·5 for $R_e = 3{\cdot}5 \times 10^{6}$. Penlands results are stated as having been corrected to free stream static pressure on the base. The differences in $(^{L}/D)_{max}$ are within the possible margin of error, but taken together with comparisons with results on similar, but not identical, wings such as Penlands 5^{o} wings and the 11^{o} wings of Blackstock and Ladson (ref. 31.) the present results would appear a little high. Since the above mentioned results were obtained in continuous facilities with model surface temperatures nearer to the equilibrium values than are obtained in a gun tunnel it is probable that transition occurred at correspondingly lower values of Reynolds number.*

5.1.2. Effect of variations of shape.

The overriding impression obtained from the results is that there is very little to choose between the three cross-sectional shapes and that each had advantages and disadvantages which tended to cancel. As would be expected, the caret wings, with near two-dimensional flow over the lower surfaces, gave results which were generally closest to the theoretical estimates. There was some evidence of viscous effects at low incidence and at the lower Reynolds number and, on average, the higher skin friction drag of the larger wetted area could be noticed.

The plain wings gave lift forces the expected few percent below the two-dimensional values; the effect of shock detachment was small. It has been pointed out that the loss of lift at high incidence has little effect on the lift/drag ratio at a given incidence. For constant C_L however, a wing developing less lift at a given incidence would have to be operated at a higher incidence and hence would achieve a lower

---

* These remarks also apply to the results recently obtained by Weinstein and Neal (ref. 88.) on a 6^o plain wing which was tested at a Reynolds number of $1{\cdot}4 \times 10^6$.

$^L/D$ than a wing developing 2-D pressures. The lower aspect ratio wing showed distinct advantages in skin friction over the higher aspect ratio wing, though this effect is probably a result of the particular conditions of these tests. At very least, the lower aspect ratio showed no disadvantages and hence, for the highest value of the volume parameter $\underline{\bar{V}}$, it is desirable to go to the slenderest shape found possible from other considerations.

Comparisons with the twisted wing are more difficult as there is no satisfactory inviscid theory with which to compare the results. Surprisingly, the results for the twisted wing followed those for the caret wing to a very large extent and there does not appear to be any loss due to the cross sectional shape. The close identity of behavior of two such dissimilar shaped wings as a caret and a twisted wing, supports the other evidence that such changes have comparatively little effect.

One aspect, which only arises incidentally in the present investigation, is that of upper surface shape. The separation that occurred as a result of the presence of the comparatively slender balance indicates the extreme sensitivity of suction surfaces to outside influences. However, the proportion of lift developed by the upper surfaces is comparatively small (e.g. about 8% at 12° incidence for the 6° wing). From the theoretical point of view, in conditions where the upper surfaces are producing pressure, caret wings and especially thick caret wings of low aspect ratio, show an advantage because of the angling of the upper surfaces relative to the flow. It is evident that it will be possible to influence the lift/drag ratio by varying the contours of the upper surface, but in general gains are only achieved at the expense of volume.

As would be expected, the thinner wings gave higher lift/drag ratios, thickness being the most important geometric parameter in determining lift/drag ratio. The question of optimum thickness and the interplay between thickness, Reynolds number, lift/drag ratio and the incidence for maximum lift/drag ratio have been fully explored and illustrated in section 2. Because of the involved nature of these relationships and the comparatively few test configurations, meaningfull conclusions can only be arrived at by comparing the results with the theoretical predictions of that section. The comparison given in paragraph 4.2. shows that in general, the relationships of section 2 regarding the effect of thickness and Reynolds number are clearly substantiated by the results.

Tunnel results taken at the comparatively low Reynolds numbers of these tests must be taken together with theoretical considerations if they are to have any meaning in relation to full scale cruise vehicles. This applies equally to comparisons between different shapes as it does to the absolute values obtained.

5.1.3. Significance for cruise vehicles

Most of the variations discussed so far have arisen from viscous effects and as such are peculiar to the conditions and especially the Reynolds numbers of the tests. Even quite small practical vehicles in the atmosphere will be operating at Reynolds numbers at least an order of magnitude larger and even though large areas of laminar flow could still exist, the very peculiar variations of the present tests are unlikely to be directly applicable. The significance of the results must lie rather in substantiating the theory, where this is possible, and in indicating caution in the use of results obtained under similar tunnel conditions.

For cruise vehicles of optimum thickness θ' (see section 2.) viscous effects will, by definition, be important. However, even here the characteristics are likely to be different at full scale Reynolds numbers and it has been shown in section 2 that practical vehicles will in any case be well away from this optimum condition and into regions where the viscous drag is only a small proportion of the total drag.

Thus 'inviscid' conclusions are likely to have most significance.

Though there might well be other reasons for prefering caret wings (e.g. engine intakes, external burning, stability) they do not, in general, have any advantages in maximum lift/drag ratio except where leading edge shock detachment on upper surface pressure is important.

A most interesting result was that for the twisted wing. This showed no losses relative to the other wings and even occasional gains. On the other hand it gave centre of pressure positions forward of the other wings and it has a more useful cross sectional area distribution. Because the generation of sufficient lift is a problem in the atmosphere a significant comparison between the wings, with respect to cruise vehicles, is the comparison of lift/drag ratio at given lift. In figures 5.1. the achieved lift/drag ratios are shown plotted against lift coefficient for the Reynolds numbers of $0{\cdot}9 \times 10^6$ and $3{\cdot}5 \times 10^6$ respectively. For the conditions of these tests the caret and twisted wings show a slight advantage in that they achieve their maximum $^L/D$ at a higher lift coefficient. At lift coefficients of 0·12 and greater there was little to choose between any of the wings, indicating the overriding importance of lower surface pressure over all other effects.

This is, in fact, the way in which the greater lifting efficiency of the caret wing shows itself (providing the gain is not lost in viscous drag on the greater wetted area, i.e., at reasonably high Reynolds numbers and lift coefficients). Although the lift/drag ratio is a similar proportion of cot. α for plain and caret wings, the caret wing produces more lift at the same incidence and hence at about the same lift/drag ratio. Hence in appropriate conditions, the same lift coefficient occurs at a slightly lower incidence, resulting in a higher lift/drag ratio for the same lift.

Although the maximum lift/drag ratios are little different, the above advantage could be significant when base drag is considered since a caret wing would produce the same lift as a plain wing of equal thickness but at a higher altitude and hence at a lower value of base drag.

Many of the estimates of range performance (refs.1, 2, 3, 6.) have used values of $^L/D$ of 4 to 6. The experimental results, taken together with the theoretical considerations of section 2, give additional evidence that these values should be easily attainable, perhaps with a little extra in hand to allow for trim, stability and control requirements.

5.2. Optimum cruise vehicle operating conditions.

The analysis of optimum conditions of section 2 was carried out for the particular case of upper surfaces streamwise but the pattern would be the same for any fixed value of upper surface incidence. However, it was shown that for the values of thickness and wing loading likely to be useful for practical purposes in the atmosphere, the maximum lift/drag ratios occur at or near the condition of upper surface streamwise.

An optimum thickness, θ', was derived at which maximum lift/drag ratio was achieved, again with upper surfaces maintained streamwise. The value of θ' varied with Mach number and Reynolds number and when operating at the appropriate conditions, the viscous drag would be a significant proportion (just under half) of the total drag. However, these optimum conditions proved to be unrealistic when translated to a practical 200 ft. long vehicle in the atmosphere. Vehicles of thickness θ' were too thin at low altitudes and had much too low wing loadings at high altitudes. The corollary to this was that vehicles with sufficient thickness and wing loading were substantially thicker than θ' and hence had viscous drags (laminar) that were only a small proportion of the total drag throughout the atmosphere.

These facts lead to the situation where the lift/drag ratio is virtually determined by the thickness while the required wing loading can be achieved by selecting the appropriate altitude. The resultant change of viscous drag due to a change of altitude has only a secondary effect on the lift/drag ratio for the reasons given above. It also follows, incidentally, that advantages of performance derived from lower viscous drag and obtained in tunnel tests would show little benefit in full scale, even if the advantages were maintained at full scale Reynolds numbers. Thus the effect of transition on $^L/D$ will also be small.

If base drag is important, i.e. if no provision is made to eliminate it (as in some proposed vehicles with external or integrated propulsion), then the effect of changing altitude can in fact be reversed since the base drag is reduced by an increase in altitude. Increasing Mach number enables the same wing loading to be achieved at a higher altitude and is therefore beneficial.

The above conclusions represent a considerable simplification of the situation and they were only possible because, for the 200 ft vehicle considered, it was possible to show that viscous effects would be small in all conditions. As the vehicle under consideration becomes smaller, and hence θ' increases, so the pattern will become more complicated in various parts of the flight spectrum.

Several authors (refs. 16, 17, 18 & 19) have presented performance estimates, and estimates of boundary layer drag, thickness and surface temperatures. In most cases, more recent work has improved upon and superseded the earlier estimates, especially as regards the inclusion of realistic values of thickness and wing loadings in the atmosphere. (In some cases, while the effect of various wing loadings were considered, these were coupled to conditions in which the required loading could not have been generated.)

A most recent independent analysis by Collingbourne and Peckham, ref. 22., calculates the performance of caret delta wings and includes the effect of altitude, wing loading, laminar and turbulent flow and the position of transition. Parasite drags such as base drag, are also included. On the theoretical side, they carry out an analysis, similar in part to that of section 2. to arrive at expressions for maximum lift/drag ratio with upper surface streamwise, and corresponding lower surface incidence, hence thickness. They also, in an appendix, consider the relationship of the upper surface streamwise condition to the incidence for maximum lift/drag ratio for fixed thickness and arrive at the same conclusion, that for thicknesses of about 5^{o}

in the atmosphere, the two conditions are co-incident.

The essential difference between Collingbourne's and Peckham's analysis and that of section 2. is in the assumption made with respect to the variation of skin friction with thickness and incidence. In section 2. it was assumed that the skin friction was invarient with wing incidence for a wing of constant thickness and this assumption was justified theoretically and can be seen to be reasonable from the experimental results, (in the absence of transition). It follows that there is a change of friction drag with thickness.

This variation and the variation with changing Reynolds number and surface heat transfer, were included in the analysis, enabling the variation of optimum conditions with Mach number and Reynolds number to be explicitly determined.

In ref. 22. the assumption was made that the skin friction drag is independent of flow deflection, i.e. does not vary with incidence or thickness, and a fixed value of friction drag was obtained from other estimates for the particular atmospheric conditions considered. As is pointed out by the authors, this assumption is not really valid and hence part of their results are not strictly correct.

Their most interesting results are those for maximum lift/drag ratio, including various assumptions on transition Reynolds number and including details of the proportion of laminar to turbulent flow, surface temperatures and lift coefficients, for various wing loadings and Mach numbers. The quoted lift/drag ratios or rather weight/drag ratios, include the effect of centrifugal lift which was not included in the present analysis.

The curves are for constant values of $\bar{V}$ of 0·08 and s/l of 0·2 which corresponds to a constant thickness of $6 \cdot 1^{o}$. The variation of C_L (and E.A.S.) at constant wing loading (and Mach number) implies a particular variation of altitude. The curves show an optimum lift coefficient which is close to that for upper surface streamwise, as would be expected for a thickness of about 6^{o}. It is interesting to note, confirming earlier predictions, how little the optimum varies with onset of transition and the comparatively small loss of $^{L}/D$ at the higher wing loadings. The beneficial effect of increasing Mach number is here largely due to the inclusion of the centrifugal lift. (It would have been greater if the effect of base drag had been included also.)

Because the chosen variables, volume parameter and slenderness ratio, are not the primary variables causing the calculated variations, some of the conclusions given by Collingbourne and Peckham do not have the universal applicability apparently implied in their presentation. With all the difficulties of interpretation however, the report presents much useful information including reviews of present knowledge on transition, sweep, leading edge radii and the effect of sweep and blunting on transition and aerodynamic heating.

5.3. Optimum configurations.

There have been many investigations, both theoretical and experimental, into the problem of the optimum configurations for a hypersonic cruise vehicle. In the present author's opinion, several fallacies, which have been consistently repeated, have served to thoroughly confuse the situation. They are discussed below and the results of several investigations are reviewed in the light of these conclusions in order to see what applicable information remains.

Penland, in appendix A of ref. 30. writes; "The relatively widespread use of the non-dimensional ratio of volume $^{2}/_{3}$ to the planform areas as an efficiency correlating parameter, further complicates the issue and makes separation of the effects of shape variables difficult." The fact is, that unlike Mach number, Reynolds number etc. which can be derived from dimensional analysis and can be demonstrated to have significance in particular circumstances, the volume parameter has no such specific and definable significance and indeed, as mentioned by Penland, has certain drawbacks. Although no better alternative exists, in the present author's opinion its use does more harm than good. The factors involved are too complicated to be correlated by a single simple parameter.

An assumption often implicitly made is that a flat wing and underslung body configuration, when tested in the inverted body position, corresponds to a normal flat-bottomed wing. Although this arrangement has been proposed in order to shield the body from high heating rates in low lift atmospheric re-entries, it has little merit in the present application and is unlikely to give the optimum upper surface configuration. The assumption is that the exact upper surface shape is irrelevant, an assumption which is demonstrably wrong.

A contributory factor in the effect of the shape of the upper surface is the incidence under consideration and this also determines the available lift to a large extent. Many results are presented in the form of $(^L/D)_{max}$ vs volume parameter but the lift coefficient corresponding to the quoted maximum lift/drag ratio is not taken into consideration. In many cases the actual lift coefficient developed is impractically small and the relative merit of different shapes totally different at realistic lift coefficients. An example of this is the caret wing which has similar maximum lift coefficients to plain wings but shows to advantage when compared on a C_L basis at high C_L's. Similarly rectangular wings which, on a volume parameter basis, are better than triangular wings at low C_L's due to their higher average Reynolds number, lose this advantage at high C_L's due to increasing tip losses. Interference designs show a similar loss of $(^L/D)_{max}$ with increasing lift coefficient.

The overriding effect of Reynolds number as between tunnel tests and full scale flight has already been mentioned. This affects almost all the published results as most of the variations found were caused or largely influenced by viscous effects and the test Reynolds numbers were generally in the $0{\cdot}7 \times 10^6$ to $4{\cdot}5 \times 10^6$ range, mostly about $1{\cdot}5 \times 10^6$. The result is that little of the experimental evidence available can be used directly (i.e. without theoretical consideration of the effect of increasing Reynolds numbers) for estimating the optimum configuration of a full scale hypersonic cruise vehicle.

Caution is evidently necessary in extracting any universally applicable conclusions from tunnel tests at these Reynolds numbers. For that reason alone, Penland's work (ref. 30.) is perhaps the best as it concerns itself with simple shapes and presents the full data, where others often give the results for $(^L/D)_{max}$ only.

Although aware of the limitations of the volume parameter, he could not resist using it but also supplies sufficient information to enable the important features to be clearly and quickly seen. The results for triangular wings extracted from his report are shown in fig. 5.2. with the result of the present tests (ref. 70.) at the same Reynolds number of $1{\cdot}5 \times 10^6$ added. It can be seen that the lift/drag ratio is practically invariant with volume coefficient at constant thickness while a wide range of lift/drag ratios is available for any value of volume coefficient with varying thickness and sweep, - a perfect example of the care needed in using the volume parameter.

Penland, nevertheless, optimises the lift/drag ratio with respect to volume parameter in a composite plot, to obtain the combinations of sweep and thickness which give maximum $^L/D$ for a given value of $\frac{V^{2}/3}{S}$. It is interesting that very high angles of sweep are obtained, - $>85^{o}$ for $^t/c > 0{\cdot}06$ - and thus shock detachment would be an important effect.

The effect of increasing sweep at constant thickness is shown to give a decrease in $^L/D$, due to the increase of wetted to plan area ratio. A different Reynolds number could give a different result.

Fetterman et al. (ref. 27.) give another plot of $(^L/D)_{max}$ versus $\frac{V^{2}/3}{S}$ for a variety of triangular and rectangular shapes. Although the sweep angles are given in most cases and thus thickness angles can be computed, this is a rather laborious process. The results of the present investigation are generally slightly higher than the corresponding ones on this plot. The presentation does nothing to show what an optimum configuration would be. Results are presented for wing body configurations in 'flat-top' and 'flat-bottom' arrangement.

One pressure plot of the upper surface of a half-cone wing arrangement in the flat-bottom position is presented as evidence that unknown effects exist which give rise to much larger upper surface pressures (or lower suctions) than would be expected and there is some speculation about premature leading edge shock detachment. In fact, the quoted case which is a

$7{\cdot}5^{o}$ half angle cone at 7^{o} incidence, has its upper centre line developing pressure and this pressure has spread through the boundary layer to the leading edges in much the same way as has been observed for lower surfaces, (e.g. ref. 44.).

Much of the information from the above reports, and from others, is presented in a review paper by Becker ref. 32. This contains much useful information but the appreciation of the results is marred by the use of the doubtful concepts discussed earlier.

In particular, optima are consistently judged in terms of the volume parameter and no account is taken of the possible effects of the large difference of Reynolds number in translating the results to full scale. To give a particularly pertinent example, Becker dismisses the caret wing as a result of one comparison with a rectangular wing because it had a lower $(^{L}/D)_{max}$ in terms of volume parameter at the test Reynolds number of $1{\cdot}5 \times 10^{6}$. The plain rectangular wing (of very low aspect ratio) is in any case not practical as an aeroplane and, as has been shown, the picture is entirely different when caret wings are considered at practical lift coefficients and Reynolds numbers. No real indications of optimum configurations emerge from the material presented in this paper.

The conclusion to be drawn from the remarks of this paragraph is that experimental determination of the effect of variations in shape and of the optimum configuration for a hypersonic cruise vehicle can only be achieved together with theoretical consideration at least until tests are carried out at substantially higher Reynolds numbers. At present, the most realistic answers are probably those derived from theoretical analyses such as that of Collingbourne and Peckham (ref. 22.) and of section 2, supported, where possible, by experimental evidence.

5.4. Conclusions.

In carrying out an experimental investigation into the forces developed by hypersonic lifting vehicles, it was found necessary to carry out a concurrent theoretical study to aid in defining a smaller area for the experimental programme and to help in the interpretation of the results. Apart from the direct results of the theoretical study, it showed that viscous forces would be proportionately less important in full scale than at the test Reynolds numbers and hence many of the experimental results would not be directly applicable. The main use of the experimental results would be to substantiate the theoretical methods used in estimating full scale characteristics. Alternatively, by isolating the discreet factors producing the measured results, these could be translated to full scale.

The results confirmed theoretical predictions that the mean pressure over flat delta surfaces with attached leading edge shocks is around 5% less than the value obtained by assuming complete two dimensional flow. The initial loss with shock detachment was also small. The lift of the caret wings was closely predicted by two-dimensional oblique shock theory except at the lower test Reynolds number of $0 \cdot 9 \times 10^6$ where there was some evidence of an increase of lift due to viscous effects on the lower surfaces.

Analysis of the skin friction drag gave good agreement with theory within the margin of unknowns arising from experimental error and base drag. Those variations outside of this margin indicated the onset of transition on the high aspect ratio plain wing which was not present on the corresponding low aspect ratio wing; an apparent delaying of transition with reducing aspect ratio. There were also significant increases in friction drag on the caret and twisted wings indicating viscous effects on the concave lower surfaces.

The viscous effects, evident on the caret and twisted wings relative to the plain wings at a Reynolds number of $0 \cdot 9 \times 10^6$ were no longer present or reduced at a Reynolds number of $3 \cdot 5 \times 10^6$. This highlights the problem of translating tests at these Reynolds numbers to full scale.

At the test Reynolds numbers there was little difference between the maximum lift/drag ratios achieved on the flat-bottomed, caret or twisted wings of similar aspect ratio. The caret wing showed an advantage in that it achieved its maximum lift/drag ratio at a higher value of lift coefficient and this advantage would be expected to remain or be enlarged at full scale. The twisted wing showed a similar advantage and in addition had a centre of pressure position some 2% further forward than the other wings and a more useful cross sectional area distribution.

The results also confirmed predictions for the incidence for maximum lift/drag ratio and the Reynolds number at which this would coincide with the condition of upper surface streamwise obtained from the theoretical analysis.

This analysis gave simple expressions for the variation of optimum thickness with Mach number, Reynolds number and surface heat transfer for the case of upper surfaces streamwise. The upper surface streamwise condition was shown to be near to the condition for maximum $^L/D$ for vehicles with realistic wing loadings and lift/drag ratios in the atmosphere. In these conditions skin friction drag would be a small proportion of the total drag.

Theoretical estimates indicated that lift/drag ratios from 5 - 10 should be obtainable on wings of thickness angles of 5° to 10° in the altitude range 80,000 to 150,000 ft. Plain, caret or twisted wings would be satisfactory from the lift/drag ratio point of view, with the caret and twisted wings having slight advantages for different reasons.

In the course of the investigation much useful information was obtained on gun tunnel balance design and a new approximation was developed for pressure versus flow deflection at hypersonic speeds.

Appendix A. Incidence for maximum lift/drag ratio.

Let α = wing centre line incidence

$$\beta = \frac{\theta}{2} .$$

and remaining notation as on pages 16 to 18.

The pressure coefficient will be assumed to be given to sufficient accuracy by a second order expression, i.e. for $M \gg 1$,

$$C_p = \frac{2\delta}{M} + A\delta^2 \qquad \ldots\ldots\ldots(A.1.)$$

then

$$C_D = C_{D_U} + C_{D_L} + C_{D_F}$$

$$= \frac{4}{M}(\beta^2 + \alpha^2) + 2A\beta(\beta^2 + 3\alpha^2) + C_{D_F} \qquad \ldots\ldots\ldots(A.2.)$$

Similarly

$$C_L = \frac{4\alpha}{M} + 4A\beta\alpha \qquad \ldots\ldots\ldots(A.3.)$$

Considering the drag/lift ratio and differentiating with respect to α,

$$C_L^{\,2}\,\frac{\partial\left(\frac{C_D}{C_L}\right)}{\partial\alpha} = \left(\frac{4\alpha}{M} + 4A\beta\alpha\right)\left(\frac{8\alpha}{M} + 12A\beta\alpha\right)$$

$$-\left[\frac{4}{M}(\beta^2 + \alpha^2) + 2A\beta(\beta^2 + 3\alpha^2) + C_{D_F}\right]\left[\frac{4}{M} + 4A\beta\right] \qquad \ldots\ldots\ldots(A.4.)$$

$= 0$ for maximum or minimum.

At $\left(\frac{C_D}{C_L}\right)_{min}$ $\alpha = \alpha'$

Hence

$$\alpha'^2\left(\frac{4}{M} + 6A\beta\right) - \left(\frac{4}{M}\beta^2 + 2A\beta^3 + C_{D_F}\right) = 0 \qquad \text{.......(A.5.)}$$

and

$$\alpha' = \sqrt{\frac{\beta^2(1 + 0{\cdot}5MA\beta) + 0{\cdot}25MC_{D_F}}{(1 + 1{\cdot}5\ MA\beta)}} \qquad \text{.......(A.6.)}$$

Thus it can be seen that for linear theory (A = 0) and inviscid flow ($C_{D_F} = 0$), the optimum incidence is achieved with the upper surface streamwise ($\alpha' = \beta$). The Mach number term in the numerator is one third of that in the denomenator and so the effect of the non-linear pressure term is to decrease α' while the skin friction term will increase it. Taking the Newtonian limit of $C_p = 2\delta^2$, i.e. letting $M \rightarrow \infty$, gives $\alpha' = \frac{1}{\sqrt{3}}\beta$ and this is the other limit to the linear result in the absence of skin friction. Numerical calculation for the range of wing loadings and altitudes considered in section 2., show that the upper surface streamwise condition is optimum for wings of about 5^{o} thickness angle.

[A similar analysis, using different methods and assumptions, is carried out by Collingbourne and Peckham in ref. 22, with the same result.]

Appendix B. Detailed development of theory of paragraph 2.2.

B.1. Lift.

Ref. 74 gives the derivation of a new approximation to pressure versus flow deflection at hypersonic speeds which is used in the theoretical development of this appendix. In the approximation the pressure is given by:-

$$\left(\frac{p}{p_\infty} - 1\right) \simeq \gamma M\delta + 1\cdot 1\ (M\delta)^{2\cdot 15} \qquad \ldots\ldots\ldots (B.1.)$$

For slender bodies with upper surfaces streamwise,

$$C_L \simeq C_{p_L} \qquad \ldots\ldots\ldots (B.3.)$$

and hence from (B.1.) above,

$$C_L = \frac{2\theta}{M} + 1\cdot 5\ M^{0\cdot 15}\ \theta^{2\cdot 15} \qquad \ldots\ldots\ldots (B.4.)$$

for $\gamma = 1\cdot 4$.

B.2. Skin friction drag.

The Blasius solution for the laminar boundary layer on a flat plate with zero pressure gradient is,

$$C_f = \frac{\tau_o}{0\cdot 5\rho U^2} = \frac{0\cdot 664}{\sqrt{R_{e_x}}} \qquad \ldots\ldots\ldots (B.5.)$$

In high speed flow, the reference temperatures method (see for example ref. 71.) gives the same expression except that conditions are evaluated at a reference temperature T^*, (where $T^* = T_3 + 0\cdot 5(T_W - T_3) + 0\cdot 22\ (T_{W_O} - T_3)$ see page 123.) giving:-

$$C_F = 0{\cdot}664 \sqrt{\frac{C_{\infty}^*}{R_{e_x}}} \quad \text{........(B.6.)}$$

where C_{∞}^* is the constant of proportionality in the viscosity/ temperature relationship,

$$\frac{\mu^*}{\mu_{\infty}} = C_{\infty}^* \frac{T^*}{T_{\infty}} \quad \text{........(B.7.)}$$

and

$$C_{\infty}^* = \frac{T_{\infty} + 110}{T^* + 110} \left(\frac{T^*}{T_{\infty}} \right) \quad \text{........(B.8.)}$$

from Sutherlands law (e.g. ref 53.) and with temperature in ^oK.

If the less accurate but more amenable relationship

$$\frac{\mu^*}{\mu_{\infty}} = \left(\frac{T^*}{T_{\infty}}\right)^n \quad \text{........(B.9.)}$$

is used then

$$\bar{C}_{\infty}^* = \left(\frac{T^*}{T_{\infty}}\right)^{n-1} \quad \text{........(B.10.)}$$

where the bar distinguishes this value from that obtained using the previous formula.

For a triangular surface with conditions on its surface shown by suffix $'$, the skin friction drag is given (obtained by integrating over the surface, e.g. ref. 19.) by,

$$C_{D_{F'}} = 1{\cdot}77\ Q' \sqrt{\frac{C'}{R_{e'_L}}} \quad \text{........(B.11.)}$$

where

$$Q_{?} = \frac{\rho_{?} U_{?}^{2}}{\rho_{2} \cdot U_{\infty}^{2}} \qquad \ldots\ldots\ldots(B.12.)$$

and $R_{e_{?}L}$ is the Reynolds number based on conditions $_{?}$ and the wing length L.

It can be seen from equation (B.26a.) that the skin friction coefficient on any surface varies as $\left(\frac{p}{p_{\infty}}\right)^{\frac{1}{2}}$. Thus $C_{D_F} \sim \delta^{n}$ with n increasing with M. For slender wings near zero incidence the two surfaces have nearly equal and opposite variation of skin friction drag with flow deflection. Thus the skin friction can be taken as approximately independent of incidence (but not of thickness) and can be determined at any convenient incidence.

If the small change due to the angled vee roof is ignored, the upper and lower surfaces are at equal incidence when each is at half the thickness angle to the flow. With suffix $_3$ designating conditions on the surfaces in this case, the total skin friction drag is given approximately by:-

$$C_{D_F} \simeq 1{\cdot}77\ Q_3\ (E_L + E_U) \sqrt{\frac{\overline{C}_3}{R_{e_{3_L}}}} \qquad \ldots\ldots\ldots(B.13.)$$

where $E_L = \dfrac{\text{Lower surface area}}{\text{plan area}}$

$E_U = \dfrac{\text{Upper surface area}}{\text{plan area}}$

other terms are as previously defined but for conditions $_3$, and

$$\bar{C}_3 \equiv \left(\frac{T^*}{T_3}\right)^{1-n} \qquad \text{.......(B.14.)}$$

where,

$$T^* = T_3 + 0{\cdot}5(T_W - T_3) + 0{\cdot}22(T_{W_0} - T_3)$$

(ref. 71.) ....(B.15.)

where

T_W = wall temperature

T_{W_0} = adiabatic wall temperature

and $T_{W_0} = T_3(1 + \sigma_p^{1/2} \frac{\gamma-1}{2} M_3^2)$

Hence $T_{W_0} - T_3 \simeq \frac{\gamma-1}{2} M_3^2 T_3$ ....(B.16.)

for $\sigma_p \simeq 1$.

The practical extremes of wall temperatures T_W in (B.15.) above can be taken as,

$T_W = T_3$ for '100%' cooling,

and $T_W = T_{W_0}$ for zero cooling.

Thus, substituting (B.16.) into (B.15.) for $M \gg 1$,

$$T^* \simeq T_3 + H(T_{W_0} - T_3)$$

$$\simeq T_3 \left(1 + \frac{H(\gamma-1)}{2} M_3^2\right)$$

$$T^* \simeq \frac{H(\gamma-1)}{2} \cdot M_3^2 \cdot T_3 \qquad \text{.......(B.17a.)}$$

where H varies from 0.22 to 0.72 as cooling varies from 100% to zero.

For hypersonic flow and slender bodies,

$$\frac{U_3}{U_\infty} \doteq \frac{U_3^2}{U_\infty^2} \doteq 1 \qquad \text{.......(B.18.)}$$

Hence,

$$M_\infty = \frac{U_\infty}{a_\infty} \doteq \frac{U_3}{a_\infty} \doteq \frac{U_3}{a_3} \cdot \frac{a_3}{a_\infty} \doteq M_3 \frac{a_3}{a_\infty}$$

but

$$\left(\frac{a_3}{a_\infty}\right)^2 = \frac{T_3}{T_\infty}$$

$$\therefore \quad M_3^2 \, T_3 = M_\infty^2 \, T_\infty \qquad \text{.......(B.19.)}$$

and hence

$$T^* \doteq H \cdot \frac{(\gamma-1)}{2} \cdot M_\infty^2 \, T_\infty \qquad \text{.......(B.17b.)}$$

$$\therefore \quad Q_3 \sqrt{\frac{\bar{C}_3}{R_{e_{3_L}}}} = \frac{\rho_3}{\rho_\infty} \sqrt{\left(\frac{T^*}{T_3}\right)^{n-1} \cdot \frac{\mu_3}{\rho_3 U_3 L}}$$

$$= \sqrt{\left[\frac{H(\gamma-1)}{2}\right]^{n-1} \left(\frac{M_\infty^2 T_\infty}{T_3}\right)^{n-1} \frac{\mu_\infty}{\rho_\infty U_\infty L} \cdot \frac{\rho_3}{\rho_\infty} \cdot \left(\frac{T_3}{T_\infty}\right)^n}$$

$$= \frac{1}{\bar{H} \, M^{1-n}} \cdot \left(\frac{p_3}{p_\infty}\right)^{1/2} \cdot \sqrt{\frac{1}{R_{e_{\infty_L}}}} \qquad \text{.......(B.20a.)}$$

where

$$\bar{H} = \left[H \cdot \frac{(\gamma-1)}{2}\right]^{\frac{1-n}{2}} \qquad \text{.......(B.21.)}$$

$\bar{H}$ varies from 0·7 to 0·8 as the wall cooling varies from

100% to zero for n = 0·76, the usual value. (n = 0·84 for tunnel).

For conditions in the atmosphere, the effect of altitude can be more clearly seen by writing the Reynolds number in terms of a standard Reynolds number taken at some defined standard conditions. With suffix $_s$ to define standard values,

$$R_{e_{\infty L}} = \sigma_s \; R_{e_s} \left(\frac{T_s}{T_\infty}\right)^{1-n} M_\infty \qquad \text{.......(B.22.)}$$

where $\sigma_s = \dfrac{\rho_\infty}{\rho_s}$ the relative density ....(B.23.)

and $R_{e_s} = \dfrac{\rho_s \, a_{s} L}{\mu_s}$ ....(B.24.)

In the atmosphere, the temperature range 216°K to 266°K covers the range 13,000ft. to 200,000 ft. (ref. 73.) and using 242°K constant in this range introduces only ±2·5% error. The appropriate standard conditions are those at 125,000 ft. In terms of standard conditions,

$$Q_3\sqrt{\frac{\bar{C}_3}{R_{e_{3_L}}}} = \frac{1}{\sigma_s^{\frac{1}{2}} \; \bar{H} \; M^{1\cdot 5-n}} \sqrt{\frac{1}{R_{e_s}}} \left(\frac{p_3}{p_\infty}\right)^{\frac{1}{2}} \qquad \text{.......(B.20b.)}$$

The term $\left(\dfrac{p_3}{p_\infty}\right)^{\frac{1}{2}}$ has been treated in the same way as $\left(\dfrac{p}{p_\infty} - 1\right)$ in ref. 74. to arrive at the approximation,

$$\left(\frac{p_3}{p_\infty}\right)^{\frac{1}{2}} = 1 + 0\cdot 25\gamma M\theta + 0\cdot 0485\,(M\theta)^{1\cdot 77} \qquad \text{.......(B.25.)}$$

which is valied to 5% for $M\theta \leqslant 4$, sufficient for the present purpose.

Then, substituting (B.20a.) into (B.13.),

$$C_{D_F} = \frac{1{\cdot}77(E_L + E_U)}{\bar{H}\, M_\infty^{1-n}\, R_{e_{\infty_L}}^{1/2}} \cdot \left(\frac{p_3}{p_\infty}\right)^{1/2} \qquad \ldots\ldots\ldots(B.26a.)$$

or in terms of conditions at a standard altitude,

$$C_{D_F} = \frac{1{\cdot}77\,(E_L + E_U)}{\bar{H}\, M_\infty^{1\cdot5-n}\, \tau_s^{1/2}\, R_{e_s}^{1/2}} \cdot \left(\frac{p_3}{p_\infty}\right)^{1/2} \qquad \ldots\ldots\ldots(B.26b.)$$

B.3. Lift/drag ratio.

It is more convenient to treat the reciprocal,

$$\frac{C_D}{C_L} = \theta + \frac{C_{D_F}}{C_L} + \frac{C_{D_B}}{C_L} \qquad \ldots\ldots\ldots(B.27.)$$

for upper surfaces streamwise and where

C_{D_B} = base drag coefficient based on plan area.

Let $p_B \equiv$ base pressure $\equiv (1-b)p_\infty$ ....(B.28a.)

then

$$C_{D_B} = \frac{2.bp_\infty}{\gamma M^2 p_\infty} \cdot \frac{\theta Ls}{sL}$$

$$C_{D_B} = \frac{2b\theta}{\gamma M^2} \qquad \ldots\ldots\ldots(B.28b.)$$

Hence from equation (B.4.) (B.25.) (B.26a.) (B.28b.) and (B.27.)

$$\frac{C_D}{C_L} = \theta \quad \frac{1{\cdot}77(E_L + E_U) \quad M^{(1+n)}\left[1+0{\cdot}35(M\theta) + 0{\cdot}0485(M\theta)^{1\cdot77}\right]}{\bar{H} \quad R_{e_{\infty_L}}^{1/2} \quad \left[2\theta M + 1{\cdot}5\ (M\theta)^{2\cdot15}\right]} + \frac{b\theta}{1{\cdot}4M\theta+1{\cdot}05(m\theta)^{2\cdot15}}$$

........(B.29a.)

Or, for flight in the atmosphere,

$$\frac{C_D}{C_L} = \theta + \frac{1{\cdot}77(E_L+E_U)\ M^{(0\cdot5+n)}\ \left[1+0{\cdot}35\ M\theta\ +\ 0{\cdot}048(M\theta)^{1\cdot77}\right]}{\bar{H}\,\tau_s^{\frac{1}{2}}\,R_{e_s}^{\frac{1}{2}}\ \left[2\theta M\ +\ 1{\cdot}5(M\theta)^{\ 2\cdot15}\right]}$$

$$+ \qquad \frac{b\theta}{1{\cdot}4M\theta\ +\ 1{\cdot}05(M\theta)^{2\cdot15}} \qquad \ldots\ldots\ldots(B.29b.)$$

B.4. Thickness for $(^L/D)_{max}$ with upper surfaces streamwise

For a maximum or minimum

$$\frac{\partial\,(\frac{D}{L})}{\partial\theta} = 0$$

$$\therefore\ \frac{\partial}{\partial\theta}\left[\frac{C_L\,\theta\ +\ C_{D_F}\ +\ C_{D_B}}{C_L}\right] = 0$$

It will be assumed that the base drag has little effect on the thickness for maximum lift/drag ratio, an assumption confirmed by the numerical results, and hence,

$$\frac{\partial\,(\frac{D}{L})}{\partial\,\theta} = C_L\frac{\partial\,(C_L\ \theta)}{\partial\,\theta} - C_L\theta\frac{\partial C_L}{\partial\theta} + C_L\frac{\partial C_{D_F}}{\partial\theta} - C_{D_F}\frac{\partial C_L}{\partial\theta}$$

$$= C_L^{\ 2} + C_L\frac{\partial C_{D_F}}{\partial\theta} - C_{D_F}\frac{\partial C_L}{\partial\theta}$$

$$= 0$$

With the expressions for C_{D_F} and C_L obtained from equations (B.26.) and (B.4.), the following expression can be obtained,

$$\left[2(M\theta') + 1\cdot5(M\theta')^{2\cdot15}\right]^2 = K\left[2 + 3\cdot23(M\theta')^{1\cdot15} - 0\cdot075(M\theta')^{1\cdot77} + 0\cdot604(M\theta')^{2\cdot15} + 0\cdot028(M\theta')^{2\cdot92}\right] \qquad \ldots\ldots\ldots(B.30.)$$

where θ' is the thickness angle for maximum lift/drag ratio with upper surfaces streamwise and K is given by

$$K = \frac{1\cdot77(E_L+E_U)\ M^{(2+n)}}{\bar{H}\ R_{e_{\infty_L}}^{\frac{1}{2}}} \qquad \ldots\ldots\ldots(B.31a.)$$

$$= \frac{1\cdot77(E_L + E_U)\ M^{(1\cdot5+n)}}{\bar{H}\ \nabla_s^{\cdot\frac{1}{2}}\ R_{e_s}^{\frac{1}{2}}} \qquad \ldots\ldots\ldots(B.31b.)$$

Equation (B.30.) has been solved (graphically)* to give:-

$$M\theta' = 0\cdot688K^{0\cdot477} \qquad \ldots\ldots\ldots(B.32a.)$$

$$\text{or} \qquad \theta' = \frac{0\cdot688K^{0\cdot477}}{M} \qquad \ldots\ldots\ldots(B.32b.)$$

Then, substituting equations (B.32a.) and (B.32b.) into

---

* Plotting the L.H.S. and R.H.S. of equation (B.30.) against $(M\theta)$ for various values of K produces a series of solutions which when plotted against K on log log paper, produce a straight line.

equation (B.29.) gives:-

$$M\left(\frac{D}{L}\right)_{\theta'} = \left[0{\cdot}688K^{0\cdot477} + \frac{K(1+0{\cdot}241K^{0\cdot477} + 0{\cdot}025K^{0\cdot845})}{1{\cdot}376K^{0\cdot477} + 0{\cdot}672K^{1\cdot03}} + \frac{0{\cdot}688bK^{0\cdot477}}{(0{\cdot}95K^{0\cdot477}+0{\cdot}47K^{1\cdot03})} \right] \qquad \ldots\ldots\ldots(B.33.)$$

Equation (B.33.) has been approximated (graphically) to give:-

$$M\left(\frac{D}{L}\right)_{\theta'} = 1{\cdot}28K^{0\cdot466} + \frac{b}{1{\cdot}38 + 0{\cdot}684K^{0\cdot553}} \qquad \ldots\ldots\ldots(B.34b.)$$

or, for zero base drag,

$$M\left(\frac{D}{L}\right)_{\theta'} = 1{\cdot}28K^{0\cdot466} \qquad \ldots\ldots\ldots(B.34a.)$$

Finally, it is possible to show the effect of Mach number explicitly by combining that part included in the parameter K with that outside to give,

$$\theta' = 0{\cdot}688\left[\frac{1{\cdot}77(E_L + E_U)\ M^{n-0\cdot6}}{\bar{H}\,\sigma_s^{\frac{1}{2}}\ R_{e_s}^{\frac{1}{2}}}\right]^{0\cdot477} \qquad \ldots\ldots\ldots(B.35a.)$$

and

$$\left(\frac{D}{L}\right)_{\theta'} = 1{\cdot}28\left[\frac{1{\cdot}77(E_L + E_U)\ M^{n-0\cdot66}}{\bar{H}\ \sigma^{\frac{1}{2}}\ R_{e_s}^{\frac{1}{2}}}\right]^{0\cdot466} \qquad \ldots\ldots\ldots(B.36a.)$$

for zero base drag.

Taking the usual value of n = 0.76, this gives,

$$\theta' \sim M^{0\cdot076} \qquad \ldots\ldots\ldots(B.35b.)$$

and

$$\left(\frac{L}{D}\right)_{\theta'} \sim M^{-0\cdot047} \qquad \ldots\ldots\ldots(B.36b.)$$

which confirms the insensitivity of maximum lift/drag ratio to

Mach number at hypersonic speeds, shown by experimental results.

The wing loading, ω, corresponding to optimum conditions can be obtained from,

$$C_L \simeq C_p = \frac{\omega}{0.5\gamma M^2 p_\infty} \qquad \text{........(B.37.)}$$

hence,

$$\omega = p_\infty(\gamma M\theta + 1.1(M\theta)^{2.15}) \qquad \text{........(B.38.)}$$

The various approximations used in deriving the expressions of this appendix have been accurate to within 5% in the required range of variables. Hence it is estimated that the results obtained from these expressions would be accurate to about ±20% (including possible inaccuracies in the theoretical assumptions) while the trends would be accurate to ±5%.

Appendix C. Derivation of expressions for the twisted wing.

It is desired to find the dimensions of a twisted delta wing of given twist that will have the same volume as a plain delta wing of equal plan area and aspect ratio. With system of axis, origin at the rear, on the centreline of lower surface, x forwards, z upwards +ve, and y sideways let the body dimensions be length l, span $\pm S$ and trailing edge thickness Z as shown below.

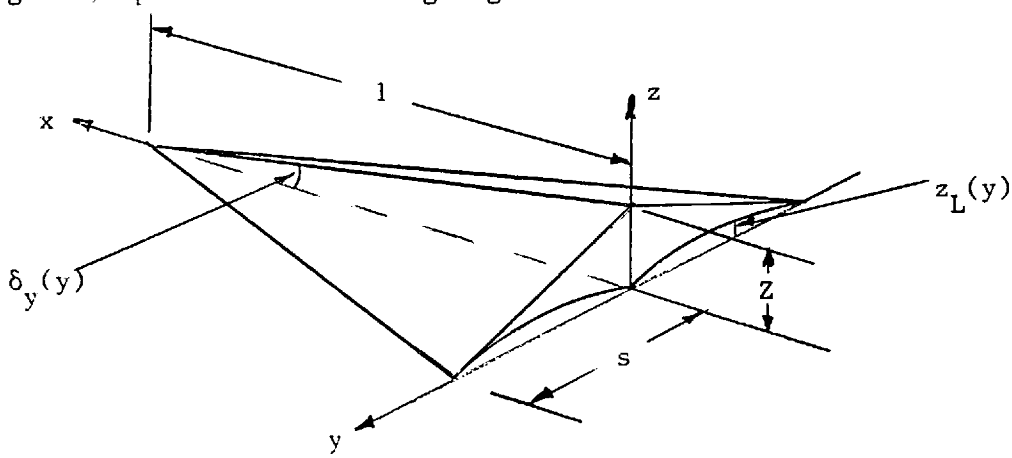

Let the thickness angle taken along y = constant be $\delta y(y)$ and the height of the lower surface at the trailing edge be $z_L(y)$, and upper surface $z_U(y)$.

Then $\quad x = l(1-\frac{y}{S})$ ....(C.1.)

and for linear twist

$$\delta y = \delta_o(1-\frac{ay}{S}) \qquad \text{........(C.2.)}$$

where δ_o is root thickness angle

and $\quad a = (1-\frac{\delta t}{\delta_o})$ ....(C.3.)

where δt is tip thickness angle.

Also let $z_U(y) - z_L(y) = z_y$ the local trailing edge thickness, then the elemental volume at any plane y = const. is,

$$\delta V = 0{\cdot}5 x_y z_y \delta_y \qquad \ldots\ldots\ldots(C.4.)$$

$$dV = 0{\cdot}5 l^2 \delta_o (1-\frac{y}{S})^2 \ (1-\frac{ay}{S})\ dy \qquad \ldots\ldots\ldots(C.5.)$$

Transforming the variable to $Y = \frac{y}{S}$, $dy = SdY$, and

$$dV = 0{\cdot}5 S l^2 \delta_o (1-Y)^2 \ (1-aY)dY$$

$$V = 0{\cdot}5 S l^2 \delta_o \ (1-Y)^2 (1-aY)dY \qquad \ldots\ldots\ldots(C.6.)$$

$$= \frac{S l^2 \delta_o}{12} \left[4 - a \right]$$

$$= \frac{(25)Zl}{b} (1 - \frac{a}{4}) \qquad \ldots\ldots\ldots(C.7.)$$

where $\frac{a}{4}$ respresents the change of volume due to twist and a, the twist ratio is given by (C.3.).

For equal length and aspect ratio, with suffix $_1$ for plain wing and suffix $_2$ for the twisted wing of equal volume,

$$\delta_{o_1} = \delta_{o_2} (1 - \frac{a}{4}) \qquad \ldots\ldots\ldots(C.8.)$$

and for the twisted wing of the present tests where the tip thickness was half the root thickness,

$$a = 0{\cdot}5$$

and $\therefore$ $\delta_{o_2} = 1{\cdot}143\ \delta_{o_1}$ $\qquad \ldots\ldots\ldots(C.9.)$

The trailing edge contour z_L is given by,

$$z_L = Z(1-\frac{y}{S}) - zy = Z\left[(1-\frac{y}{S}) - 1 + (1+a)\frac{y}{S} - a(\frac{y}{S})^2\right]$$

$$z_L = aZ\left[\frac{y}{S}(1-\frac{y}{S})\right] \qquad \ldots\ldots\ldots(C.10.)$$

References

1. Küchemann D. Hypersonic Aircraft and their Aerodynamic Problems. Progress in Aeronautical sciences Vol.6. Pergammon Press 1965.
2. Peckham D.H. Crabtree L.F. The range performance of hypersonic aircraft. R.A.E. Tech Report No. 66178 June 1966.
3. Küchemann D. Weber J. An analysis of some performance aspects of various types of aircraft designed to fly over different ranges at different speeds. R.A.E. T.R.66188 June 1966.
4. Eggers Jn.A. Allen H.J. Neice S.E. A comparative analysis of the performance of long-range Hypervelocity Vehicles. N.A.C.A. Report 1382 1958.
5. Crabtree L.F. Boundary layer effects on hypersonic aircraft. Unpublished R.A.E. Memo.
6. Nonweiler T. Delta wings of shapes amenable to exact shock-wave theory. ARC,22644 1961.
7. Townend L.H. On lifting bodies which contain two dimensional supersonic flows. R.A.E. T.N.Aero 2675 ARC,25277.
8. Flower J.W. Configurations for high supersonic speeds derived from simple shock waves and expansions. ARC,24,750 and Jn. of Royal Aero. Soc.Vol 67 May 1963.
9. Jones J.G. A method for designing lifting configurations for high supersonic speeds using the flow fields of non-lifting cones. R.A.E. Rep. Aero.2674 (ARC 24,846) March 1963.
10. Mölder S. Lifting configurations for high supersonic speeds derived from internal axisymmetric conical flow fields. McGill University report 1965.
11. Woods B.A. The construction of a compression surface based on an axisymmetric conical flow field. R.A.E. T.N. Aero 2900 June 1963.
12. Moore K.C. The application of known flow fields to the design

of wings with lifting upper surfaces at hypersonic speeds. R.A.E. Tech.Rep. 65034 February 1965.

13. Pike J. The analytical performance of lifting surfaces supporting plane shock waves. R.A.E. Tech.Rep. 66127. April 1966.

14. Pike J. Minimum drag surfaces of given lift which support two dimensional supersonic flow fields. R.A.E. Tech.Rep. 66305 September 1966

15. Bartlett R.S. High lift-drag ratio double wedges of given volume which support two-dimensional supersonic flow fields. RA.E. Tech.Rep. 66306. October 1966.

16. Peckham D.H. On three dimensional bodies of delta planform which can support plane attached shock waves. R.A.E. T.N. Aero 2812 March 1962. (ARC 23887)

17. Catherall D. Boundary layer characteristics of caret wings. R.A.E. T.N. Aero 2835 August 1962. (ARC 24222)

18. Cooke J.C. Leading edge effects on caret wings. RA.E. T.N. Aero 2943 January 1964 (ARC25840)

19. Catherall D. Boundary layer effects on caret wings. R.A.E. T.N. Aero 2972 August 1964.

20. Squire L.C. Pressure distributions and flow patterns at M=4·0 on some delta wings of inverted 'V' cross-section R.A.E. T.N. Aero 2838. August 1962 and R & M 3373 1964. and Part II Flat wings.

21. Pennelegion L. Cash R.F. Preliminary measurements in a shock tunnel of shock angles and under surface pressure related to a Nonweiler wing. N.P.L. Aero Rep. 1037 July 1962. (ARC 23,945)

22. Collingbourne J.R. Peckham D.H. The lift and drag characteristics of caret wings at Mach No.'s between 5 and 10. R.A.E. Tech.Rep. 66036 February 1966. (ARC 28172)

23. Trimpi R.L. et al. Aerodynamic and heating problems of advanced re-entry vehicles. N.A.S.A. SP-23 December 1962.

24. Roe P.L. Some exact calculations of the lift and drag produced by a wedge in supersonic flow either directly or by interference. R.A.E. T.N. Aero 2981 August 1964.

25. McLellan C.H. Ladson C.L. A summary of the aerodynamic performance of hypersonic gliders. N.A.S.A. TM X-237 March 1960.

26. Fetterman D. Favorable interference effects on the maximum lift-drag ratios of half-cone delta-wing configurations at Mach 6·86. N.A.S.A. TN D-2942 August 1965.

27. Fetterman D. et al. Studies relating to the attainment of high lift-drag ratios at hypersonic speeds. N.A.S.A TN D-2956 August 1965.

28. Baines D. Estimates of leading-edge bluntness for a swept-wing hypersonic aircraft. RA.E. Unpublished (ARC 24972)

29. Capey E.C. Alleviation of leading-edge heating by conduction and radiation. R.A.E. Tech.Rep. 66311 October 1966.

30. Penland J.A. Maximum lift-drag-ratio characteristics of rectangular and delta wings at Mach 6·9. N.A.S.A. TN D-2925 August 1965.

31. Blackstock T.A. Ladson C.L. Comparison of the hypersonic aerodynamic characteristics of some simple winged shapes in air and helium. N.A.S.A. TN D-2328 June 1964.

32. Becker J.V. Studies of high lift/drag configurations. A.I.A.A. paper 64-551. 1964. also I.C.A.S. Congress (4th) Paris 1964. Spartan and MacMillan & Co. Ltd. 1965.

33. Geiger R.E. Experimental lift and drag of a series of glide configurations at Mach numbers of 12·6 and 17·5. Jn. of Aero Space Sci. Vol.29.No.4. April 1962.

34. Eggers Jn.A. Syvertson C. Aircraft configurations developing high lift-drag ratios at high supersonic speeds. N.A.C.A. RM A55L05 1956.

35. Small W.J. Bertram M.H. Effect of geometric modifications on the maximum lift-drag ratios of slender wing-body configurations

at hypersonic speeds. N.A.S.A. TN D-3276 March 1966.

36. Mead H.R. Koch F. Hartsfilis S. Theroetical prediction of pressures in hypersonic flow with special reference to configurations having attached leading edge shocks.

(a) Part III Experimental measurements of forces at Mach 8 and pressures at Mach 21. ASD TR 61-60; ASTIA 291219; P111920.

(b) Part II Experimental pressure measurements at Mach 5 and Mach 8. Details as Part III.

37. Penland J.A. Aerodynamic force characteristics of a series of lifting cone and cone cyliner configurations at a Mach No. of 6.83 and angles of attack up to 130° NA.S.A. TN D-840 June 1961.

38. Penland J.A. A study of the stability and location of the centre of pressure on sharp, right circular cones at hypersonic speeds. N.A.S.A. TN D-2283 May 1964.

39. Ladson C.L. Blackstock T.A. Air-helium simulation of the aerodynamic force coefficients of cones at hypersonic speeds. N.A.S.A. TN D-1473 October 1962.

40. Spencer Jn.B. Fox Jn.C.H. Hypersonic aerodynamic performance of minimum-wave-drag bodies. N.A.S.A. TR R-250 November 1966.

41. Wells W.R. Armstrong W. Tables of aerodynamic coefficients obtained from developed Newtonian expressions for complete and partial conic and spheric bodies at combined angles of attack and sideslip with some comparisons with hypersonic experimental data. N.A.S.A. TR R-127

42. Peckham D.H. Pressure distribution measurements on a series of slender delta body shapes at Mach numbers of 6.85 and 8.6. R.A.E. Tech. Note Aero 2952 ARC 25966 February 1964.

43. Nagel A.L. et al. Analysis of hypersonic pressure and heat transfer tests on delta wings with laminar and turbulent boundary layers. N.A.S.A. CR-535 August 1966.

44. Dunavant J.C. Heat transfer to a delta-wing-half-cone combination at Mach numbers of 7 and 10. N.A.S.A. TN D-2199 March 1964.

45. Peckham D.H. Experiments at hypersonic speeds on circular cones at incidence. R.A.E. Tech Note Aero 2863. January 1963. ARC 24,946.

46. Amick J.L. Pressure measurements on sharp and blunt 5° and 15° half-angle cones at Mach number 3·86 and angles of attack to 100°. N.A.S.A. Tech Note D-753 February 1961.

47. Dunavant J.C. Investigation of heat transfer and pressures on highly swept flat and dihedraled delta wings at Mach numbers of 6·8 and 9·6 and angles of attack to 90°. N.A.S.A. TM X-688 1962.

48. Bertram M.H. et al. The aerodynamics of hypersonic cruising and boost vehicles. N.A.S.A. SP 23 December 1962.

49. Bertram M.H. et al. Recent hypersonic studies of wings and bodies. A.R.S. Jn. Vol 31 No.8 August 1961 pp1129-1139.

50. Polak A. Li T.Y. Hypersonic viscous flow past a flat delta wing at moderate angle of attack. University of Cincinnati Tech.Rep. AE6601.

51. Wallace J.E. Burke A.F. Skin-friction, heat transfer and pressure distributions over a flat plate and highly swept delta wings with sharp and blunt leading edges at angles of attack in hypersonic flow. ASD - TDR - 63-772 September 1963.

52. Hopkins H.B. Scheuing R.A. Leng J. Investigation of pressure distributions over planar, twisted and cambered wings in a hypersonic shock tunnel. ASD - TDR - 62-171 P105305 May 1962.

53. Ames Staff Equations, tables and charts for compressible flow. N.A.C.A. Report 1135. 1953.

54. Taylor G.I. Maccol J.W. The air pressure on a cone moving at high speeds. Proc. of Royal Soc. No139. Page 278 1933.

55. Kopal et al Tables of supersonic flow around cones. M.I.T. centre of analysis Tech Rep. No1. 1947.

56. As 55. As 55 Tech Report No3. 1947.

57. Bussemann A. Aerodynamic lift at supersonic speeds. Luftfohrtforschung Bd. 12, No6. October 1935. pages 40 - 220.

58. Linnell R.D. Two-dimensional aerofoils in hypersonic flows. Jn. Aero. Sci. Jan 1949 pp22-30.

59. Bertram M.H., Cook B.S. The correlation of oblique shock parameters for ratios of specific heats from 1 to $^{5}/3$ with application to real gas flows. N.A.S.A. TR-R-171 1963.

60. Cleary J.W., Axelson J.A. Theoretical aerodynamic characteristics of sharp and circularly blunted wedge airfoils. N.A.S.A. TR-R-202 1964.

61. Trimpi R.L., Jones R.A. A method of solution with tabulated results for the attached oblique shock wave system for surfaces at various angles of attack, sweep and dihedral in an equilibrium real gas including the atmosphere. N.A.S.A. TR R-63 1960.

62. Fowell L.R. Exact and approximate solutions for the supersonic delta wing. Jn. Aero. Si. Vol. 23, No. 8. August 1956. p. 709.

63. Babaev D.A. Numerical solution of the problem of supersonic flow past the lower surface of a delta wing. A.I.A.A. Jn. Vol.1. No. 9 September 1963.

64. Crabtree L.F. Survey of inviscid hypersonic flow-theory for geometrically slender shapes. R.A.E. Tech. Note Aero 2695 June 1960.

65. Love E.S., Henderson A. Some aspects of air-helium simulation and hypersonic approximations. N.A.S.A. TN D-49 October 1959.

66. Scheuing R.A. et al. Theoretical prediction of pressures in hypersonic flow with special reference to configurations having attached leading-edge shocks. Part I. Theoretical Investigation ASD TR 61-60 May 1962 p. 106480.

67.Gentry A.E. Aerodynamic characteristics of arbitrary three-dimensional shapes at hypersonic speeds. I.C.A.S. Paper 66-25 September 1966.

68.Edwards J.B. Some properties of wedge section aerofoils at supersonic and hypersonic speeds. R.A.E. TN Aero 2938 December 1963.

69.Deney Jn.C.F. Bluntness and viscous interaction effects on slender bodies at hypersonic speeds. Rand Corp. AD605249 from T.I.L.

70.Opatowski T. Lift drag and pitching moment measurements on a 20° cone, a flat delta and a caret delta wing at a Mach number of 8·3. ARC CP908 1966.

71.Monagham R.J. Formulae and approximations for aerodynamic heating rates in high speed flight. ARC CP360 1957.

72.Monagham R.J. An approximate solution of the compressible laminar boundary layer on a flat plate. R & M 2760 1953.

73. - U.S. Standard Atmosphere 1962.

74.Opatowski T. A new approximation for pressure versus flow deflection at hypersonic speeds. Jn. R.Ae.S. May 1967.

75.Picken. J. Greenwood.G. Free-flight measurements of heat transfer and observations of transition on a caret wing at Mach numbers up to 3·6. R.A.E. TR 65237. October 1965.

76.Needham D.A. Progress report on the Imperial College Hypersonic Gun Tunnel. Imperial College of Science and Technology, Aeronautics Dept. Tech Note.No.118.1963.

77.Hoerner S.F. Fluid-dynamic drag. Published by the author. 148, Busteed Drive, Midland Park, N.5. U.S.A. 1958.

78.King H.H. A tabulation of base flow properties for cones and wedges. Electro-optical Systems Inc. Rep.RN-17.

79.Pennelegion L. Smith G.S. Dolman K. Millisecond measurements of aerodynamic forces in a high pressure shock tunnel. N.P.L. Aero Report 1120 ARC 26309 1964.

80. McLellan C.H. Bertram M.H. Moore J.A. An investigation of four wings of square plan form at a Mach number of 6.9 in the Langley 11-inch hypersonic tunnel. N.A.C.A. Report 1310 1957.

81. Martin J.R. Duryea C.R. Stevenson L. Instrumentation for force and pressure measurements in a hypersonic shock tunnel. Proceedings of Second Symposium on Hypervelocity Techniques. University of Denver. 1962. Plenum Press N.Y.

82. Platov A.S. Ricci H.A. Wind tunnel tests of solid state strain gauges. Proceedings of the 1st International Congress on Instrumentation in Aerospace Simulation facilities. L'École Nationale Supérieur de l'Aéronautique, Paris. 1964.

83. Crabtree L.F. Treadgold D. Experiments on hypersonic lifting bodies. Paper presented at I.C.A.S. meeting 1966.

84. Album H.H. Flow inclination measurements in hypersonic tunnels. Jn. A.I.A.A. Vol.2.No.1 January 1964 p.104.

85. Hara F.R. Experimental studies on the lip shock. A.I.A.A. paper No.67-29. 5th Aerospace Sciences Meeting, New York. January 1967.

86. Richards B. Film cooling in hypersonic flow. Ph.D. Thesis. Imperial College of Science and Technology. 1966.

87. Crane J R.A.E. report. To be published.

88. Weinstein L. Neal Jn. L. Hypersonic performance of several basic and modified diamond-cross-section delta wing configurations. N.A.S.A. TN D-3894 1967.

89. Hall I.M. Transonic flow in two-dimensional and axially-symmetric nozzles. ARC 23,347 1961.

90. Stratford B. Beavers G.S. The calculation of the compressible turbulent boundary layer in an arbitrary pressure gradient. - a correlation of certain previous methods. ARC R & M 3207.

91. Deem R.E. Murphy J.S. Flat plate boundary layer transition at hypersonic speeds. A.I.A.A. Paper No.65-128 January 1965.

92. Pennelegion L. Cash R.F. Shilling M.J. Free flight tests in the N.P.L. 6-in.(15cm.) shock tunnel of model HB-2 using multiple spark recording. N.P.L. Aero Report. 1212.

93. MacArthur R. Martin J.F. Use of field effect transistors in shock tunnel instrumentation circuits. Proceedings of 2nd International Congress on Instrumentation in Aerospace simulation facilities. Arnold Air Force Station. Tennessee. U.S.A.

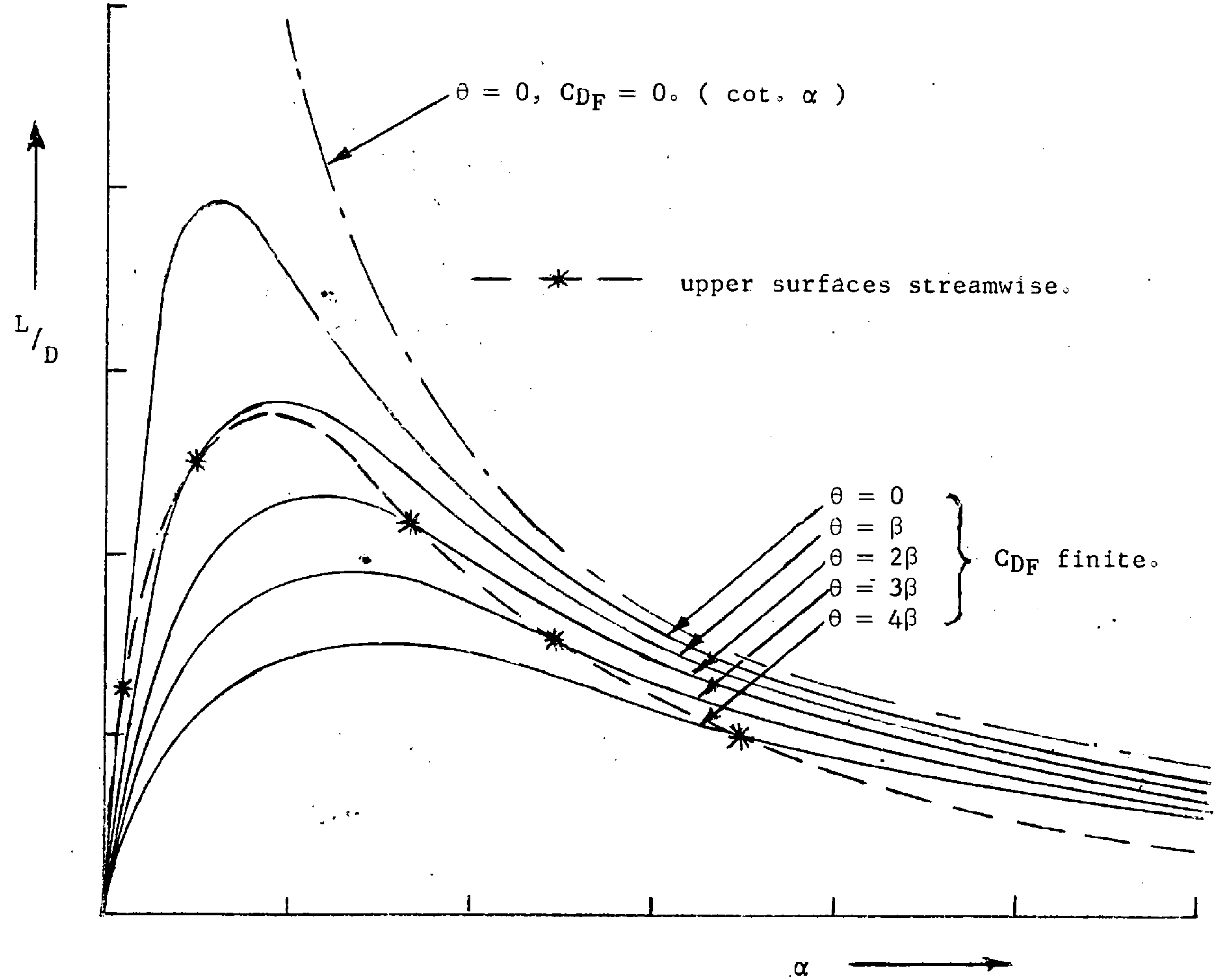

FIG. 2.1 Sketch showing the variation of L/D with incidence for various thickness angles.

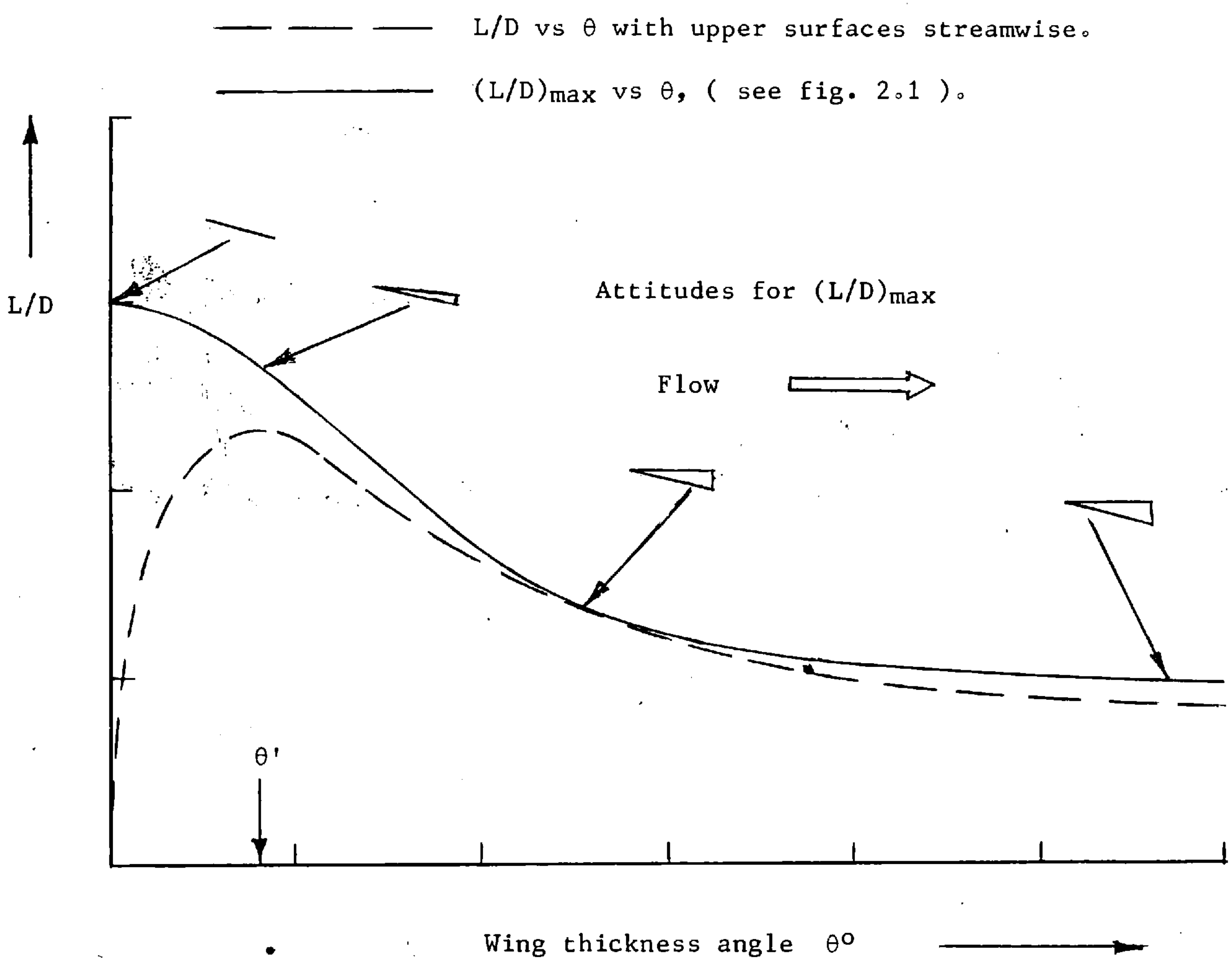

FIG. 2.2 Sketch showing relationship between $(L/D)_{max}$ and the L/D with upper surfaces streamwise.

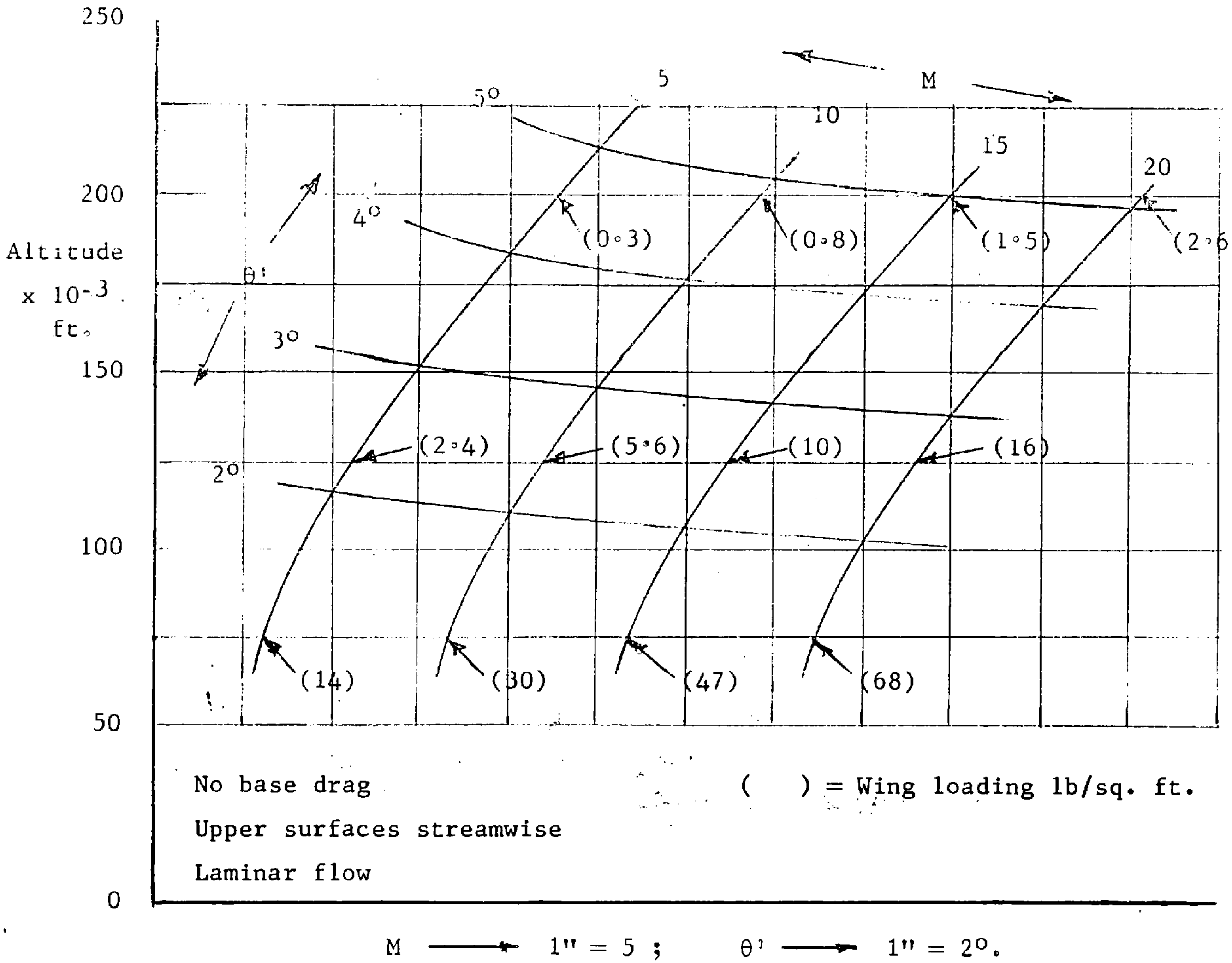

FIG. 2.3 Optimum thickness angle θ' for a delta wing of 200ft length in the atmosphere.

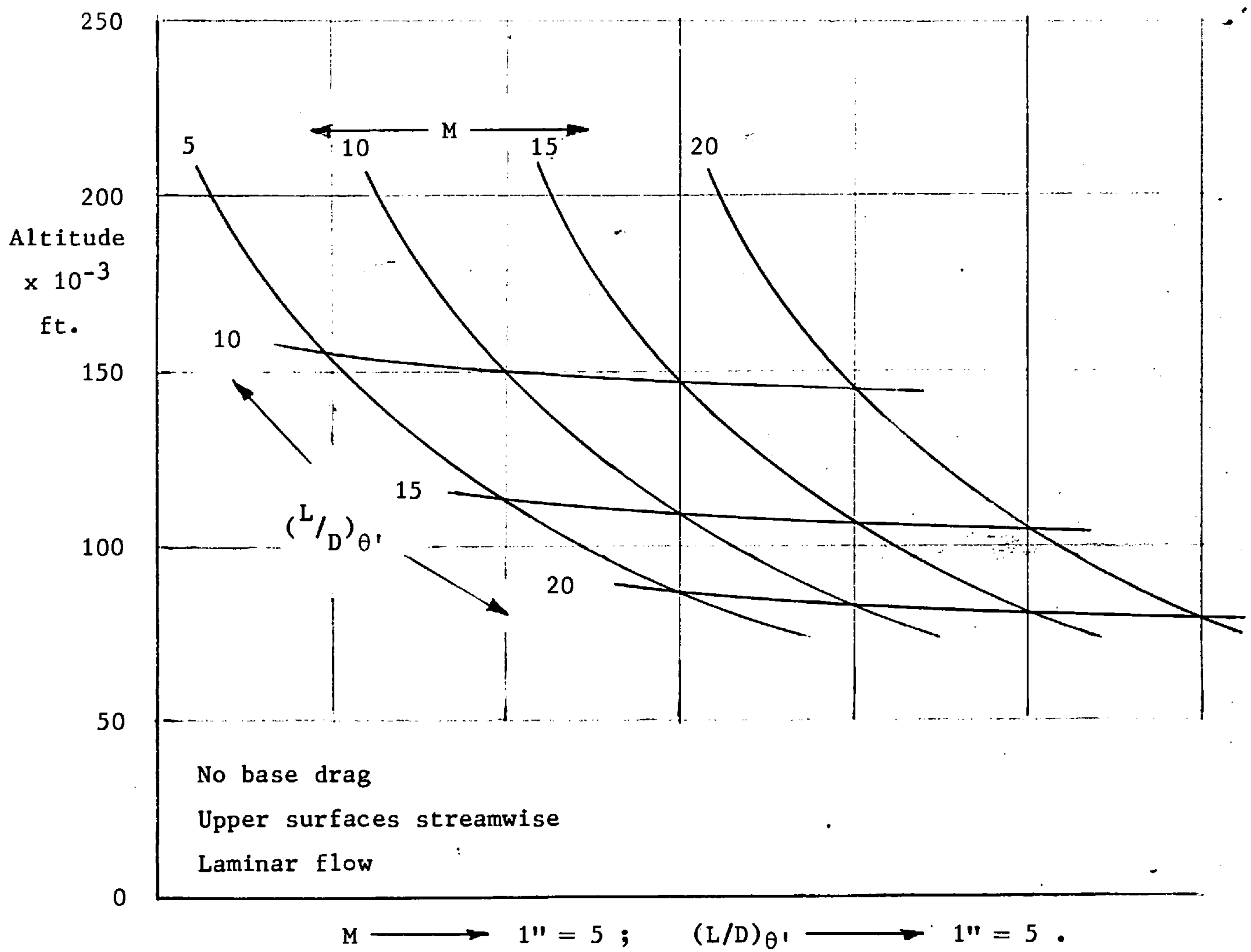

FIG. 2.4 $(L/D)_{\theta'}$ for a delta wing of 200ft length in the atmosphere.

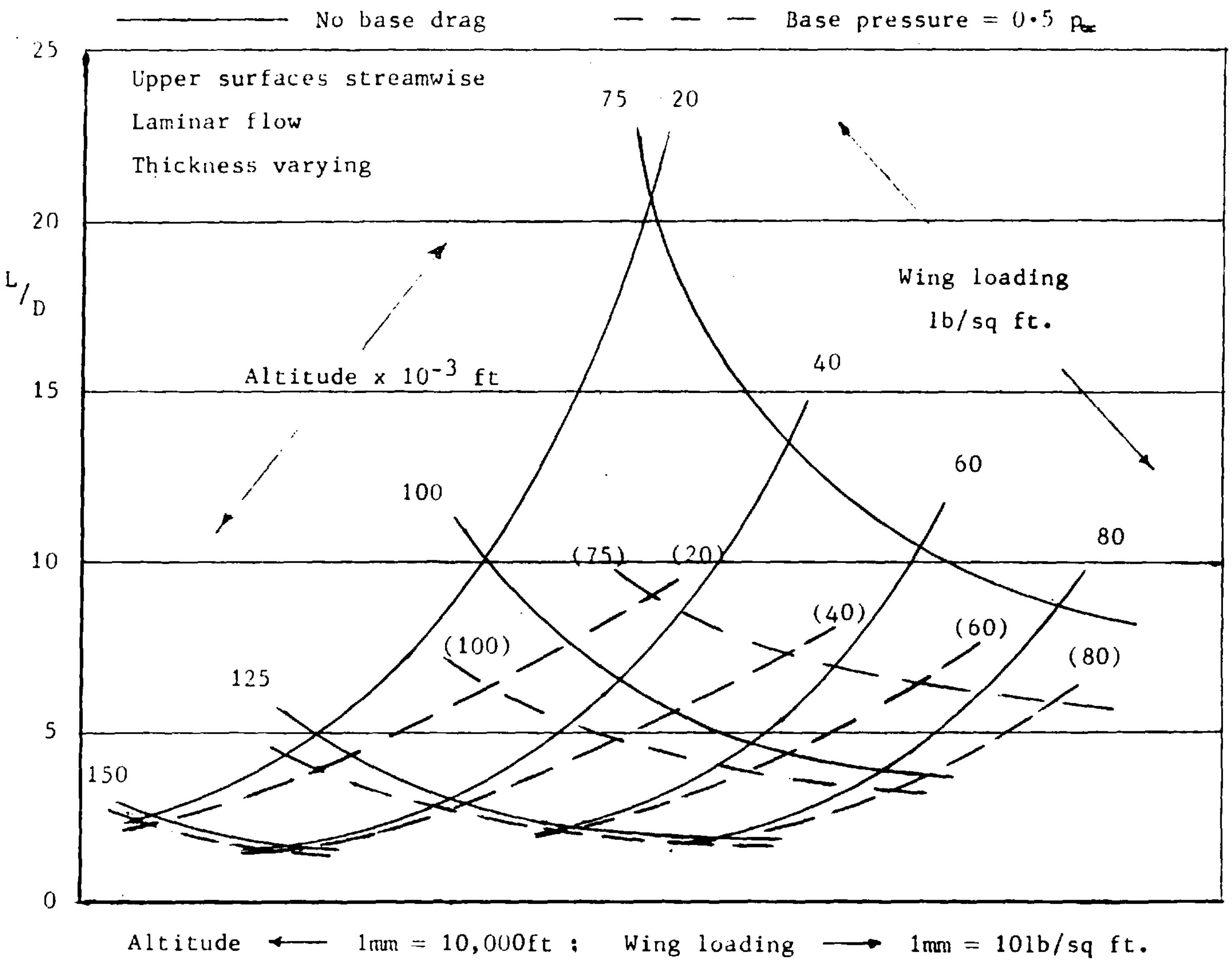

FIG. 2.5 (a) L/D vs wing loading and altitude for a delta wing of 200ft length at M = 5.

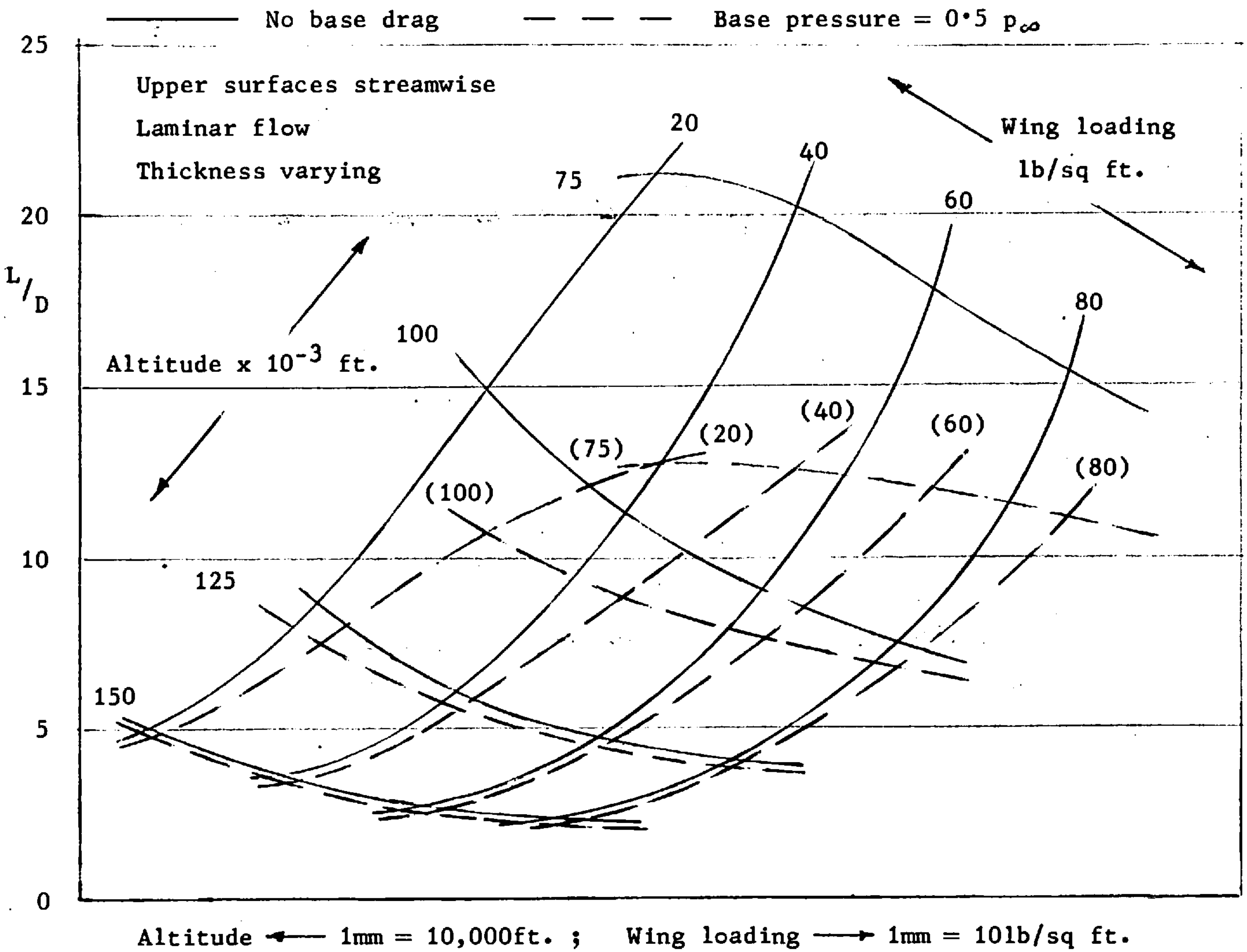

FIG. 2.5 (b) L/D vs wing loading and altitude for a delta wing of 200ft length at M = 10.

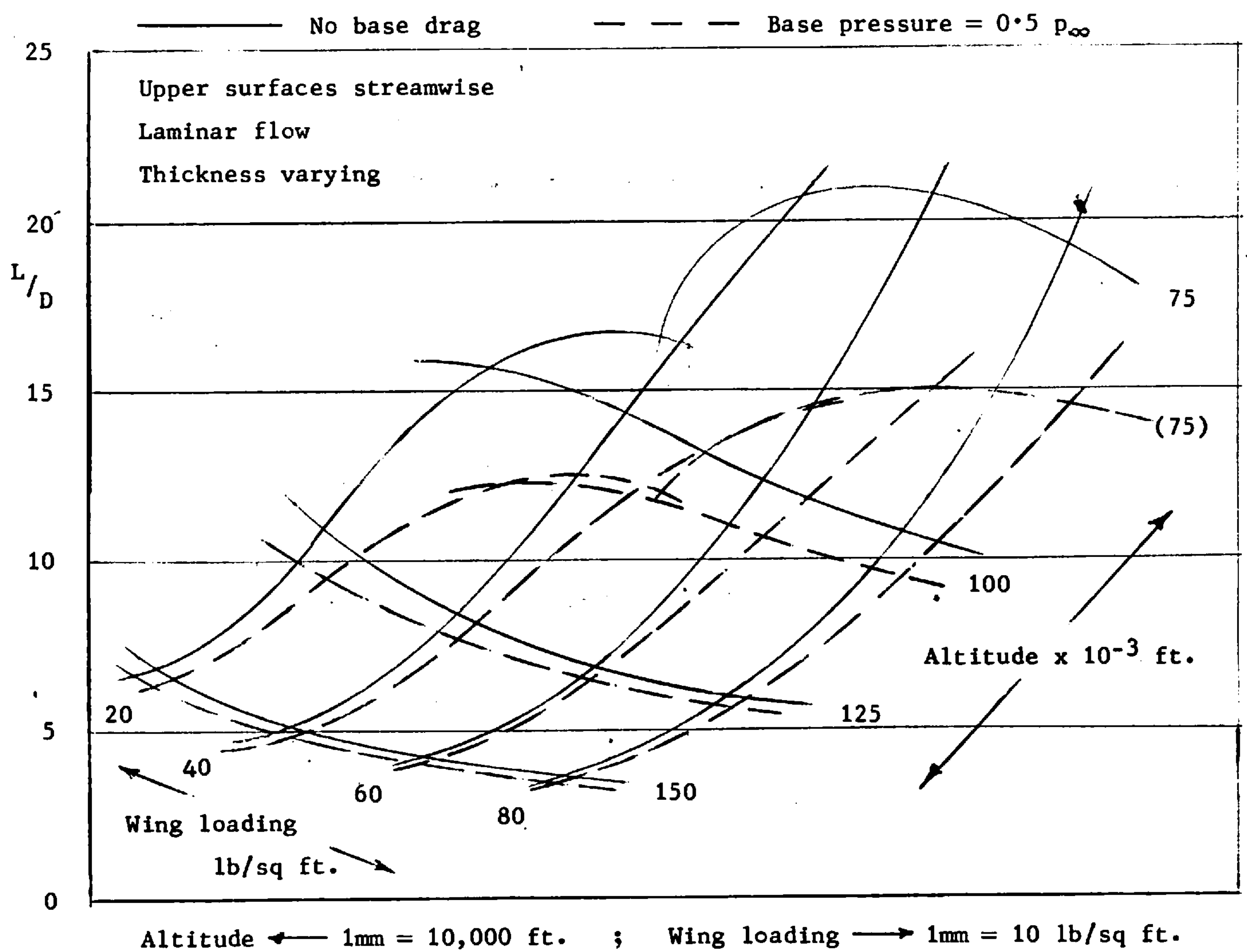

FIG. 2.5 (c) L/D vs wing loading and altitude for a delta wing of 200 ft length at M = 15.

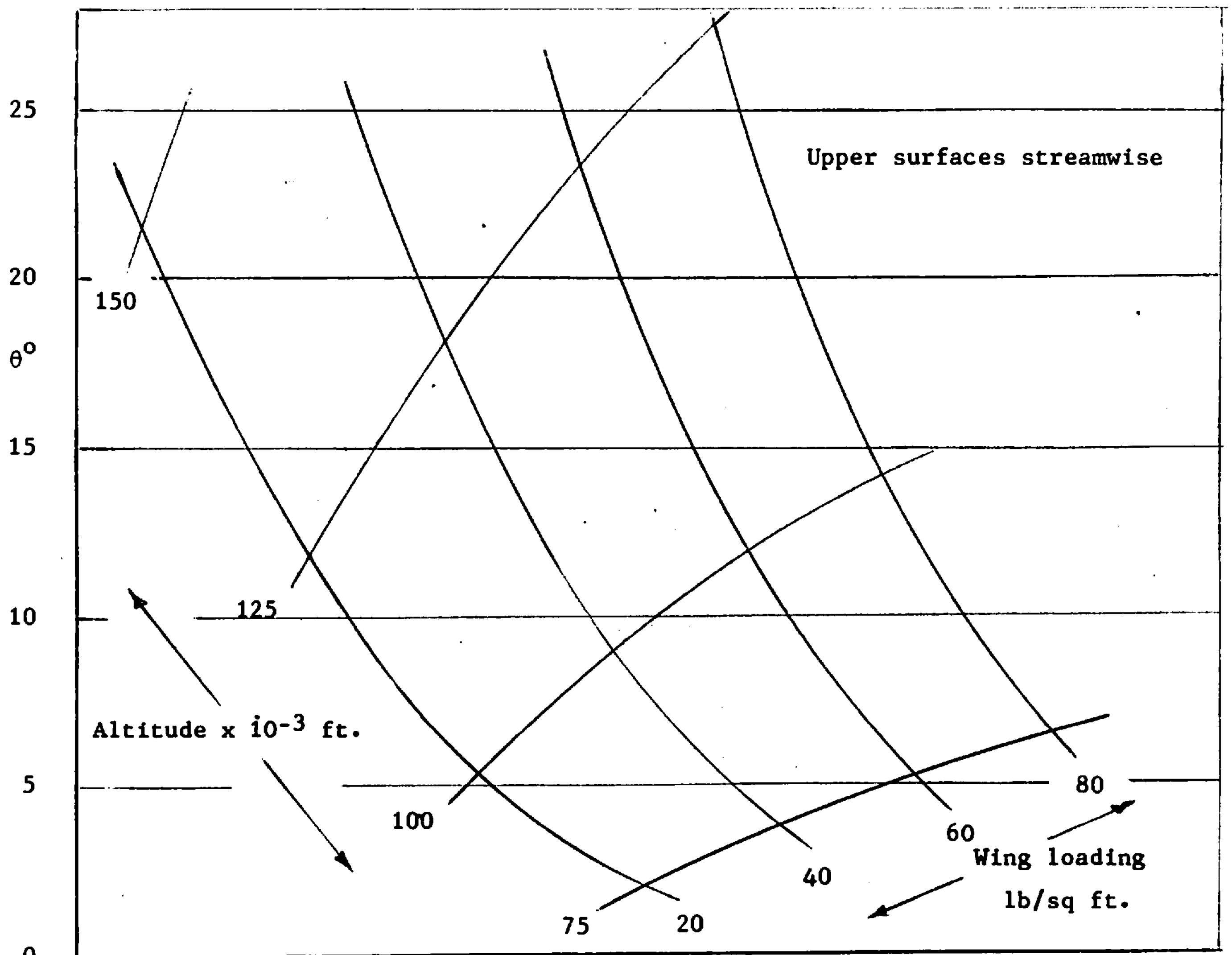

Altitude ← 1mm = 10,000ft ; Wing loading → 1mm = 10lb/sq ft.

FIG. 2.6 (a) Wing thickness angle θ vs wing loading and altitude for a delta wing at M = 5.

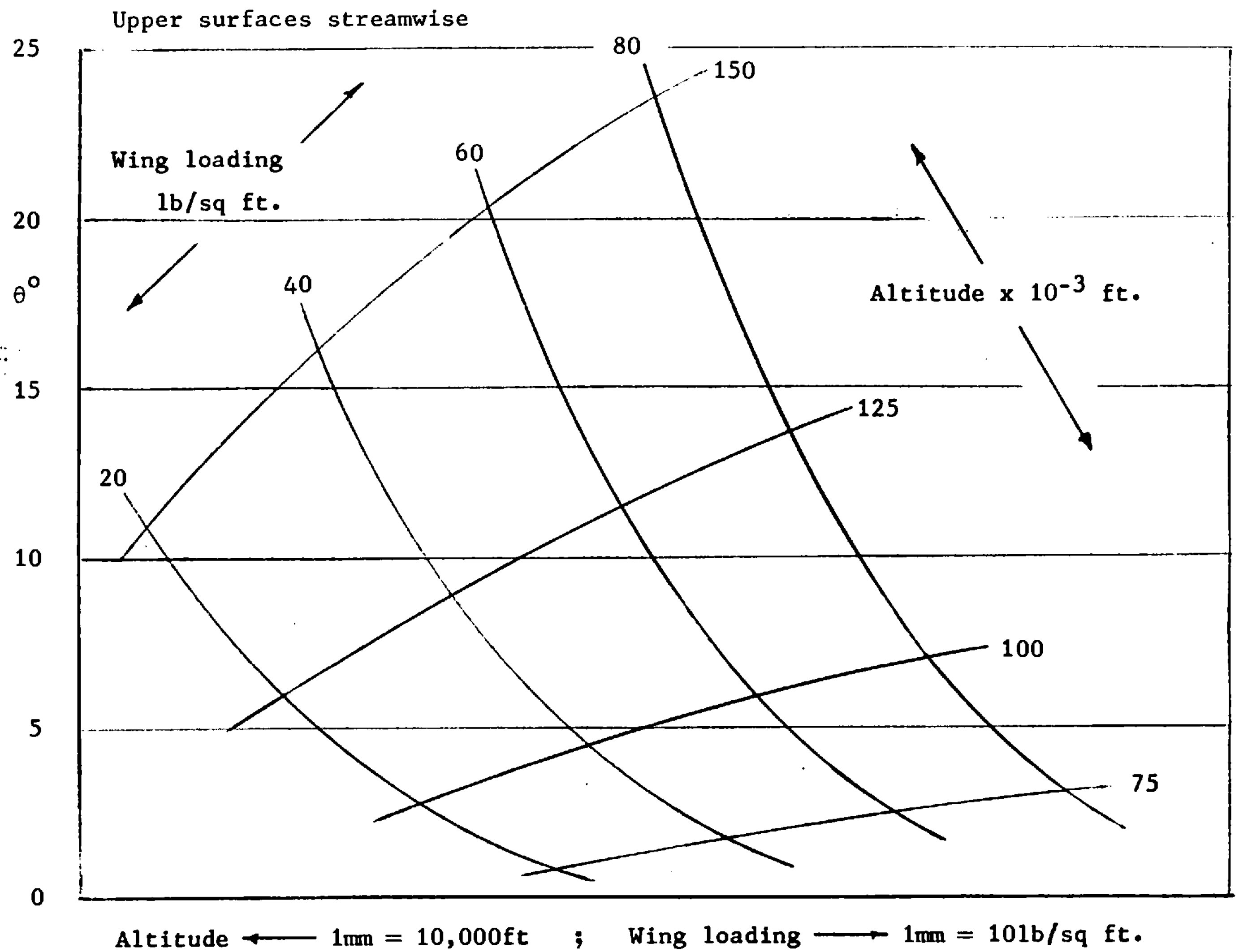

FIG. 2.6 (b) Wing thickness θ vs wing loading and altitude for a delta wing at M = 10.

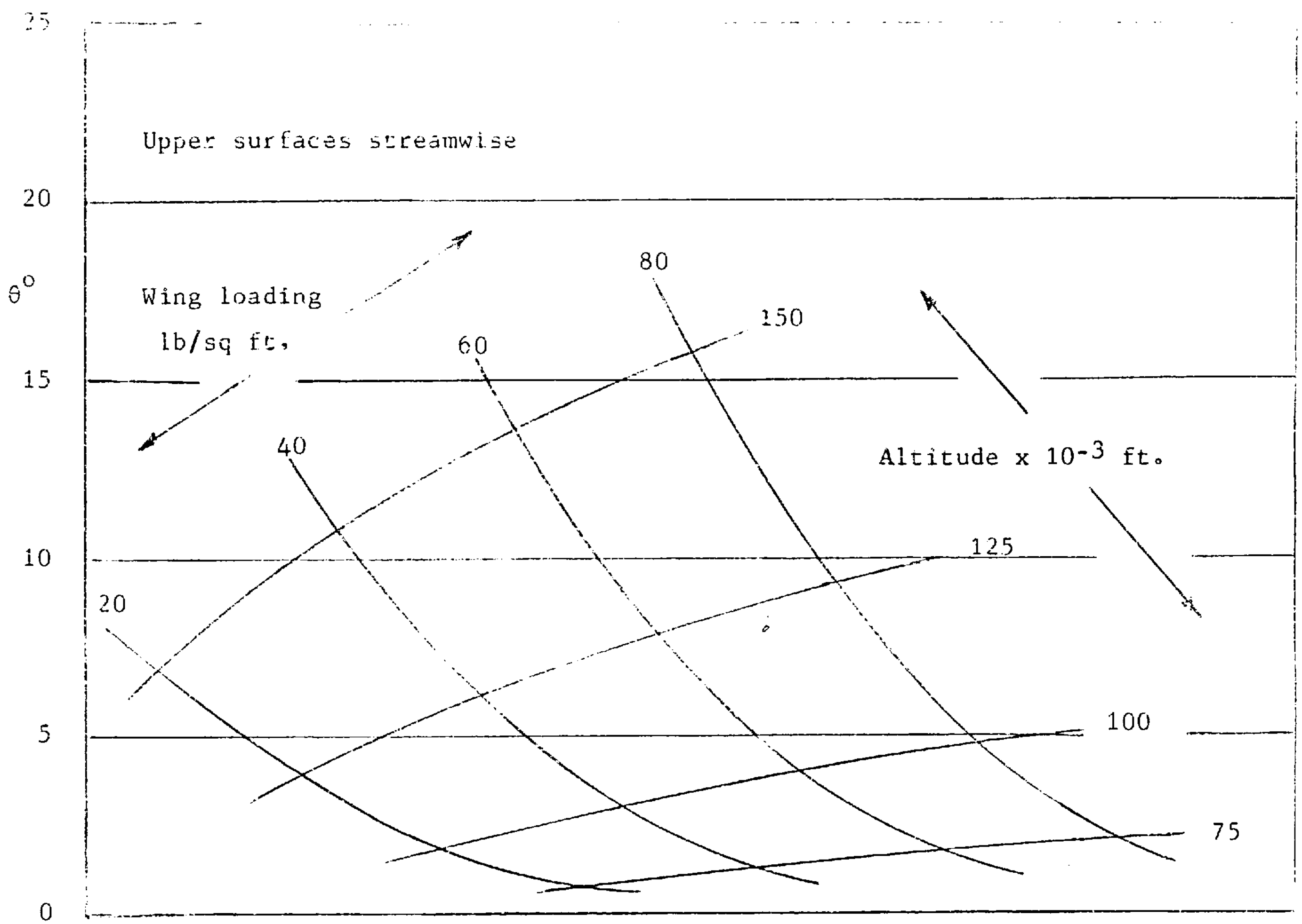

Altitude —— 1mm = 10,000ft. ; Wing loading —— 1mm = 10lb/sq ft.

FIG. 2.6 (c) Wing thickness θ vs Wing loading and altitude for a delta wing at M = 15.

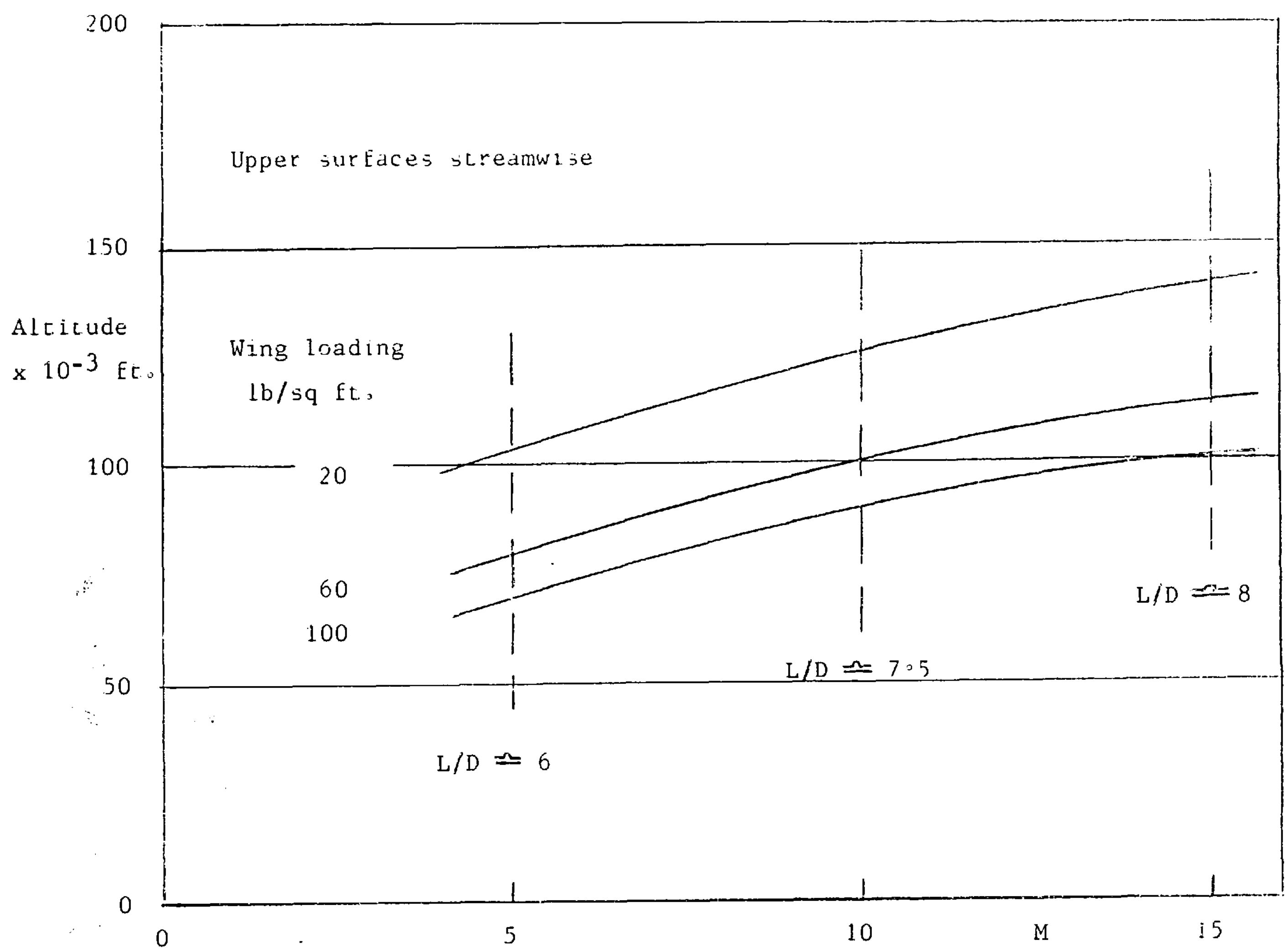

FIG 2.7 (a) Performance of a 200ft delta wing of constant thickness angle in the atmosphere, $\theta = 6^{\circ}$.

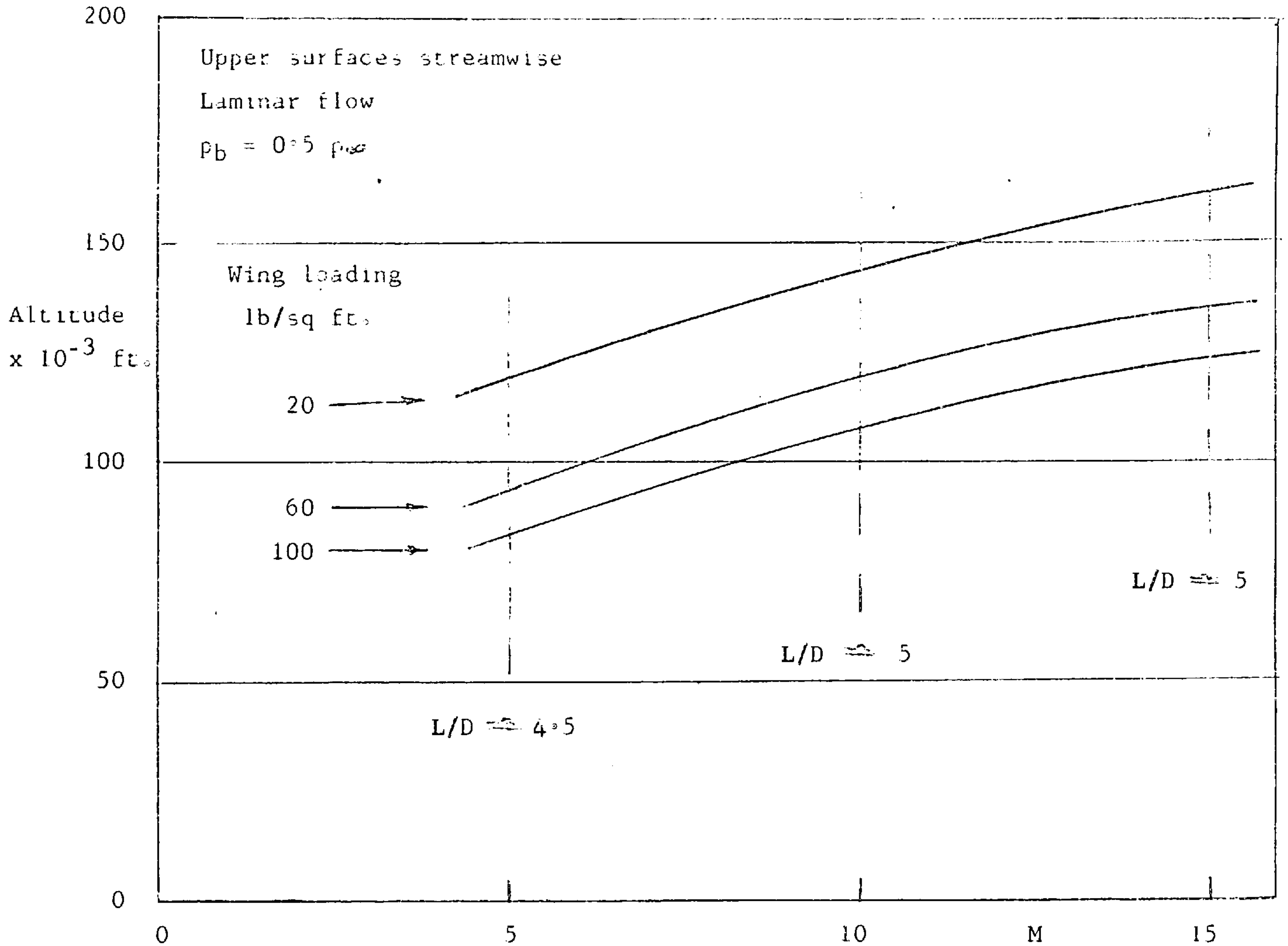

FIG. 2.7 (b) Performance of a 200ft delta wing of constant thickness angle in the atmosphere, $\theta = 10^{o}$.

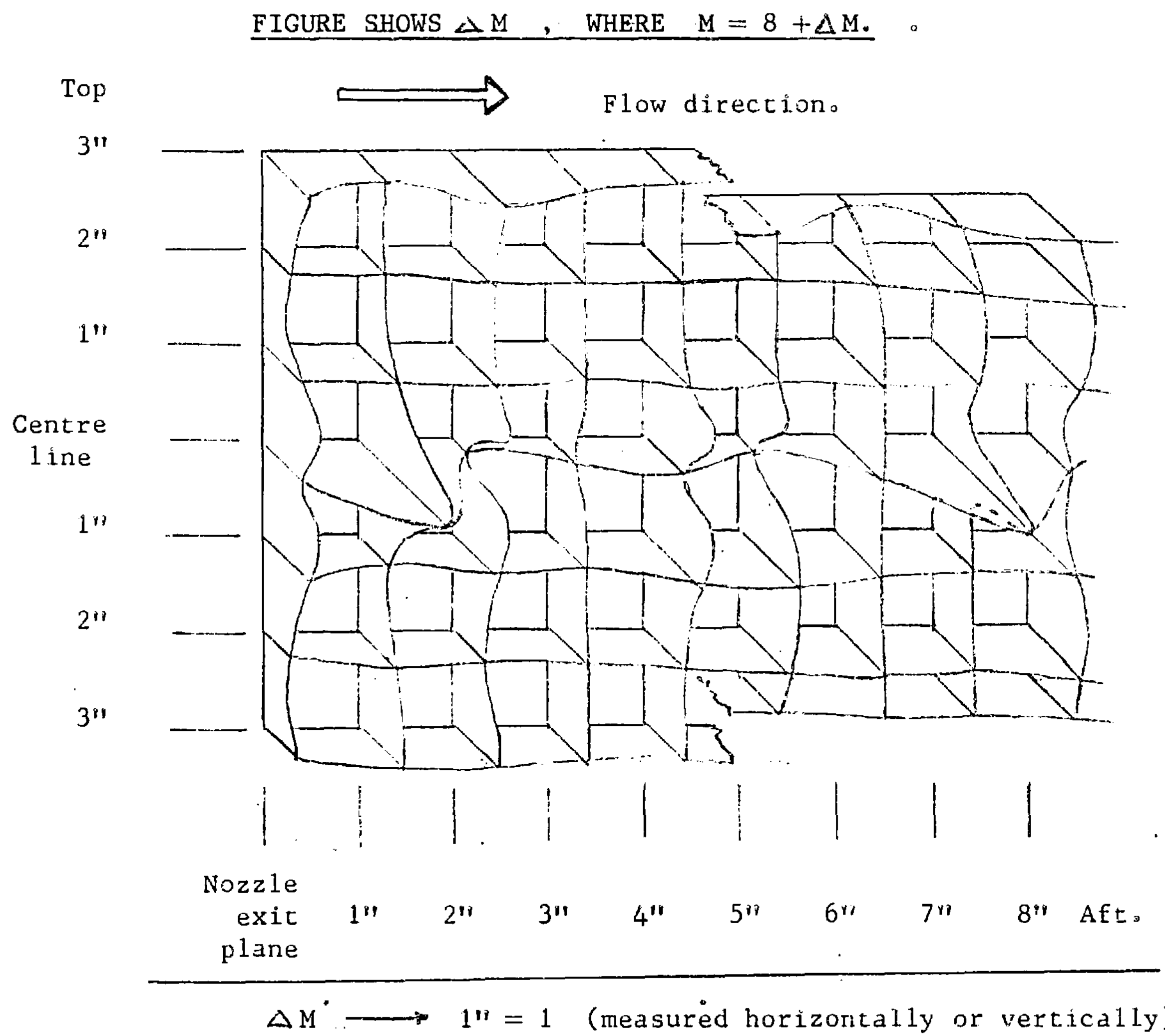

FIG. 3.1 (a) Mach No. distribution in the tunnel on the vertical centre line.

FIGURE SHOWS ΔM , WHERE $M = 8 + \Delta M$.

Flow direction, into paper.

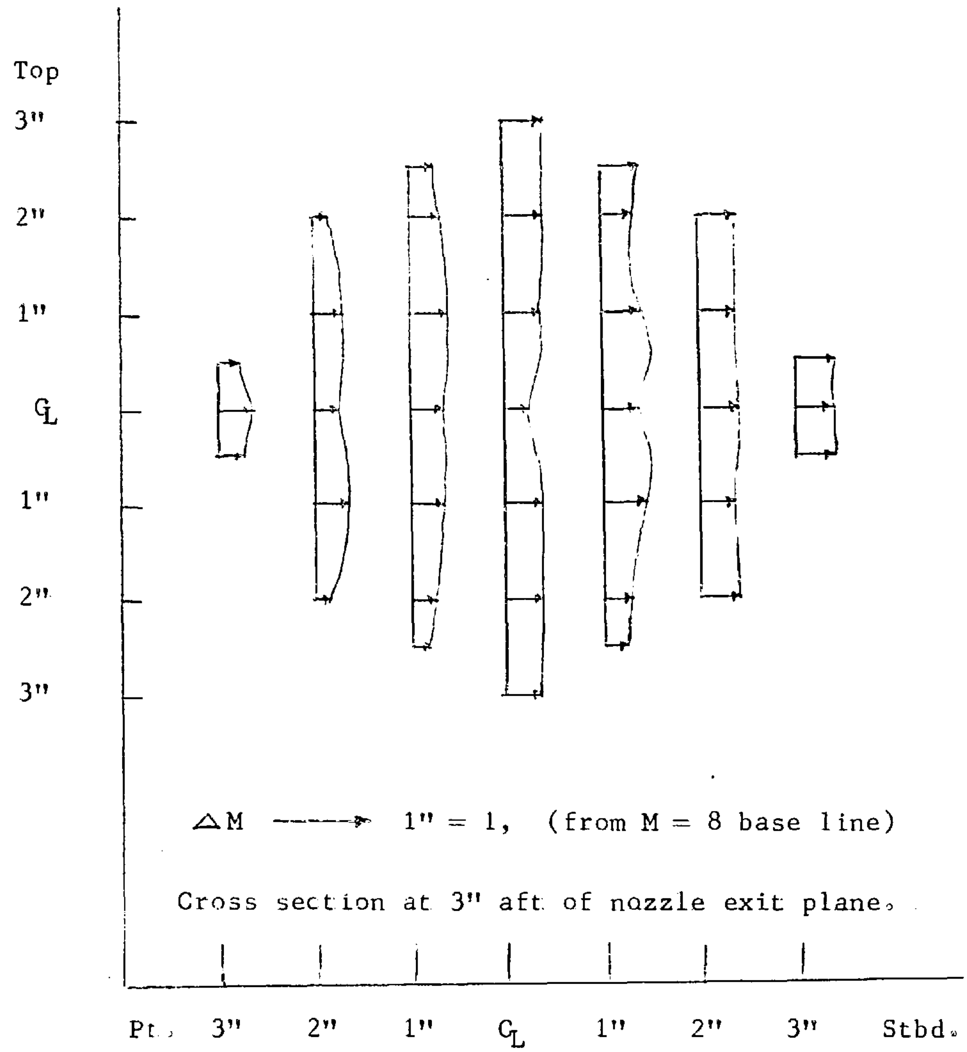

Fig. 3.1 (b) Mach No. distribution in the tunnel. Lateral cross section.

Pitot
pressure.

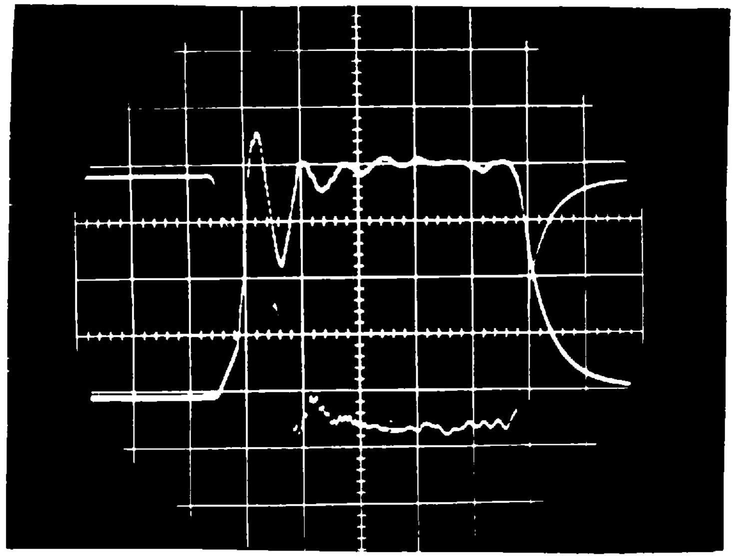

10msec/cm.

(a) Normal

Pitot
pressure.

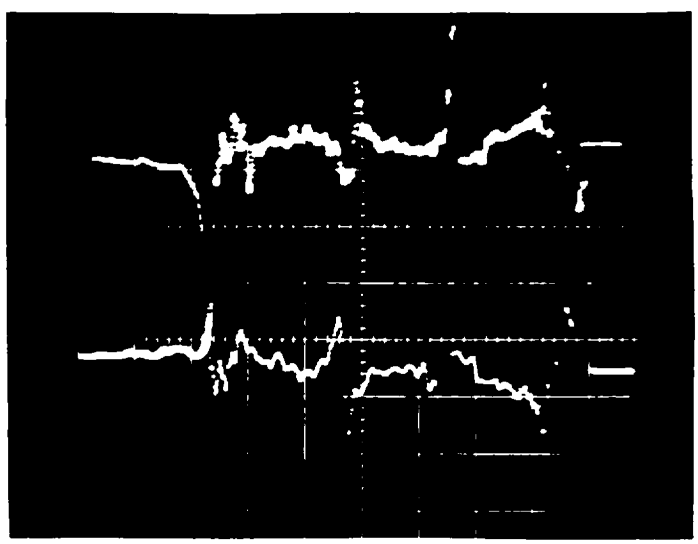

10msec/cm.

(b) With pressurized barrel.

FIG. 3.2 Tunnel calibration; typical traces.

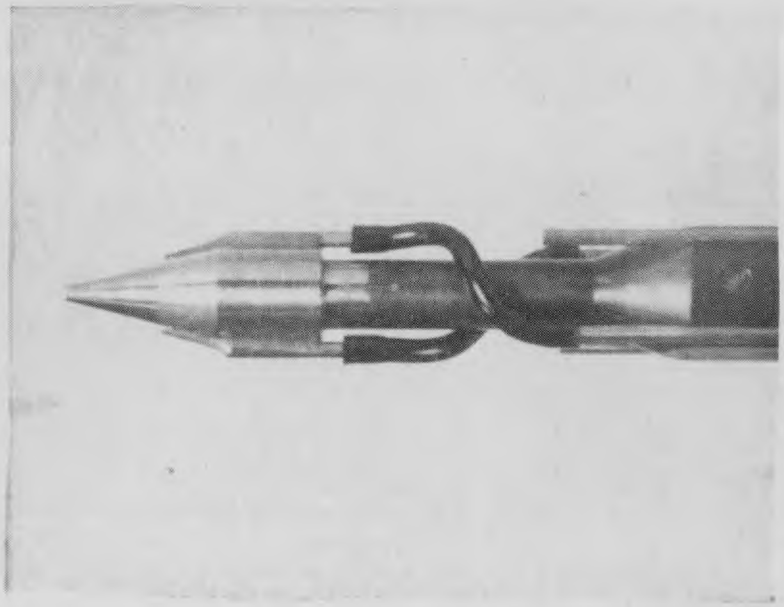

(a) Sensing head.

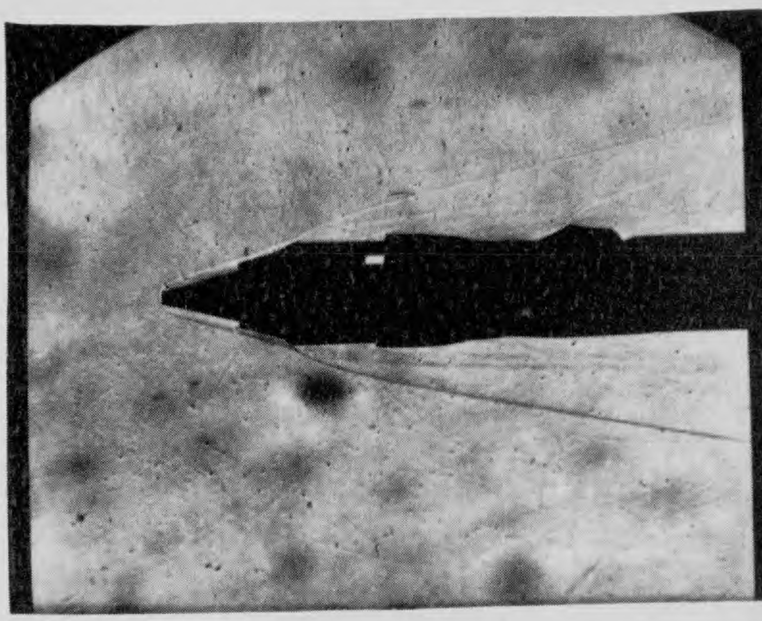

(b) [illegible] flow.

FIG. 3.3 The 'pressure recovery' flow inclination probe.

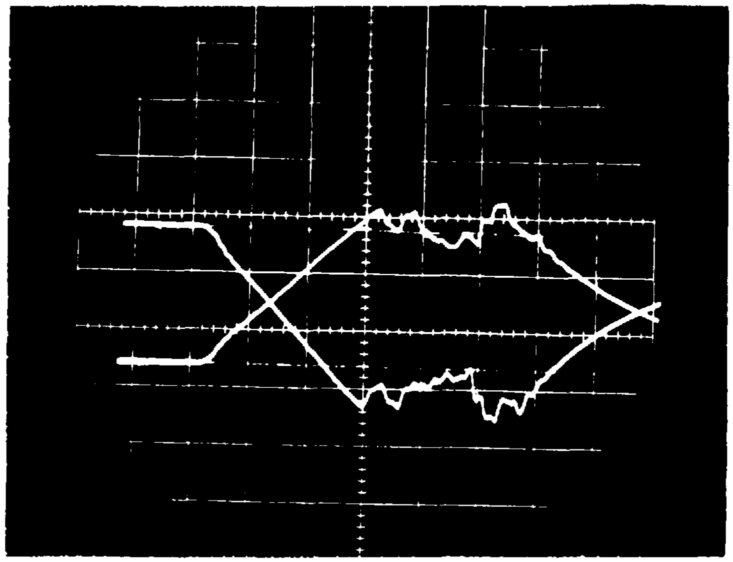

FIG. 3.3 (c) Typical flow inclination probe trace.

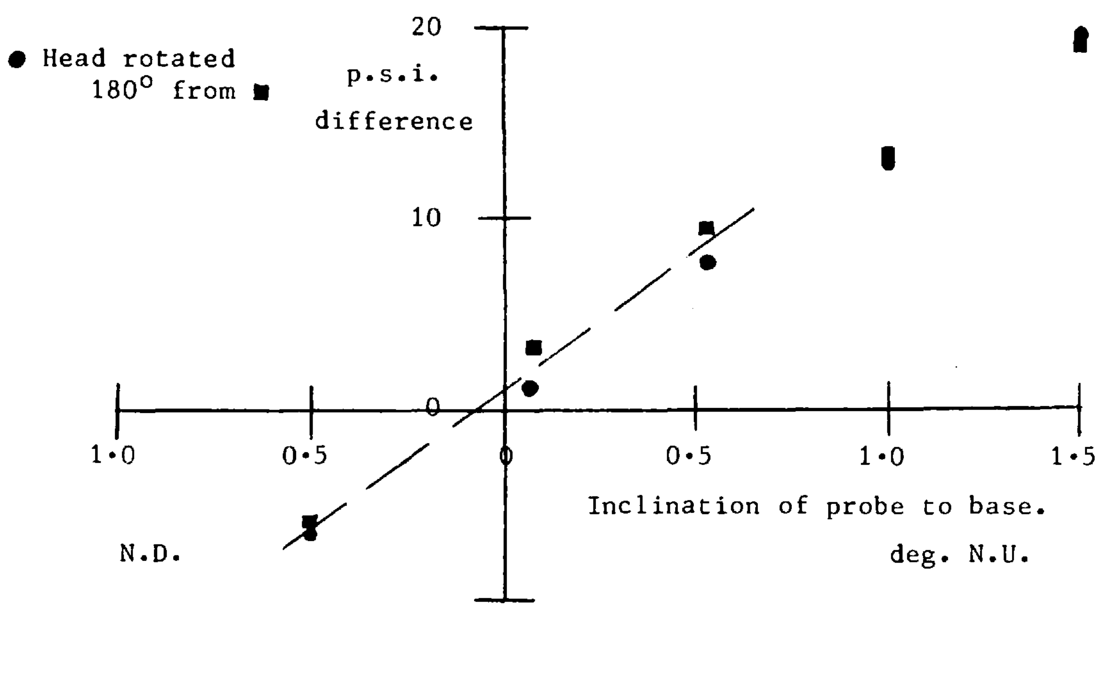

FIG. 3.4 Results of flow inclination probe measurements at 1" below centre line.

Top.

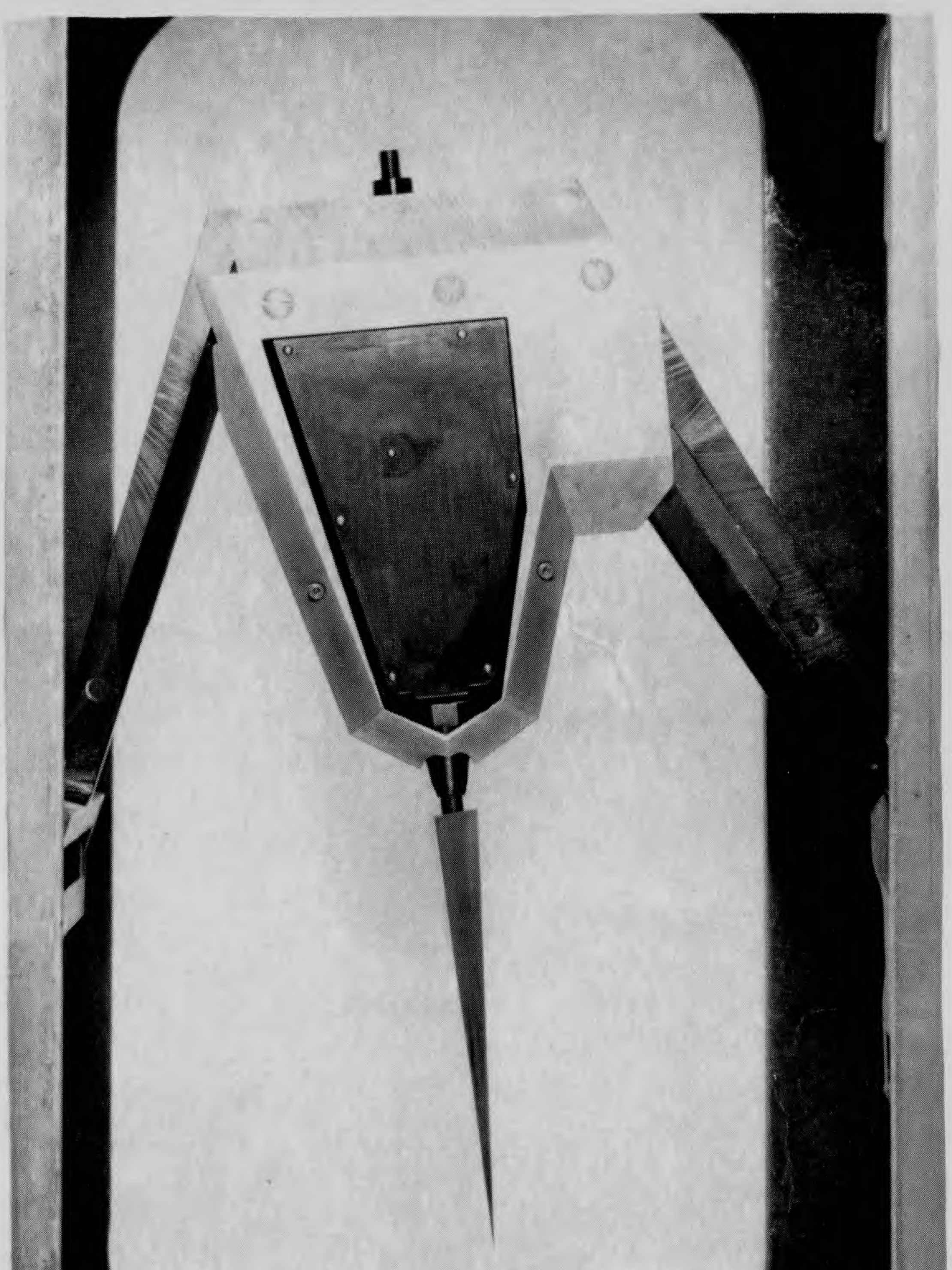

FIG. 3.5 The Mk III balance and a model in the tunnel.

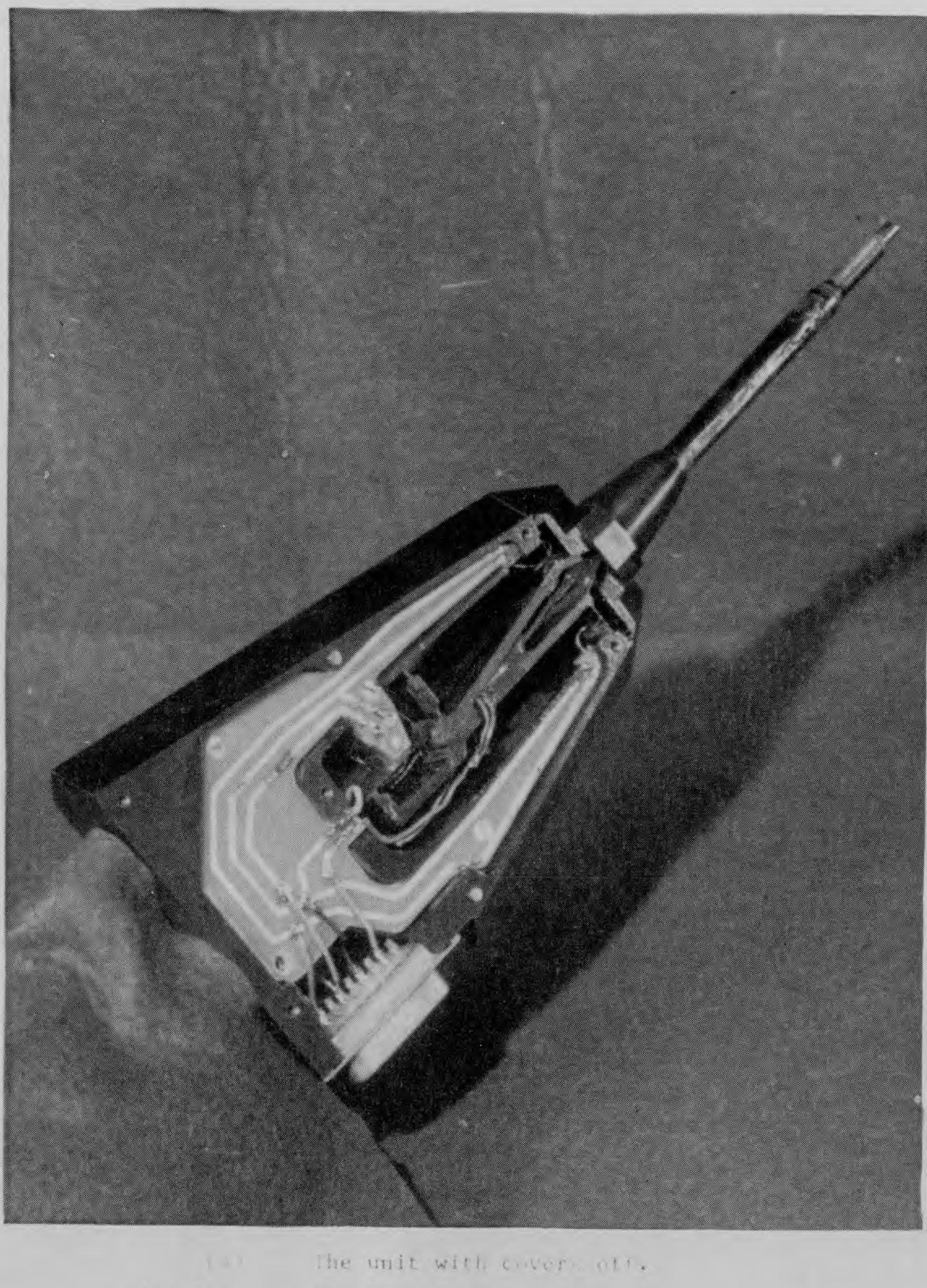

(a) The unit with covers off.

FIG. 3.6 The balance 'plug-in' unit.

FIG. 3.6 (b) The balance " plug-in " unit.
General arrangement.

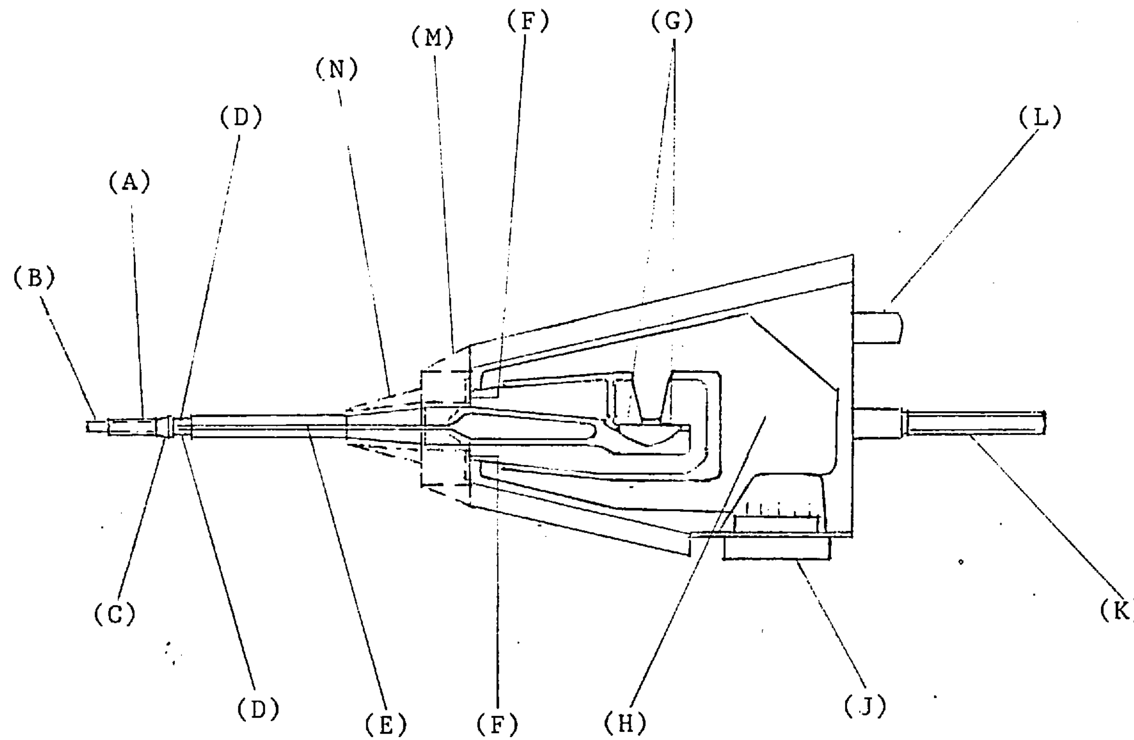

$^1/_2$ Scale. Gauges at (D),(F) and (G).

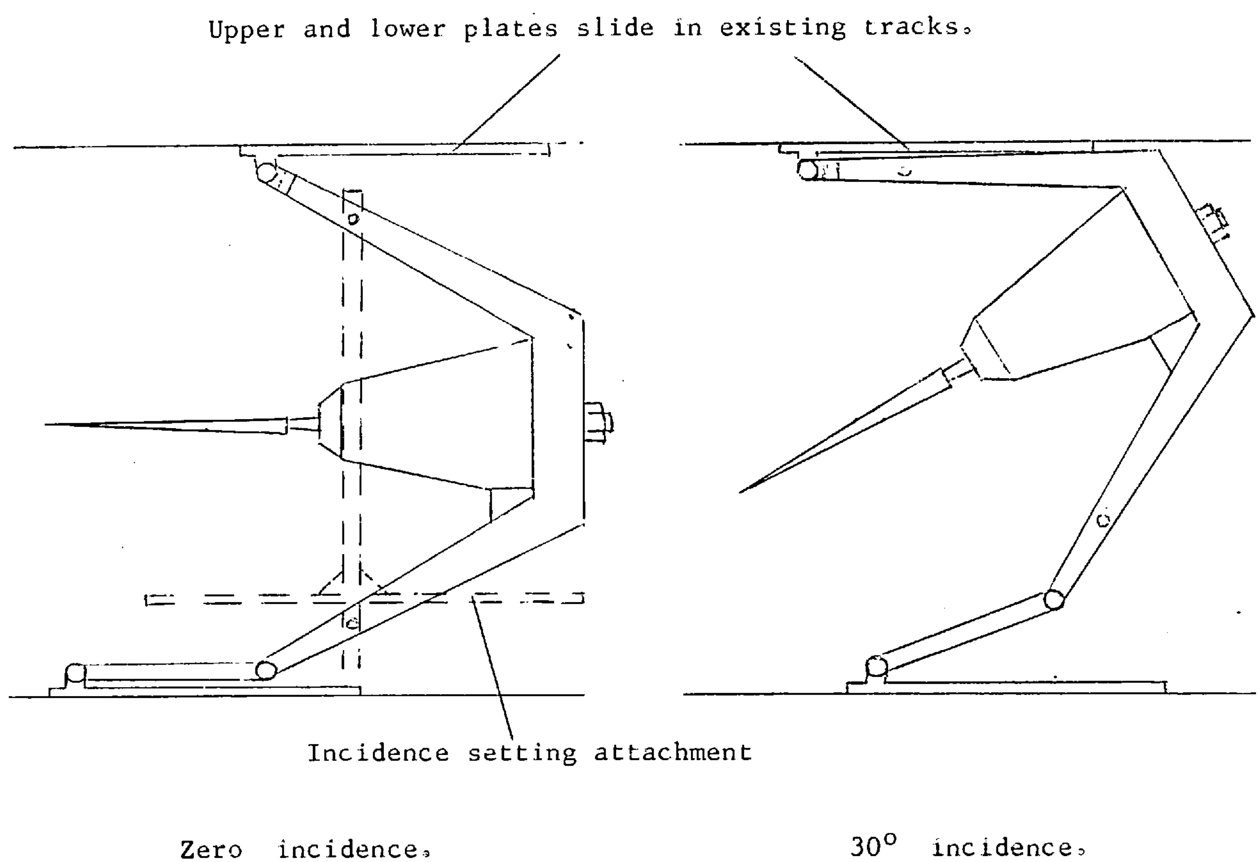

FIG. 3.7 (a) Incidence setting and adjustment.

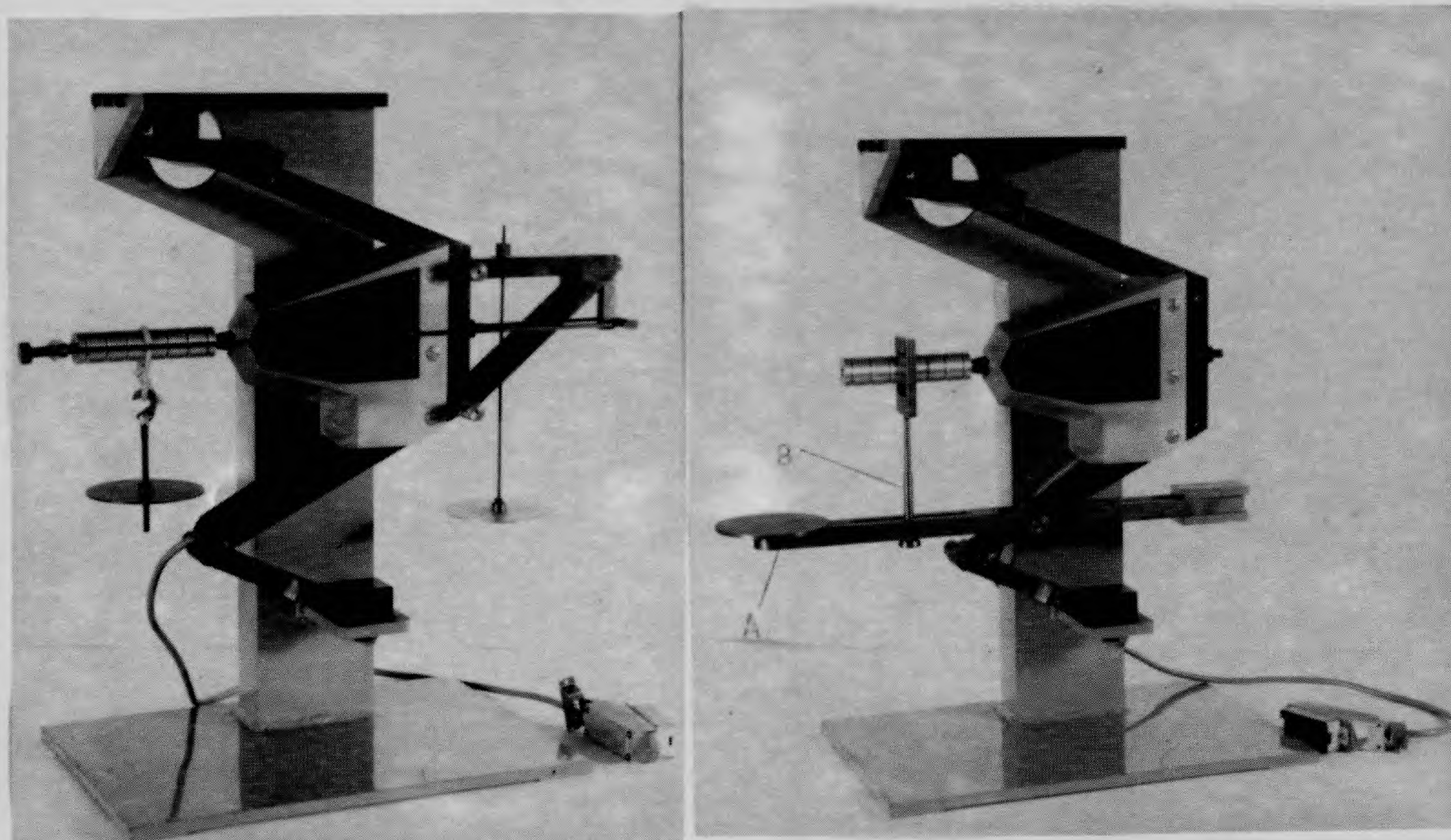

for static calibration. for dynamic interaction.

FIG. 3.7 (b) Calibration equipment.

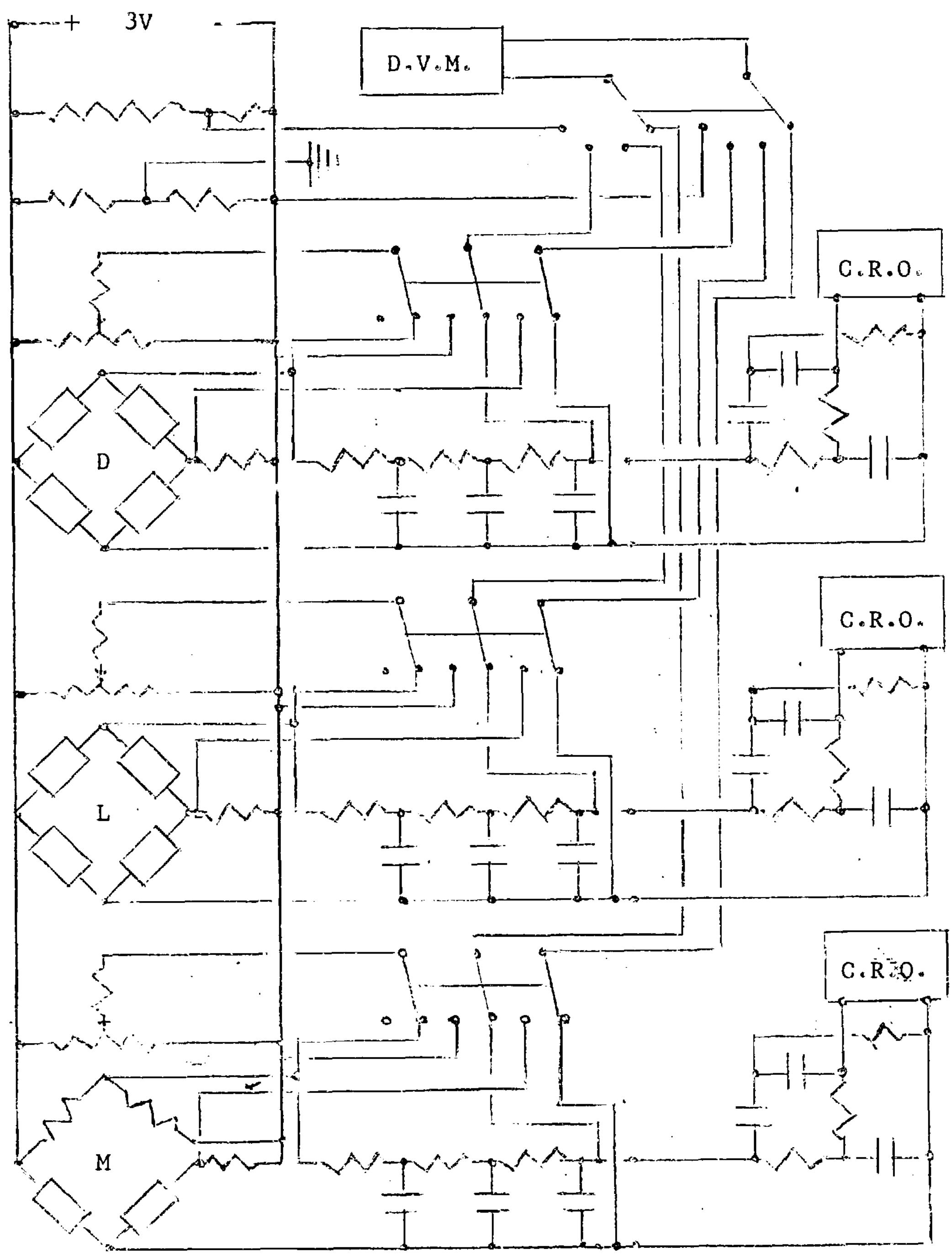

FIG. 3.8 Circuit diagram.

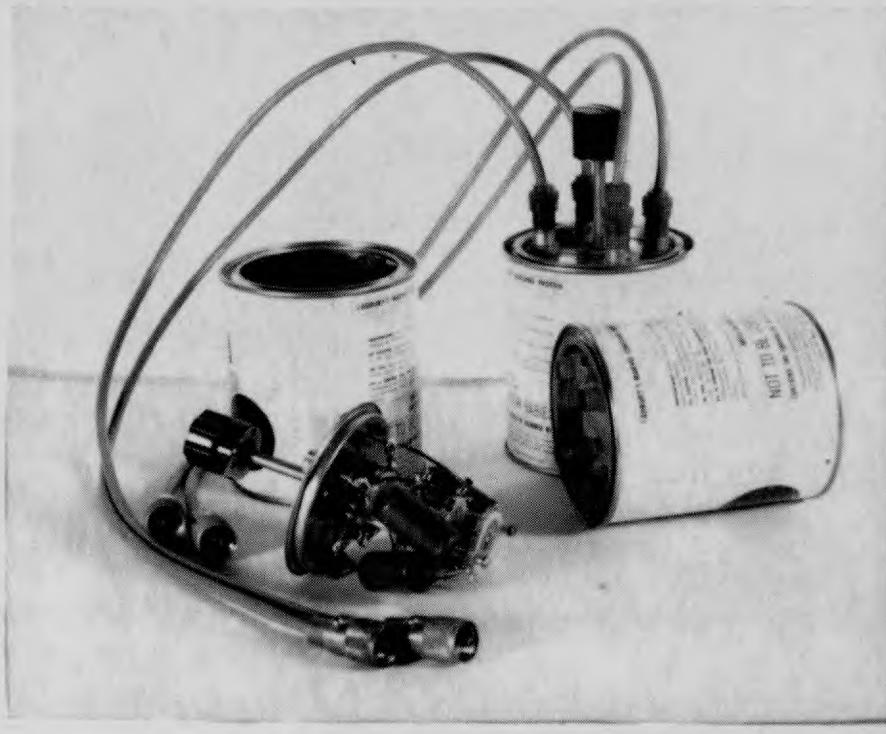

(b) Photograph of units.

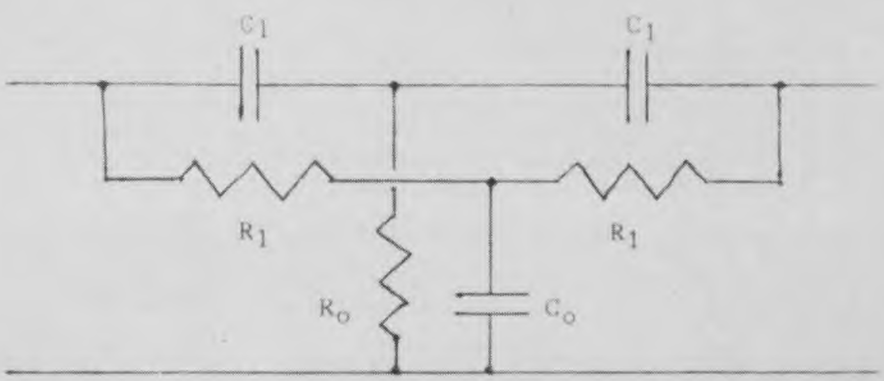

$R_1 = 2R_o$: $C_o = 2C_1$.

(a) Circuit.

FIG. 3.9 The 'parallel T' filters.

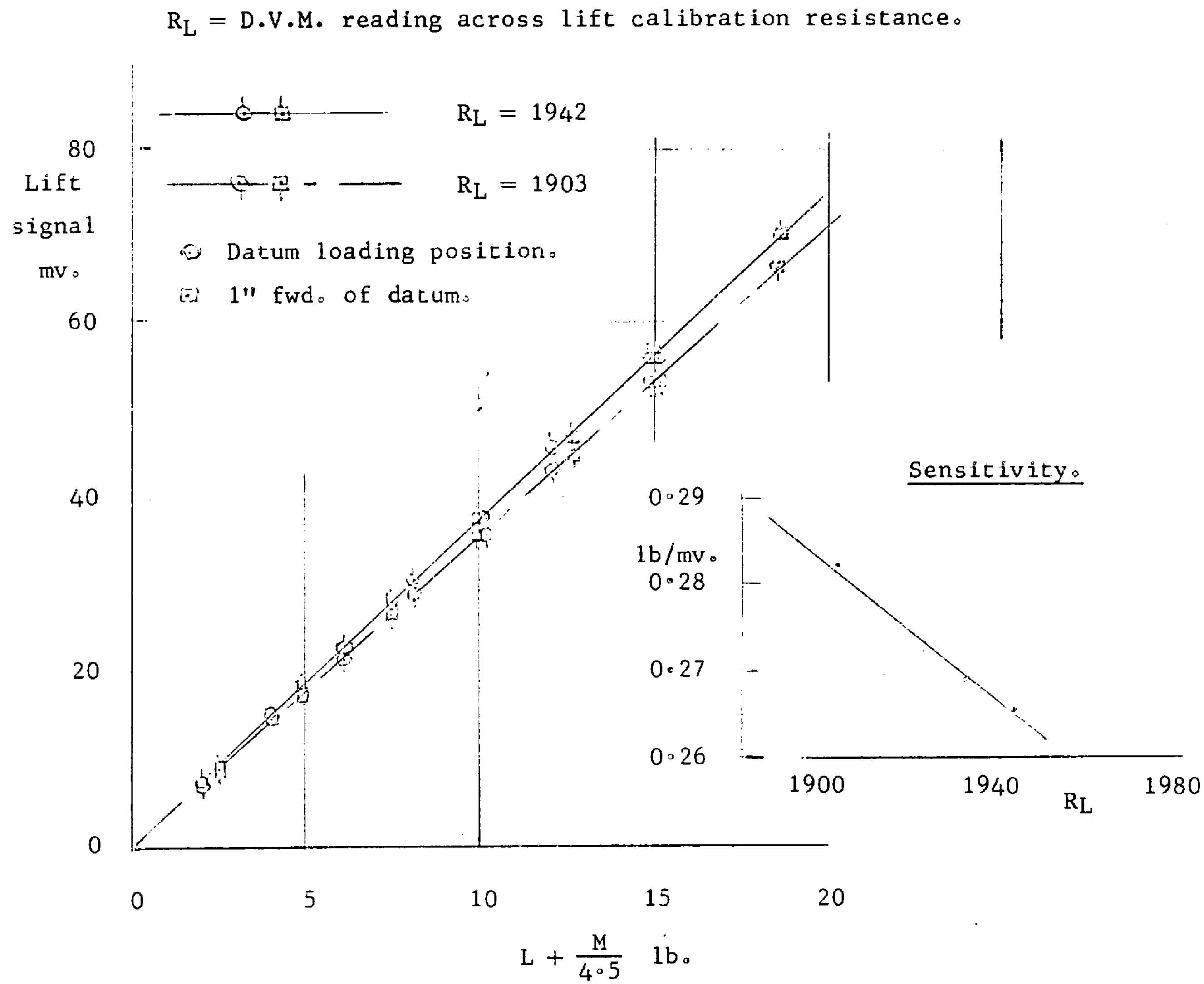

FIG. 3.10 (a) Lift. Static calibration.

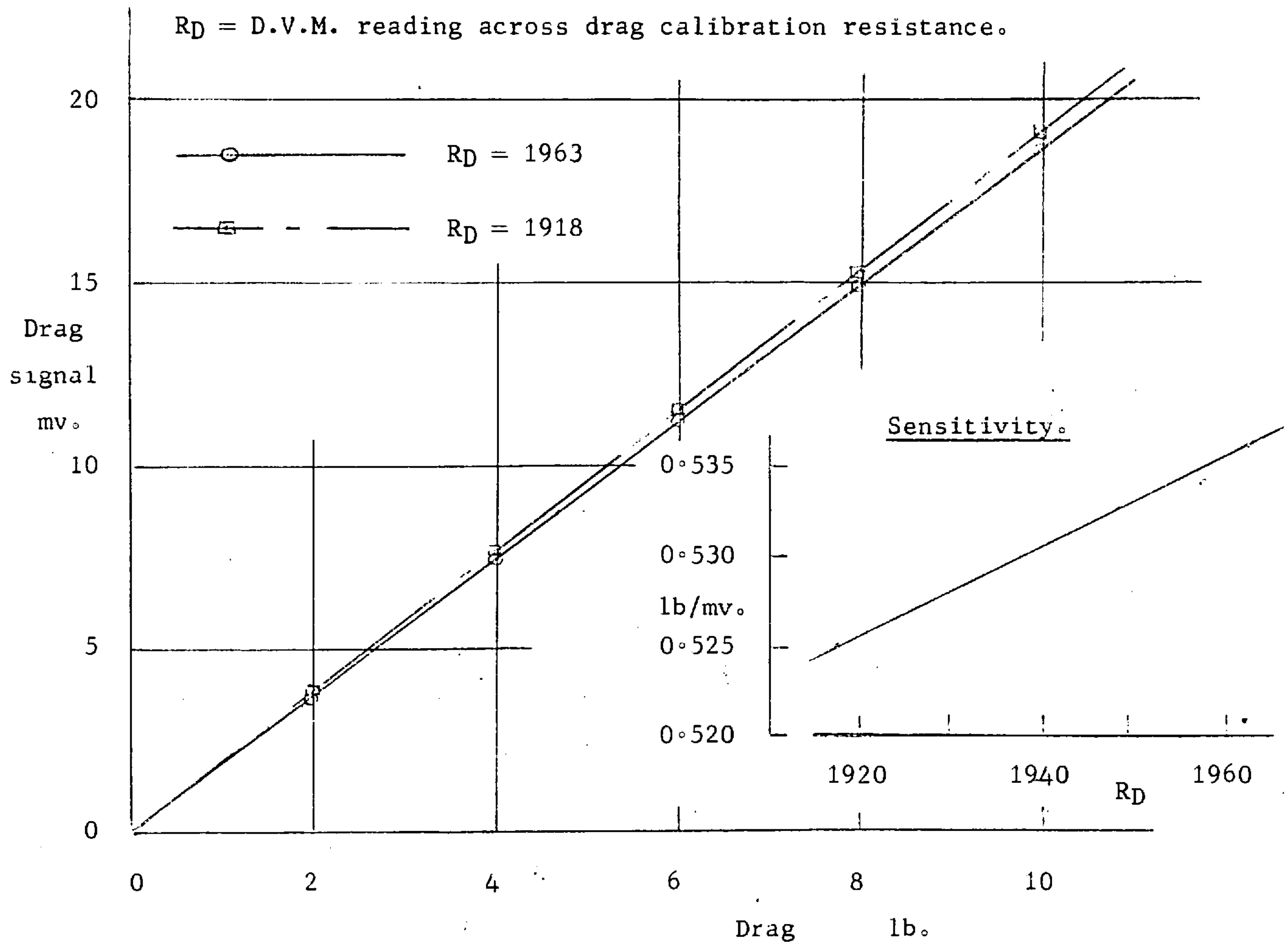

FIG. 3.10 (b) Drag. Static calibration.

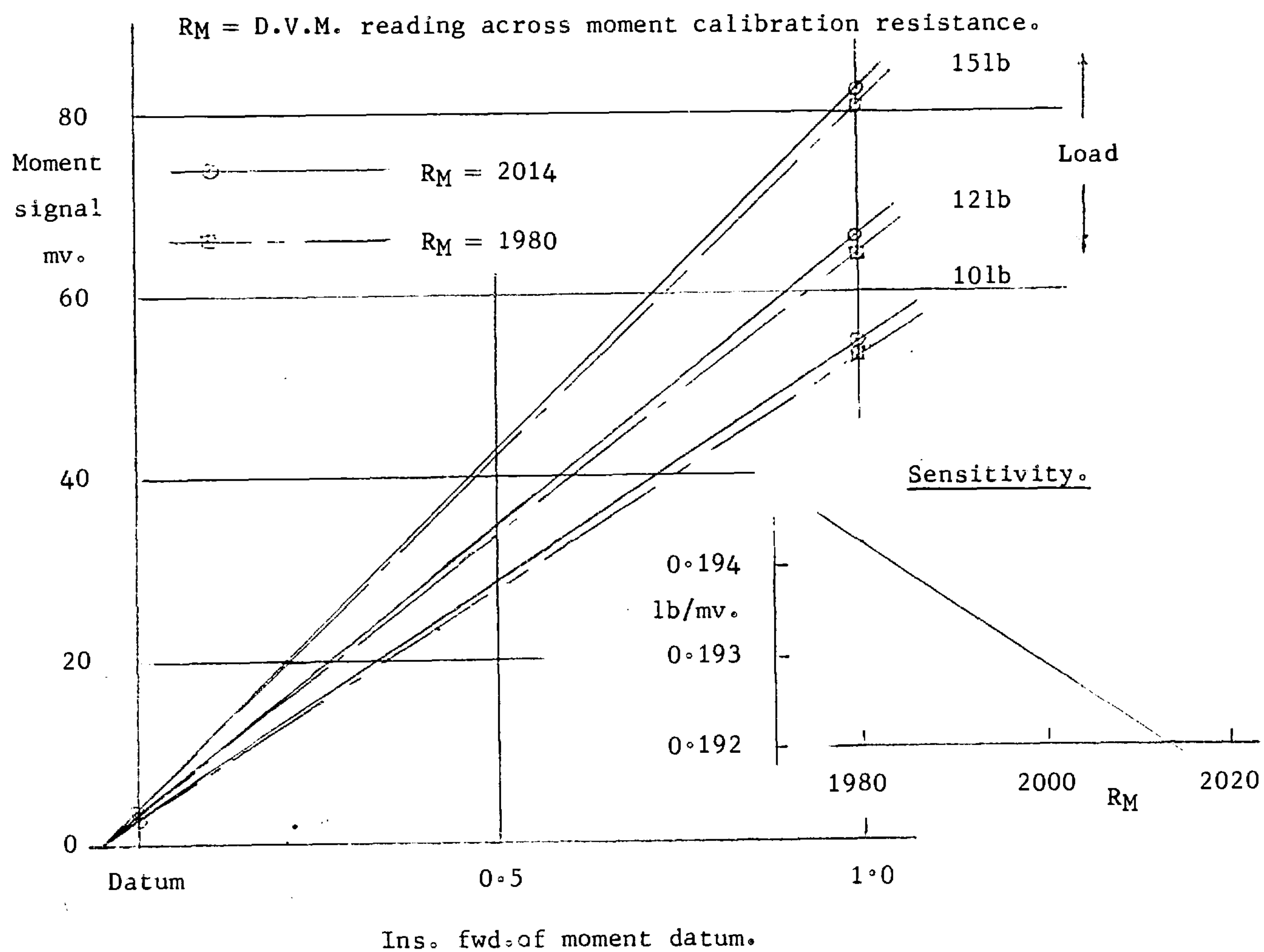

FIG. 3.10 (c) Pitching moment. Static calibration.

Drag

200μv/cm.

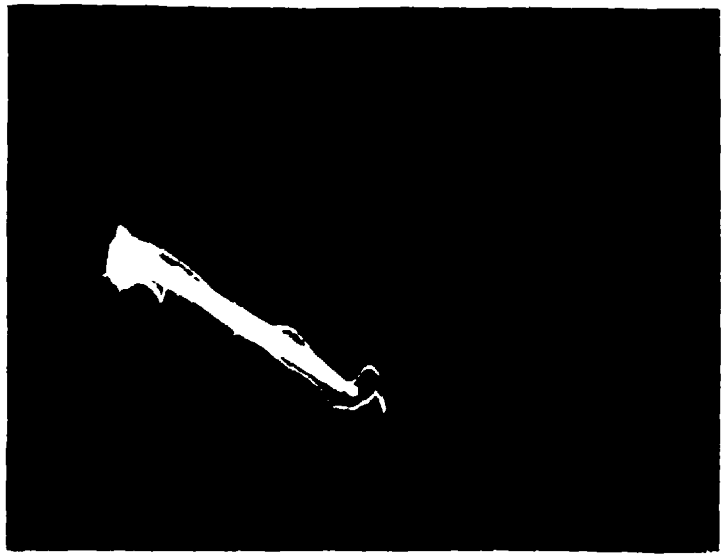

Lift 10mv / cm. →

(a) Lift on drag.

Drag ↑

2mv/cm.

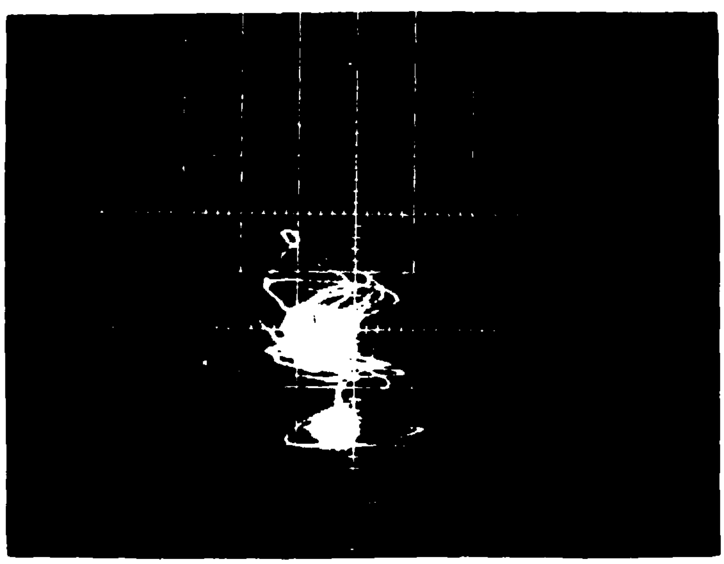

Lift 200μv / cm.

(b) Drag on lift.

FIG. 3.11 Dynamic interaction; typical traces.

Drag
200μv/cm.

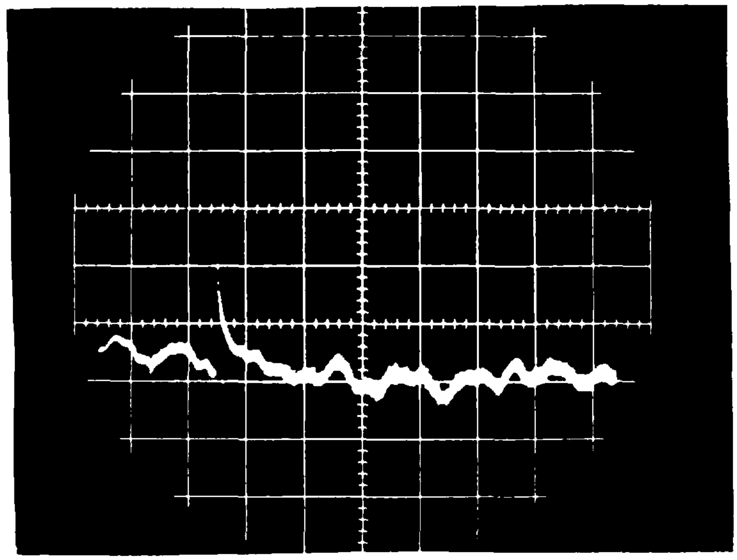

→ 20msec/cm.

Conditions for $R_e = 0{\cdot}9 \times 10^6$ runs.

Drag
200μv/cm.

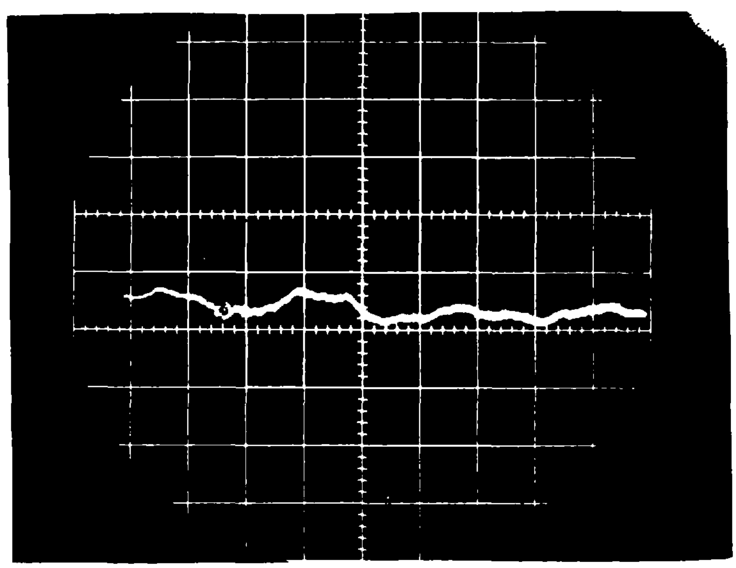

→ 20msec/cm.

Conditions for $R_e = 3{\cdot}5 \times 10^6$ runs.

FIG. 3.12 Tare calibration; typical traces.

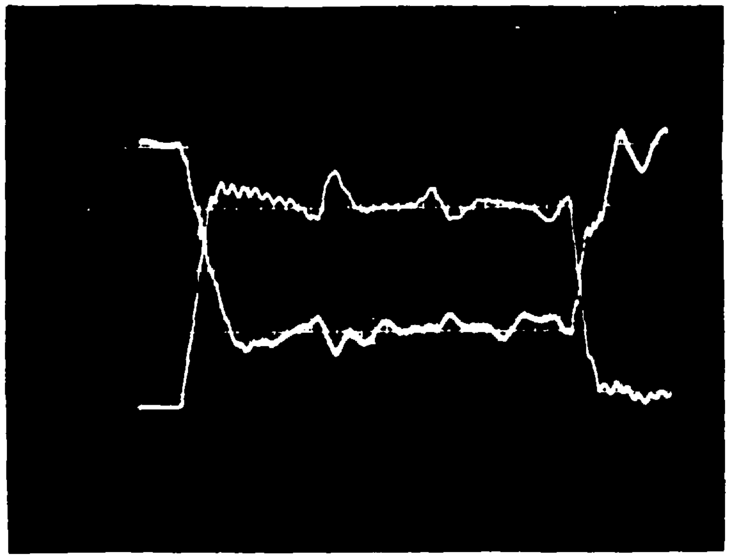

(a) Lift and drag, $R_e = 3{\cdot}5 \times 10^6$.

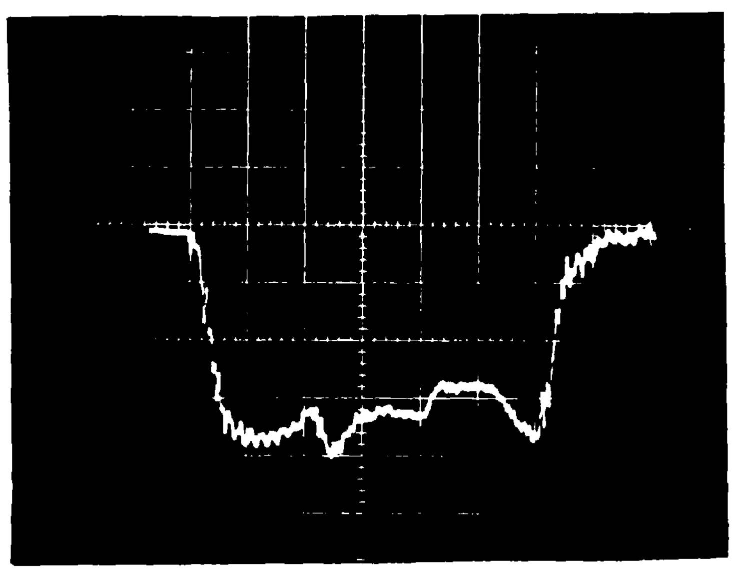

(b) Pitching moment, $R_e = 3{\cdot}5 \times 10^6$.

FIG. 3.13 Force measurement: typical traces, $M = 8{\cdot}3$.

Drag.

Lift

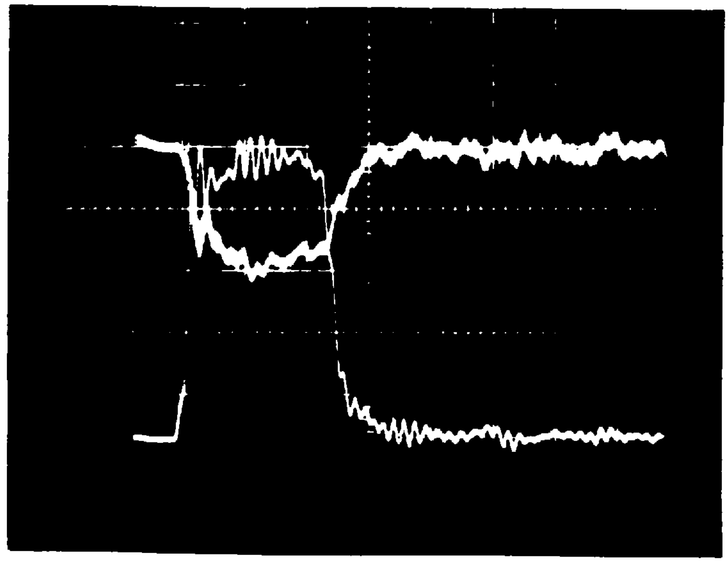

20msec/cm.

(c) Lift and drag, $R_e = 0 \cdot 9 \times 10^6$.

Drag

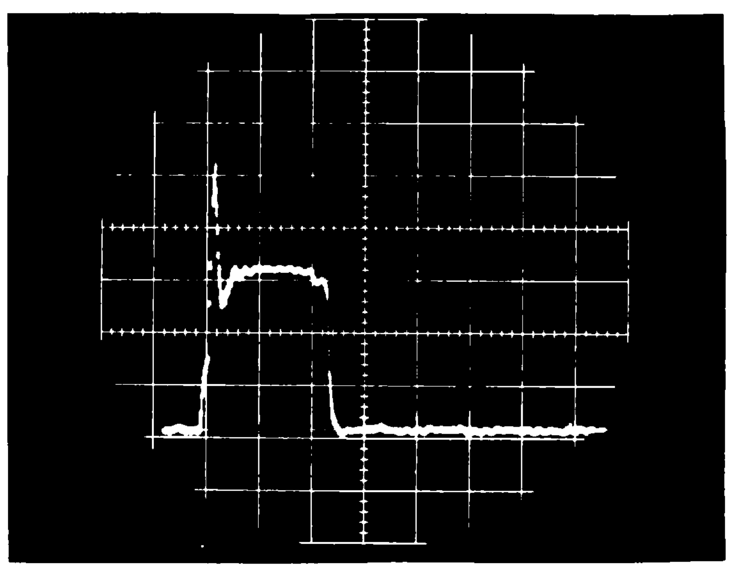

20msec/cm.

(d) Hemisphere drag.

FIG. 3.13 Concluded.

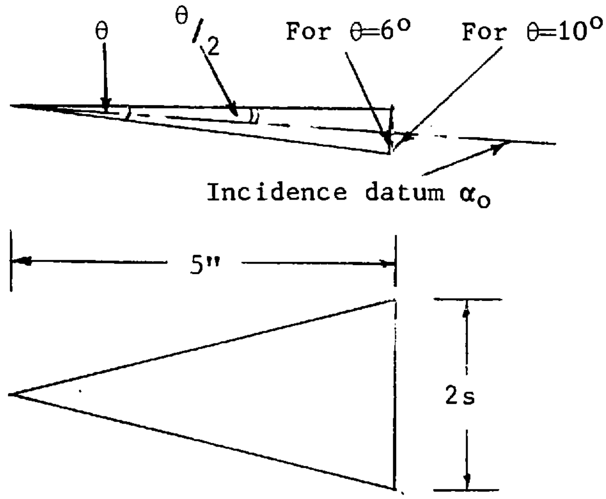

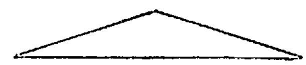

Model	2s	θ
1	2·5"	10°
3	2·5"	6°
4	3·75"	6°

(a) Plain wings.

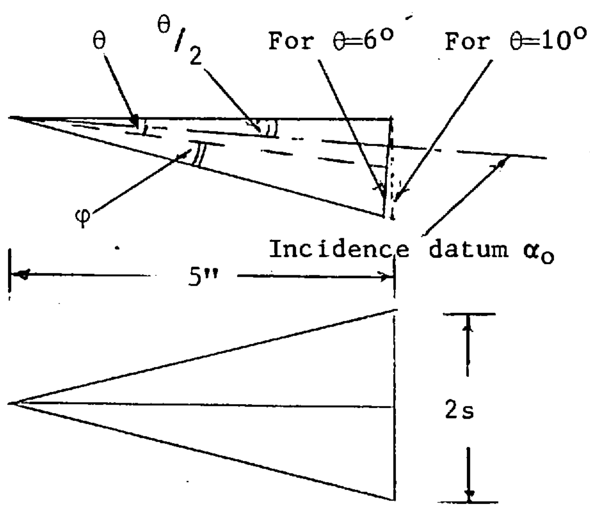

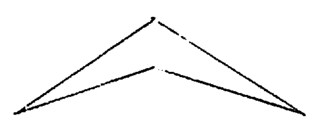

Model	2s	θ	φ
2	2·5"	10°	6°
5	3·75"	6°	6°

(b) Caret wings.

FIG. 4.1 Model dimensions and details.

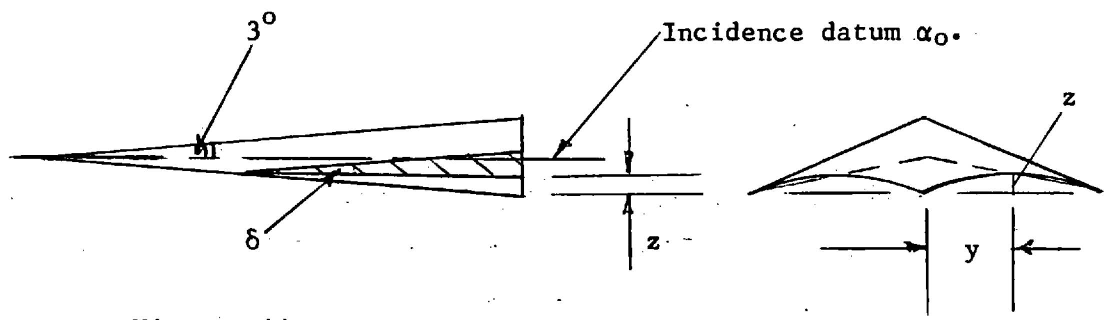

View on AA.

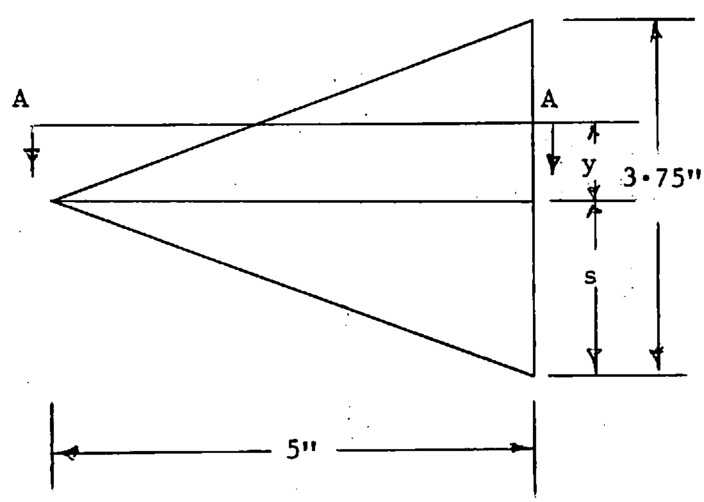

Model 6, having same volume as other 6° wings.

δ varies linearly from root to tip.

Upper surfaces are flat.

$y/_s$	0	0·1	0·2	0·3	0·4	0·5	0·6	0·7	0·8	0·9	1·0
z"	0	·027	·048	·063	·072	·075	·072	·063	·048	·027	0
δ^o	6·85	6·51	6·17	5·82	5·48	5·14	4·80	4·45	4·11	3·77	3·43

(c) Twisted wing.

FIG. 4.1 Concluded.

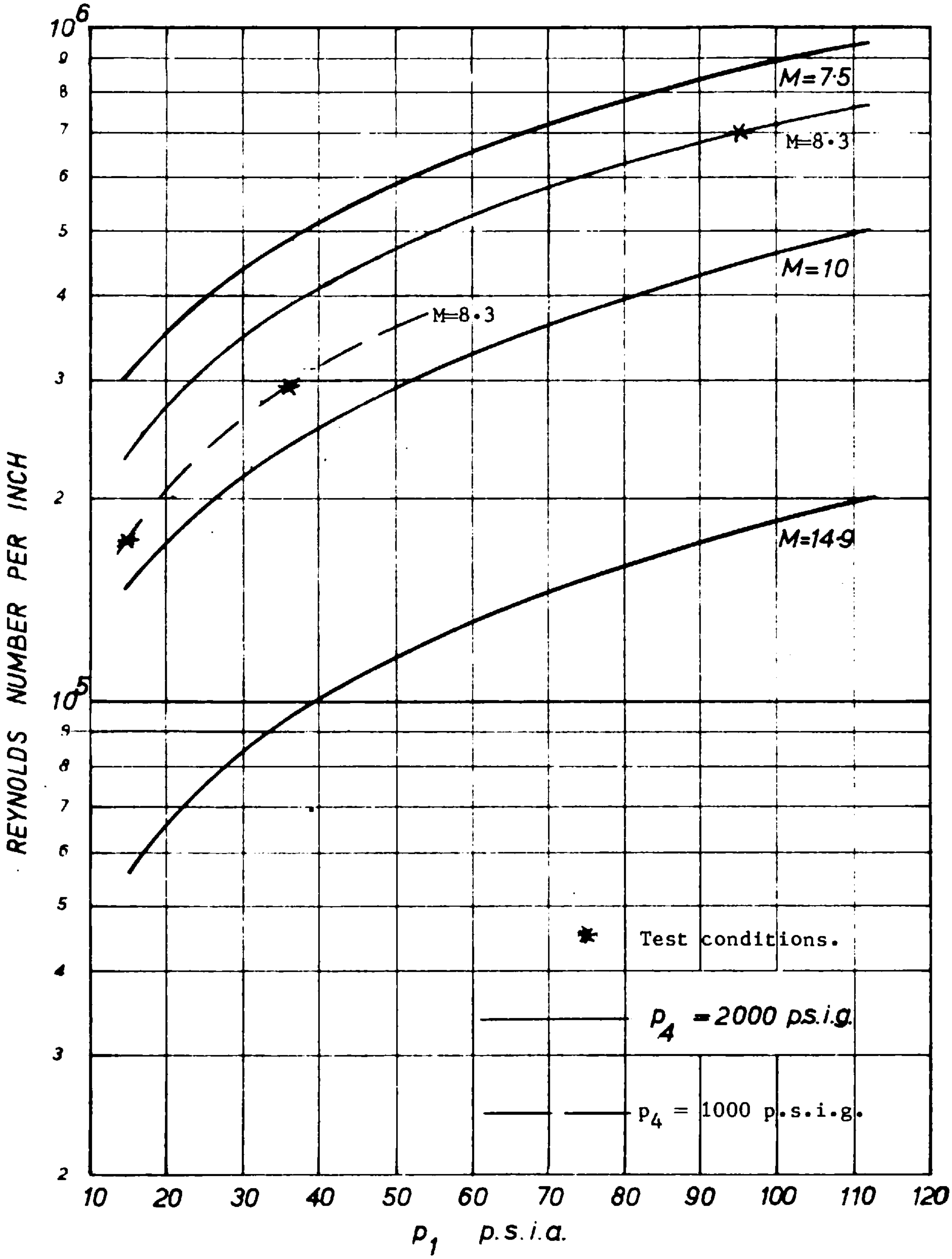

FIG. 4.2 Tunnel Reynolds number vs driver conditions.

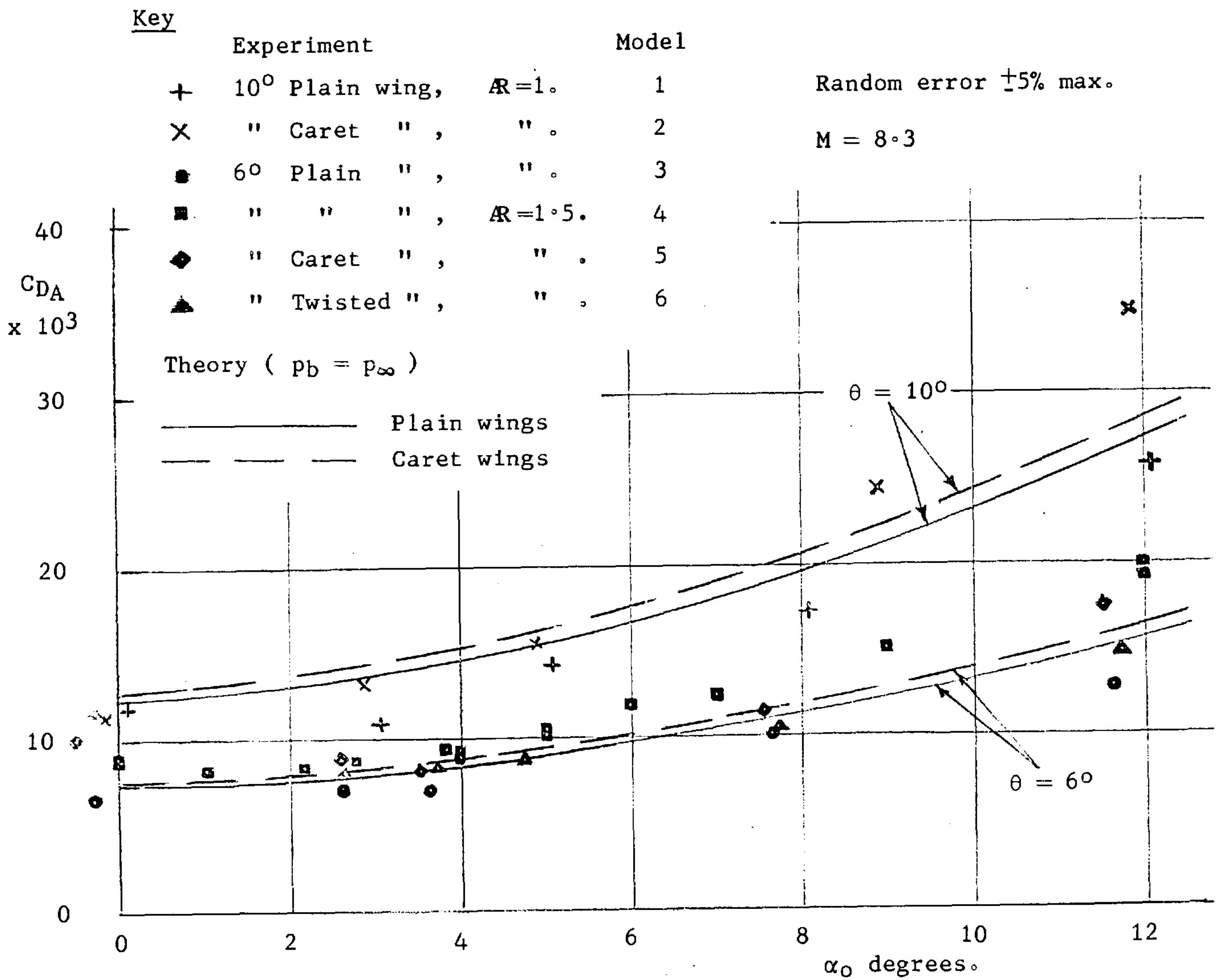

FIG. 4.3 (a) Axial force coefficient, C_{DA}, vs incidence for $R_e = 0{\cdot}9 \times 10^6$.

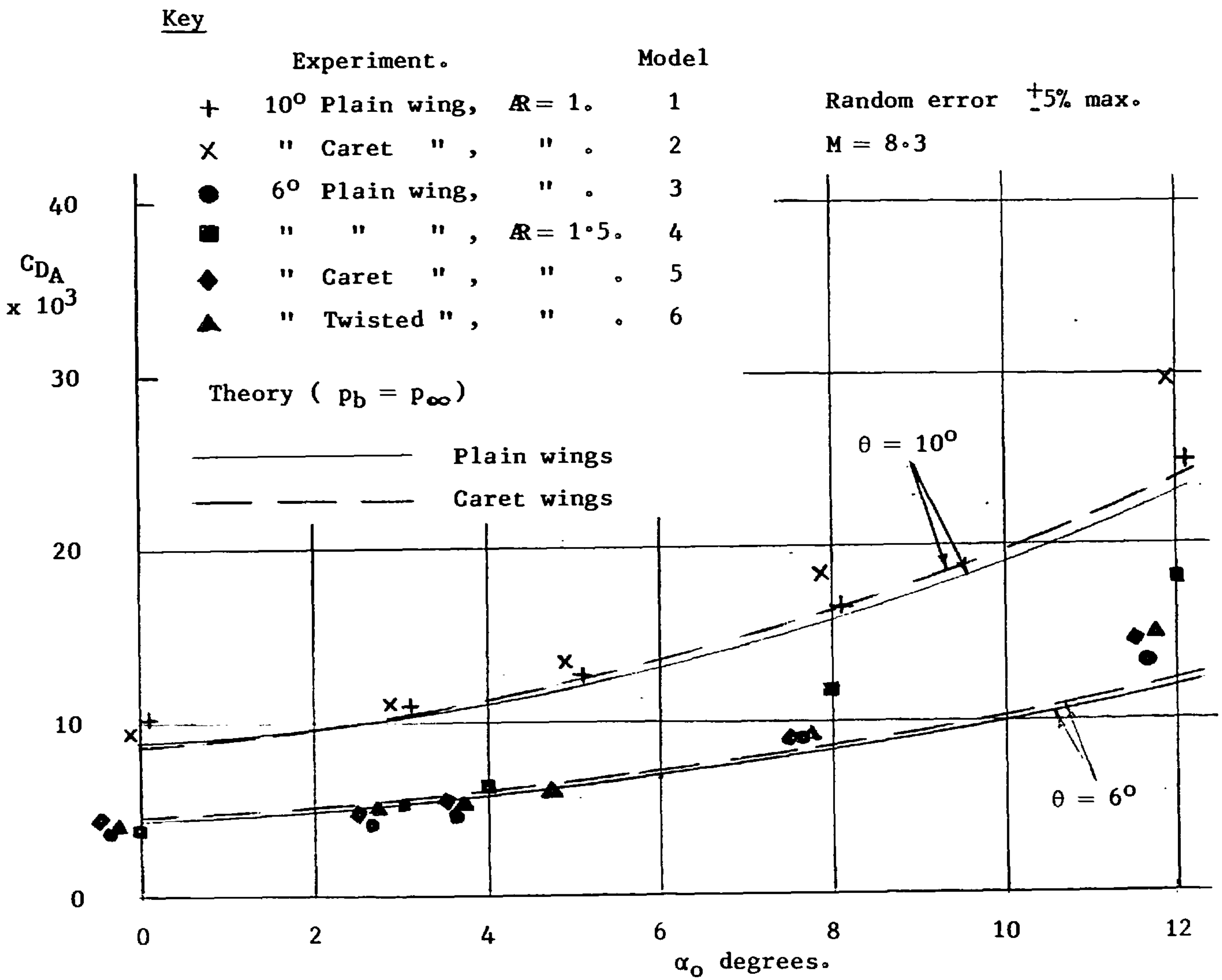

FIG. 4.3 (b) Axial force coefficient, C_{D_A}, vs incidence for $R_e = 3\cdot5 \times 10^6$.

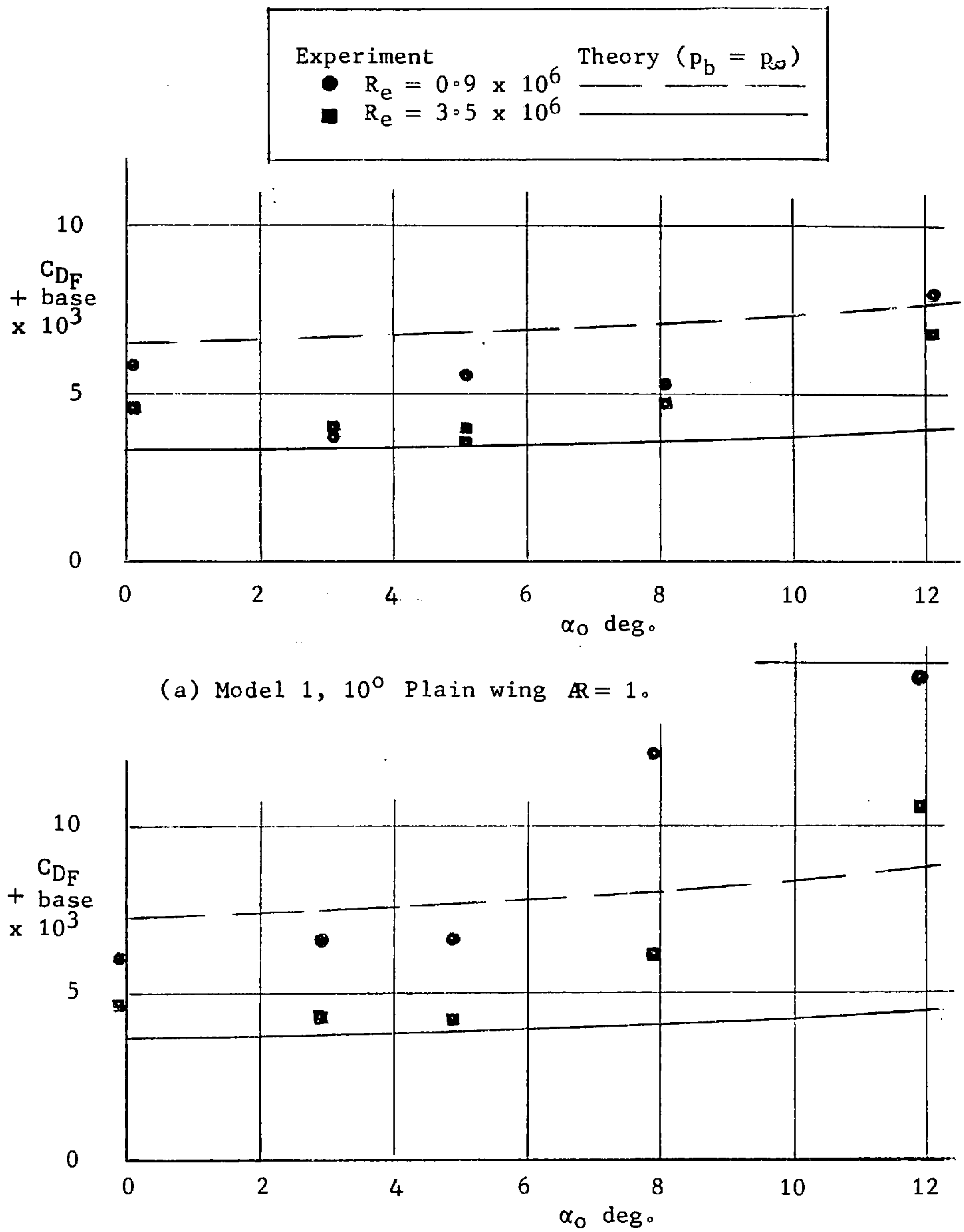

(a) Model 1, 10° Plain wing Æ = 1.

(b) Model 2, 10° Caret wing Æ = 1.

FIG. 4.4 Skin friction plus base drag vs incidence for $R_e = 0{\cdot}9 \times 10^6$ and $R_e = 3{\cdot}5 \times 10^6$.

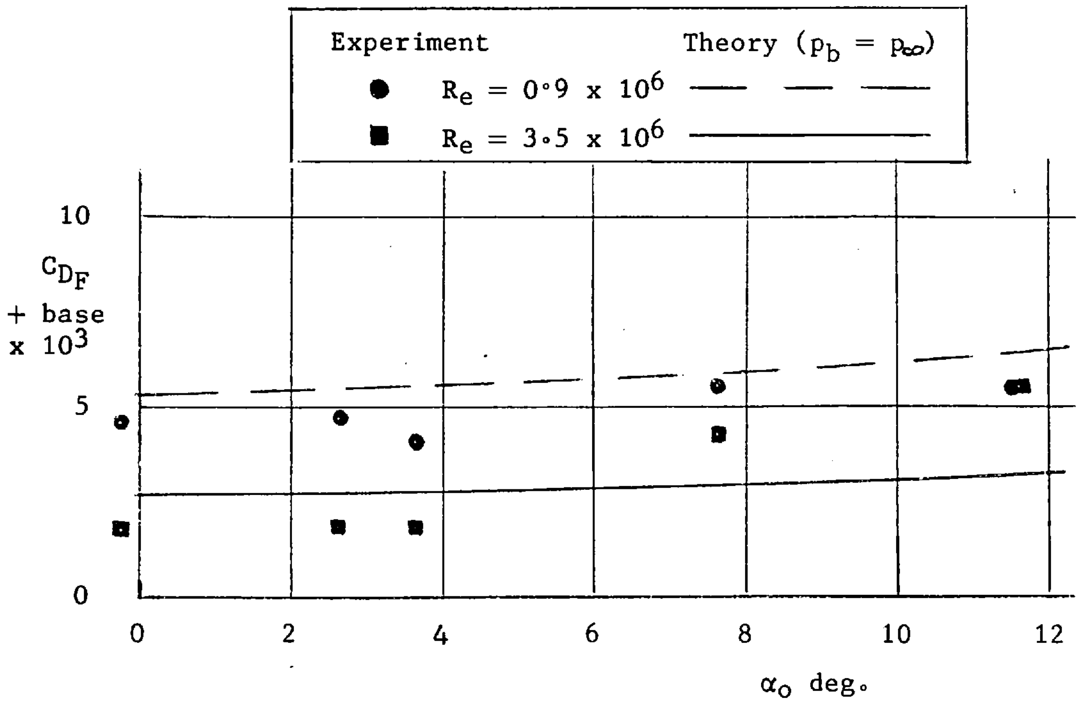

(c) Model 3, 6° plain wing Æ = 1.

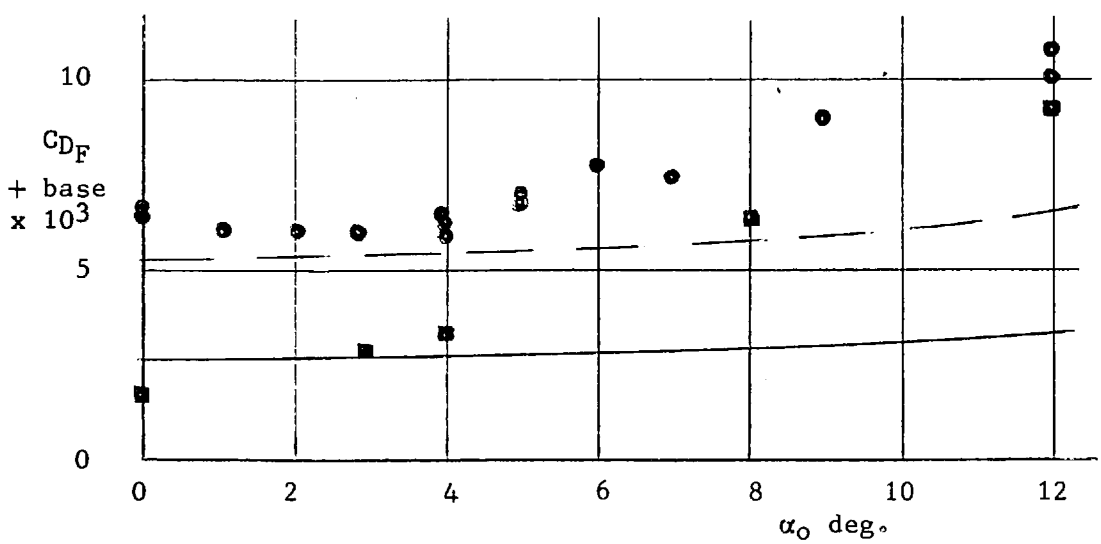

(d) Model 4, 6° plain wing Æ = 1·5.

FIG. 4.4 Continued.

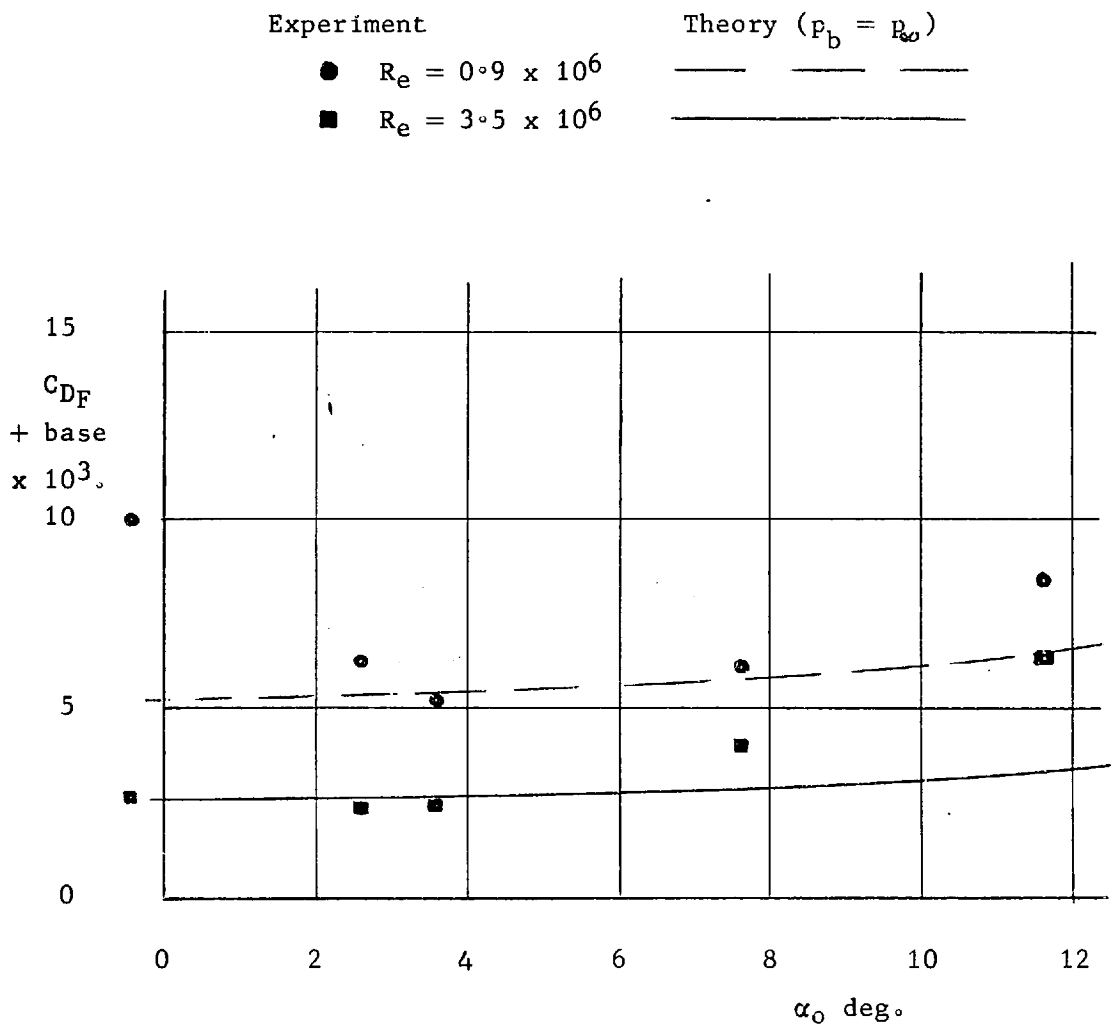

(e) Model 5, 6^o caret wing, Æ = 1·5.

FIG. 4.4 Concluded.

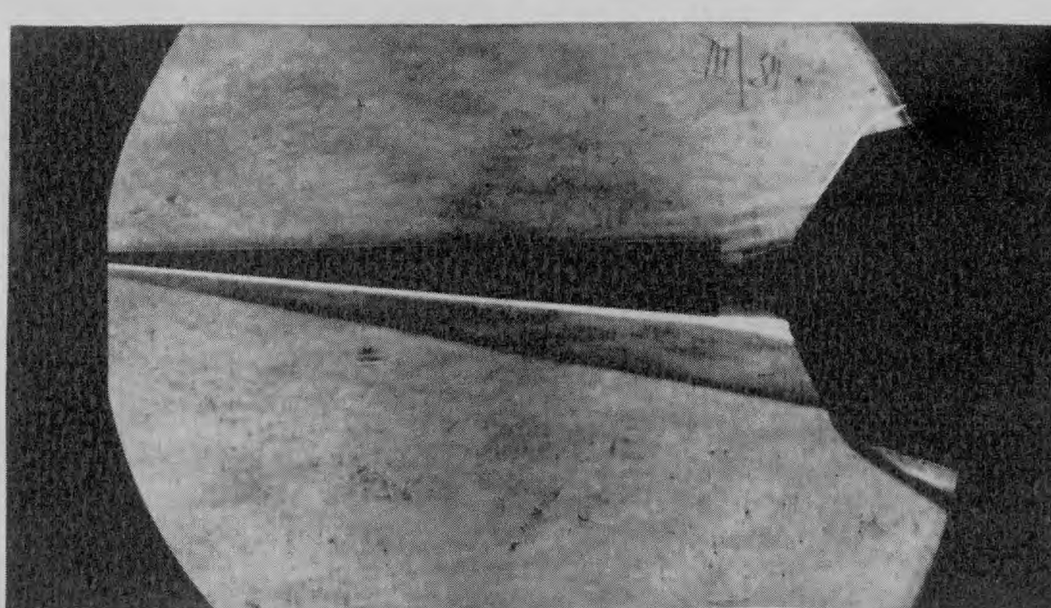

(a) α_0 3^0.

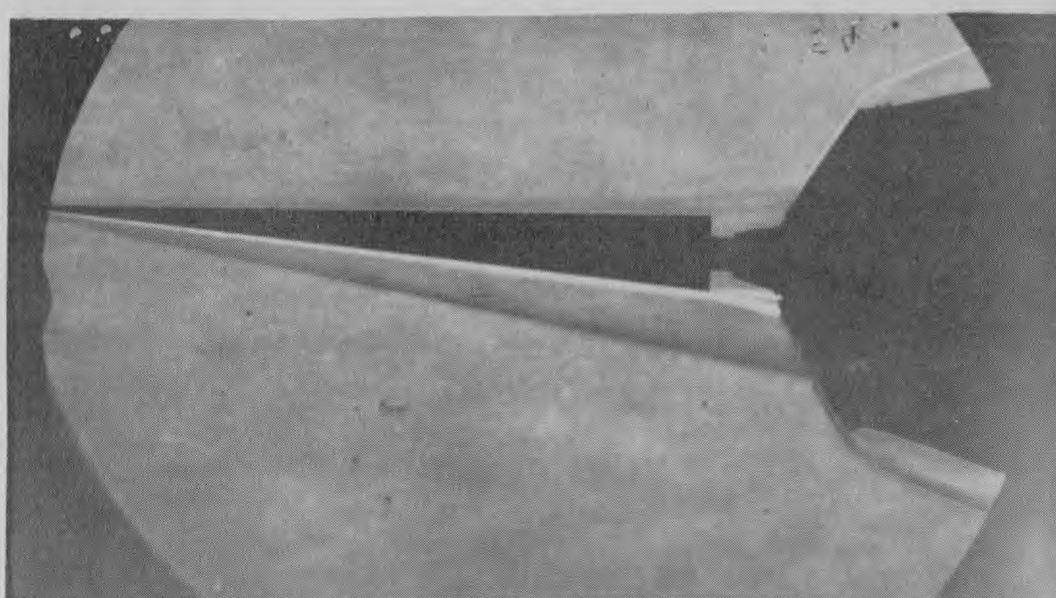

(b) α_0 [illegible].

FIG. 4.5 Schlieren photographs of flow separation on [illegible] models.

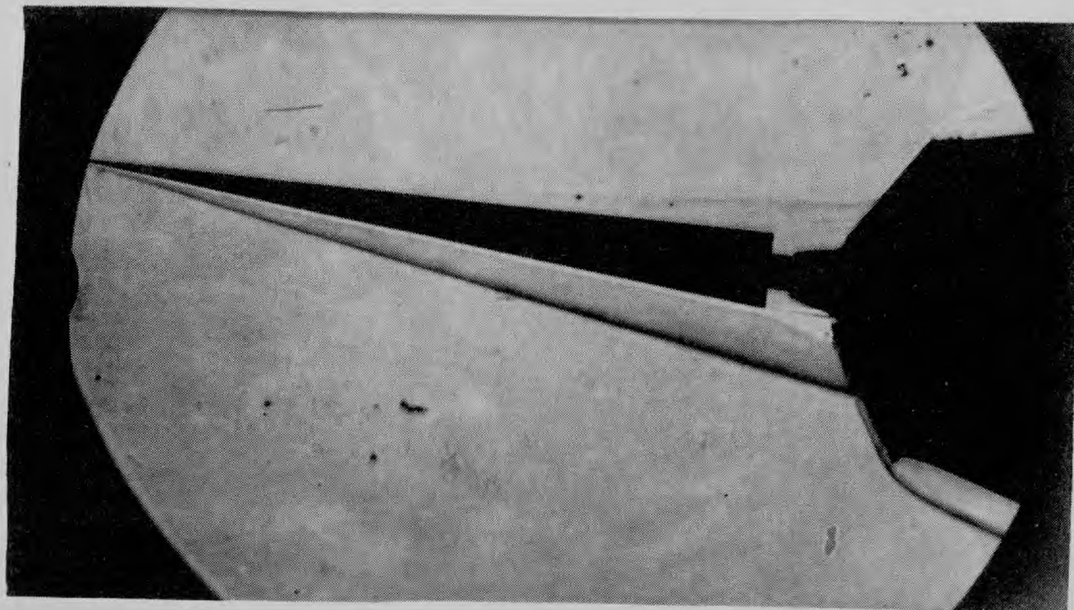

(c) $\alpha_0 = 8^\circ$.

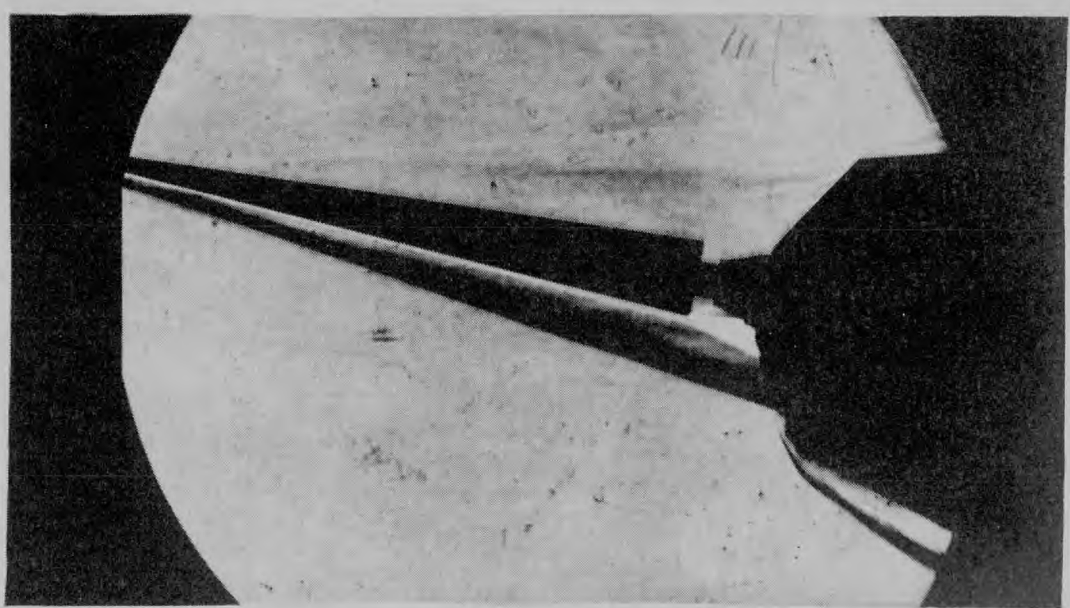

(d) $\alpha_0 = 12^\circ$.

FIG. 4.5 Concluded.

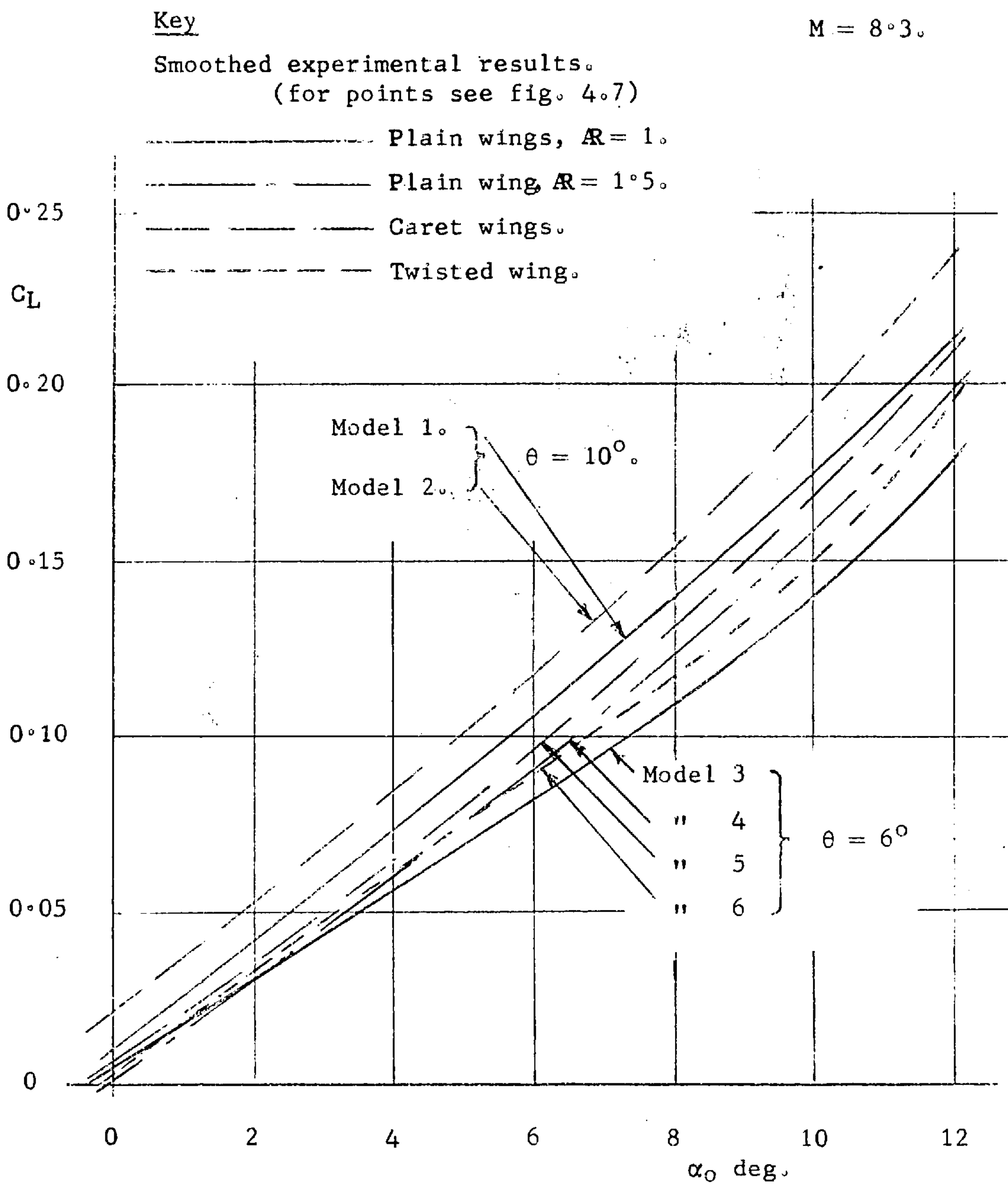

FIG. 4.6 (a) Lift coefficient vs incidence for all models at $R_e = 0{\cdot}9 \times 10^6$.

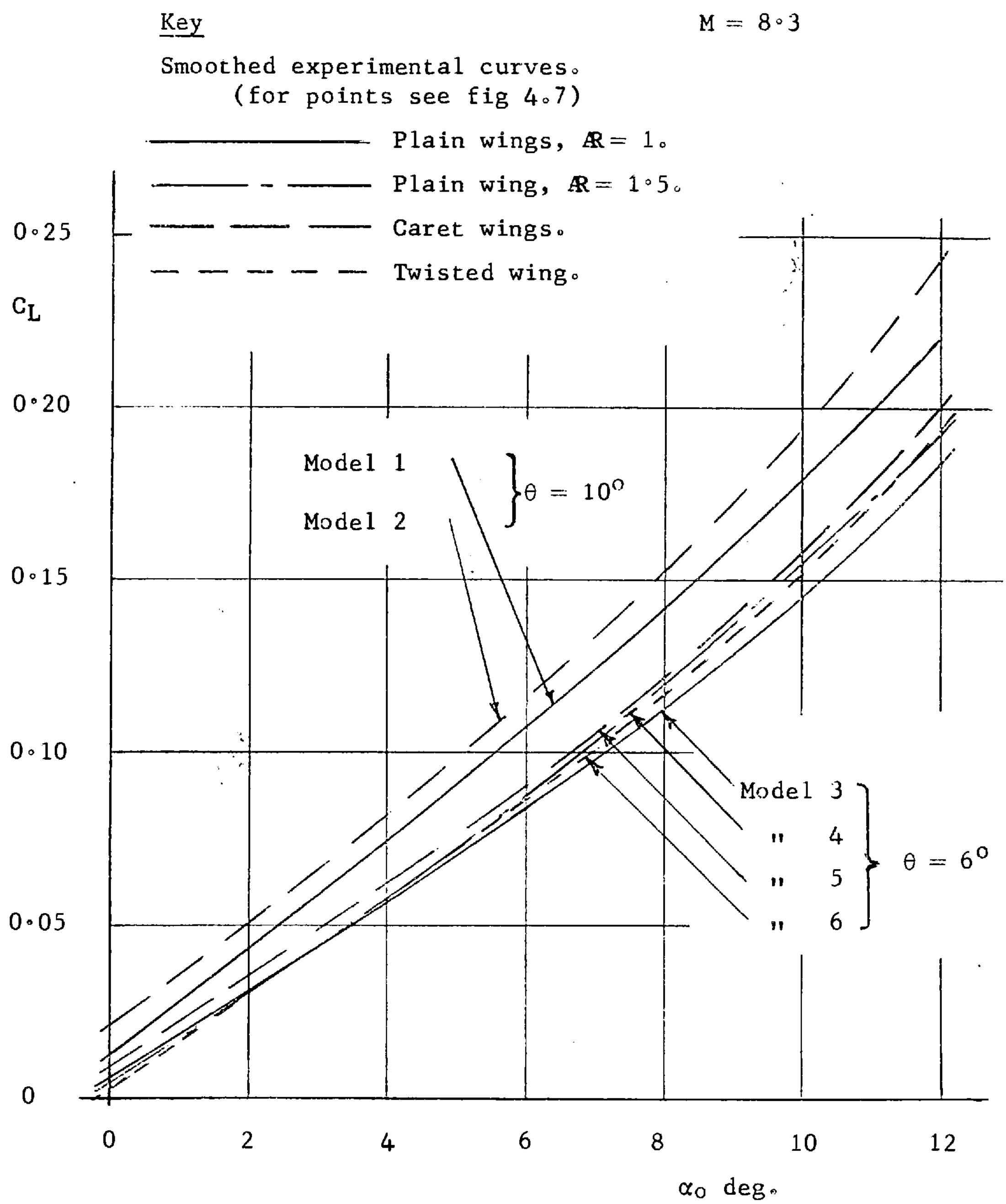

FIG. 4.6 (b) Lift coefficient vs incidence for all wings at $R_e = 3{\cdot}5 \times 10^6$.

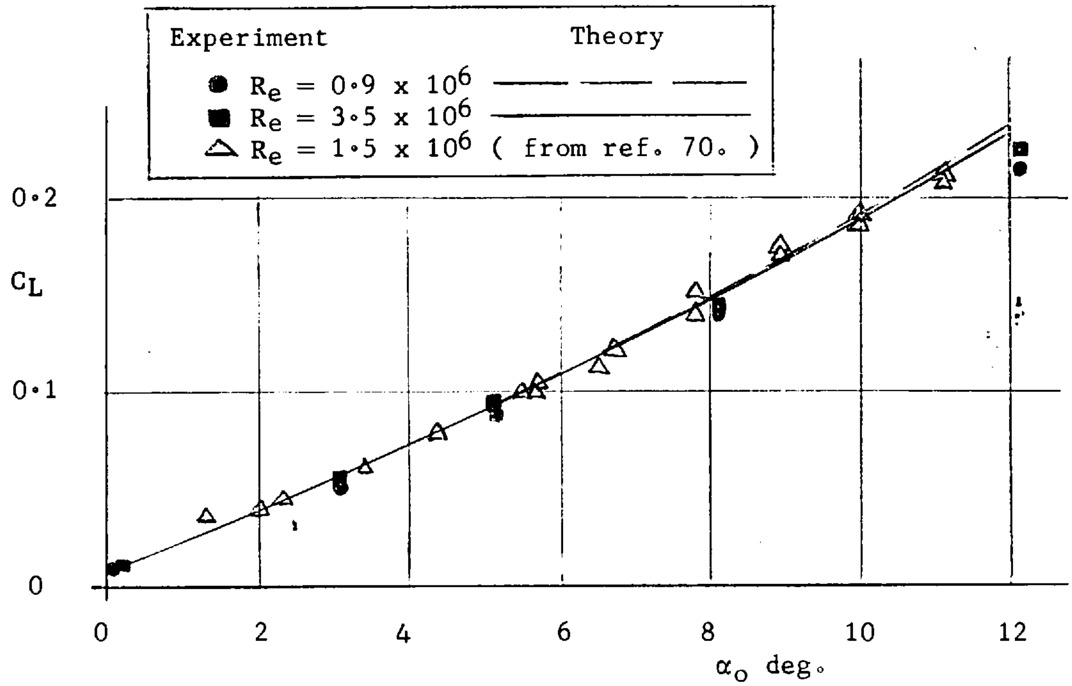

(a) Model 1, 10^o plain wing $AR = 1$.

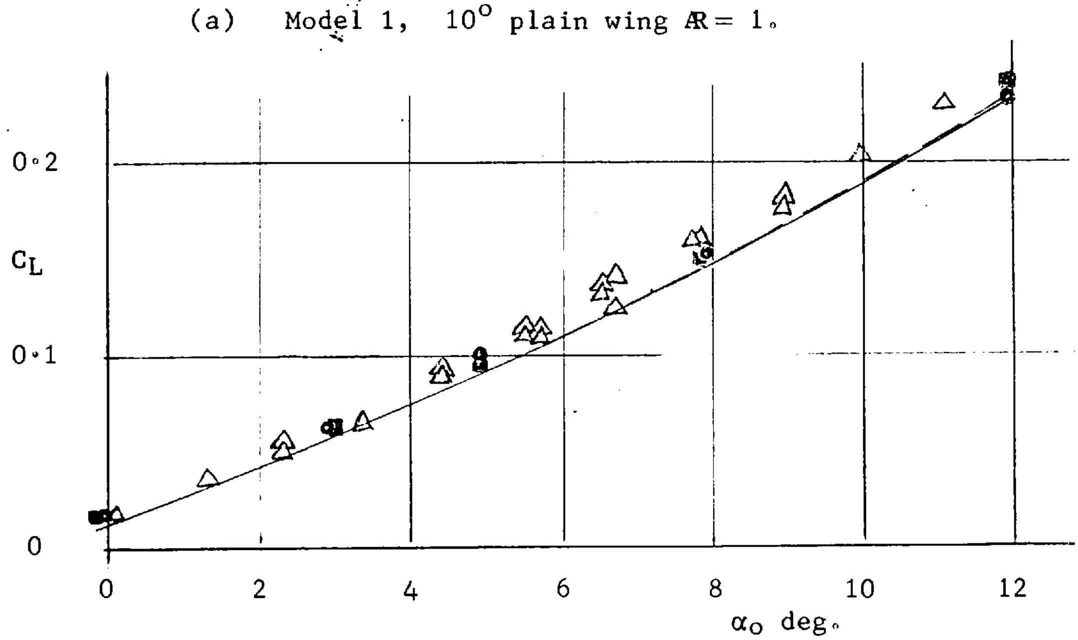

(b) Model 2, 10^o caret wing $AR = 1$.

FIG. 4.7 Lift coefficient vs incidence and Reynolds number with theoretical estimates.

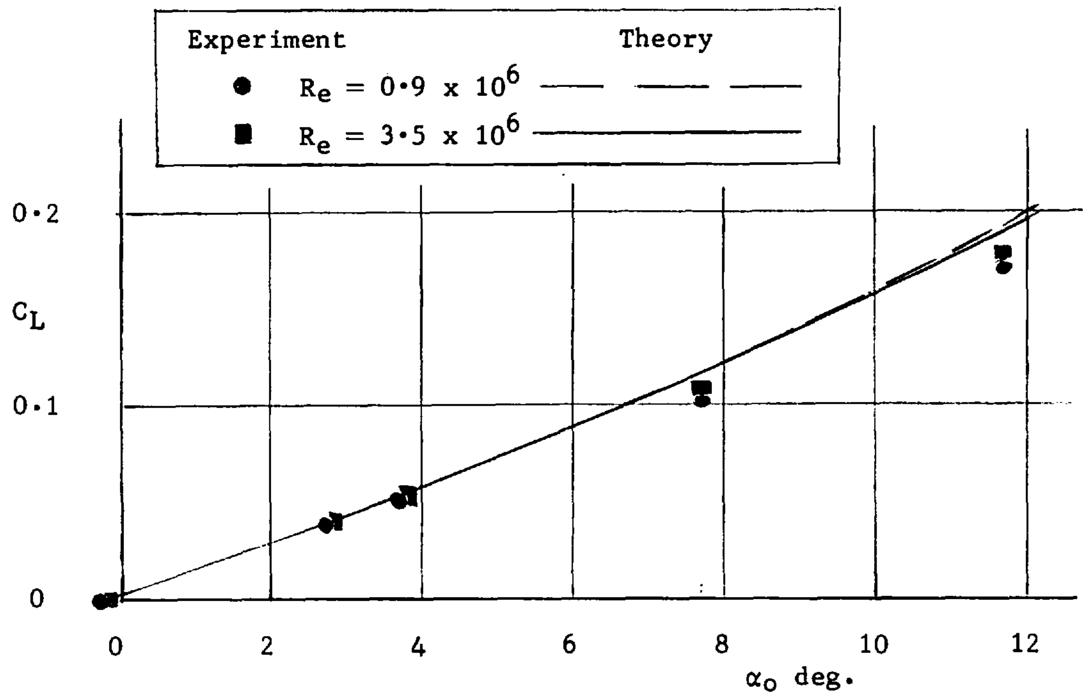

(c) Model 3, 6^o plain wing, Æ= 1.

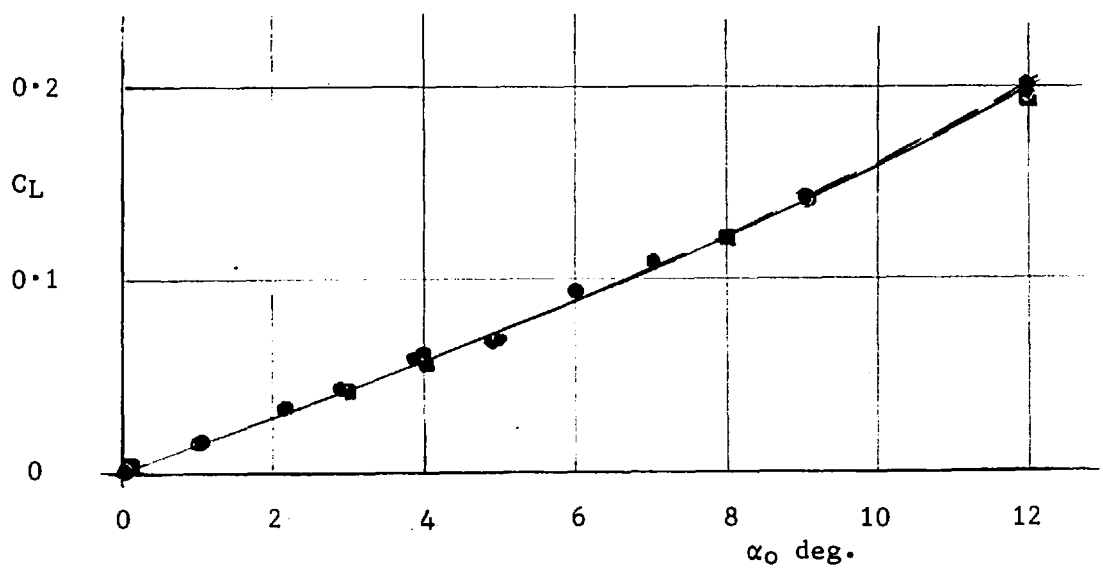

(d) Model 4, 6^o plain wing, Æ= 1·5.

FIG. 4.7 Continued.

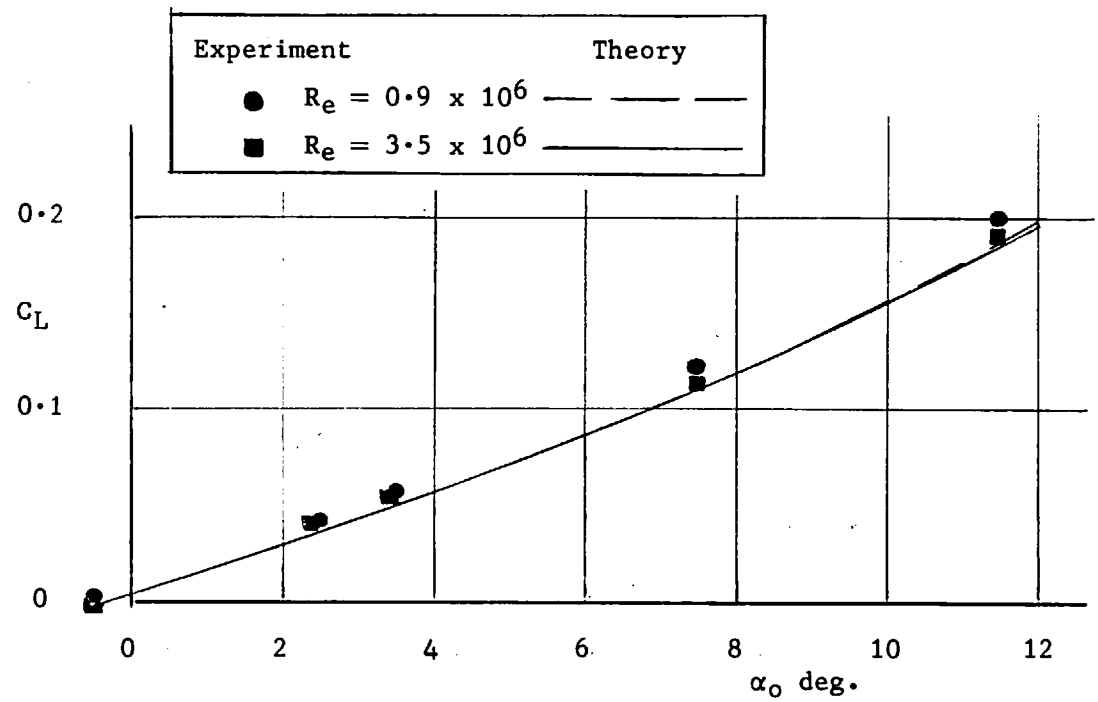

(e) Model 5, 6° caret wing, Æ = 1·5.

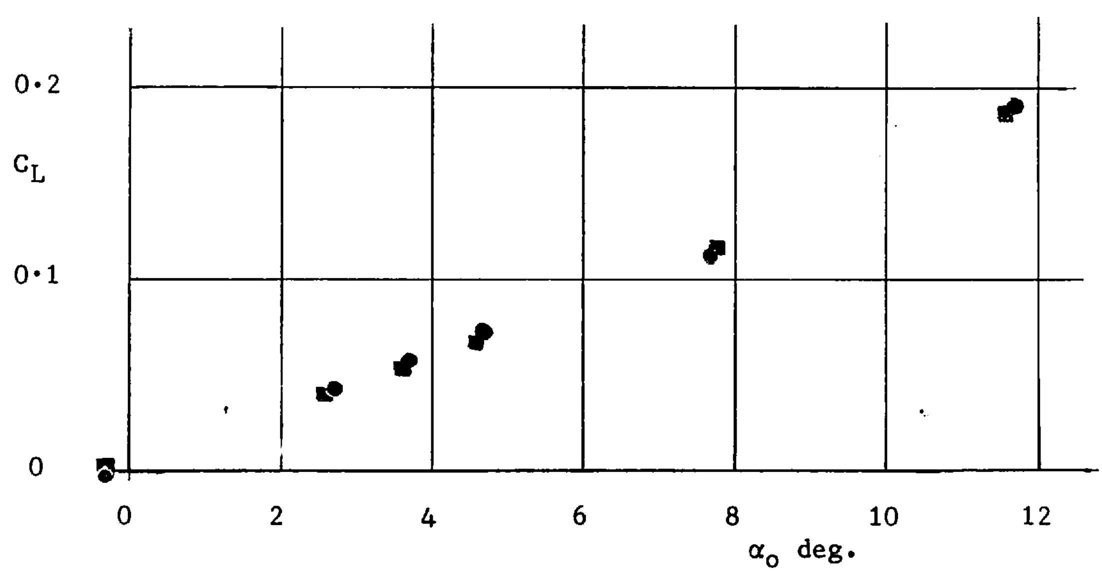

(f) Model 6, 6° twisted wing, Æ = 1·5.

FIG. 4.7 Concluded.

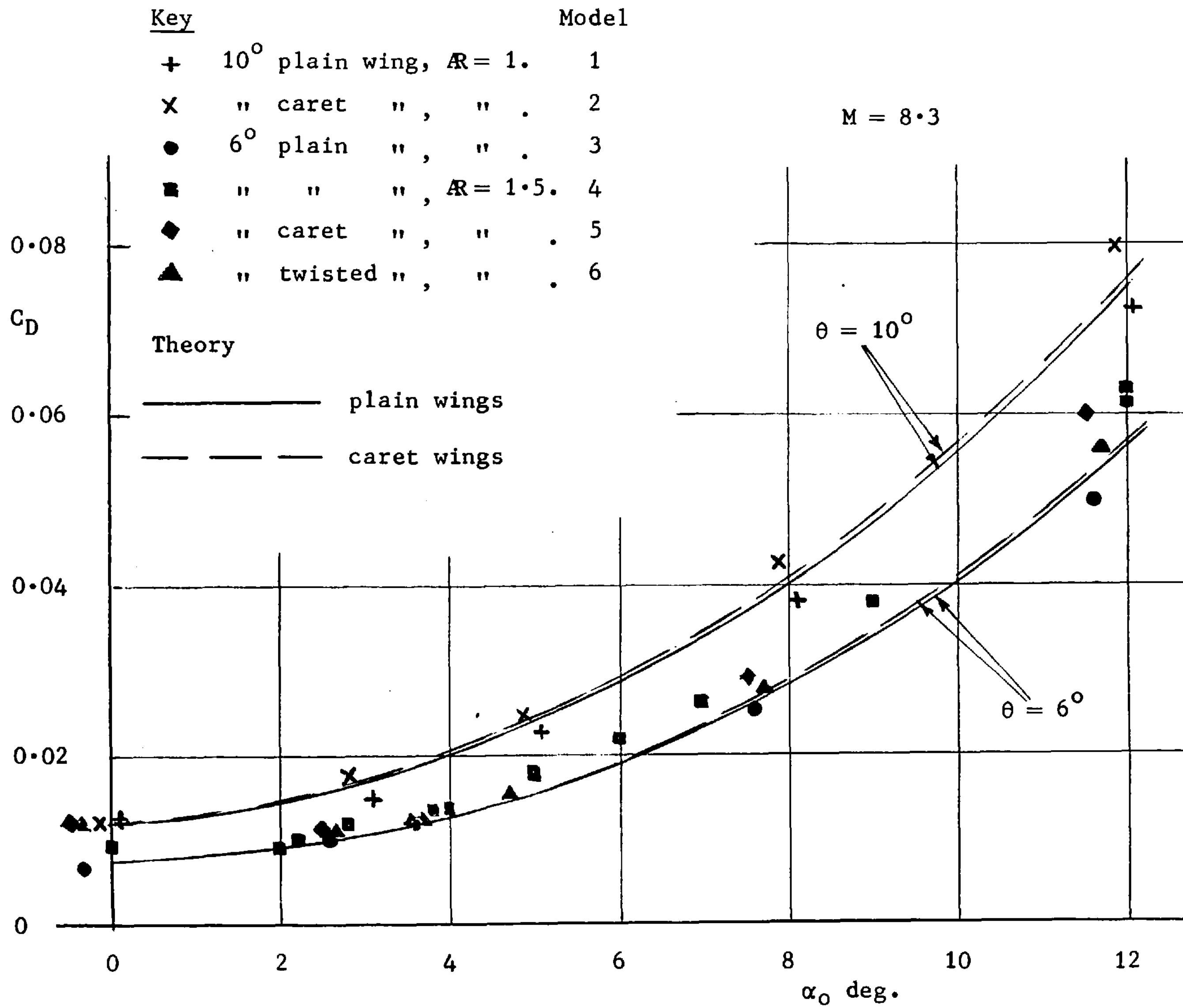

FIG. 4.8 (a) Drag coefficient vs incidence for $R_e = 0{\cdot}9 \times 10^6$.

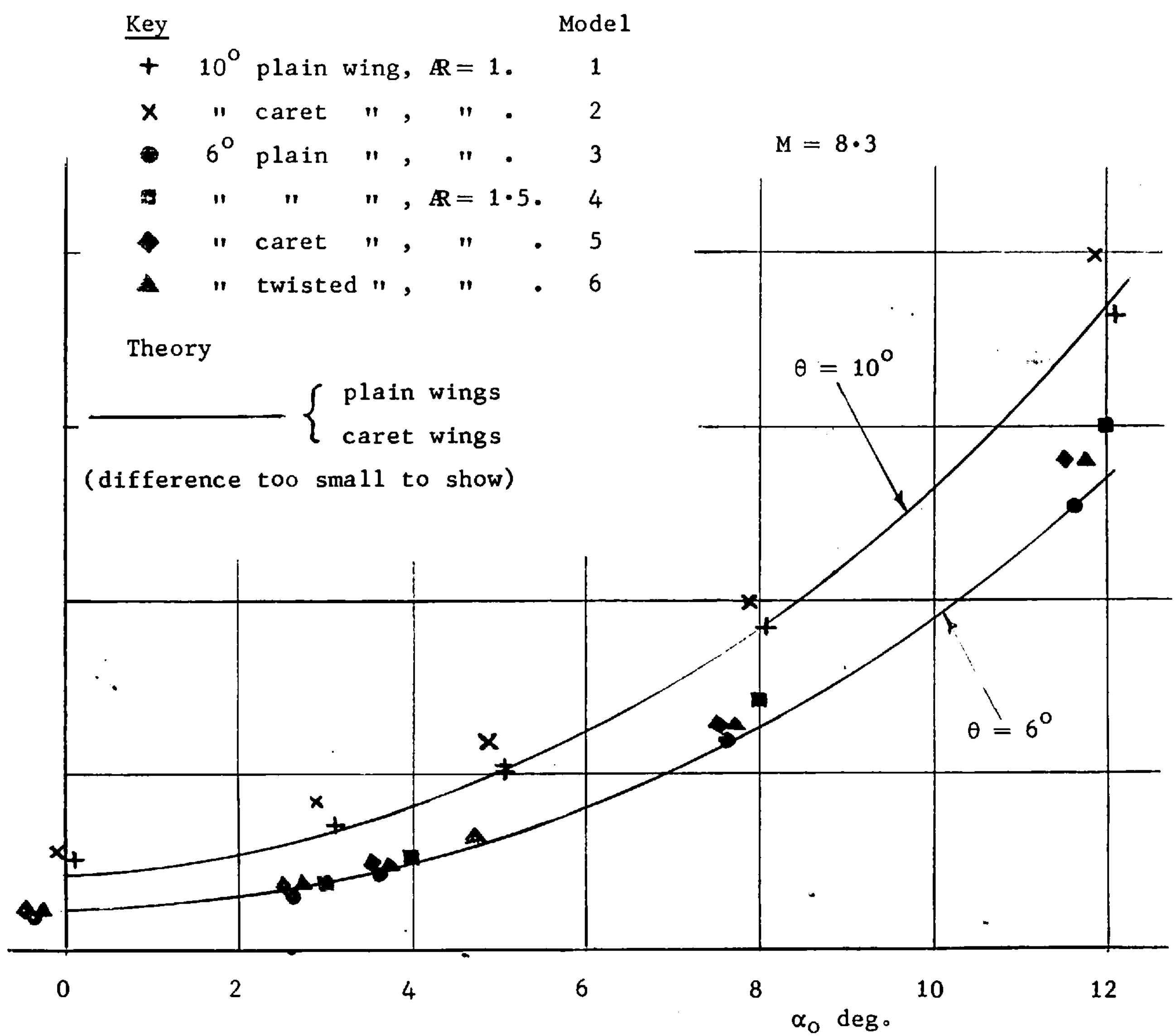

FIG. 4.8 (b) Drag coefficient vs incidence for $R_e = 3{\cdot}5 \times 10^6$.

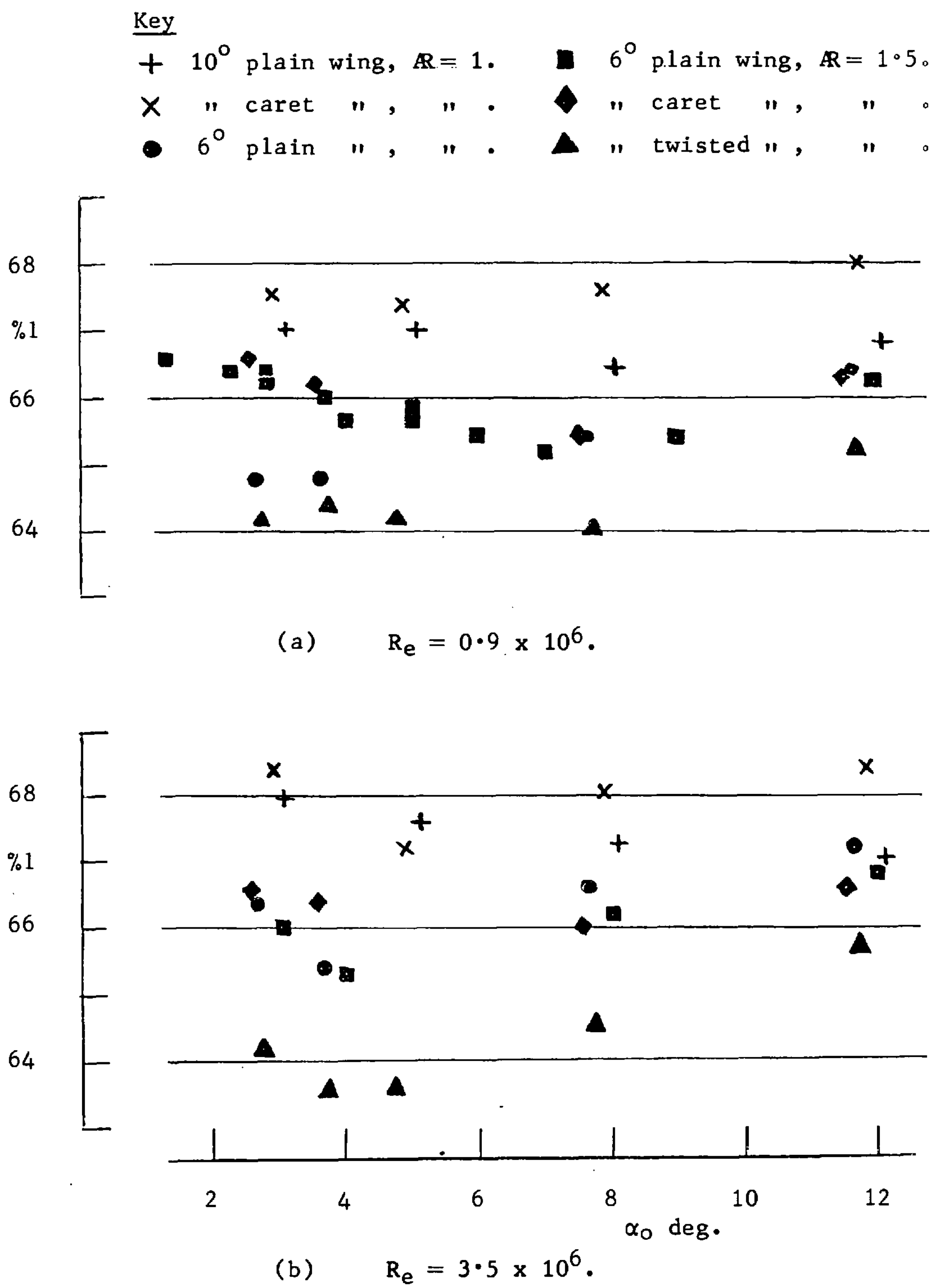

FIG. 4.9 Centre of pressure position vs incidence.

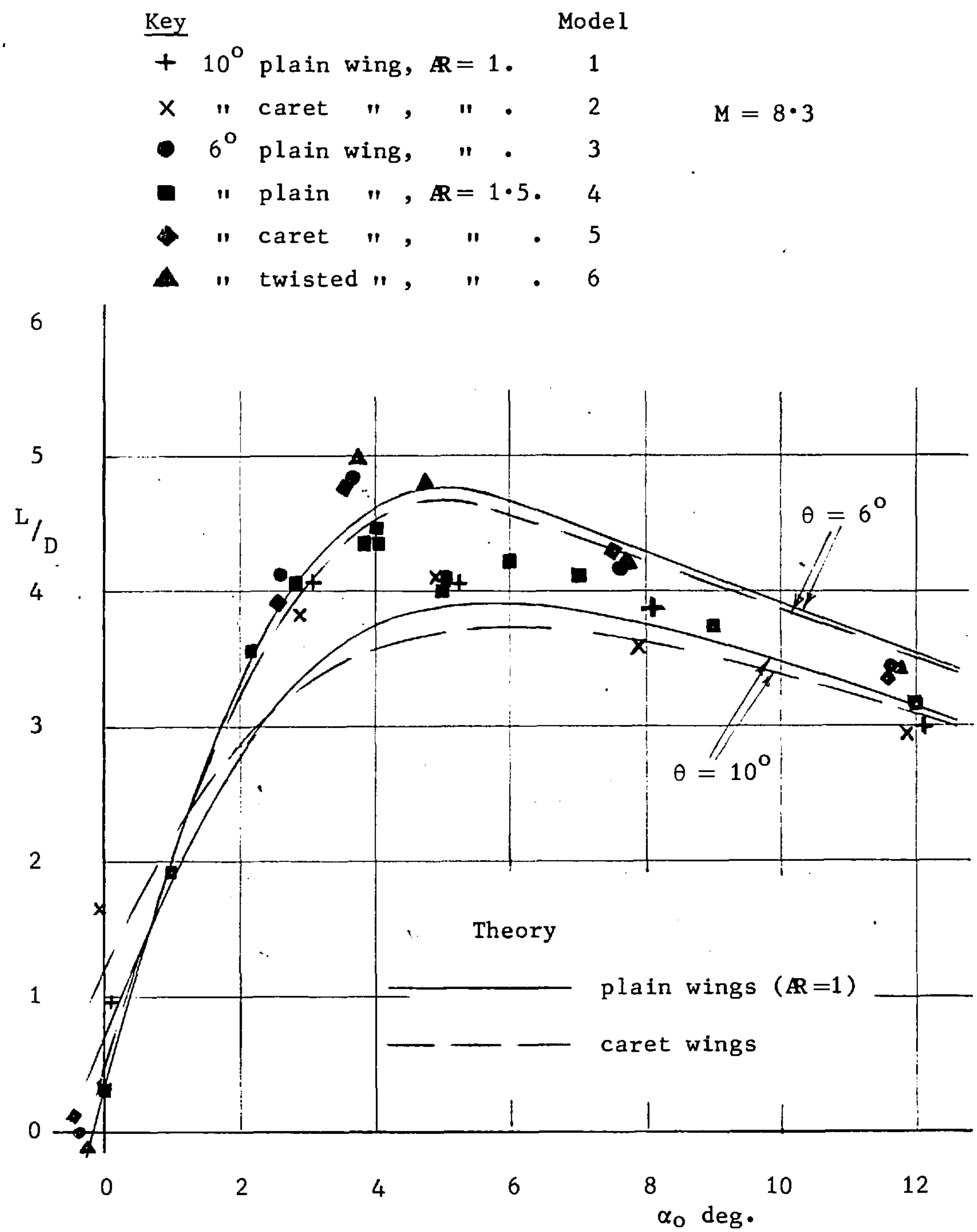

FIG. 4.10 (a) Lift/drag ratio vs incidence for $R_e = 0{\cdot}9 \times 10^6$.

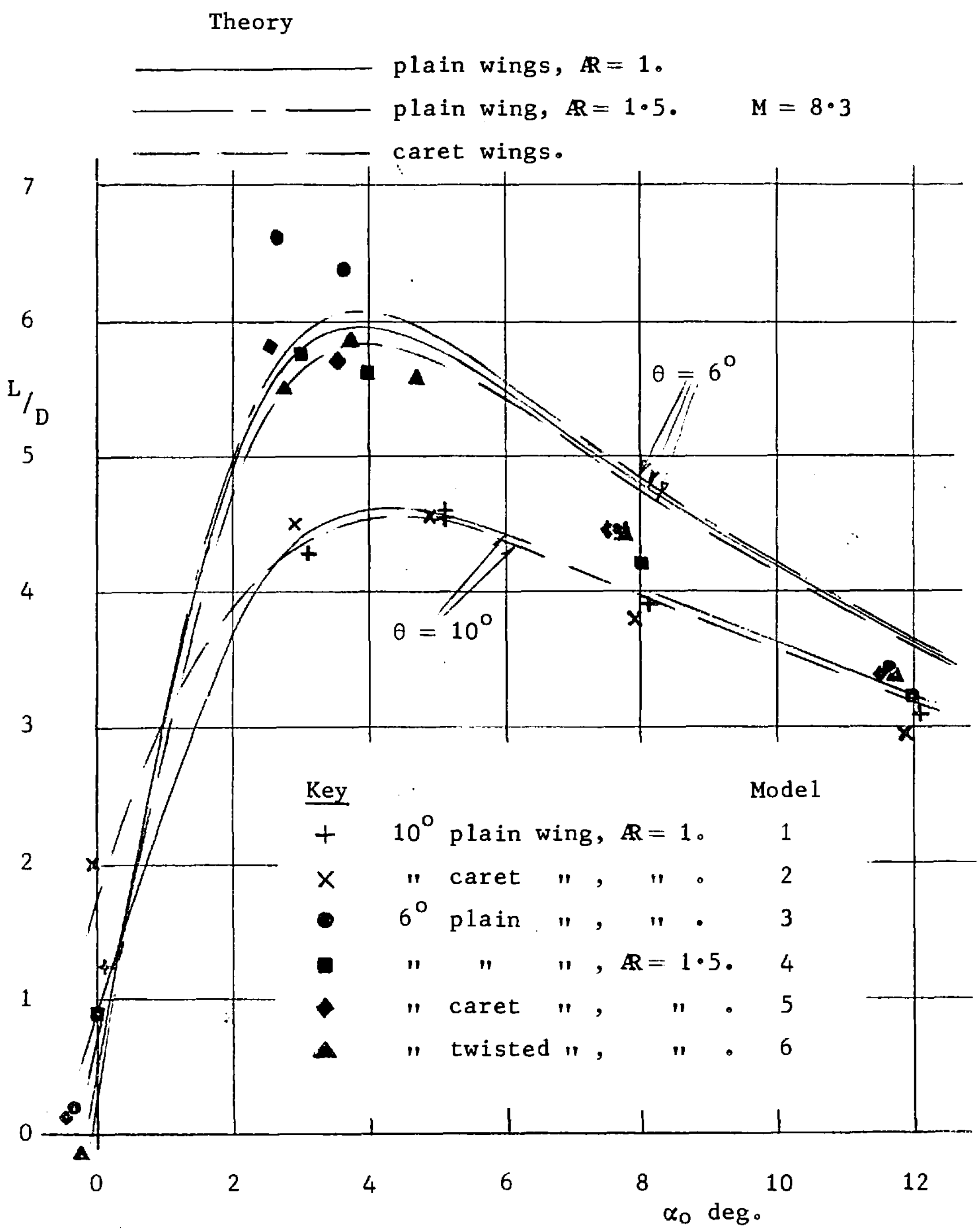

FIG. 4.10 (b) Lift/drag ratio vs incidence for $R_e = 3{\cdot}5 \times 10^6$.

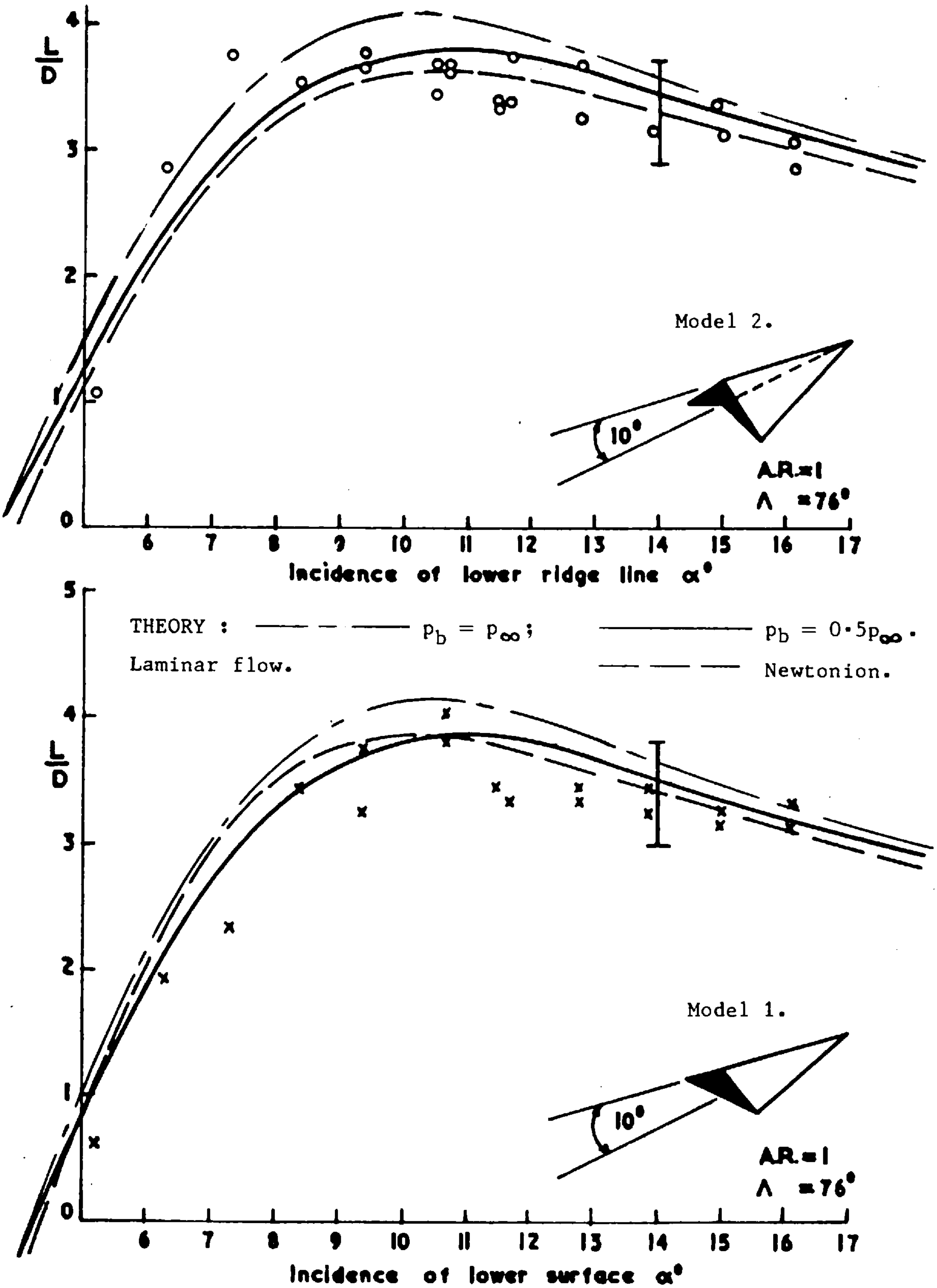

FIG. 4.10 (c) Lift/drag ratio vs incidence for $R_e = 1{\cdot}48 \times 10^6$.

Experimental results from smoothed lift and drag curves.

plain wings, Æ = 1.

plain wing, Æ = 1·5.

caret wings.

twisted wing.

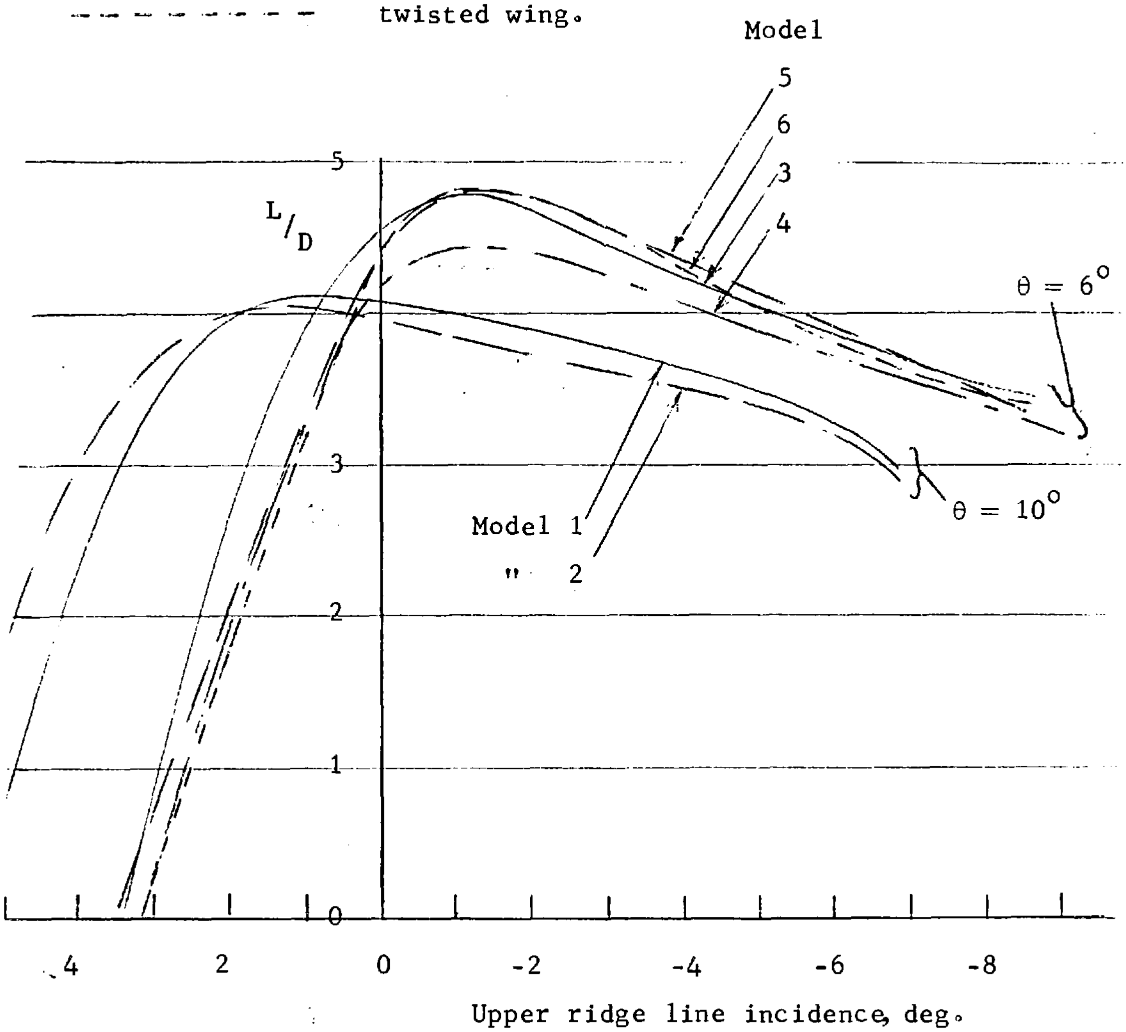

(a) $R_e = 0{\cdot}9 \times 10^6$.

FIG. 4.11 Smoothed curves of lift/drag ratio vs upper ridge line incidence.

Experimental results from smoothed lift and drag curves.

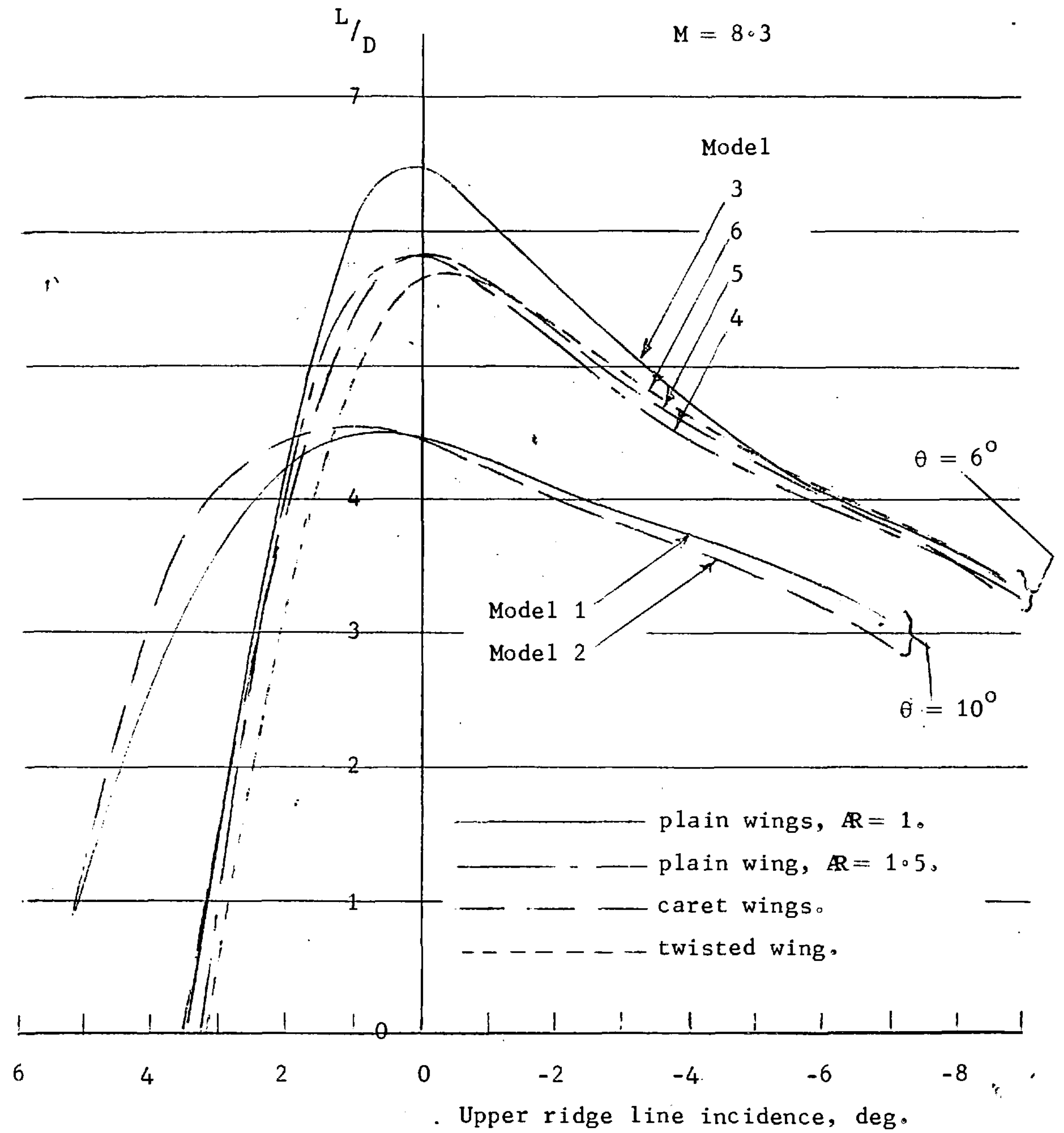

(b) $R_e = 3\cdot5 \times 10^6$.

FIG. 4.11 Concluded.

Experimental results from smoothed lift and drag curves.

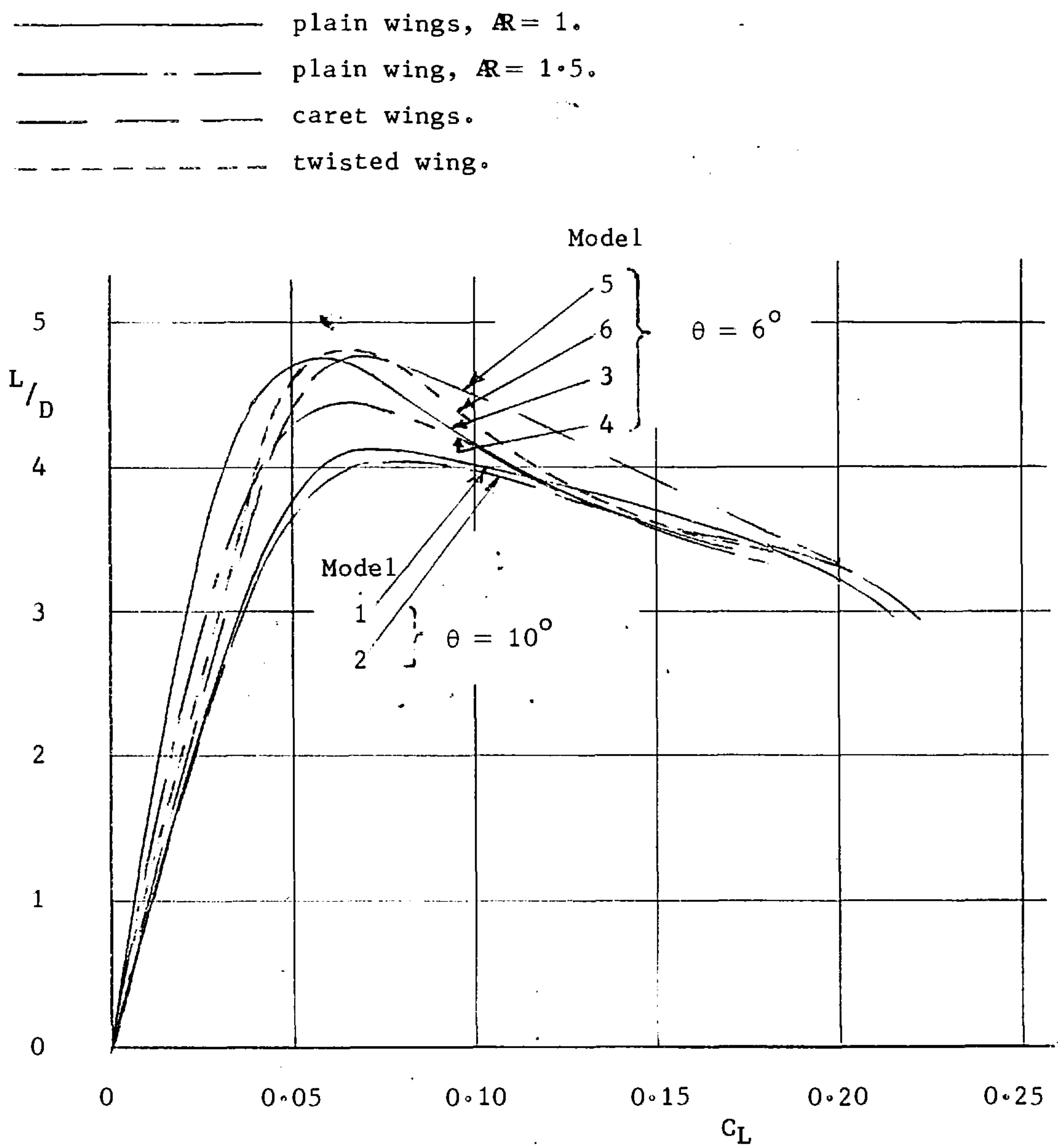

(a) $R_e = 0{\cdot}9 \times 10^6$.

FIG. 5.1 Lift/drag ratio vs lift coefficient.

Experimental results from smoothed lift and drag curves.

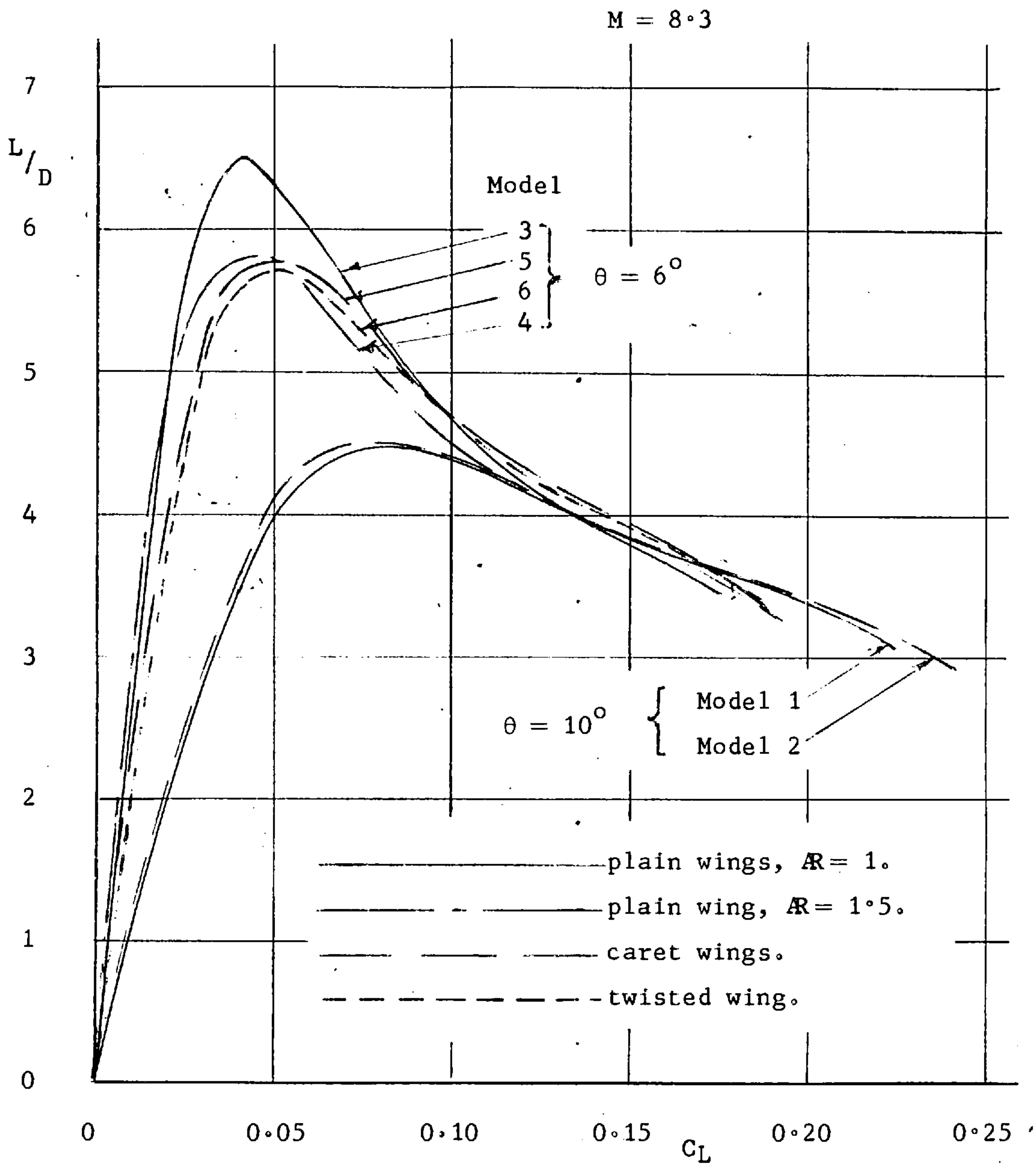

(b) $R_e = 3 \cdot 5 \times 10^6$.

FIG. 5.1 Concluded.

FIG. 5.2 Maximum lift/drag ratio for delta wings from Penland, (ref.30).

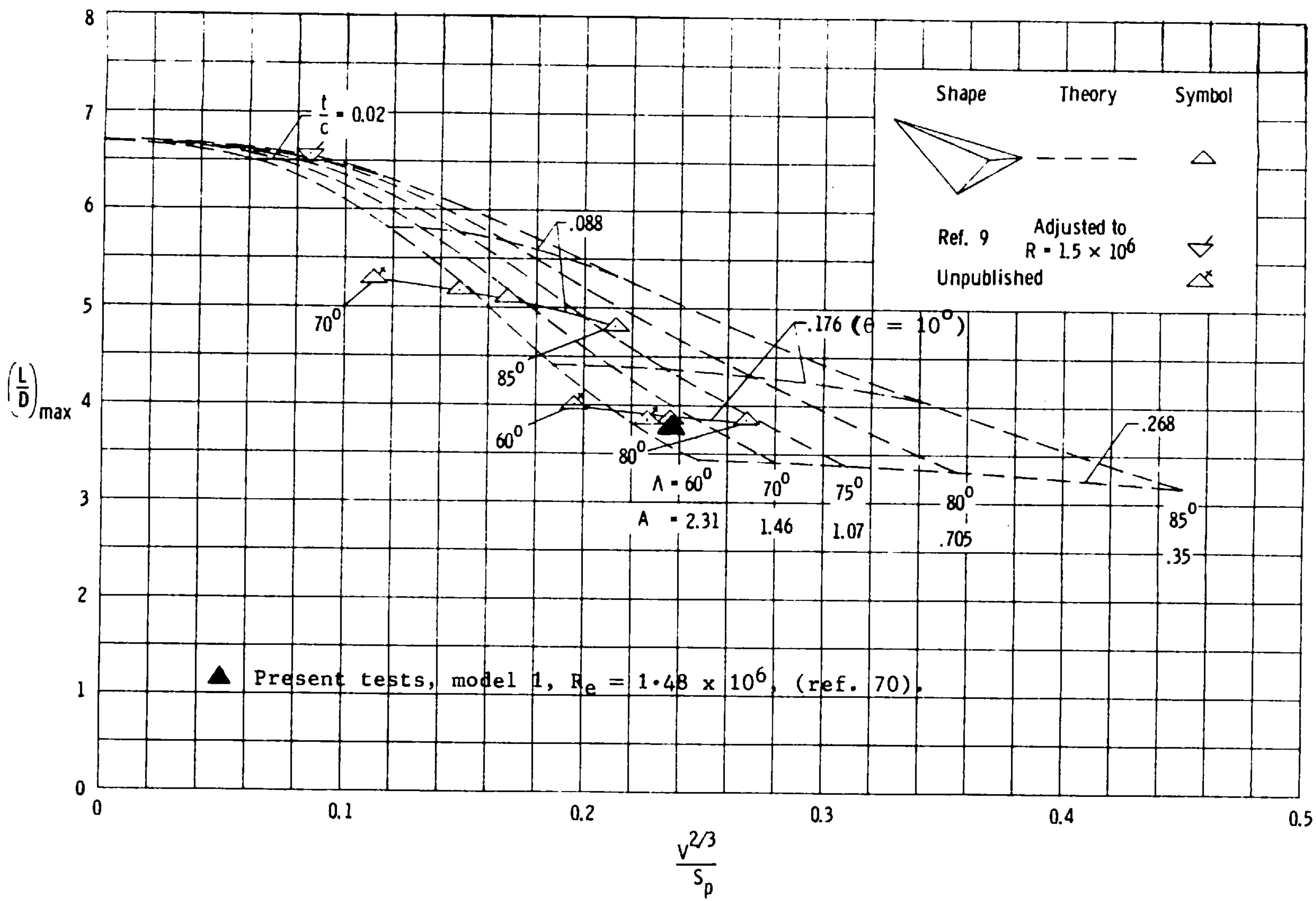

(b) Roof delta wings.

Figure 6.- Concluded.

Ph.D. 1967 OPATOWSKI (T. P. S.)

[*Reprinted from the* JOURNAL OF THE ROYAL AERONAUTICAL SOCIETY, *May* 1967]

A New Formula for Pressure Versus Flow Deflection at Hypersonic Speeds

T. OPATOWSKI, DCAe, CEng, AFRAeS

Department of Aeronautics, Imperial College of Science and Technology

ANALYTICAL studies involving the pressure on inclined surfaces in hypersonic flow are made difficult by the lack of an explicit and simple relationship connecting the pressure p with the flow deflection angle δ. The various existing relationships are either too complicated or valid only over a very limited range.

For small deflection angles, series expansions in powers of δ such as Busemann's[1, 2] are sufficiently accurate but still complicated. At hypersonic speeds his series can be simplified as the Mach number $M \longrightarrow \infty$ to give:—

$$\left(\frac{p}{p_\infty}-1\right)=\gamma M\delta+\frac{\gamma(\gamma+1)}{4}(M\delta)^2+\frac{\gamma(\gamma+1)^2}{32}(M\delta)^3+\ldots \quad . \quad . \quad (1)$$

where γ is the ratio of specific heats and the first term is the linear result for high M.

Linnell[3] gives an expression (eqn. (2)) which is valid for high Mach numbers and δ's up to 2/3 shock detachment angle but, although explicit, it is still too complicated for general analytic use.

$$\left(\frac{p}{p_\infty}-1\right)=\frac{\gamma(\gamma+1)}{4}(M\delta)^2+\gamma M\delta\sqrt{1+\left(\frac{\gamma+1}{4}M\delta\right)^2} \quad . \quad . \quad (2)$$

If expanded for small $M\delta$ (the series converges for $M\delta < 4/(\gamma+1)$) it reduces to eqn. (1) above. For $M\delta > 1{\cdot}67$ one can obtain

$$\left(\frac{p}{p_\infty}-1\right)=\frac{2\gamma}{\gamma+1}+\frac{\gamma(\gamma+1)}{2}(M\delta)^2-f\left[\frac{1}{(M\delta)^2}\right] \quad . \quad (3)$$

In ref. 4, Bertram and Cook suggested that by replacing $M\delta$ by $(M^2/\beta)\sin\delta$ (where $\beta=\sqrt{M^2-1}$) eqn. (2) could be made to link up with linear theory and Newtonian theory, thus extending the range of applicability but not the simplicity.

A similar substitution (in effect) is suggested by Collingbourne and Peckham[5] into eqn. (1) to give a rather complicated third order expression valid for $\delta < 15°$ and $M\delta < 2{\cdot}25$.

Cleary and Axelson[6] give an expression which is valid for high Mach numbers and δ's almost up to shock detachment but not valid for small δ. It is also rather complicated for analytic use.

Finally, Newtonian theory, *ie*

$$C_P=2\sin^2\delta \quad \text{for} \quad \gamma=1$$

$$\text{or } =(\gamma+1)\sin^2\delta \text{ in modified form;}$$

Originally received 13*th September* 1966. *Revised* 25*th October* 1966.

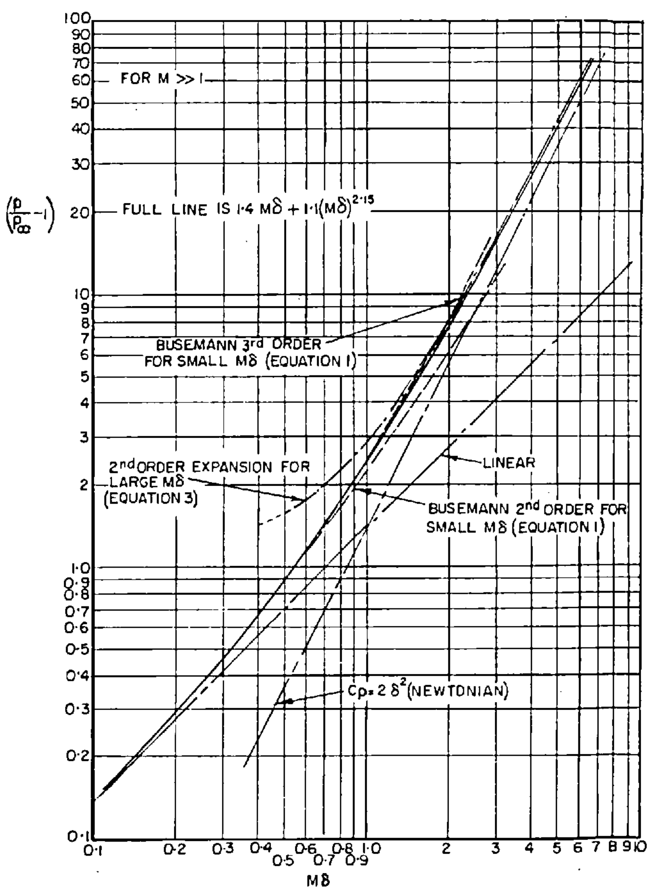

Figure 1.

or for small δ,

$$\left(\frac{p}{p_\infty}-1\right)=1{\cdot}4\,(M\delta)^2 \quad \text{or}=\frac{\gamma(\gamma+1)}{2}(M\delta)^2 \text{ respectively} \quad . \quad . \quad (4)$$

is inaccurate at small δ's and only moderate Mach numbers.

Thus there is a region of moderate δ's and Mach numbers where none of the existing approximations are sufficiently accurate or sufficiently simple. A new formula has been developed to extend to this range by looking for a single term of non-integer power to replace the second order and subsequent terms of the series expansions with the result:—

$$\left(\frac{p}{p_\infty}-1\right)=\gamma M\delta+1{\cdot}1(M\delta)^{2{\cdot}15} \quad \text{for } \gamma=1{\cdot}4 \quad . \quad (5)$$

This expression is compared with eqns. (1), (3), (4) and the linear result in Fig. 1. The exact results and Linnell (eqn. (2)) are so close to eqn. (5) that they could not be conveniently shown on this figure. It is evident that none of the approximations are sufficiently accurate over all the range. Eqns. (1) and (3) together are a good approximation although still with appreciable error in the central range unless the third order term is used. They would not be convenient in use.

In Fig. 2 eqn. (5) is compared with the exact results (from ref. 7). The accuracy of the approximation is evident. While an improvement over some of the range could be achieved by changing the constant of the second order term in the Busemann expansion, it could not be made to be as accurate as eqn. (5).

A new approximation for the pressure on inclined surfaces at hypersonic speeds has been developed. This approximation is simple, accurate and useful over the range $0 < M\delta \leq 10$ and flow deflection angles almost up to shock detachment.

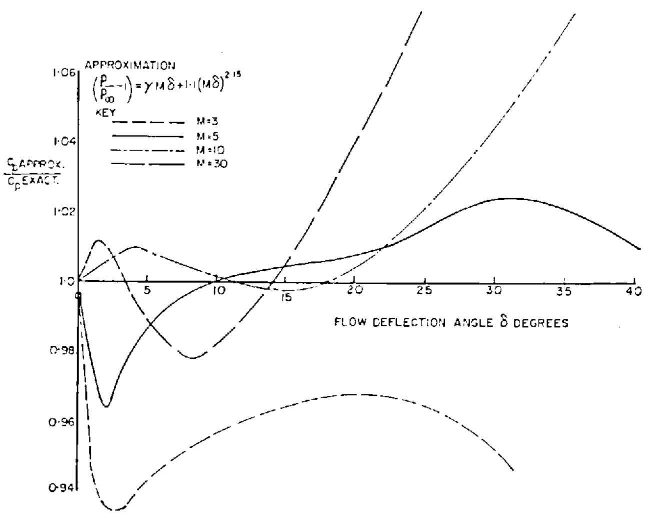

Figure 2.

References

1. BUSEMANN, A. Aerodynamic Lift at Supersonic Speeds. Luftfohrtforschung Bd 12, No. 6, pp 40-220, October 1935.
2. Ames Research Staff. Equations, Tables and Charts for Compressible Flow. NACA 1135, 1953.
3. LINNELL, R. D. Two-dimensional Aerofoils in Hypersonic Flows. *J Aero Sci*, pp 22-30, January 1949.
4. BERTRAM, M. H. and COOK, B. S. The Correlation of Oblique Shock Parameters for Ratios of Specific Heats from 1 to 5/3 with Application to Real Gas Flows. NASA TR R-171.
5. COLLINGBOURNE, J. R. and PECKHAM, D. H. The Lift and Drag Characteristics of Caret Wings at Mach Nos between 5 and 10. RAE Tech Rep No 66036, February 1966.
6. CLEARY, J. W. and AXELSON, J. A. Theoretical Aerodynamic Characteristics of Sharp and Circularly Blunted Wedge Airfoils. NASA TR R-202.
7. TRIMPI, R. L. and JONES, R. A. A method of Solution with Tabulated Results for the Attached Oblique Shock Wave System for Surfaces at Various Angles of Attach Sweep and Dihedral in an Equilibrium Real Gas Including the Atmosphere. NASA, TR-R63.

PRINTED BY THE LEWES PRESS WIGHTMAN & CO. LTD., LEWES, SUSSEX, ENGLAND, AND PUBLISHED BY THE ROYAL AERONAUTICAL SOCIETY, 4 HAMILTON PLACE, LONDON W.1. ENGLAND.

Ph.D. 1967. OPATOWSKI (T.P.S.) 2

C.P. No. 908

C.P. No. 908

MINISTRY OF AVIATION

AERONAUTICAL RESEARCH COUNCIL

CURRENT PAPERS

Gun Tunnel Measurements of Lift, Drag and pitching Moment on a 20° Cone, a Flat Delta and a Caret Delta Wing at a Mach number of 8.3

By

T. Opatowski
Imperial College of Science and Technology

LONDON: HER MAJESTY'S STATIONERY OFFICE

1966

Price 10s. 6d. net

C.P. No. 908

December, 1965

Gun Tunnel Measurements of Lift, Drag and Pitching Moment on a 20° Cone, a Flat Delta and a Caret Delta Wing at a Mach number of 8·3

- By -

T. Opatowski,

Imperial College of Science and Technology

Communicated by Prof. P. R. Owen

SUMMARY

Measurements of lift drag and pitching moment have been made on a 20° half-angle, right-circular cone and on two delta wings of triangular and caret cross section, 10° wedge angle and aspect ratio 1 in the Imperial College gun tunnel.

The strain gauge balance developed for this purpose gave results which were within 5% of other published cone data.

Maximum lift/drag ratios of about 3·7 were obtained for both wings at the test Mach number of 8·3 and Reynolds number based on root chord of $1{\cdot}5 \times 10^6$.

The measured lift, drag and lift/drag ratio agreed well with estimates based on two-dimensional oblique shock theory and laminar skin friction.

List/

Replaces A.R.C. 27 582

List of Contents

---

1. Introduction

The object of the work, which is covered in part by this report, was to make force measurements in the gun tunnel on models of hypersonic lifting vehicles. This entailed considerable modification and development of an existing strain gauge balance. Other strain gauge balances for short duration facilities have either been inertia compensated (e.g., Ref. 14) or made extremely stiff with electronic filtering of the vibratory signal components (e.g., Ref. 12). As the natural frequency of the present balance plus models was too low for electronic filtering a hydraulic damper was fitted.

A 20° half-angle cone was chosen as a calibration model and showed, by comparison with existing data from conventional wind tunnels, that reasonable results could be obtained. The two delta wings tested, one plain and one caret or Nonweiler, were the first of a series of slender wings to be tested and though they presented a more difficult task for the balance, useful results have also been obtained.

2. The Gun Tunnel Balance

2.1 Physical details

The layout of the modified balance is shown in Fig. 1(a) and diagramatically in Fig. 1(b). There are three cantilevers (A, B & C) in what was part of the original balance and these are connected through the flexure hinges (D) to the balance beam via tapered pins. The aft cantilever measures drag while the other two together measure lift and were intended to measure pitching moment, but proved insufficiently accurate for this purpose.

At the front of the balance beam is mounted a combined moment sensor and incidence adjustor. The whole unit (E & F) is free to rotate about a phosphor bronze bush (J) but the end of the moment sub-beam (E) is restrained by a pin which is free to slide fore and aft in the balance beam.

The catch shown (G) together with another underneath, not shown, connect the model mounting plate to the moment sub-beam allowing incidence adjustments in steps of $7\frac{1}{2}°$. Adjustment within these steps was accomplished by tilting the whole balance on a special mount.

Damping was provided by the hydraulic damper (H). Highly viscous silicon fluid of 10^5 centistoke was used and the desired damping achieved by progressively reducing the size of the piston. In the optimum damping configuration the piston was less than half the area of the dashpot. Typical lift traces with and without damping are given in Fig. 2(b).

The lift and drag cantilevers used foil type Budd gauges while the moment sensor used two silicon strain gauges (Type 3A-1A-120P made by Ether Ltd.). These gauges have a sensitivity sixty times that of the foil gauges. Silicon gauges change their resistance and gauge factor with temperature, a characteristic that causes difficulties in continuous facilities necessitating special compensating techniques (see Ref. 15 for example). No change in temperature occurred during the short running time of the gun tunnel (checked by recording the output of the bridge in the 'calibrate' configuration (Fig. 3) and hence its resistance through a run) and it was

found/

found possible to allow for variations caused by atmospheric changes of temperature by measuring the gauge resistance before each run. The P type gauges have the larger variation of resistance with temperature and these were chosen to give the best sensitivity in determining the temperature and hence gauge factor (see Fig. A1).

The circuit for the moment sensor is shown in Fig. 3. All channels were fed from a 9v stabilized voltage source but the voltage input to the moment channel was dropped to 3v by resistors. The six component bridge network in the moment channel (Fig. 3) was so arranged that for test each gauge was in a separate leg of a Wheatstone bridge circuit while for gauge factor measurement both gauges were in one leg of the bridge. The arrangement of the voltage dropping resistors was such that the current through the gauges was approximately the same when switched to 'test' or 'calibrate' in order to maintain a constant level of self-heating.

2.2 Performance

Because of mishandling the balance was slightly strained and this resulted in non-linear readings which changed slightly from time to time. It was essential to check the calibration frequently in order to achieve reliable data. Calibrations were carried out before and after each series of tests with spot checks about every ten runs as shown in Figures A1 to A5.

The load capacity of the balance was:-

Lift	10 lb
Drag	24 lb
Moment	200 lb in.

and the sensitivities were approximately

Lift, front	0·54 mv/lb
Lift, rear	0·33 mv/lb
Drag	0·16 mv/lb
Moment	1·82 mv/lb in.

The vibratory frequencies were complicated by the damper which tended to couple the lift and drag. With the cone model which weighed 51 gm a predominant 170 c.p.s. was evident on the lift trace (shown in Fig. 2(a)) and this seemed to be superimposed on an aperiodic decay. The level of damping was chosen to ensure that the mean line had reached its steady value; which limited the amount of damping possible on the higher frequency mode.

The wing models, which weighed 135 gm were mounted much further forward on the balance and had a dominant lift frequency (damped) of 100 c.p.s. The drag traces were very irregular with no clearly dominant frequency. Typical drag traces are given in Fig. 2.

As/

As the model centres of gravity were not at the moment pivot point (para. 2.1) the lift vibrations were reflected in the moment trace. The natural frequency of the moment cantilever was calculated to be 500 c.p.s. and was not discernible on the traces.

The main unusual design features, namely the use of uncompensated silicon gauges, the plain bearing and the hydraulic damper; worked satisfactorily. The change in gauge factor due to temperature change was never more than 3% during these tests and could be determined to better than 5% of this 3% variation. The friction from the plain bearing made calibration more difficult but gave no trouble in use because of the short running time during which the readings never settled completely. By calibrating with increasing and decreasing loads and with extreme care, consistent calibrations were achieved.

Full details of the balance calibration are given in Appendix A.

3. Force Measurements

3.1 Models tested

The cone and delta wing models are shown in Fig. 4, together with their relevant physical details. A $2\frac{1}{2}$ in. diameter hemisphere was also tested for tunnel calibration purposes. (See para. 4.1).

The angle between the plane of the leading edge and the lower ridge line of the caret wing was 6°. At the test Mach number of 8·3 this would result in the shock lying in the leading edge plane at 4° and 16° incidence for inviscid 2-D flow and be within 0·7° of this plane between the above angles[7].

3.2 Test conditions

The cone was tested at incidences up to 30° in steps of $7\frac{1}{2}$°. The moment pivot was located at about the 3/4 chord point of the cone and this limited the incidence obtainable to 37° as the base of the cone came in contact with the balance beam.

The wings were tested in the incidence range α = 5° to 16°, the upper limit being dictated by balance strength considerations.

The actual incidences in the case of the cone were determined with a precision protractor. The deflection under load was negligible (see Appendix A). In the case of the wings two methods were used. The flat bottomed wing was measured with an inclinometer of known weight and the deflection under load measured and allowed for. The incidence was also measured from the schlieren photographs. The two methods agreed to within a maximum difference of 0·2°.

The tests were performed in the Imperial College gun tunnel described in Ref. 1. Since that report, the conical nozzle has been replaced by a Mach 8 (nominal) contoured nozzle. With atmospheric pressure in the barrel the test conditions were:-

Driving Pressure p.s.i.	Mach No.	Re/Inch
2000	8·25	$0{\cdot}23 \times 10^6$
1000	8·3	$0{\cdot}17 \times 10^6$

The/

The calibration of the contoured nozzle was carried out at 2000 p.s.i. driving pressure and gave a mean Mach number of 8·25 with negligible Mach number gradient. The test Mach number at 1000 p.s.i. driving pressure was deduced from drag measurements on a hemisphere as described in para. 4.1. Most of the tests were carried out at 1000 p.s.i. driver pressure because of balance strength limitations.

All the wing tests were run with 1000 p.s.i. driver pressure and 40 p.s.i.a. in the barrel giving a Reynolds number per inch of $0{\cdot}296 \times 10^6$ in the free stream.

4. Results and Discussion

4.1 Hemisphere

The drag coefficient of the hemisphere measured with 2000 p.s.i. driving pressure at a Mach number of 8·25 was 0·915. This compared well with that given, for example, by Hoerner[2] and served as a check on both the balance and the tunnel calibration. The hemisphere was then used to determine the effective Mach number when operating with 1000 p.s.i. driving pressure, using the calibration of the reservoir pressure of the tunnel given in Ref. 1.

4.2 20° Cone

Figures 5, 6 and 7 give the measured lift coefficient, drag coefficient and centre of pressure position against incidence, respectively.

Also plotted on these figures are some experimental results from several sources[3,4,5,6], and Newtonian values as calculated in Ref. 3. In each case the coefficients are based on plan area.

Good agreement with both experiment and Newtonian theory has been achieved in each case. The lift coefficient would appear to be somewhat higher than the comparative results but the difference is within the accuracy of the balance (see para. 5.3). The conditions of the comparative tests ranged from $M_N = 6{\cdot}8$ to $M_N = 9{\cdot}6$ and $Re = 0{\cdot}56 \times 10^6$ to $1{\cdot}2 \times 10^6$ thus bridging the conditions of the present experiments.

The drag and pitching moments are in excellent agreement. The pitching moment was so close to zero that it has had to be plotted on a very much expanded scale.

4.3 Delta wings

4.3.1 Lift

The measured values are compared with two simple theoretical estimates in Figure 8. For the full line in the figure, two-dimensional flow has been assumed to exist on all surfaces (i.e., as if the surface was part of an infinite unswept plane) and the appropriate oblique shock or expansion pressures from Ref. 7 used to determine the lift coefficient. The under surface of the caret wing has been assumed to have two-dimensional flow over it for all the incidences tested and hence the two wings have the same estimated pressures on this surface. Thus the estimated lifts cannot show any direct benefit from the caret configuration. Allowance has also been made for the effect of boundary-layer thickness (see para. 4.3.2) though this only amounted to about 0·002 in lift coefficient.

The/

The dashed line is the Newtonian value using $C_p = 2 \sin^2\delta$ and the appropriate flow deflection angles (δ) for all surfaces.

Good agreement with the two-dimensional approximation has been obtained.

This is in accord with the recent numerical solutions of Babaev[16]. Although his solutions do not cover the present configuration, a mean pressure on the under surface of the order of 3 - 4% less than the true 2-D value would be indicated by his results and it is possible to see a difference of this order between the plain and caret wing results at the higher incidences where the influence of the upper surfaces is least.

Babaev's solutions apply strictly only to flows with attached leading edge shocks. For the plain delta of the present tests, shock detachment would be expected to occur at about 7° incidence. This is substantiated by the plan view schlieren photographs presented in Figs. 12 (d)-(g) and discussed in para. 4.3.4. The fact that the difference between the plain and caret wings was still of the order of magnitude indicated by Babaev's work suggests that slight shock detachment has only a small effect on the results for truly independent surfaces. This can also be deduced from Squire's results[19] where pressures close to those obtained from oblique attached shock theory were measured on the lower surface of a flat delta wing despite shock detachment due to the incidence of the upper surface.

The Newtonian estimate of lift is poor, as might be expected at these low flow deflection angles and moderate Mach numbers.

4.3.2 Drag

The experimental and theoretical drag results are shown in Fig. 9. The inviscid part of the theoretical drag was obtained in the same way as the theoretical lift.

Laminar flow has been assumed throughout and this was largely confirmed by schlieren photographs though in a few cases the flow appeared transitional towards the trailing edge of the root chord. The skin friction drag and boundary-layer thickness were calculated using the methods given by Monaghan[8], and Catherall[9], assuming that each streamwise strip was independent of its neighbour and behaved as a sharp flat plate with zero pressure gradient with appropriate free stream conditions. The free stream conditions used were those calculated for the inviscid lift (see para. 4.3.1).

The base pressure has been taken as half the free stream static pressure which is approximately the value given by King[10], for conditions similar to these tests. This value was also found in measurements made by McLellan, Bertram and Moore[13], on the base of a 20° wedge at a Mach number of 6·9 and Reynolds number of $0{\cdot}98 \times 10^6$.

The agreement of the experimental results with the theoretical drags obtained as above is reasonably good. The measured drags were generally slightly higher than the theoretical for both wings but both values are amply covered by the possible inaccuracies of the balance. The effect of leading edge sweep, three-dimensionality of the flow and the streamwise corner on the caret wing on the boundary layer or on transition have not been considered.

The/

The boundary-layer corrections to drag and lift have been included for each surface by taking the trailing edge, centre line displacement thickness (δ^*root) calculated as stated before and assuming an effective change of surface incidence given by $\frac{\delta^* \text{root}}{\ell}$, where ℓ is the model length.

Leading edge boundary-layer interaction would not be expected to have any significant effect under the test conditions[11].

As would be expected, both the theory and measured results show the caret wing to have a higher drag at incidence due to its greater wetted area. At lower incidences this is offset to some extent by the greater anhedral of the upper surface which gives less lift reduction. The greater drag is also offset in practice, though not in the present theory, by the slightly higher lift developed by the caret wing.

Newtonian theory, even with skin friction added, can again be seen to give a poor estimate.

4.3.3 Lift drag ratio

The measured and theoretical lift/drag ratios are shown in Fig. 10. Fortuitously, the Newtonian theory with laminar skin friction added now shows excellent agreement with the experimental data.

A maximum lift/drag ratio of about 3·7 was obtained in both cases. All the differences between the maximum lift/drag ratios, both measured and theoretical, are small and it is evident that the extra drag of the caret wing is balanced by the decreased lift of the plain delta.

The results agree well with similar measurements obtained by Becker[17], and Blackstock and Ladson[18].

4.3.4 Shock angles

The centre line shock angles were measured from schlieren photographs, and are plotted in Fig. 12(a). These angles corrected for boundary-layer displacement are also plotted and hence the size of the correction can be seen. Also plotted are the two-dimensional and conical shock angles. The shock angles on the caret wing were close to the two-dimensional values while the plain delta shock angles lay between the two-dimensional and the conical values as given in Ref. 7.

Typical schlieren photographs in side and plan view are presented in Figs. 12(b)-(g). The side view photographs are for incidences of approximately 10°, the 'design' incidence, when the upper surfaces of both models are streamwise.

The plan view photographs show the plain delta wing at 6°, 10° and 16° incidence and the caret delta at 16° incidence. At 6° the shock is still attached to the leading edge of the plain delta while it is slightly detached at 10°. At 16° the detachment is more noticeable while, by contrast, the shock is still attached on the caret wing for which this is the upper design shock closure angle.

4.3.5/

4.3.5 Centre of pressure position

Fig. 11 gives the measured centre of pressure positions. These models were the thinnest that could be accommodated on the balance and had to be mounted well forward of the moment sensor. This resulted in poor accuracy as compared to the cone results where the sensor could be buried in the model. (See para. 5.6.) All that can be said is that the C.P. was at about the expected 2/3 chord position.

5. Accuracy of Results

5.1 General

For those traces which exhibited a sinusoidal and decaying wave form the mean line could be determined quite accurately. The measurements were taken to 0·2 millimetres but were probably not repeatable to better than 0·7 millimetre.

Assuming a typical trace deflection of $3\frac{1}{2}$ cm for lift and moment this gives ± 2% reading accuracy.

A better estimate of the performance than the worst possible error is probably that error which is exceeded on say less than 20% of occasions and it is with this concept in mind that the following accuracies have been assessed, in so far as the greater errors of occasional traces with poor wave forms have been ignored.

5.2 Moments

The moment sensor was independent of the other channels and the obtainable accuracy is assessed at ± 3%, being made up from a calibration error of ± 1% and an error in trace reading of ± 2%.

5.3 Lift

In order to get a realistic estimate of the accuracy of the balance, the maximum possible errors for a typical run (wing), corresponding to a mean lift coefficient of 0·15, have been calculated with the following results:

Trace reading ± 2% of lift reading

Calibration ± 3% " " "

Moment calibration ± 3% of moment reading

Since the moment term, which is subtracted from the lift reading to get the true lift (see Appendix A) is typically about 1/3rd of the lift reading, a total error of ± 9% of the true lift results.

5.4 Drag

The main sources of error were those of trace reading and interaction from lift. The wing tests gave minute deflections at maximum sensitivity and (indeed because) the interaction from lift was considerable. For the cone tests both these factors were better and hence the accuracies are different for the two cases.

For/

For the run considered in para. 5.3 above and a similarly typical cone test corresponding to an incidence of $22\frac{1}{2}°$, the following maximum errors have been calculated.

	Cone	Wing
Trace reading	± 2%	± 27%
Calibration of drag	± 2%	± 2%
Calibration of interaction	± 3%	± 3%
Lift error (used in interaction)	± 5%	± 5%

The interaction corrections are additive and are typically 1/10th and 4 times the drag readings respectively and thus the errors as a percentage of the final drag are ± 5% and ± 12% for cone and wing tests respectively.

5.5 Lift/drag ratio

The possible error for L/D, for small errors, is the sum of the component errors, giving ± 21% for the wing results. When the % error is not small (i.e., near zero lift) this figure can be much increased.

5.6 Centre of pressure position

The accuracy obtainable in centre of pressure position measurement is shown in Appendix C to be given by

$$\frac{\Delta x}{L} = \left(\frac{\Delta M}{M} + \frac{\Delta L'}{L'}\right)\frac{x(x+a)}{aL}$$

with notation as listed and shown in Fig. 1(b).

The dominant effect of the distance of the centre of pressure from the moment sensor datum is evident.

The above expressions together with the errors for lift and moment given before, gives accuracies of ± 0·25% for the cone tests and ± 13% for the wing tests.

5.7 Tunnel running conditions

Measurements of tunnel conditions were not made for each run. A repeatability of 3% over 6 runs was achieved during calibration. Since these runs included instrumentation errors the tunnel repeatability would be expected to be better than 3%.

6. Conclusions

The lift, drag and pitching moment of a 20° half-angle cone and two thin delta wings of triangular and caret cross section have been measured with a strain gauge balance in the Imperial College gun tunnel.

The/

The results of the measurements on the cone agree with previously published data to within ± 5% in lift and ± 3% and ± 1% in drag and centre of pressure position respectively.

The measured values of wing lift, drag, and lift drag ratio agreed well with theoretical estimates based on the two-dimensional oblique shock relationships and laminar skin friction. Newtonian theory with laminar skin friction included gave good estimates of lift/drag ratio though poor estimates of lift and drag.

A maximum lift drag ratio of about 3·7 was obtained for both wings. The slightly greater skin friction drag of the caret wing appeared to be approximately balanced by a slightly higher lift.

Achnowledgements

The work reported here was carried out under a contract from the Science Research Council (formerly D.S.I.R.) and monitored by Dr. L. Pennelegion of the National Physical Laboratory.

Thanks are also due to my Supervisor, Mr. J. L. Stollery, to other members of staff and of the workshop of Imperial College who have helped in various ways and to several members of the Aerodynamics Department, R.A.E., Farnborough, for their constructive comments.

Notation/

Notation

a	Distance from moment datum to L hinge
a'	" " " " " L "
b	a' - a (Fig. 16 and Appendix C)
c_L	Lift coefficient
c_D	Drag coefficient
D	Drag
d	Drag bridge signal
K_L	L bridge constant
$K_{L'}$	L' bridge constant
ℓ	Length of body
l	Signal from L bridge
l'	Signal from L' bridge
L	Lift when used generally
L_1	Symbol for front lift cantilever
L'	Symbol for rear lift cantilever
L_T	True lift. Sometimes lift as determined from L cantilever
$L_{T'}$	Lift as determined from L' cantilever
M_N	Mach number
M	Moment about datum (Fig. 16)
m	Signal from moment bridge
p	Static pressure
R_N	Reynolds number
S	Wing area projected perpendicular to upper ridge line
T_L, T'_L	Loads in appropriate flexure hinges (Appendix B and C)
V	Volume of vehicle
x	Distance from moment datum to centre of pressure
α	Wing incidence. The angle between the free stream and the model centre line; lower centre line for wings
δ^*	Boundary-layer displacement thickness
θ	Angle between shock wave and free stream

References/

References

No.	Author(s)	Title, etc.
1	D. A. Needham	Progress report on the Imperial College Hypersonic Gun Tunnel. Imperial College of Science and Technology, Aeronautics Dept., Tech. Note No.118. August, 1963.
2	S. F. Hoerner	Fluid-Dynamic Drag. Published by the author - 148, Busteed Drive, Midland Park, N.J., U.S.A. 1958.
3	W. R. Wells and W. O. Armstrong	Tables of aerodynamic coefficients obtained from developed Newtonian expressions for complete and partial conic and spheric bodies at combined angles of attack and sideslip with some comparisons with hypersonic experimental data. N.A.S.A. TR R-127. 1962.
4	C. L. Ladson and T. A. Blackstock	Air-helium simulation of the aerodynamic force coefficients of cones at hypersonic speeds. N.A.S.A. TN D-1473. October, 1962.
5	J. A. Penland	Aerodynamic force characteristics of a series of lifting cone and cone-cylinder configurations at a Mach number of 6·83 and angles of attack up to 130°. N.A.S.A. TN D-840. June, 1961.
6	J. A. Penland	A study of the stability and location of the centre of pressure on sharp, right circular cones at hypersonic speeds. N.A.S.A. TN-2283. May, 1964.
7	-	Equations, tables, and charts for compressible flow. Ames Research Staff. N.A.C.A. Report 1135. 1953.
8	R. J. Monaghan	An approximate solution of the compressible laminar boundary layer on a flat plate. A.R.C. R. & M. 2760. November, 1949.
9	D. Catherall	Boundary-layer characteristics of caret wings. A.R.C. C.P. 694 August, 1962.

No.	Author(s)	Title, etc.
10	H. H. King	A tabulation of base flow properties for cones and wedges. Electro-Optical Systems Inc., Report RN - 17. (AD 426983).
11	J. C. Cooke	Leading edge effects on caret wings. R.A.E. Tech. Note Aero.2943. A.R.C.25 840 - F.M.3449 - Hyp.418. January, 1964.
12	L. Pennelegion, G. S. Smith and K. Dolman	Millisecond measurements of aerodynamic forces in a high-pressure shock tunnel. NPL Aero Report 1120. A.R.C.26 309 - Hyp.451. October, 1964.
13	C. H. McLellan, M. H. Bertram and J. A. Moore	An investigation of four wings of square plan form at a Mach number of 6·9 in the Langley 11-inch hypersonic tunnel. N.A.C.A. Report 1310. 1957.
14	J. R. Martin, G. R. Duryea and L. M. Stevenson	Instrumentation for force and pressure measurements in a hypersonic shock tunnel. Proceedings of Second Symposium on Hypervelocity Techniques, University of Denver, 20-21st March, 1962. Plenum Press, N.Y.
15	A. S. Platov and H. A. Ricci	Wind tunnel tests of solid state strain gauges. Proceedings of the 1st International Congress on Instrumentation in Aerospace Simulation facilities, L'Ecole Nationale Superièure de l'Aéronautique, Paris. September, 1964.
16	D. A. Babaev	Numerical solution of the problem of supersonic flow past the lower surface of a delta wing. A.I.A.A. Journal Vol. 1, p. 2224 - 2231. September, 1963.
17	J. Becker	Studies of high lift/drag ratio hypersonic configurations. International Council of the Aeronautical Sciences, 4th Congress, Paris, 24-28th August, 1964. ICAS Paper No. 64-551.
18	T. A. Blackstock and C. L. Ladson	Comparison of the hypersonic aerodynamic characteristics of some simple winged shapes in air and helium. N.A.S.A. TN D-2328. June, 1964.
19	L. C. Squire	Pressure distributions and flow patterns at M = 4·0 on some delta wings. A.R.C. R. & M. 3373 February, 1963.

APPENDIX A

Balance Calibrations

1. Calibrations Made

Several calibrations were carried out before, during and after the series of tests described in this report using different instruments and techniques. They are enumerated below.

(a) Before the series of tests commenced, a complete calibration including interactions was carried out using a Solartron digital voltmeter type LM 10102 as the test instrument. Checks were also made using an oscilloscope of the type used in operation (Tektronix 502) with and without the D.V.M. connected.

(b) A dynamic check on the drag interaction was made by dropping weights from the balance and recording the apparent drag changes on an oscilloscope.

(c) In situ calibrations of the lift and moment and the drag interaction were carried out before and several times during the wing tests. These were made by using a slow scan rate on the C.R.O. and lifting the weights rapidly on and off the balance.

(d) Some time after the conclusion of the tests covered by this report a further complete calibration was carried out using a Digital Measurement D.V.M.

(e) After preliminary tests with some further wings (during which high overshoot loads were encountered) the drag sensor was changed to silicon gauges and a further complete re-calibration carried out using a Solartron D.V.M. type LM 1420.

(f) Finally, in order to try and clear up certain inconsistencies in the calibrations and results, a method was devised of dropping weights consistently from the balance and a dynamic calibration of lift, moment and interaction of lift on drag was carried out.

The results of all the calibrations are shown in Figures A 1 to A 5. Due to having been strained, the balance showed some unusual characteristics and this together with the different circumstances and methods of each calibration was responsible for some of the variation between calibrations, though genuine changes of sensitivity may also have occurred.

2. Moment Channel

This was consistent throughout, though a slight shift of calibration occurred in the interval between the end of the tests described herein and the recalibration preceding the next tests. As seen in Fig. A 1, calibrations (a) and (c) agreed, giving 0·55 lb in./mv for normal temperatures (datum combined resistance reading of 470 = 249·8 Ω). The variation in gauge factor due to temperature was 0·67%/Ω or about 0·4%/°C temperature change.

The/

The later calibrations, (d), (e) and (f) (not shown on the graph for clarity) gave a sensitivity of 0·575 lb in./mv when corrected to the same datum temperature, representing an apparent change in calibration of $4\frac{1}{2}$% in about six months.

3. Drag Channel

The various calibrations are plotted in Fig. A 2. A sensitivity of 6·3 lb/mv was obtained.

4. Lift Channels

These channels showed the greatest variation. The results for the forward lift cantilever (designated L_1) are plotted in Fig. A 3 and those for the rear cantilever (designated L') in Fig. A 4.

The initial calibration of the L_1 channel was non-linear and appeared to give a slightly different non-linear line for each position of the centre of pressure. The mean line chosen did not pass through the origin and was given by

$$\text{Lift} = 1{\cdot}85 \times \text{mv reading} - 0{\cdot}2 - \frac{M}{6} \text{ lb}$$

where M is the moment of lift about the moment datum and 0·2 lb was the amount by which the chosen line did not pass through the origin.

The calibrations (c) made during the last set of the present tests confirmed this value but later calibrations (d), (e), (f) tended away from this to a minimum value of 1·65 instead of 1·85 and with the final dynamic calibration being somewhere between the two extremes.

The initial calibration of the L' channel was similar in form to the L_1 channel and the chosen line gave:-

$$\text{Lift} = 3{\cdot}03 \times \text{mv reading} - 0{\cdot}2 - \frac{M}{3} \text{ lb.}$$

The calibrations (c) gave a slightly different result:-

$$\text{Lift} = 3{\cdot}12 \times \text{mv reading} - \frac{M}{3} \text{ lb}$$

and this was used for the wing tests. Subsequent calibrations lay between the two above values. Both lift channels exhibited hysteresis and the L' channel at high loads took a finite time (about 50 m sec) to fully return to its zero (as shown by the dynamic calibrations).

To summarize, although the calibration constants of the lift channels varied slightly with time and use, the variation through the test period was small, as shown by frequent calibrations ($< 5\%$).

Subsequent calibrations showed continued variations but also showed that, at least for times greater than 50 m sec there was no difference between static and dynamic results.

5./

5. Interactions

All interactions other than that of lift on drag were negligible. The interaction of lift on drag is plotted in Fig. A 5. The initial calibration shows the hysteresis, mainly of the loading system. The mean, of 11·4% of the L' sensor reading, coincided with that obtained by dropping a weight from the balance (calibration (b)). However, three checks carried out during the wing tests (calibration (c)), each gave a value of 10% and this was used for these tests. Calibration (d), sometime after the tests again gave 11·4%. For later calibrations this channel had been changed to silicon gauges.

Also plotted in Fig. A 5 is a residual correction used for the cone results which corrected the chosen straight line to the non-linear line for the appropriate centre of pressure position.

Note: All the sensitivities quoted are for 9v basic excitation voltage (i.e., 3v on moment channel).

6. Deflections under Load

For the cone tests the incidence deflection for maximum load was 0·1°. For the wing tests it was 0·13°/lb which was allowed for, in addition to incidence measurements from the schleiren photographs.

APPENDIX B/

APPENDIX B

Method of Obtaining Lift Measurement

The lift may be obtained from any two of the three readings, front lift, rear lift and moment. It is more accurate to take either lift reading with the moment.

With the notation as listed and shown in Fig. 1(b), taking moments about the moment datum,

$$M + aT_L - a'T'_L = 0 \qquad \dots(B.1)$$

and

$$L + T'_L - T_L = 0 \qquad \dots(B.2)$$

substituting (B.2) into (B.1), rearranging, and noting that $L \equiv L_T$ when derived from T_L or $L \equiv L'_T$ when derived from T'_L,

$$L'_T = \left(\frac{a'}{a} - 1\right) T'_L - \frac{M}{a} \qquad \dots(B.3)$$

or

$$L_T = \left(1 - \frac{a}{a'}\right) T_L - \frac{M}{a'}. \qquad \dots(B.4)$$

Hence plotting $L + \dfrac{M}{a'}$ or $L + \dfrac{M}{a}$ against ℓ or ℓ' respectively will produce a straight line whose slope is $k_L\left(1 - \dfrac{a}{a'}\right)$ or $k'_L\left(\dfrac{a'}{a} - 1\right)$ respectively, where $k_L \propto T_L$ and $k'_L \propto T'_L$.

These values are plotted in Figs. A.3 and A.4.

APPENDIX C

Derivation of Balance Accuracy Estimation

1. Lift/Drag Ratio

$$\Delta \frac{L}{D} = \frac{\partial\ L/D}{\partial L} \Delta L \pm \frac{\partial\ L/D}{\partial D} \Delta D$$

$$= \frac{1}{D} \Delta L + \frac{L}{D^2} \Delta D$$

$$\therefore \frac{\Delta\ L/D}{L/D} = \frac{\Delta L}{L} + \frac{\Delta D}{D}.$$

2. Centre of Pressure Position

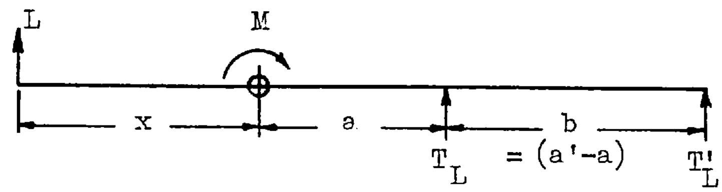

$$x = \frac{M}{L} \qquad \ldots(C.1)$$

$$\therefore \Delta x = \frac{\partial x}{\partial M} \Delta M \pm \frac{\partial x}{\partial L} \Delta L$$

$$= \frac{\Delta M}{L} + \frac{M}{L^2} \Delta L. \qquad \ldots(C.2)$$

Therefore from (C.1)

$$\frac{\Delta x}{x} = \frac{\Delta M}{M} + \frac{\Delta L}{L}. \qquad \ldots(C.3)$$

Similarly, since $L = \dfrac{T'_L b}{(x+a)}$

$$\frac{\Delta L}{L} = \frac{\Delta T'_L}{T'_L} + \frac{\Delta x}{(x+a)}. \qquad \ldots(C.4)$$

Substituting/

Substituting (C.4) into (C.3) and rearranging

$$\frac{\Delta x}{x} = \left(\frac{\Delta M}{M} + \frac{\Delta T_L'}{T_L'}\right)\left(\frac{x + a}{a}\right).$$

The % centre of pressure position for the body under test can be represented by $\frac{\Delta x}{L}$, hence finally, $\frac{\Delta x}{L} = \left(\frac{\Delta M}{M} + \frac{\Delta T_L'}{T_L'}\right)\frac{x(x+a)}{aL}$.

PC
ES

Gauge positions

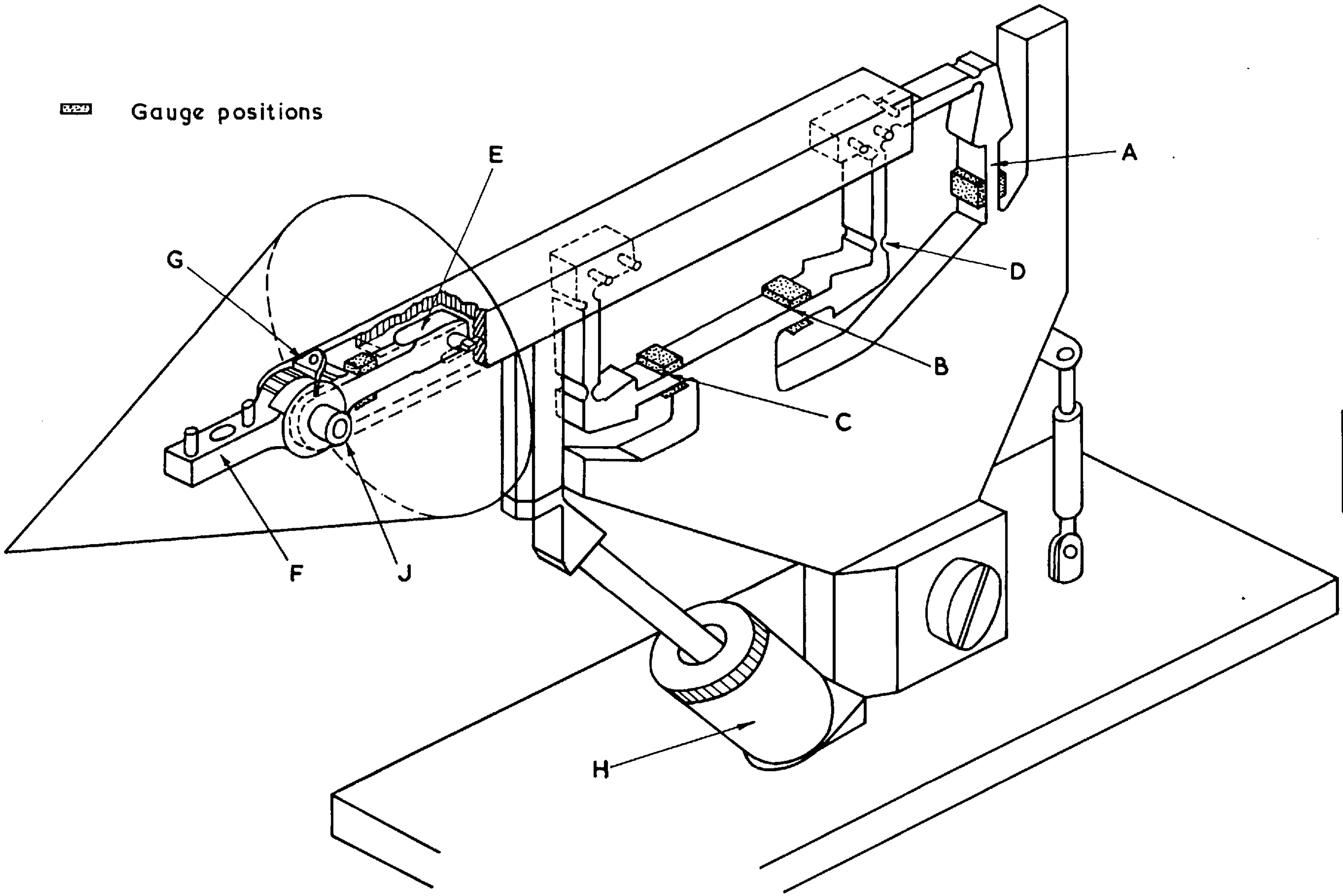

Layout of balance (Covers off)

FIG. 1(a)

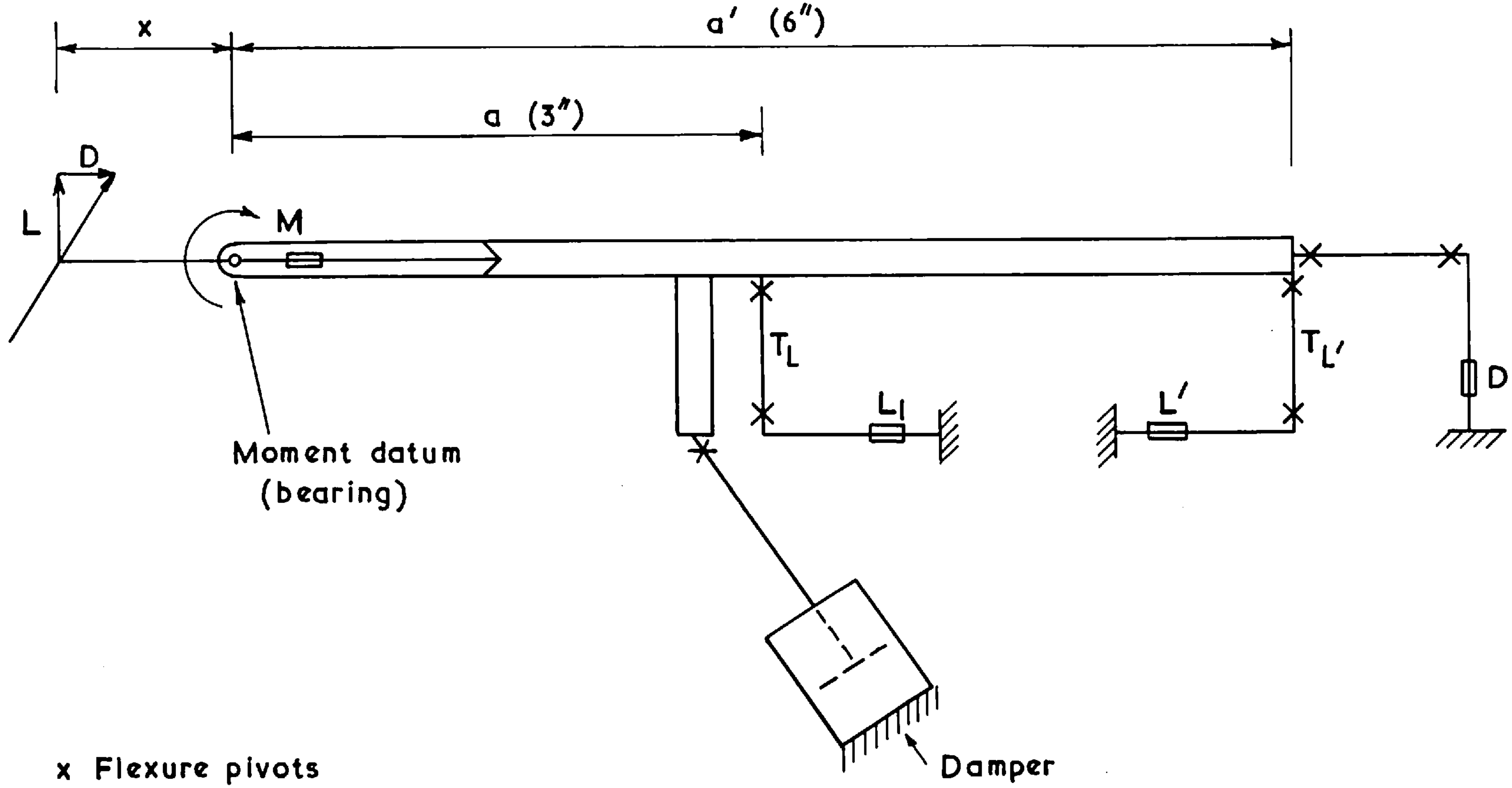

General arrangement of balance

FIG. 1(b)

FIG. 2 (a & b)

P_1 = Initial barrel pressure
P_4 = Drive vessel pressure

Drag D

Rear lift L′

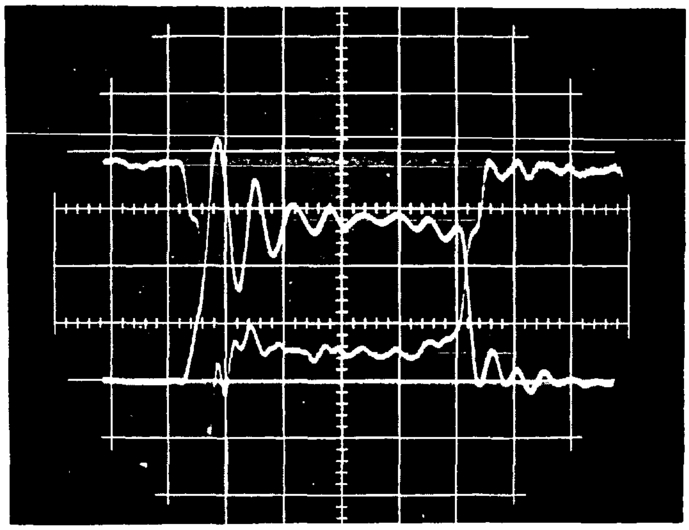

Time base
1 cm = 10 m sec
P_4 = 1000 p.s.i.
P_1 = 14 7 p.s.i.

(a) With damping (cone model)

Front lift L_1

Rear lift L′

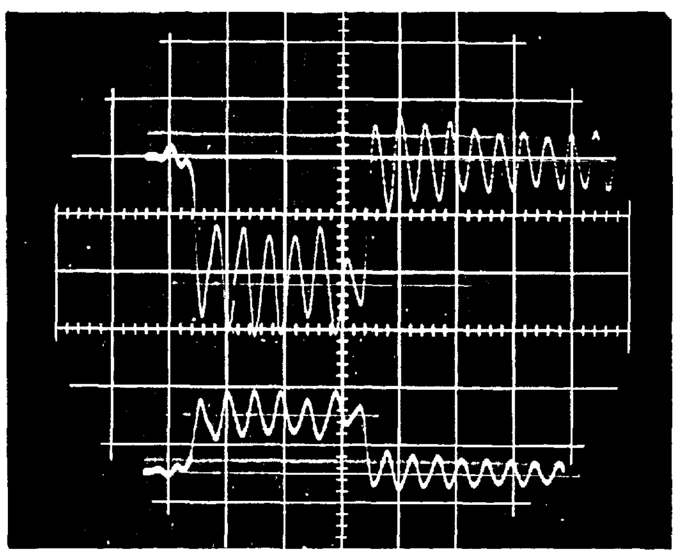

Time base
1 cm = 10 m sec
(Mach 10)
P_4 = 2000 p.s.i.
P_1 = 14·7 p.s.i.

(b) Without damping (original balance)

Typical traces with and without damping

FIG.2 (c – e)

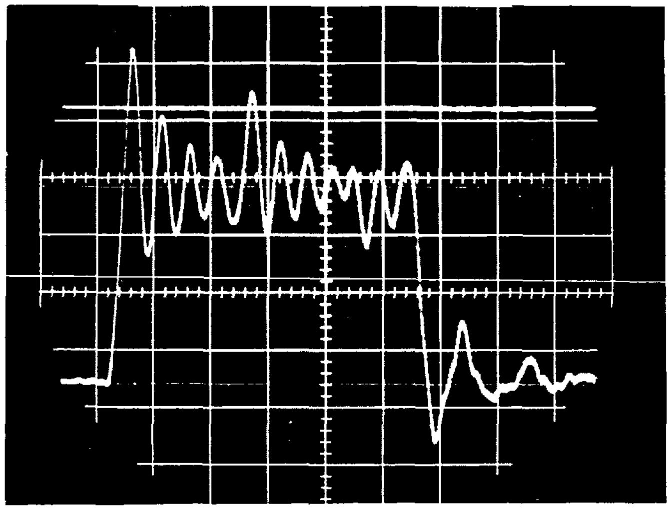

(c)

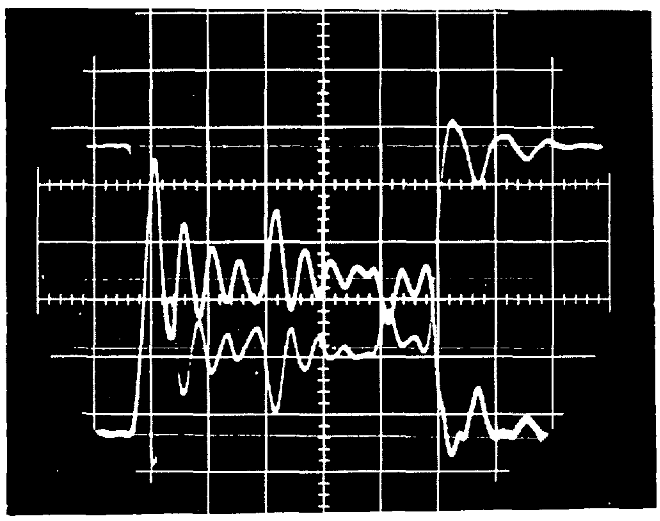

(d)

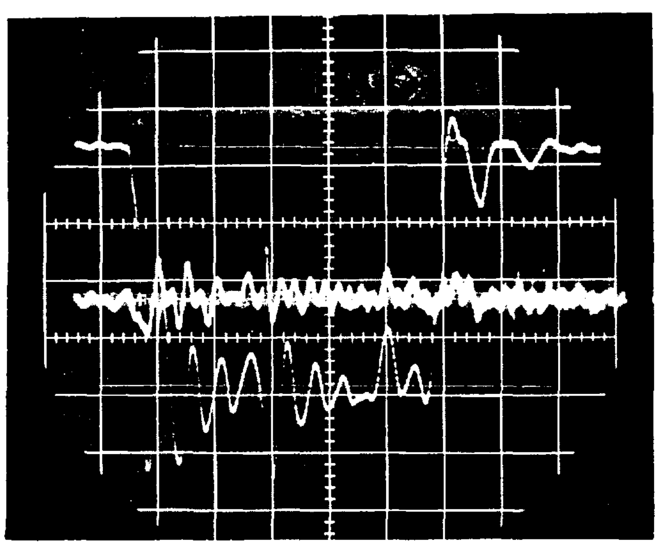

(e)

Typical traces with wing models

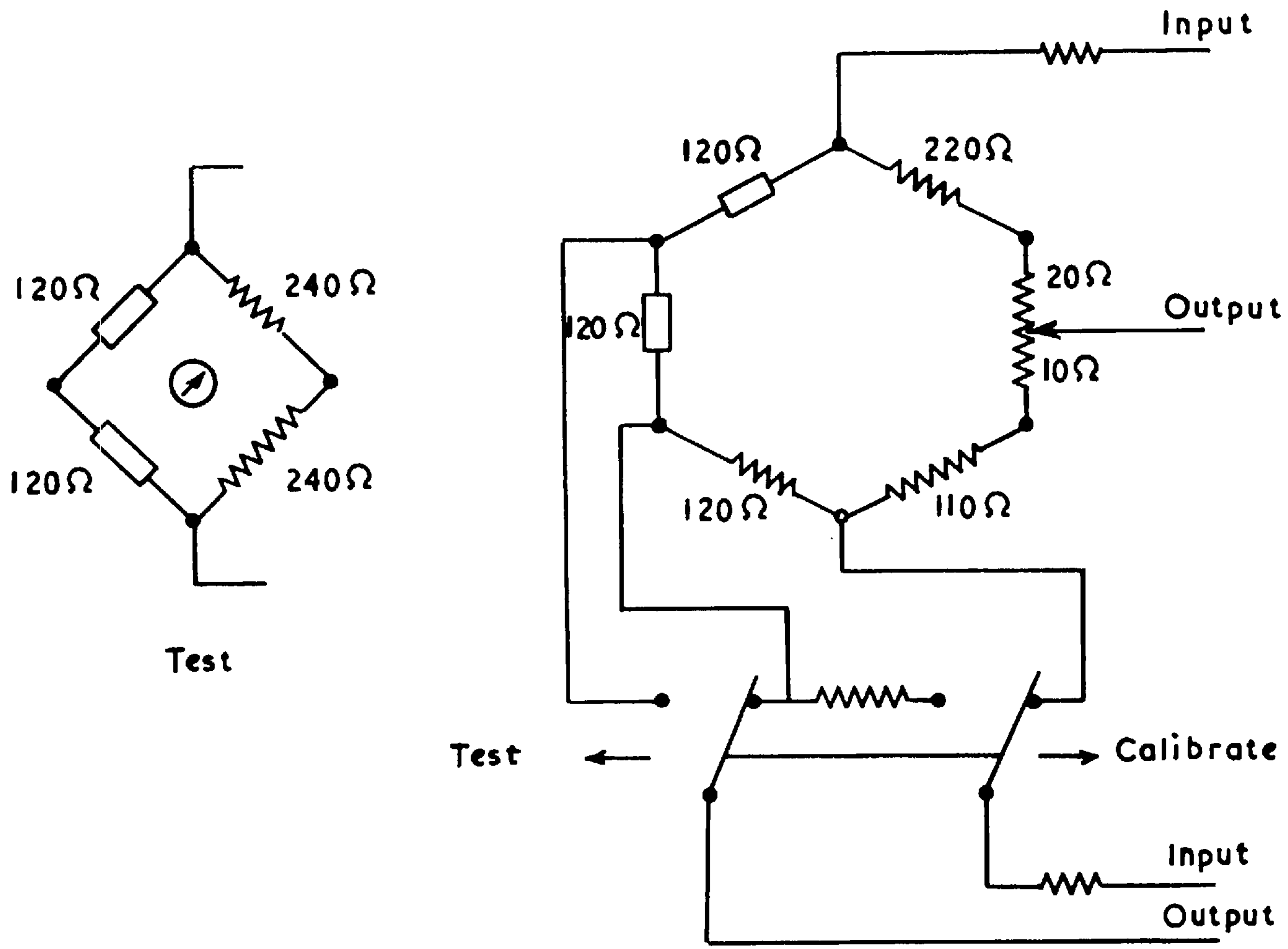

FIG 3

Moment sensor circuit

FIG. 4

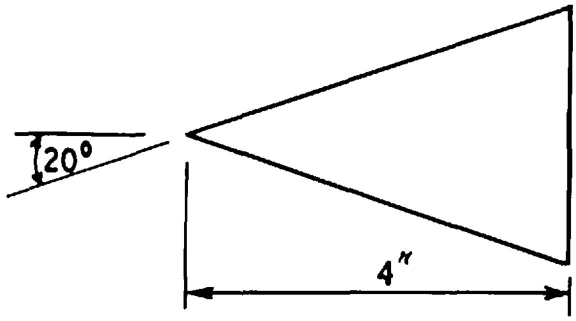

Weight 51 gms.

(a) Cone

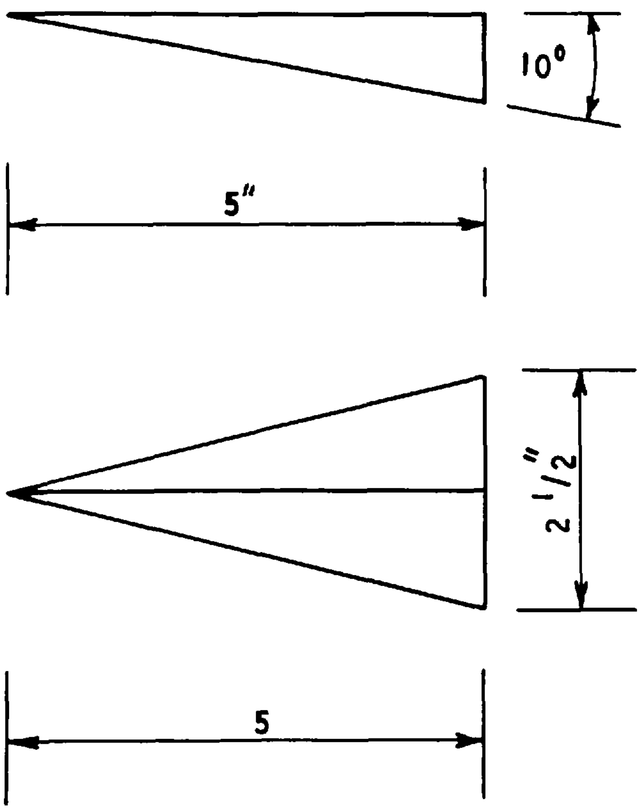

(b) Plain Delta

Both wings

AR = 1

$\frac{V}{S^{3/2}} = 0{\cdot}116$

Weight = 135 gms.

L.E. thickness
0·004" to 0·007" dia.

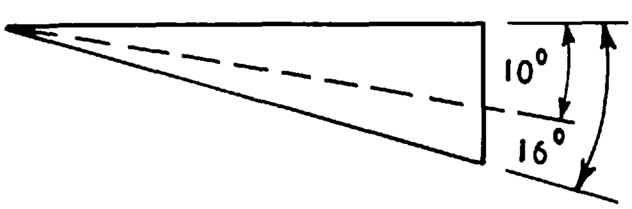

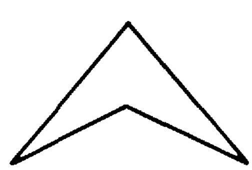

(c) Caret Delta

Sketch of models

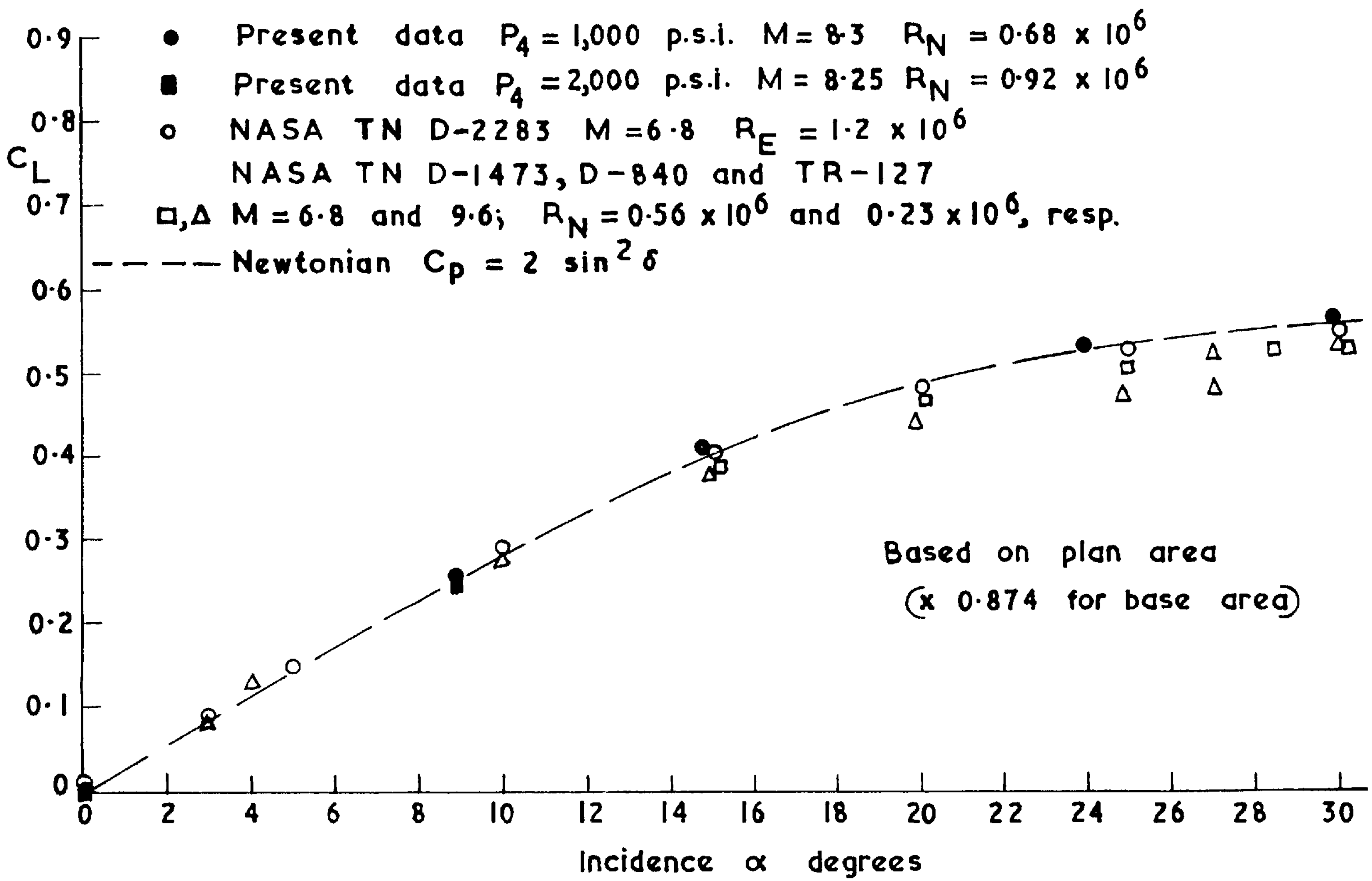

Lift of 20° half angle cone M = 8·3

FIG. 5

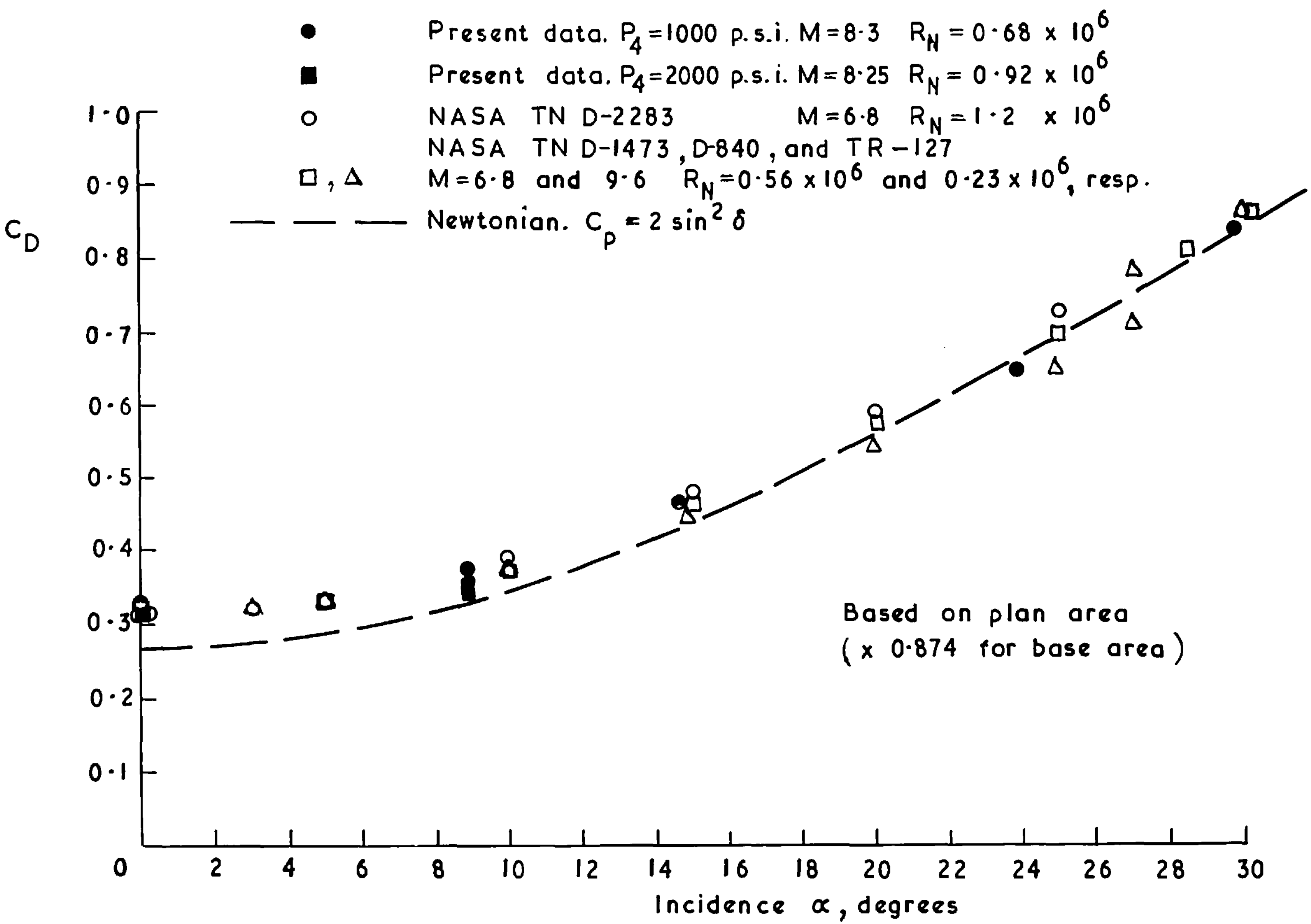

Drag of 20° half angle cone M = 8·3

FIG. 6

FIG. 7

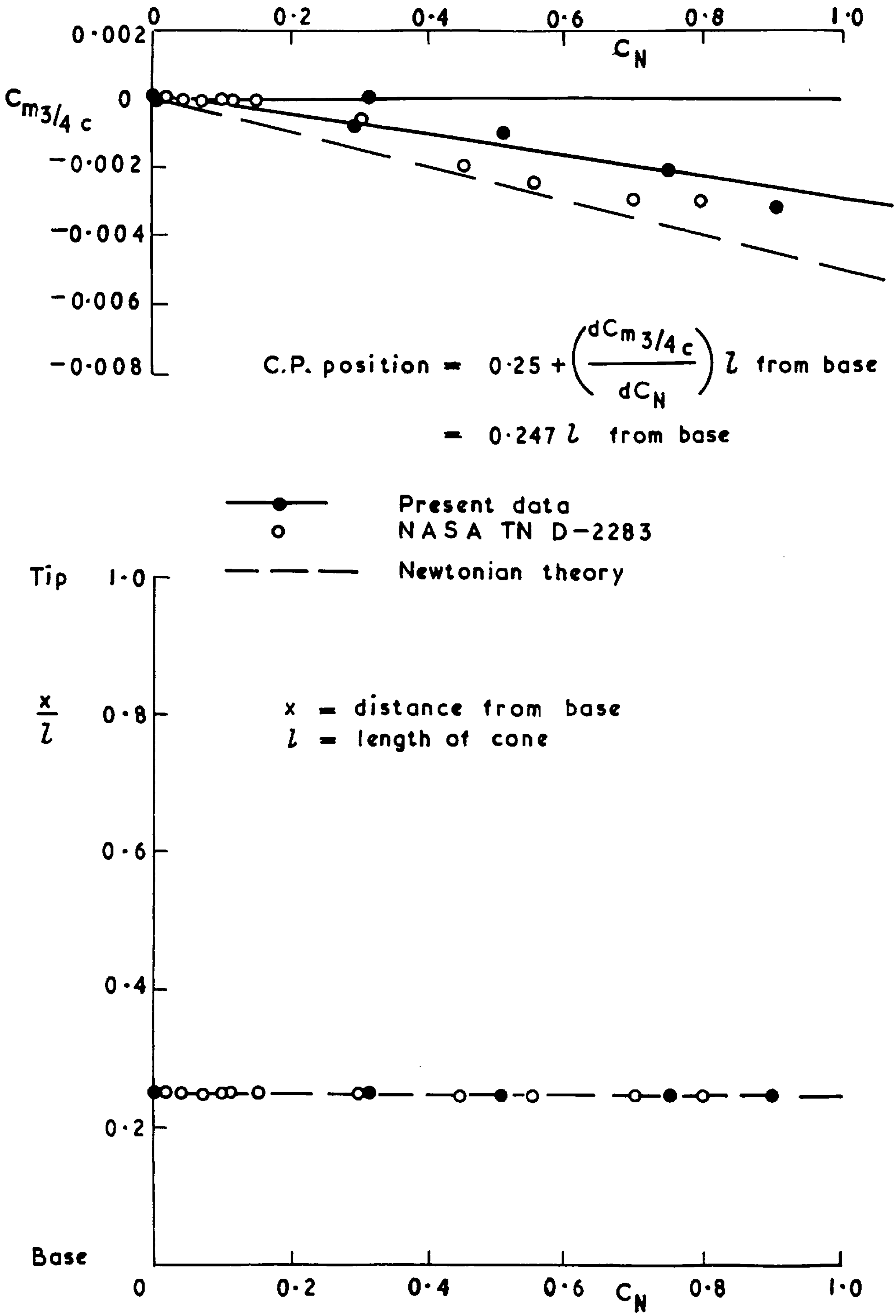

C.P. position on a 20° half angle cone

FIG. 8

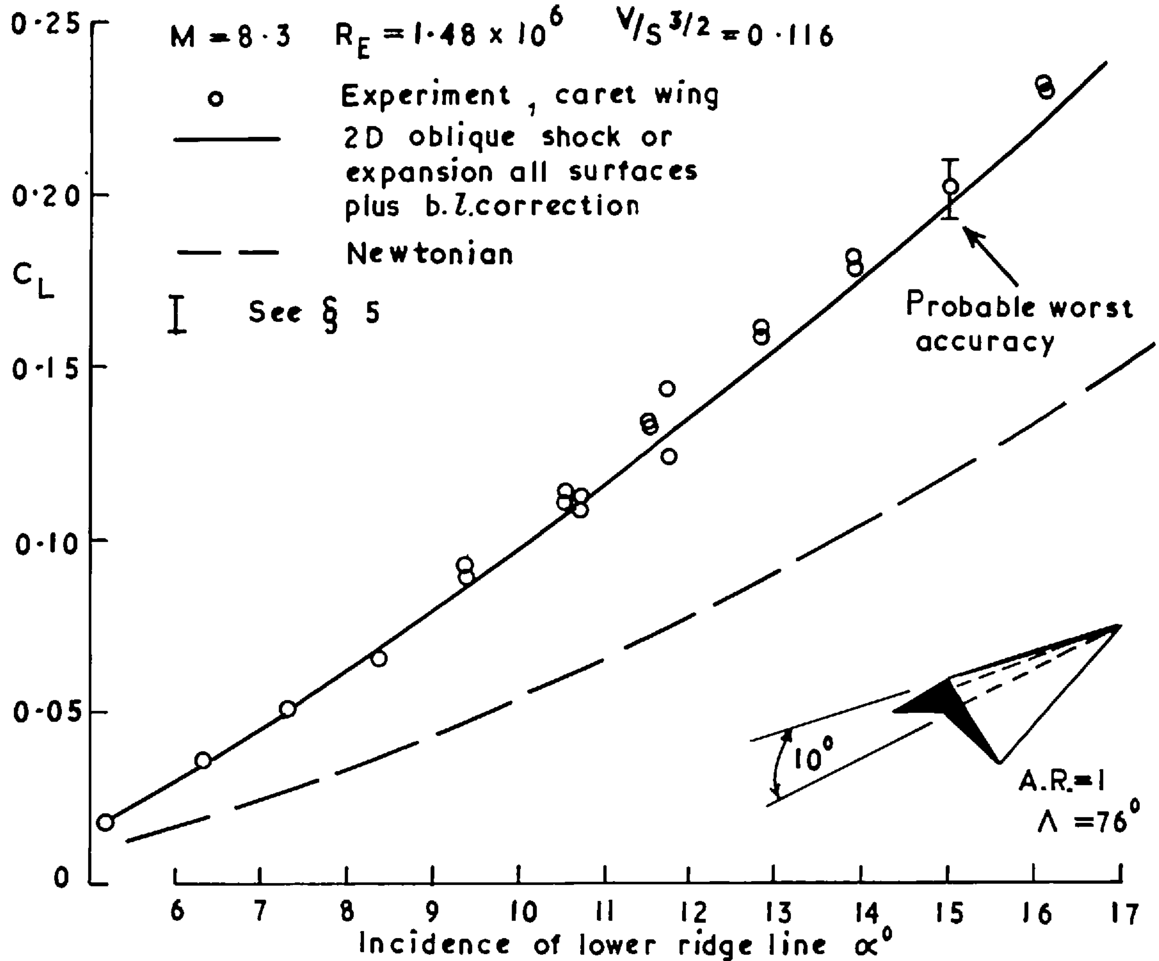

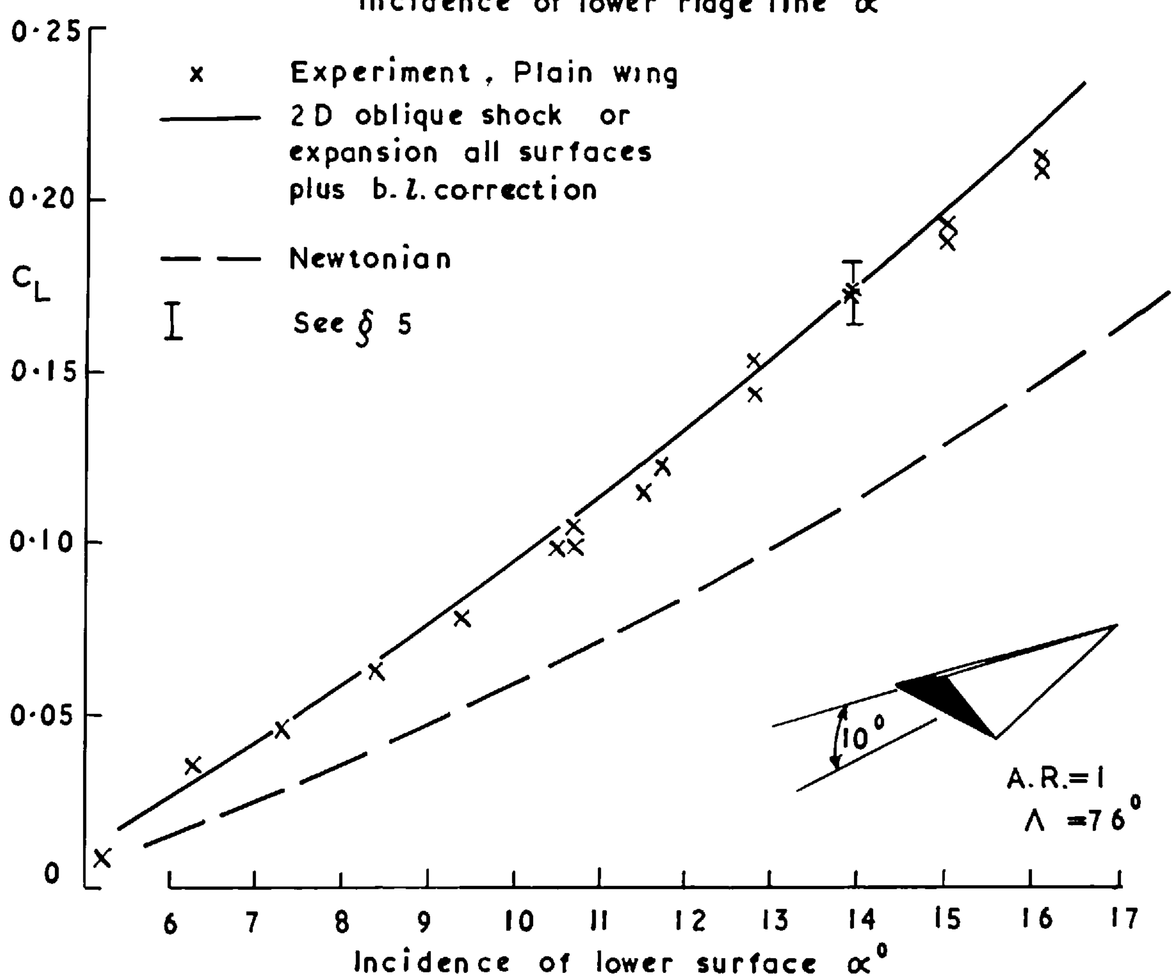

Lift of delta wings

FIG. 9

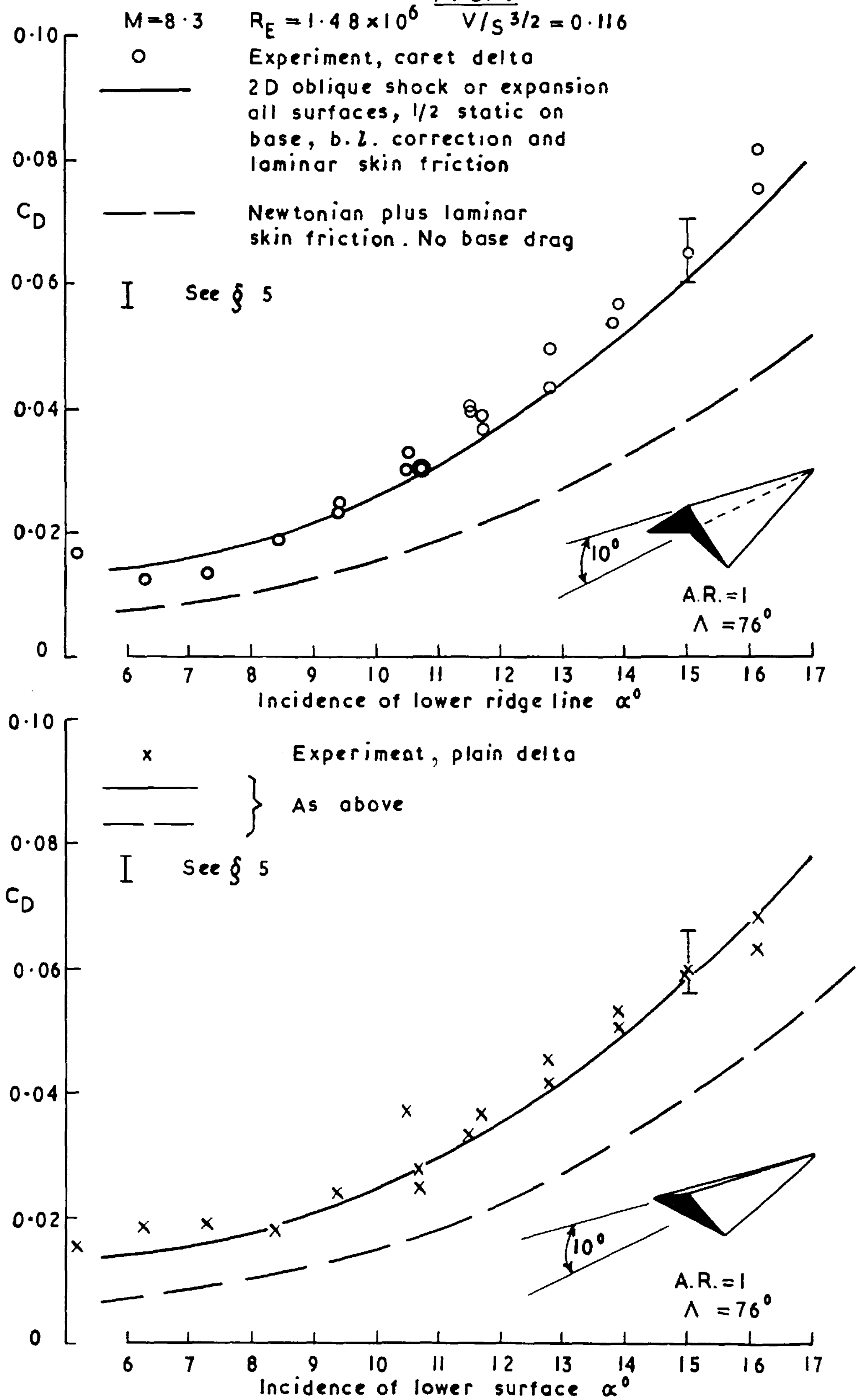

Drag of delta wings

FIG. 10

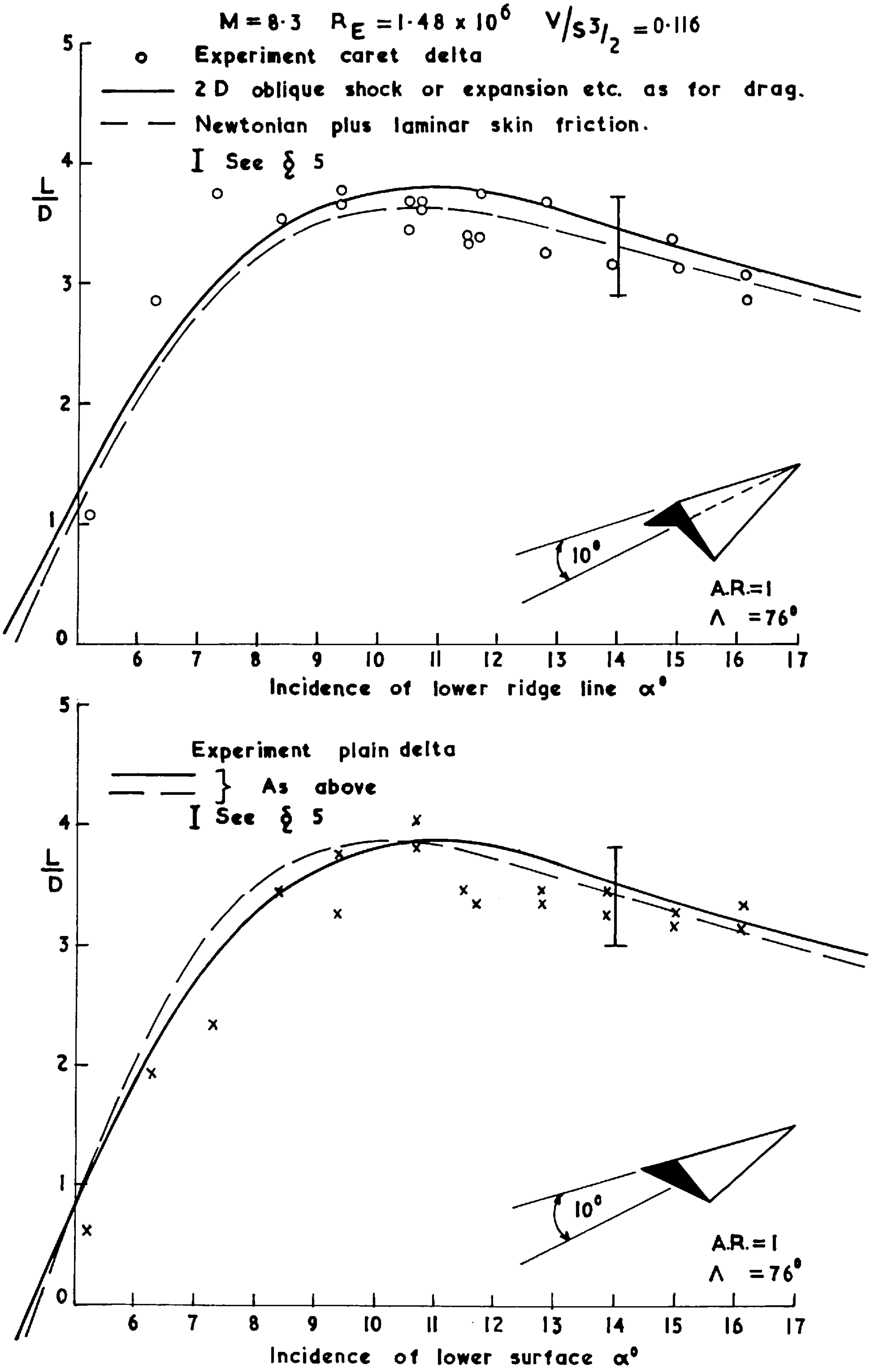

$\frac{L}{D}$ ratio of delta wings

FIG.11

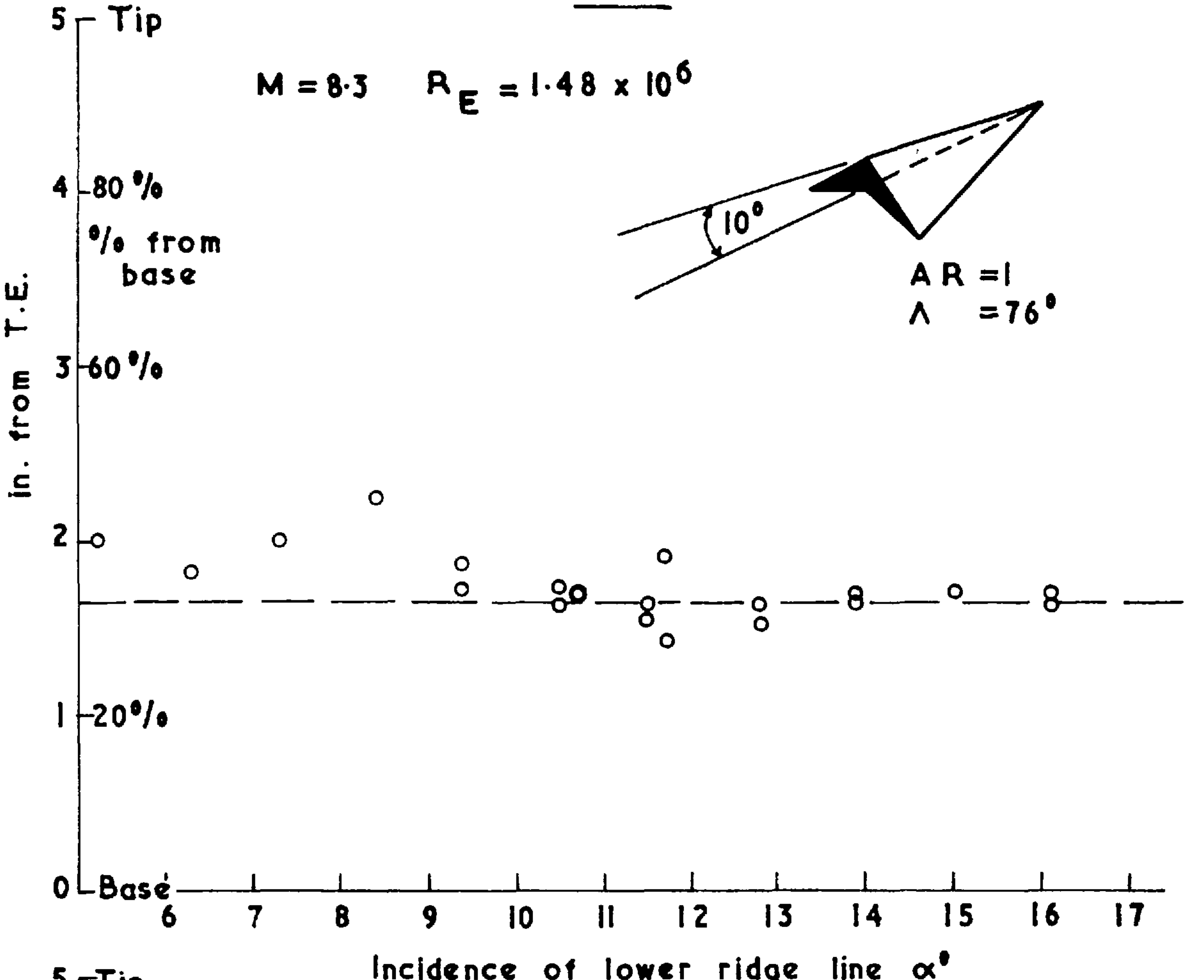

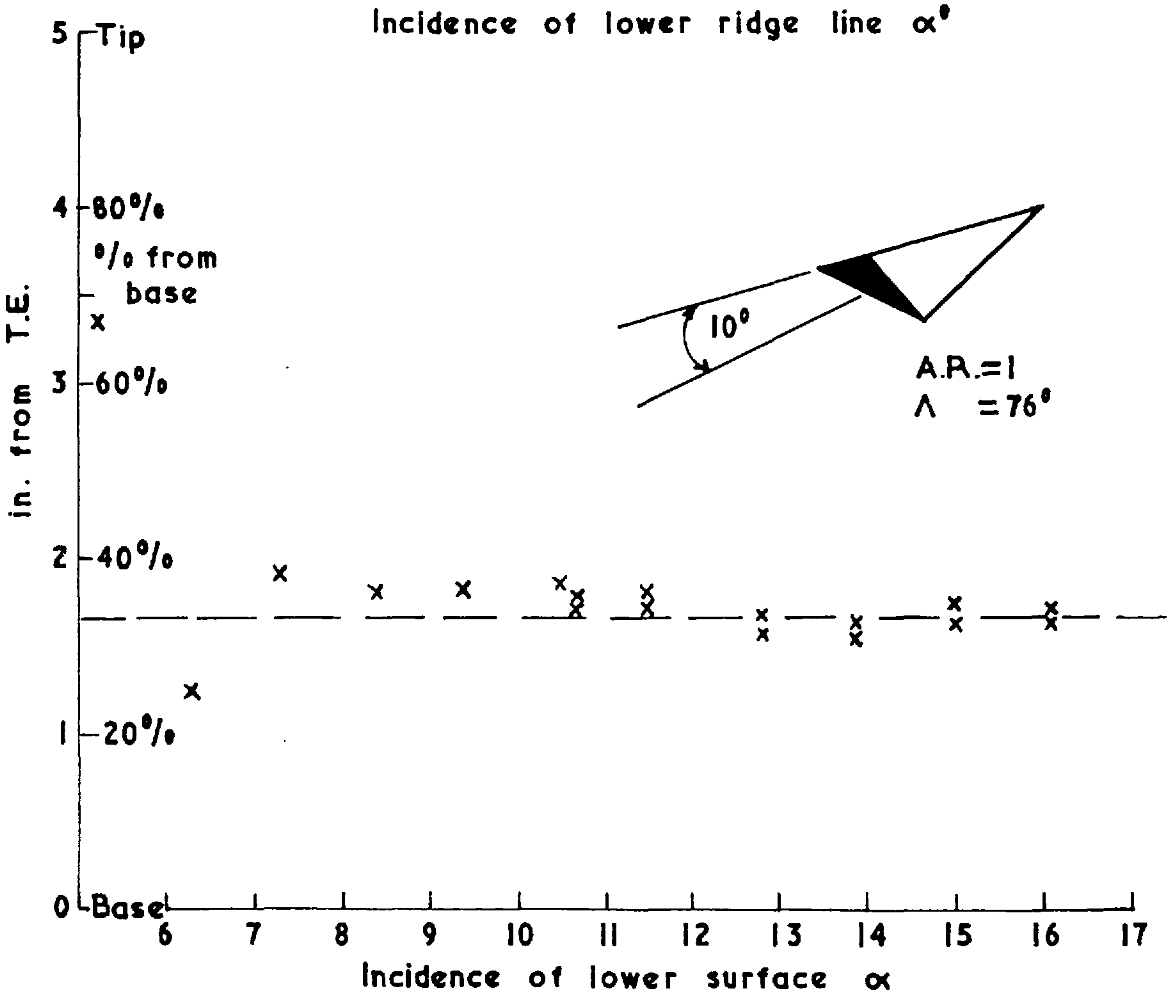

C.P. position on delta wings

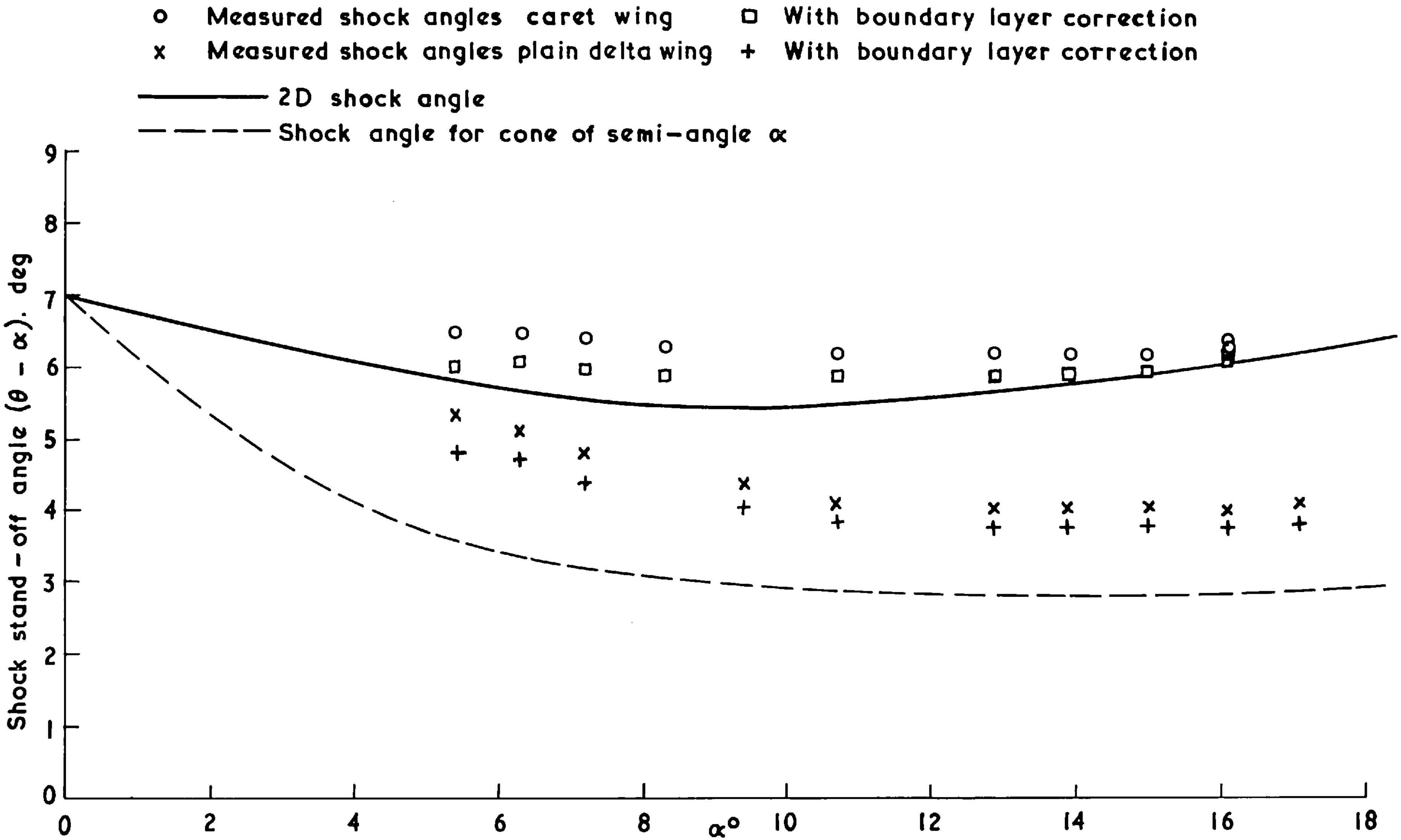

Shock angles on delta wings

FIG. 12(a)

FIG. 12 (b & c)

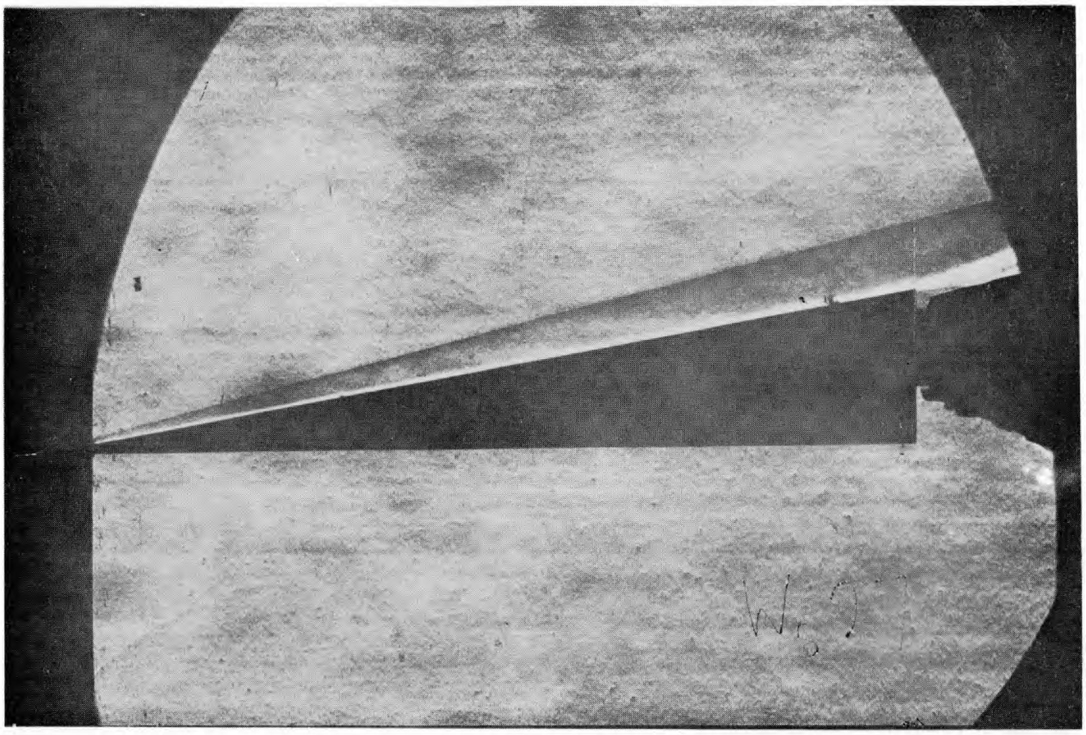

(b) Plain delta, $\alpha = 10 \cdot 7^{0}$, $M = 8 \cdot 3$

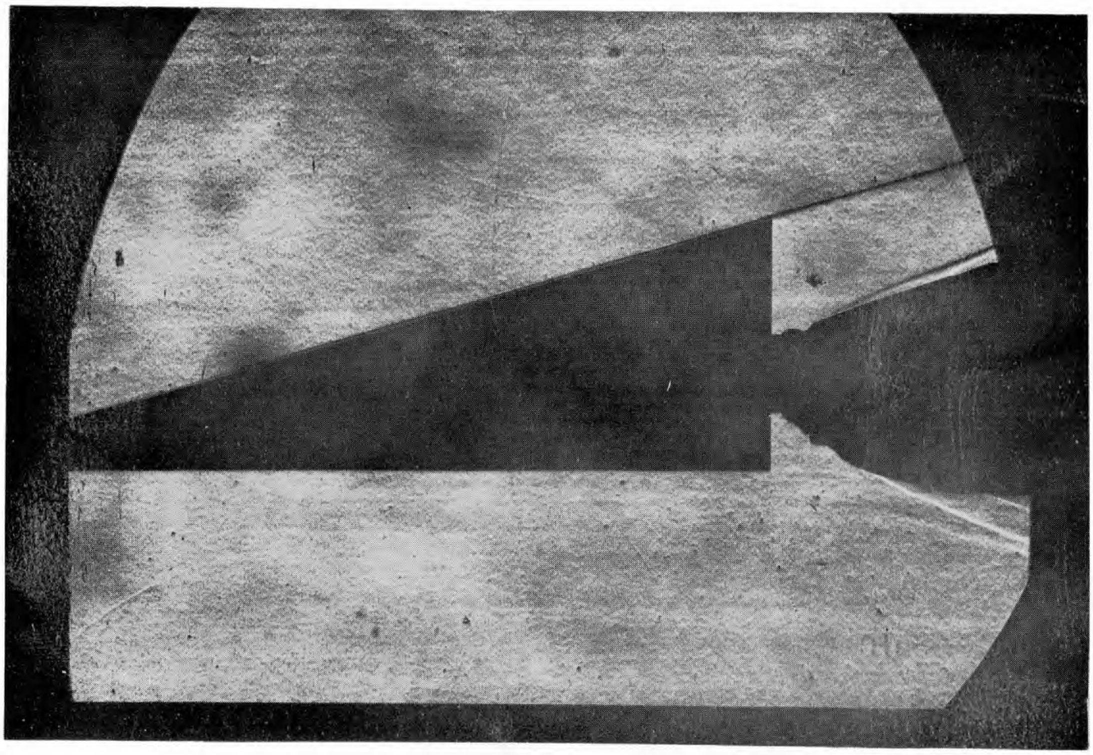

(c) Caret delta, $\alpha = 10 \cdot 3^{0}$, $M = 8 \cdot 3$

Schlieren of flow (Side view)

FIG. 12 (d & e)

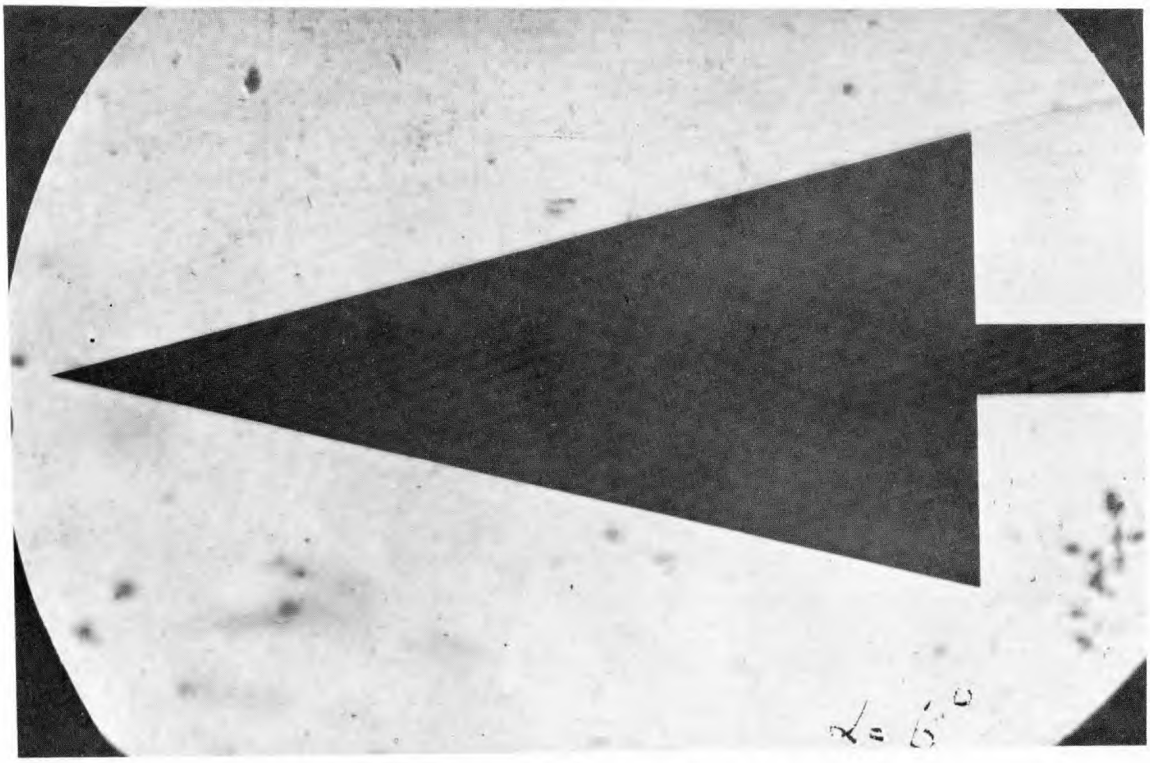

(d) Plain delta, $\alpha = 6^\circ$, $M = 8{\cdot}3$

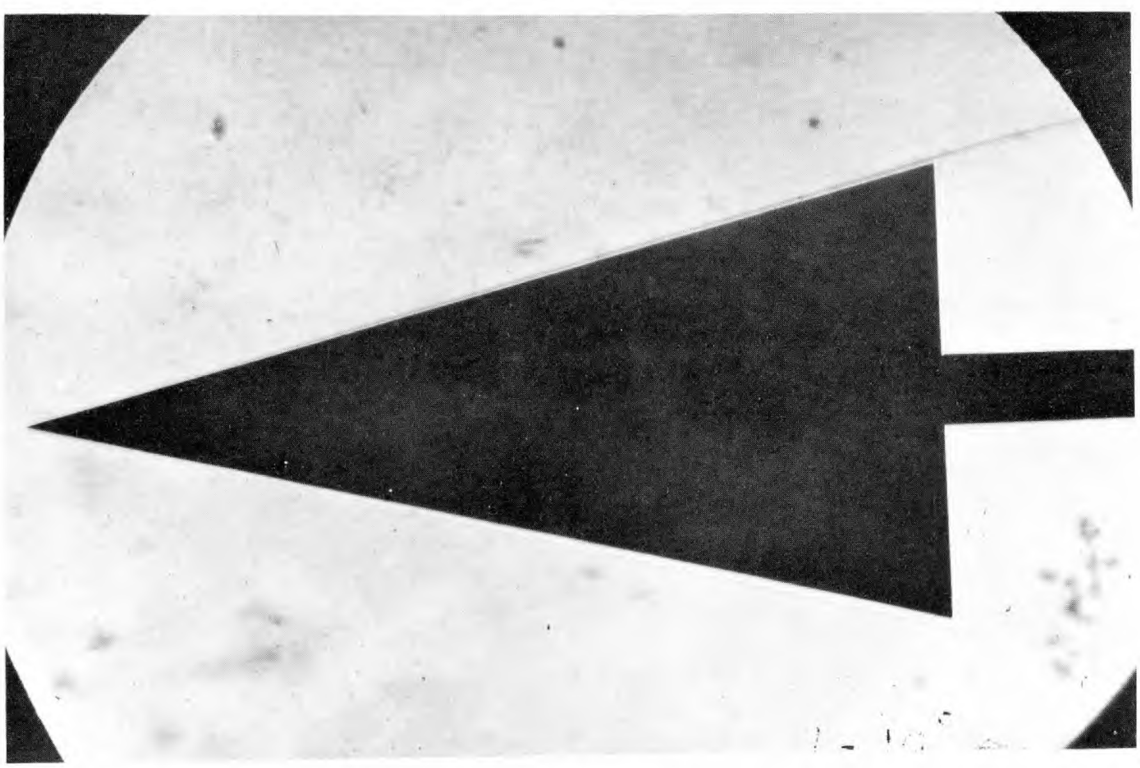

(e) Plain delta, $\alpha = 10^\circ$, $M = 8{\cdot}3$

Schlieren of flow (Plan view)

FIG. 12 (f & g)

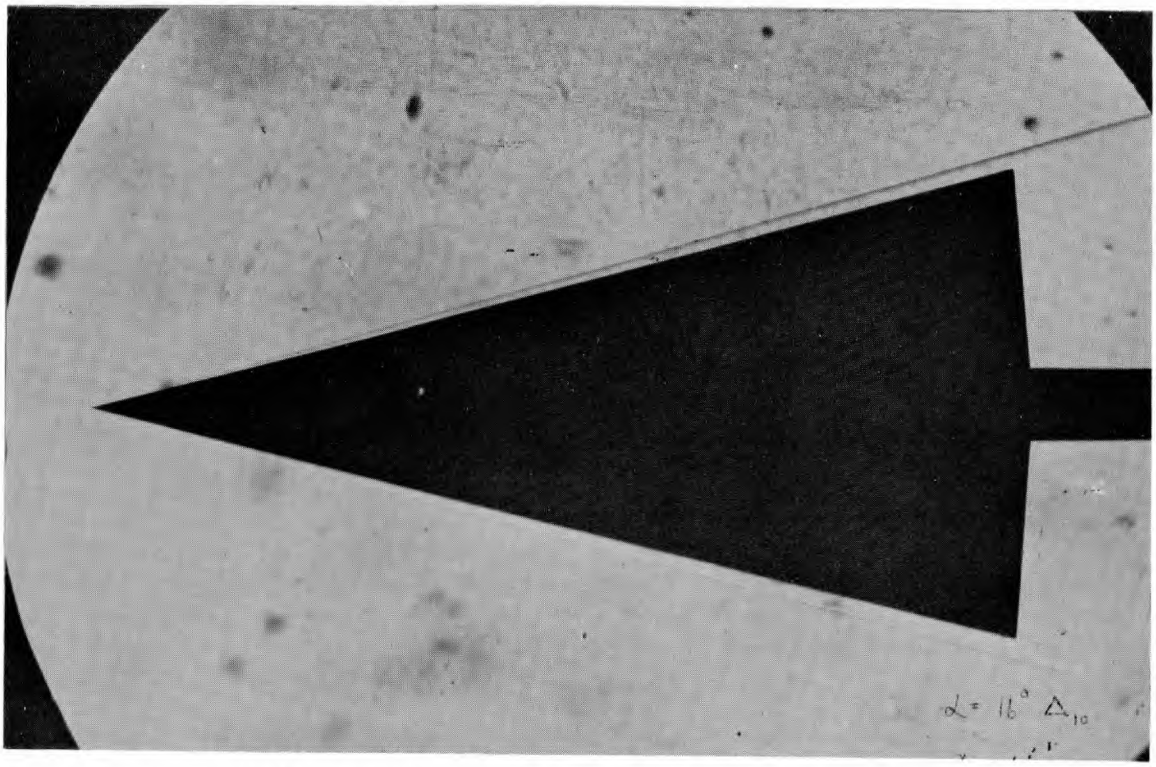

(f) Plain delta, $\alpha = 16^0$, $M = 8{\cdot}3$

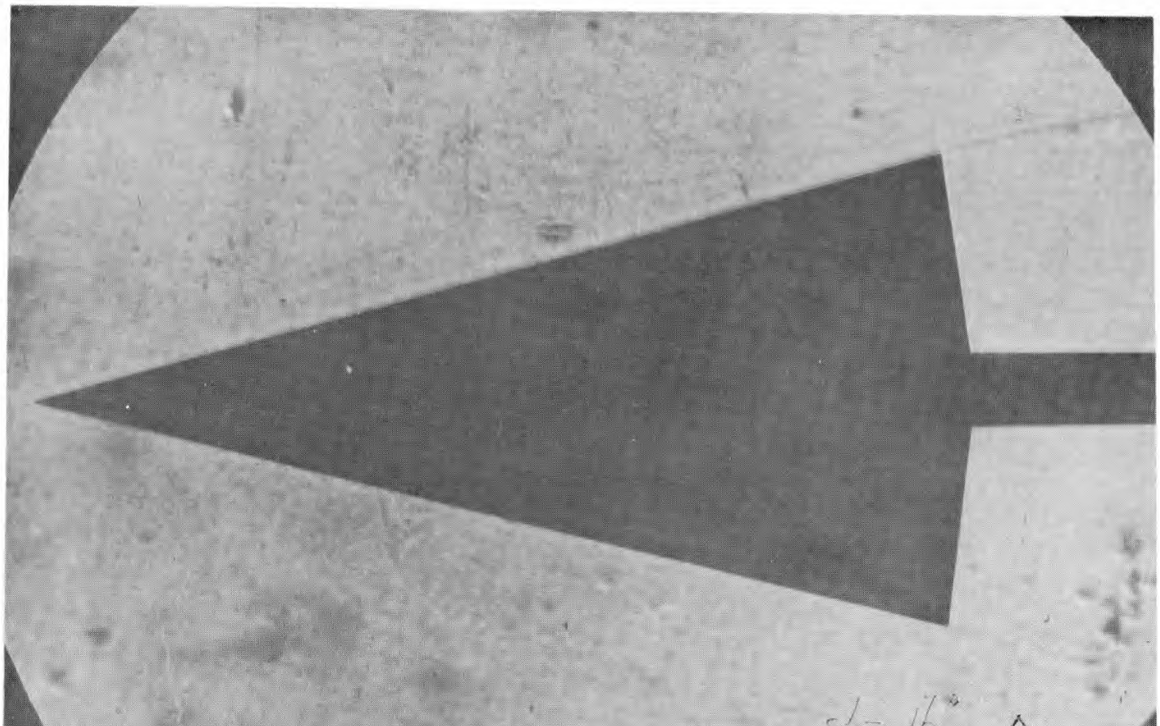

(g) Caret delta, $\alpha = 16^0$, $M = 8{\cdot}3$

Schlieren of flow (Plan view)

FIG. A1

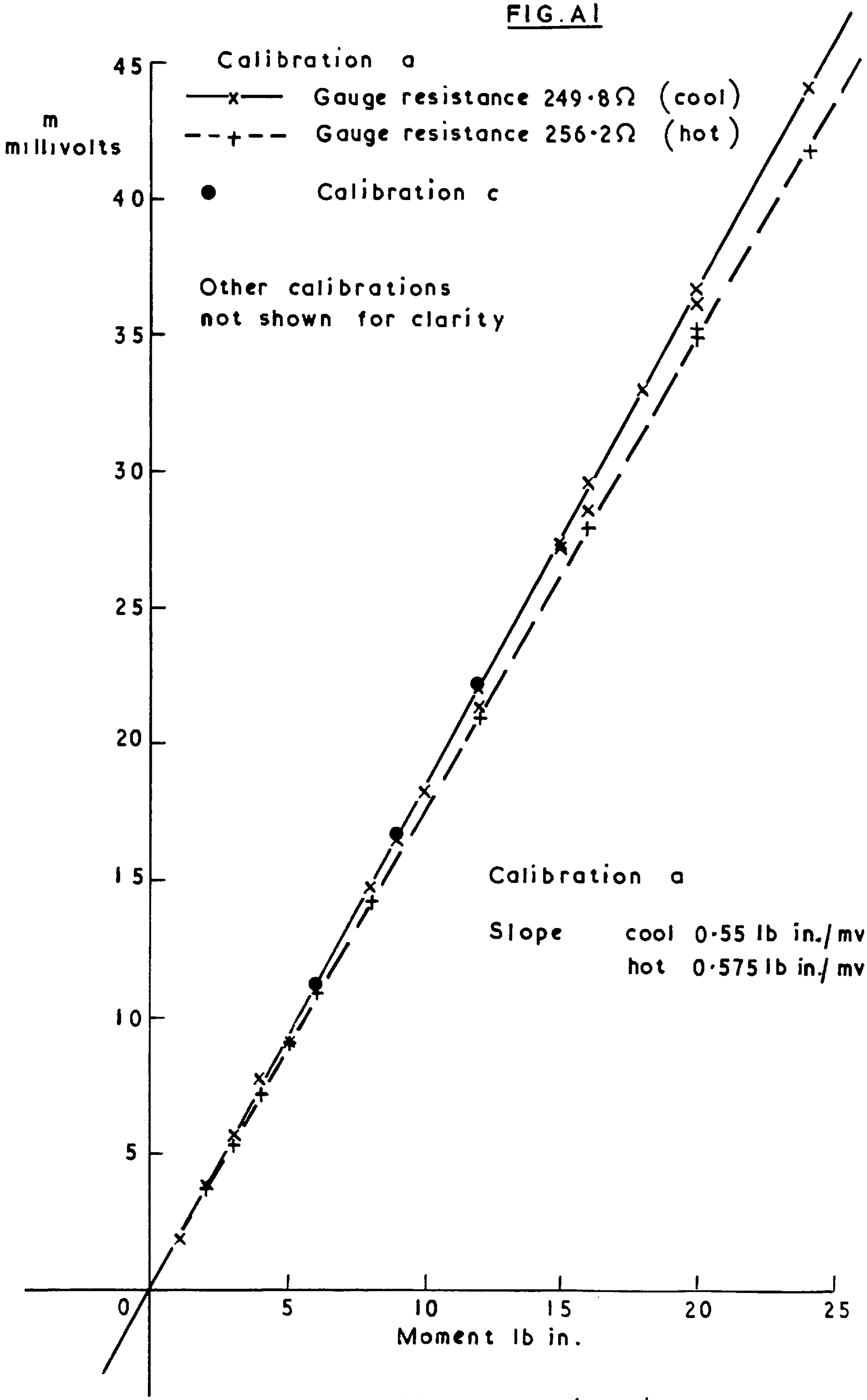

Moment calibration

FIG. A2

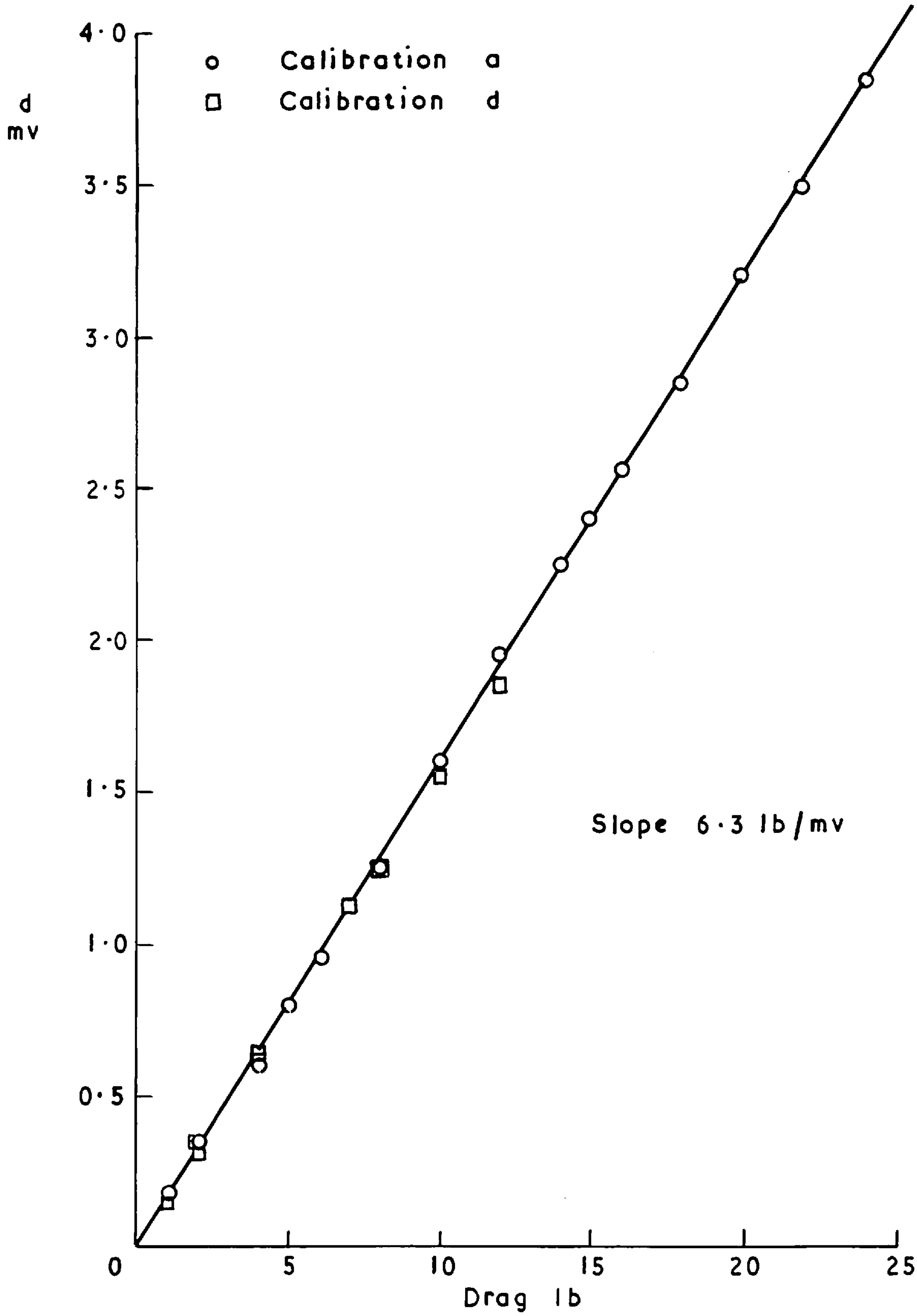

Drag calibration

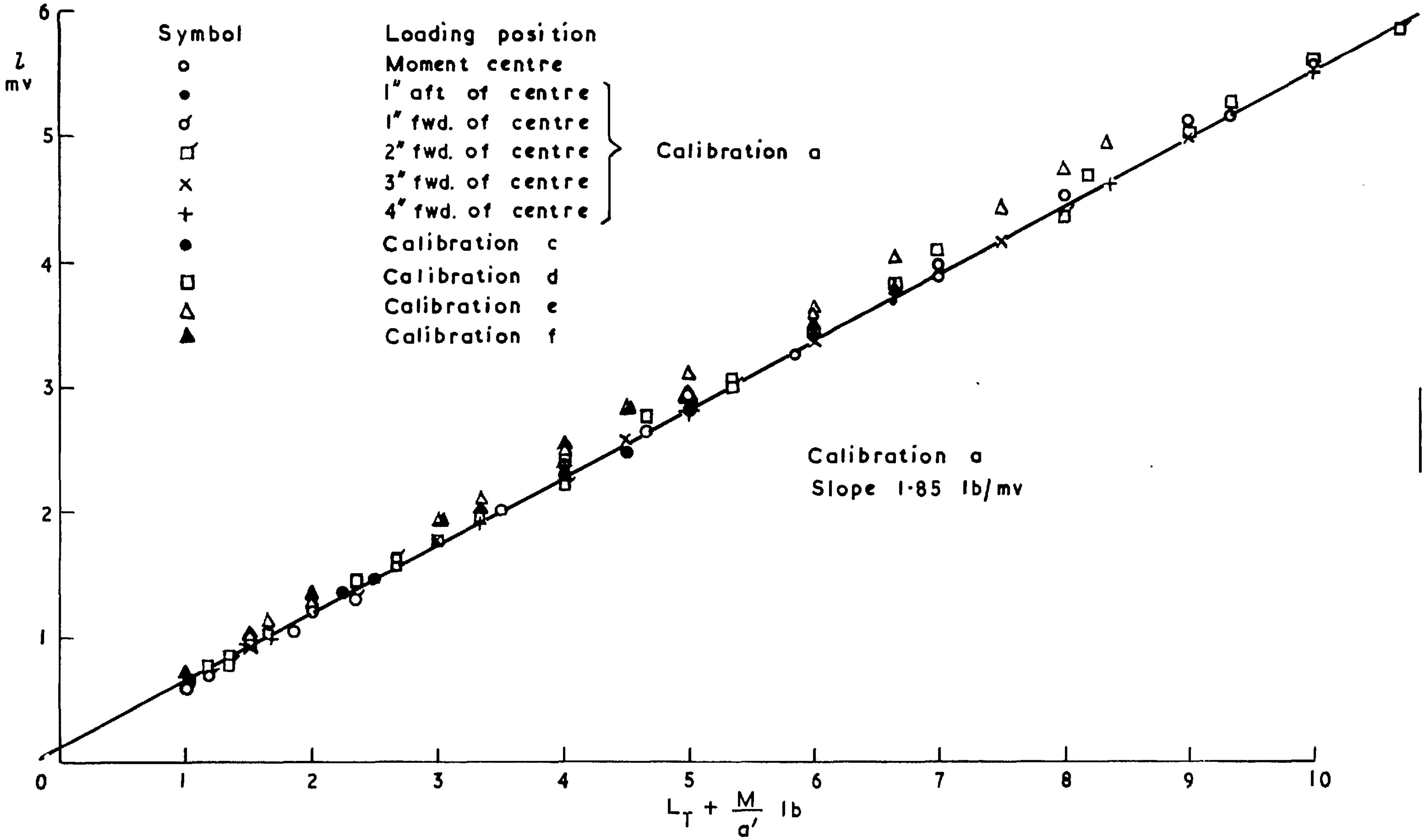

Lift calibration L_1 cantilever (fwd. lift sensor)

FIG A3

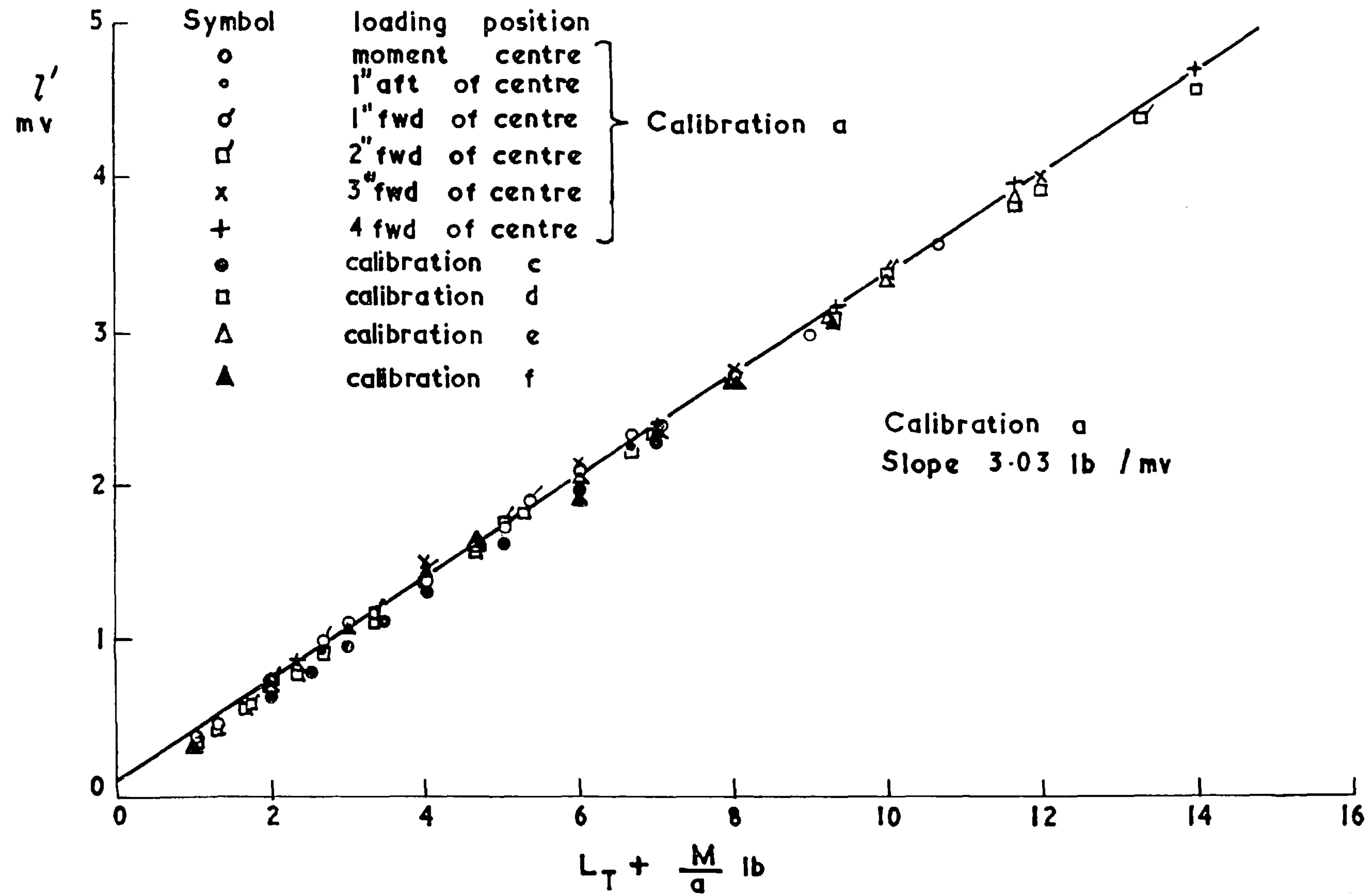

Lift calibration. – L′ cantilever

(Aft lift sensor)

FIG. A 4

FIG. A5

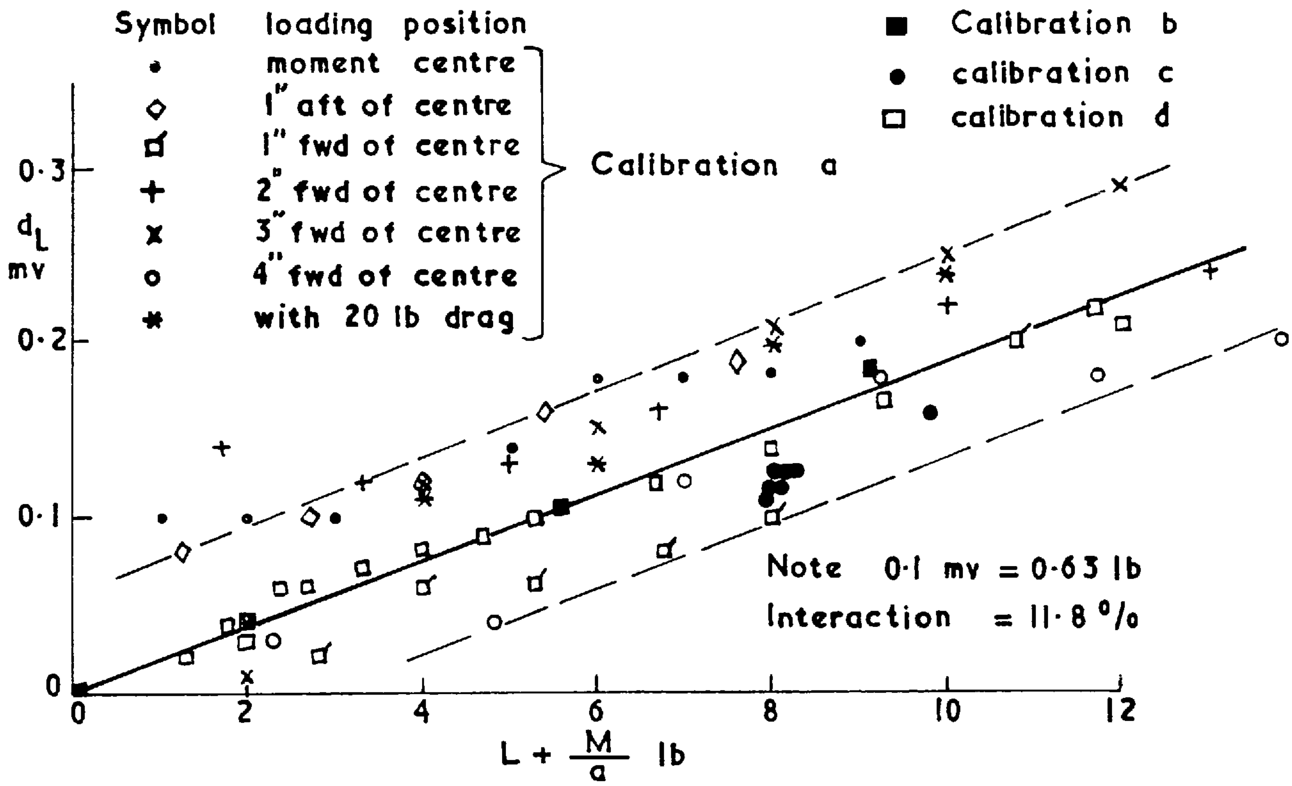

(a) Lift interaction on drag

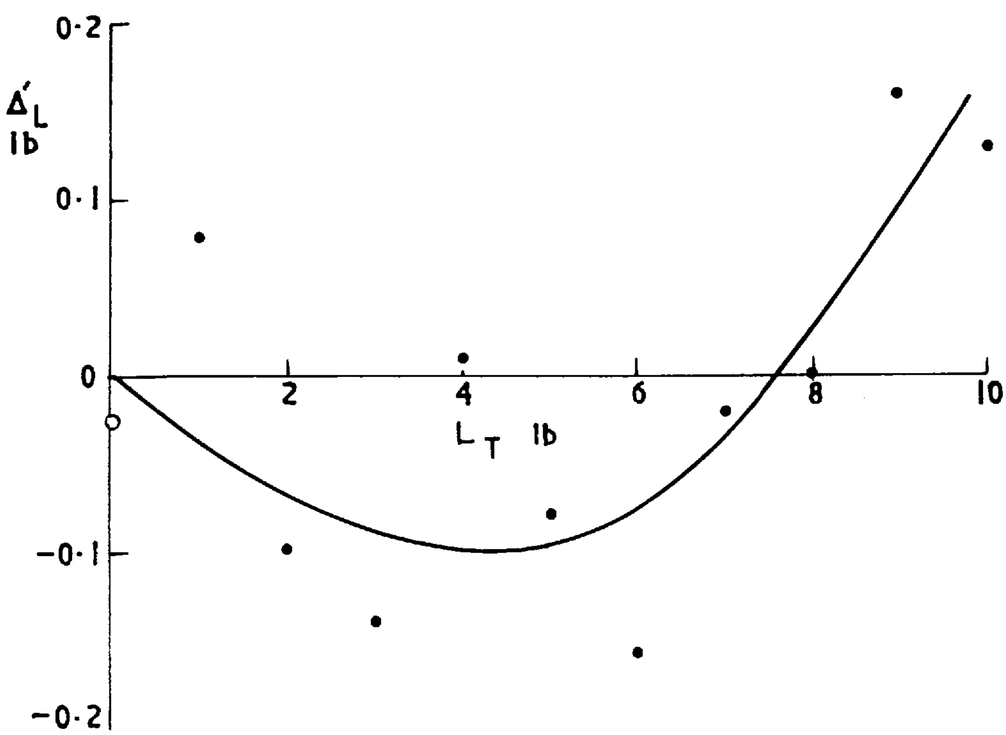

(b) Lift correction Δ'_L at zero moment.

See para. V

A.R.C. C.P. No.908
December, 1965
Opatowski, T. Imperial College of Science and Technology

GUN TUNNEL MEASUREMENTS OF LIFT, DRAG AND PITCHING MOMENT ON A 20° CONE, A FLAT DELTA AND A CARET DELTA WING AT A MACH NUMBER OF 8·3

Measurements of lift, drag and pitching moment have been made on a 20° half-angle, right-circular cone and on two delta wings of triangular and caret cross section, 10° wedge angle and aspect ratio 1 in the Imperial College gun tunnel.

The strain gauge balance developed for this purpose gave results which were within 5% of other published cone data.

Maximum lift/drag ratios of about 3·7 were obtained for both wings at the test Mach number of 8·3 and Reynolds number based on root chord of $1{\cdot}5 \times 10^6$.

The measured lift, drag and lift/drag ratio agreed well with estimates based on two-dimensional oblique shock theory and laminar skin friction.

A.R.C. C.P. No.908
December, 1965
Opatowski, T. Imperial College of Science and Technology

GUN TUNNEL MEASUREMENTS OF LIFT, DRAG AND PITCHING MOMENT ON A 20° CONE, A FLAT DELTA AND A CARET DELTA WING AT A MACH NUMBER OF 8·3

Measurements of lift, drag and pitching moment have been made on a 20° half-angle, right-circular cone and on two delta wings of triangular and caret cross section, 10° wedge angle and aspect ratio 1 in the Imperial College gun tunnel.

The strain gauge balance developed for this purpose gave results which were within 5% of other published cone data.

Maximum lift/drag ratios of about 3·7 were obtained for both wings at the test Mach number of 8·3 and Reynolds number based on root chord of $1{\cdot}5 \times 10^6$.

The measured lift, drag and lift/drag ratio agreed well with estimates based on two-dimensional oblique shock theory and laminar skin friction.

A.R.C. C.P. No.908
December, 1965
Opatowski, T. Imperial College of Science and Technology

GUN TUNNEL MEASUREMENTS OF LIFT, DRAG AND PITCHING MOMENT ON A 20° CONE, A FLAT DELTA AND A CARET DELTA WING AT A MACH NUMBER OF 8·3

Measurements of lift, drag and pitching moment have been made on a 20° half-angle, right-circular cone and on two delta wings of triangular and caret cross section, 10° wedge angle and aspect ratio 1 in the Imperial College gun tunnel.

The strain gauge balance developed for this purpose gave results which were within 5% of other published cone data.

Maximum lift/drag ratios of about 3·7 were obtained for both wings at the test Mach number of 8·3 and Reynolds number based on root chord of $1{\cdot}5 \times 10^6$.

The measured lift, drag and lift/drag ratio agreed well with estimates based on two-dimensional oblique shock theory and laminar skin friction.

A.R.C. C.P. No.908
December, 1965
Opatowski, T. Imperial College of Science and Technology

GUN TUNNEL MEASUREMENTS OF LIFT, DRAG AND PITCHING MOMENT ON A 20° CONE, A FLAT DELTA AND A CARET DELTA WING AT A MACH NUMBER OF 8·3

Measurements of lift, drag and pitching moment have been made on a 20° half-angle, right-circular cone and on two delta wings of triangular and caret cross section, 10° wedge angle and aspect ratio 1 in the Imperial College gun tunnel.

The strain gauge balance developed for this purpose gave results which were within 5% of other published cone data.

Maximum lift/drag ratios of about 3·7 were obtained for both wings at the test Mach number of 8·3 and Reynolds number based on root chord of $1{\cdot}5 \times 10^6$.

The measured lift, drag and lift/drag ratio agreed well with estimates based on two-dimensional oblique shock theory and laminar skin friction.

DETACHABLE ABSTRACT CARDS

Printed and published by
HER MAJESTY'S STATIONERY OFFICE
To be purchased from
49 High Holborn, London W.C.1
423 Oxford Street, London W.1
13A Castle Street, Edinburgh 2
109 St. Mary Street, Cardiff
Brazennose Street, Manchester 2
50 Fairfax Street, Bristol 1
35 Smallbrook, Ringway, Birmingham 5
80 Chichester Street, Belfast 1
or through any bookseller

Printed in England

C.P. No. 908

S.O. Code No. 23-9017-8